Acknowledgement

The research described in this report was carried out at the Road and Railroad research Laboratory of the Faculty of Civil Engineering of the Delft University of Technology. This report presents the Master of Science thesis that is written as final part of the study Civil Engineering at Delft University of Technology, Section Highway Engineering. The thesis constitutes part of the Ph.D. study of T.O. Medani.

The author wishes to express his appreciation to: Tarig Medani for his enthusiastic daily assistance and expertise, Marco Poot for his energetic help during the execution of the experimental program, L.J.M. Houben and A.A.A. Molenaar for their co-operation and support and finally Sandra Erkens for helping me with the determination of the ACRe model parameters.

Delft, September 2001

Allart Bosch

The M.Sc. commission consists of: Prof. dr. ir. A.A.A. Molenaar Ir. L.J.M. Houben T.O. Medani M.Sc.

i

Summary

Some of the largest bridges in the Dutch main highway network consist of an orthotropic steel deck with an asphalt surface. Examples of such bridges are the Moerdijk bridge and the Brienenoord bridge. Due to the flexible nature of the structure high deformations occur in the asphalt under increasing traffic loading. This result in a short lifetime of the asphalt, in spite of the fact that special asphalt mixes (like mastic asphalt) are applied. The frequent maintenance that is necessary is expensive and leads to hindrance for the traffic.

In this M. Sc. project first available models are used to calculate the expected asphalt strains on orthotropic steel bridges. Also the influence of temperature and dynamics is included. Because of the high strains that occur in the asphalt compared to normal pavements on a subgrade, it is doubtful the mastic asphalt on the bridge deck behaves pure linear-elastic. For a better understanding of the behaviour of mastic asphalt on orthotropic steel bridges an experimental program is carried out on mastic asphalt. Specimens were obtained during surfacing the Moerdijk bridge in June 2000. The experimental program consists of two parts:

- Four-point bending tests at different temperatures, loading frequencies and strain rates. With
 the results the master curves and the fatigue characteristics are determined and also a
 relationship that describes the stiffness of mastic asphalt as a function of loading time,
 temperature and strain level. After 2.5 months some tests were repeated to investigate the
 healing capacity of the asphalt mix.
- 2. Uniaxial monotonic tension and compression tests. With the results of these tests the ACRe material model parameters were determined.

Finally, a case study for the Moerdijk bridge is carried out to predict the fatigue lifetime of mastic asphalt based on the experimental results and assuming linear elastic material behaviour.

The main conclusions from the literature review are:

- The strains in the asphalt on orthotropic steel bridges are approximately 10 times higher than the strains in normal pavements on a basecoarse and a subgrade.
- Composite action theories are commonly used to calculate stresses and strains that occur in the mastic asphalt due to bending moment produced by loading. They are based on one of both of the following assumptions:
 - 1. Linear strain distribution in the asphalt and the steel.
 - 2. The slopes of the strain distribution through the depth of the asphalt and the steel are equal.
- From the comparison between the composite action theories from Metcalf, Kolstein, Cullimore, Nakanishi and Sedlacek/Bild the following can be concluded:
 - 1. For the high strain levels that oocur in the asphalt linear elastic behaviour of the asphalt is doubtful.
 - 2. The strains/stresses in the steel/asphalt are calculated using a beam model. However, plate theory may be more applicable.
 - 3. For certain conditions the presented theories might be true, but these conditions might not be representative for the real structure.
 - 4. For extreme values of the bond (0% and 100% bonding) the theories give the same results, but for values of the bond stiffness between both extremes the theories give different results.
- From a dynamic analysis can be concluded that vibration of the deck could lead to increasing strains in the pavement due to an increasing impact of the dynamic axle loads compared to pavements on a subgrade, because of the interaction between the bridge deck and the vehicle.

From the experimental program the following can be concluded:

- The material characteristics, like stiffness and fatigue behaviour are more or less comparable to the characteristics of some different modified mastic asphalt mixes.
- Mastic asphalt has excellent healing characteristics.

- The stiffness of mastic asphalt is not only a function of loading time and temperature, but also a function of the strain level. This indicates non-linear elastic behaviour of mastic asphalt. The mix stiffness decreases with increasing strain level, long loading times (traffic congestion) and high temperatures (summer).
- For strain rates lower than 0.05 s⁻¹ the flow surface can not be determined. Physically this might be attributed to the fact that in that case there is hardly any elastic response, meaning that the material starts to flow immediately.

Conclusions from a case study for the Moerdijk bridge are:

- Shifting the traffic lanes over a distance of 1.0 m during a certain period of the year on a bridge leads to an increased lifetime of the asphalt on orthotropic steel bridges.
- The commonly used procedure to estimate the fatigue lifetime seems not to be applicable for mastic asphalt on orthotropic steel bridges.

To calculate the fatigue lifetime of mastic asphalt in a better way the following is proposed:

- Include the strain dependent behaviour of the asphalt stiffness in the calculation of the asphalt strains
- Use a finite element program to calculate a reasonable bending moment, but take a representative part of the structure
- Use a non-linear material model to calculate the asphalt strains, for example the ACRe material model

Contents

ACKNOWLEDGEMENT	I
SUMMARY	II
1 INTRODUCTION	1
2 SCOPE OF THIS RESEARCH	3
2.1 AIM OF THIS RESEARCH	3
2.2 RESEARCH QUESTIONS	3
2.3 RESEARCH PLANNING	
2.3.1 Literature study	
2.3.2 Experiments	
2.3.3 Analysis	
2.3.4 Case study	
3 LITERATURE REVIEW	5
3.1 ORTHOTROPIC STEEL BRIDGES	5
3.1.1 Definition	
3.1.2 History of orthotropic steel bridges	
3.1.3 Deck surfacing	
3.1.3.1 Introduction	
3.1.3.2 Requirements for different layers	
3.1.3.3 Materials used in practice for different surfacing layers	
3.2 Mastic asphalt	9
3.2.1 Characteristics of mastic asphalt	9
3.2.2 Comparison composition mastic asphalt with other Dutch asphalt mixes	
3.2.3 The reason that mastic asphalt is often used on orthotropic steel bridges	12
3.2.4 History of mastic asphalt in the Netherlands	
3.2.5 Requirements for mastic asphalt in some countries	
3.2.5.1 The Netherlands	
3.2.5.2 Germany	
3.2.5.3 USA	
3.2.5.4 England	
3.2.6 Comparison between the composition of mastic asphalt in some countries Typical cross-sections in various countries	10
3.3 STRESS REDUCTION IN STEEL DECK DUE TO ASPHALT SURFACING	
3.3.1 Introduction	
3.3.2 Composite action theories	
3.3.2.1 Metcalf [1967]	
3.3.2.2 Kolstein [1990]	
3.3.2.3 Cullimore et al. [1983]	
3.3.2.4 Nakanishi et al. [2000]	
3.3.2.5 Sedlacek and Bild [1985]	
3.3.3 Comparison between the different composite action theories	31
3.3.3.1 Introduction	31
3.3.3.2 <i>Metcalf</i>	
3.3.3.3 Kolstein	
3.3.3.4 Cullimore	
3.3.3.5 Nakanishi	
0.0.0.0 Oculater and Dild	

	3.4 DA	MAGE TO BRIDGE DECK SURFACINGS	38
	3.4.1	Introduction	38
	3.4.2	Permanent deformation	
	3.4.3	Cracking	
	3.4.4	Mounds	
	3.4.5	Disintegration	
	3.4.6	Loss of bond between the steel deck and the asphalt	
	3.4.7	Distress mechanisms related to mix parameters	
	3.4.7 3.4.7.		
	3.4.7. 3.4.7.		
	3.4.7. 3.4.7.		
	3.4.7.		
		MPERATURE EFFECT	
		RATION OF THE BRIDGE DECK	
	3.6.1	Dynamic axle loads on pavements on a subgrade	
	3.6.2	Vibration of the bridge deck	
	3.6.3 3.6.3.	The effect of vibrations on the pavement	
	3.6.3. 3.6.3.	· · · · · · · · · · · · · · · · · · ·	
	3.6.3. 3.6.3.	, , ,	
	3.6.3.		
		•	
4	MATE	RIAL MODELLING	55
	44 1-		
		RODUCTION	
		E MATERIAL MODEL	
		LUENCE OF THE MODEL PARAMETERS	
	4.4 TE	STS TO DETERMINE THE MODEL PARAMETERS	61
5	FYDF	RIMENTAL PROGRAM	62
J			
	5.1 INT	RODUCTION	62
	5.2 Mi	(COMPOSITION	62
	5.3 SP	ECIMEN PREPARATION	63
	5.4 DE	NSITY MEASUREMENTS	66
		UR POINT BENDING TEST	
	5.5.1	Test set up	
	5.5.2	Survey of the four point bending testing program	
	5.5.3	Input for the four point bending fatigue testing machine	
	5.5.3.		70 70
	5.5.3.		/ 0
	553		70
	5.5.3. 5.5.3.	3 Test conditions for the first determination of the fatigue behaviour	70 70
	5.5.3.	 Test conditions for the first determination of the fatigue behaviour Test conditions for the repeated determination of the fatigue behaviour 	70 70 71
	5.5.3. 5.5.3.	Test conditions for the first determination of the fatigue behaviour	70 70 71 71
	5.5.3. 5.5.3. 5.5.4	Test conditions for the first determination of the fatigue behaviour	70 70 71 71
	5.5.3. 5.5.3. 5.5.4 5.5.5	Test conditions for the first determination of the fatigue behaviour	70 70 71 71 71
	5.5.3. 5.5.3. 5.5.4 5.5.5 5.6 O P	Test conditions for the first determination of the fatigue behaviour Test conditions for the repeated determination of the fatigue behaviour Test conditions for the determination of the strain dependency of the mix stiffness Output for the four point bending fatigue testing machine Data calculations in the four point bending test TIMISATION OF THE TENSION AND COMPRESSION EXPERIMENTAL PROGRAM	70 70 71 71 72 73
	5.5.3. 5.5.4 5.5.5 5.6 OP 5.6.1	Test conditions for the first determination of the fatigue behaviour Test conditions for the repeated determination of the fatigue behaviour Test conditions for the determination of the strain dependency of the mix stiffness Output for the four point bending fatigue testing machine Data calculations in the four point bending test TIMISATION OF THE TENSION AND COMPRESSION EXPERIMENTAL PROGRAM	70 71 71 71 72 73
	5.5.3. 5.5.4 5.5.5 5.6 OP 5.6.1 5.6.2	Test conditions for the first determination of the fatigue behaviour Test conditions for the repeated determination of the fatigue behaviour Test conditions for the determination of the strain dependency of the mix stiffness Output for the four point bending fatigue testing machine Data calculations in the four point bending test TIMISATION OF THE TENSION AND COMPRESSION EXPERIMENTAL PROGRAM	70 71 71 71 72 73 73
	5.5.3. 5.5.4 5.5.5 5.6 OP 5.6.1 5.6.2 5.7 UN	Test conditions for the first determination of the fatigue behaviour Test conditions for the repeated determination of the fatigue behaviour Test conditions for the determination of the strain dependency of the mix stiffness Output for the four point bending fatigue testing machine Data calculations in the four point bending test TIMISATION OF THE TENSION AND COMPRESSION EXPERIMENTAL PROGRAM	70 70 71 71 72 73 73 75
	5.5.3. 5.5.4 5.5.5 5.6 OP 5.6.1 5.6.2 5.7 UN 5.7.1	Test conditions for the first determination of the fatigue behaviour Test conditions for the repeated determination of the fatigue behaviour Test conditions for the determination of the strain dependency of the mix stiffness Output for the four point bending fatigue testing machine Data calculations in the four point bending test. TIMISATION OF THE TENSION AND COMPRESSION EXPERIMENTAL PROGRAM Introduction Procedure for the central rotatable design IAXIAL MONOTONIC COMPRESSION TEST Compression test set up	7071717172737373
	5.5.3. 5.5.4 5.5.5 5.6 OP 5.6.1 5.6.2 5.7 UN 5.7.1 5.7.2	Test conditions for the first determination of the fatigue behaviour Test conditions for the repeated determination of the fatigue behaviour Test conditions for the determination of the strain dependency of the mix stiffness Output for the four point bending fatigue testing machine Data calculations in the four point bending test TIMISATION OF THE TENSION AND COMPRESSION EXPERIMENTAL PROGRAM Introduction Procedure for the central rotatable design IAXIAL MONOTONIC COMPRESSION TEST Compression test set up Specimen preparation for the compression test	707171717373737375
	5.5.3. 5.5.3. 5.5.5 5.6 OP 5.6.1 5.6.2 5.7 UN 5.7.1 5.7.2 5.7.3	Test conditions for the first determination of the fatigue behaviour Test conditions for the repeated determination of the fatigue behaviour Test conditions for the determination of the strain dependency of the mix stiffness Output for the four point bending fatigue testing machine Data calculations in the four point bending test. TIMISATION OF THE TENSION AND COMPRESSION EXPERIMENTAL PROGRAM Introduction Procedure for the central rotatable design IAXIAL MONOTONIC COMPRESSION TEST Compression test set up Specimen preparation for the compression test Input for the compression test	707171717373737575
	5.5.3. 5.5.4 5.5.5 5.6 OP 5.6.1 5.6.2 5.7 UN 5.7.1 5.7.2 5.7.3	Test conditions for the first determination of the fatigue behaviour Test conditions for the repeated determination of the fatigue behaviour Test conditions for the determination of the strain dependency of the mix stiffness Output for the four point bending fatigue testing machine Data calculations in the four point bending test. TIMISATION OF THE TENSION AND COMPRESSION EXPERIMENTAL PROGRAM Introduction Procedure for the central rotatable design IAXIAL MONOTONIC COMPRESSION TEST Compression test set up Specimen preparation for the compression test Input for the compression test 1 Computer input for the compression test	707171717373737575
	5.5.3. 5.5.3. 5.5.5 5.6 OP 5.6.1 5.6.2 5.7 UN 5.7.1 5.7.2 5.7.3	Test conditions for the first determination of the fatigue behaviour Test conditions for the repeated determination of the fatigue behaviour Test conditions for the determination of the strain dependency of the mix stiffness Output for the four point bending fatigue testing machine Data calculations in the four point bending test. TIMISATION OF THE TENSION AND COMPRESSION EXPERIMENTAL PROGRAM Introduction Procedure for the central rotatable design IAXIAL MONOTONIC COMPRESSION TEST Compression test set up Specimen preparation for the compression test Input for the compression test	707171717373737575

	5.8 Uni	AXIAL MONOTONIC TENSION TEST	78
	5.8.1	Tension test set up	78
	5.8.2	Specimen preparation for the tension test	79
	5.8.3	Input for the tension test	
	5.8.3.1	Computer input for the tension test	80
	5.8.3.2		
	5.8.4	Output from the tension test	81
6	EXPER	IMENTAL RESULTS	82
	6.1 DEN	SITY MEASUREMENTS	82
	6.1.1	Introduction	82
	6.1.2	Mix composition of the specimen for the four point bending test	
	6.1.2.1		
	6.1.2.2		
	6.1.3	Mix composition of the specimen for the monotonic compression test	
	6.1.4	Mix composition of the specimen for the monotonic tension test	
		TER CURVES	
	6.2.1	Determination of the master curves	
	6.2.2	Results from the first determination of the master curves	
	6.2.3	Results from the repeated determination of master curves	
		GUE RESULTS	
	6.3.1	Results from the first fatigue test	
	6.3.2	Results from the repeated fatigue test	
		AIN DEPENDENCY OF THE MIX STIFFNESSDIFFERENCE BETWEEN THE ELASTIC MODULUS AND THE FLEXURAL STIFFNESS	
		AXIAL MONOTONIC COMPRESSION TEST	
		AXIAL MONOTONIC COMPRESSION TEST	
7	ANALY	SIS OF TEST RESULTS	. 102
	7.1 Mas	TER CURVES	102
		TER CURVES	
	7.1.1	Introduction	
		Introduction	102
	7.1.1 7.1.2	Introduction	102
	7.1.1	$\begin{tabular}{ll} Introduction &$	102 102
	7.1.1 7.1.2 7.1.3	Introduction	102 102 103
	7.1.1 7.1.2 7.1.3 7.1.4	Introduction	102 102 103 104
	7.1.1 7.1.2 7.1.3 7.1.4 7.1.5	Introduction	102 102 103 104
	7.1.1 7.1.2 7.1.3 7.1.4	Introduction	102 102 103 104 106
	7.1.1 7.1.2 7.1.3 7.1.4 7.1.5 7.1.6	Introduction	102 102 103 104 106
	7.1.1 7.1.2 7.1.3 7.1.4 7.1.5 7.1.6	Introduction	102 103 104 106 107
	7.1.1 7.1.2 7.1.3 7.1.4 7.1.5 7.1.6 7.2 FAT	Introduction Determining S _{mix} as a function of T and t for the first determination of master curves Determining S _{mix} as a function of T and t for the repeated determination of master curves. Comparison between the first and repeated determination of master curves Comparison of the stiffness behaviour of some different mastic asphalt mixes Stiffness behaviour of mastic asphalt compared to some other types of asphalt mixes Introduction	102 103 104 106 107 108
	7.1.1 7.1.2 7.1.3 7.1.4 7.1.5 7.1.6 7.2 FAT 7.2.1	Introduction Determining S _{mix} as a function of T and t for the first determination of master curves Determining S _{mix} as a function of T and t for the repeated determination of master curves. Comparison between the first and repeated determination of master curves Comparison of the stiffness behaviour of some different mastic asphalt mixes Stiffness behaviour of mastic asphalt compared to some other types of asphalt mixes IGUE CHARACTERISTICS Introduction First fatigue test.	102 103 104 106 107 108 108
	7.1.1 7.1.2 7.1.3 7.1.4 7.1.5 7.1.6 7.2 FAT 7.2.1 7.2.2	Introduction Determining S _{mix} as a function of T and t for the first determination of master curves Determining S _{mix} as a function of T and t for the repeated determination of master curves. Comparison between the first and repeated determination of master curves Comparison of the stiffness behaviour of some different mastic asphalt mixes Stiffness behaviour of mastic asphalt compared to some other types of asphalt mixes GUE CHARACTERISTICS Introduction First fatigue test. Characterisation of fatigue parameters using the Wöhler approach. Characterisation of fatigue parameters using the energy approach.	102 103 104 106 107 108 109 109
	7.1.1 7.1.2 7.1.3 7.1.4 7.1.5 7.1.6 7.2 FAT 7.2.1 7.2.2 7.2.2.1 7.2.2.2 7.2.2.3	Introduction Determining S _{mix} as a function of T and t for the first determination of master curves Determining S _{mix} as a function of T and t for the repeated determination of master curves. Comparison between the first and repeated determination of master curves Comparison of the stiffness behaviour of some different mastic asphalt mixes Stiffness behaviour of mastic asphalt compared to some other types of asphalt mixes IGUE CHARACTERISTICS Introduction First fatigue test. Characterisation of fatigue parameters using the Wöhler approach. Characterisation of fatigue parameters using the energy approach. Relationship between the strain, the mix stiffness and the number of load repetitions	102 103 104 106 107 108 109 109 110
	7.1.1 7.1.2 7.1.3 7.1.4 7.1.5 7.1.6 7.2 FAT 7.2.1 7.2.2 7.2.2.1 7.2.2.3 7.2.3	Introduction Determining S _{mix} as a function of T and t for the first determination of master curves Determining S _{mix} as a function of T and t for the repeated determination of master curves. Comparison between the first and repeated determination of master curves Comparison of the stiffness behaviour of some different mastic asphalt mixes Stiffness behaviour of mastic asphalt compared to some other types of asphalt mixes Introduction First fatigue test. Characterisation of fatigue parameters using the Wöhler approach Characterisation of fatigue parameters using the energy approach Relationship between the strain, the mix stiffness and the number of load repetitions. Repeated fatigue test	102 103 104 106 107 108 109 109 110
	7.1.1 7.1.2 7.1.3 7.1.4 7.1.5 7.1.6 7.2 FAT 7.2.1 7.2.2 7.2.2.1 7.2.2.2 7.2.2.3 7.2.3 7.2.3.1	Introduction Determining S _{mix} as a function of T and t for the first determination of master curves Determining S _{mix} as a function of T and t for the repeated determination of master curves. Comparison between the first and repeated determination of master curves Comparison of the stiffness behaviour of some different mastic asphalt mixes Stiffness behaviour of mastic asphalt compared to some other types of asphalt mixes IGUE CHARACTERISTICS Introduction First fatigue test. Characterisation of fatigue parameters using the Wöhler approach. Characterisation of fatigue parameters using the energy approach. Relationship between the strain, the mix stiffness and the number of load repetitions. Repeated fatigue test. Characterisation of fatigue parameters using the Wöhler approach.	102 103 104 106 107 108 109 109 111 112 112
	7.1.1 7.1.2 7.1.3 7.1.4 7.1.5 7.1.6 7.2 FAT 7.2.1 7.2.2 7.2.2.1 7.2.2.2 7.2.2.3 7.2.3 7.2.3.1 7.2.3.2	Introduction Determining S _{mix} as a function of T and t for the first determination of master curves Determining S _{mix} as a function of T and t for the repeated determination of master curves. Comparison between the first and repeated determination of master curves Comparison of the stiffness behaviour of some different mastic asphalt mixes Stiffness behaviour of mastic asphalt compared to some other types of asphalt mixes IGUE CHARACTERISTICS Introduction First fatigue test. Characterisation of fatigue parameters using the Wöhler approach. Characterisation of fatigue parameters using the energy approach Relationship between the strain, the mix stiffness and the number of load repetitions Repeated fatigue test Characterisation of fatigue parameters using the Wöhler approach. Characterisation of fatigue parameters using the Wöhler approach. Characterisation of fatigue parameters using the energy approach. Characterisation of fatigue parameters using the energy approach.	102 103 104 106 107 108 109 109 111 112 112
	7.1.1 7.1.2 7.1.3 7.1.4 7.1.5 7.1.6 7.2 FAT 7.2.1 7.2.2 7.2.2.3 7.2.3 7.2.3 7.2.3.1 7.2.3.2 7.2.4	Introduction	102 103 104 106 107 108 109 109 111 112 112
	7.1.1 7.1.2 7.1.3 7.1.4 7.1.5 7.1.6 7.2 FAT 7.2.1 7.2.2 7.2.2.1 7.2.2.2 7.2.2.3 7.2.3 7.2.3.1 7.2.3.2	Introduction	102 103 104 106 107 108 109 109 110 111 112 113
	7.1.1 7.1.2 7.1.3 7.1.4 7.1.5 7.1.6 7.2 FAT 7.2.1 7.2.2 7.2.2.3 7.2.3 7.2.3 7.2.3.1 7.2.3.2 7.2.4 7.2.5	Introduction Determining S _{mix} as a function of T and t for the first determination of master curves Determining S _{mix} as a function of T and t for the repeated determination of master curves Comparison between the first and repeated determination of master curves Comparison of the stiffness behaviour of some different mastic asphalt mixes Stiffness behaviour of mastic asphalt compared to some other types of asphalt mixes GUE CHARACTERISTICS Introduction First fatigue test. Characterisation of fatigue parameters using the Wöhler approach Characterisation of fatigue parameters using the energy approach Relationship between the strain, the mix stiffness and the number of load repetitions Repeated fatigue test Characterisation of fatigue parameters using the Wöhler approach Characterisation of fatigue parameters using the Wöhler approach Characterisation of fatigue parameters using the energy approach Characterisation of fatigue parameters using the energy approach Comparison between the first and repeated fatigue test for the Moerdijk mix Fatigue behaviour of the Moerdijk mix compared to some modified mastic asphalt mixes	102 103 104 106 107 108 109 109 110 111 112 113 113
	7.1.1 7.1.2 7.1.3 7.1.4 7.1.5 7.1.6 7.2 FAT 7.2.1 7.2.2 7.2.2.3 7.2.3 7.2.3 7.2.3.1 7.2.3.2 7.2.4 7.2.5 7.2.6	Introduction Determining S _{mix} as a function of T and t for the first determination of master curves Determining S _{mix} as a function of T and t for the repeated determination of master curves Comparison between the first and repeated determination of master curves Comparison of the stiffness behaviour of some different mastic asphalt mixes Stiffness behaviour of mastic asphalt compared to some other types of asphalt mixes BUE CHARACTERISTICS Introduction First fatigue test Characterisation of fatigue parameters using the Wöhler approach Characterisation of fatigue parameters using the energy approach Relationship between the strain, the mix stiffness and the number of load repetitions Repeated fatigue test Characterisation of fatigue parameters using the Wöhler approach Characterisation of fatigue parameters using the energy approach Characterisation of fatigue parameters using the energy approach Characterisation of fatigue parameters using the energy approach Comparison between the first and repeated fatigue test for the Moerdijk mix Fatigue behaviour of the Moerdijk mix compared to some modified mastic asphalt mixes Fatigue behaviour of the Moerdijk mix compared to some other mixes	102 103 104 106 107 108 109 110 111 112 113 114
	7.1.1 7.1.2 7.1.3 7.1.4 7.1.5 7.1.6 7.2 FAT 7.2.1 7.2.2 7.2.2.3 7.2.3 7.2.3 7.2.3 7.2.3 7.2.3 7.2.4 7.2.5 7.2.6 7.2.7	Introduction	102 103 104 106 107 108 109 110 111 112 113 114
	7.1.1 7.1.2 7.1.3 7.1.4 7.1.5 7.1.6 7.2 FAT 7.2.1 7.2.2 7.2.2.3 7.2.3 7.2.3 7.2.3.1 7.2.3.2 7.2.4 7.2.5 7.2.6	Introduction Determining S _{mix} as a function of T and t for the first determination of master curves Determining S _{mix} as a function of T and t for the repeated determination of master curves Comparison between the first and repeated determination of master curves Comparison of the stiffness behaviour of some different mastic asphalt mixes Stiffness behaviour of mastic asphalt compared to some other types of asphalt mixes BUE CHARACTERISTICS Introduction First fatigue test Characterisation of fatigue parameters using the Wöhler approach Characterisation of fatigue parameters using the energy approach Relationship between the strain, the mix stiffness and the number of load repetitions Repeated fatigue test Characterisation of fatigue parameters using the Wöhler approach Characterisation of fatigue parameters using the energy approach Characterisation of fatigue parameters using the energy approach Characterisation of fatigue parameters using the energy approach Comparison between the first and repeated fatigue test for the Moerdijk mix Fatigue behaviour of the Moerdijk mix compared to some modified mastic asphalt mixes Fatigue behaviour of the Moerdijk mix compared to some other mixes	102 103 104 106 107 108 109 110 111 112 113 114 115

vi

	7.3	DEPENDENCY OF THE MIX STIFFNESS ON THE STRAIN	120
	7.3.1	Introduction	120
	7.3.2	Strain dependency of some asphalt mixes	120
	7.3.3	Comparison between master curves at 80 μm/m and 800 μm/m for the Moerdijk	
		mix	123
	7.3.4		
	7.3.5		
	7.3.6		
	7.3.7		
	7.3.8		
	7.3.9		137
	7.4	UNIAXIAL MONOTONIC COMPRESSION TEST	
	7.4.1	Standardisation compression curves	138
	7.4.2		
		strain rate	139
	7.5	UNIAXIAL MONOTONIC TENSION TEST	141
	7.5.1	Standardisation of tension curves	141
	7.5.2		
		rate	141
	7.5.3		
	7.6	DETERMINATION OF THE MODEL PARAMETERS	
	7.6.1		
	7.6.2		
	7.6.3		
	7.6.4		
	7.6.5		
		$6.5.1$ Determination of α_0 at the onset of dilation	
		$6.5.2$ Determination of α as a function of the equivalent plastic strain	
		$0.5.3$ Determination of α as a function of plastic work	
	7.6.6		
	7.6	6.6.1 Effect of temperature on the response surface	172
	7.6	6.6.2 Effect of strain rate on the response surface	173
	7.6	$6.6.3$ Effect of α on the response surface	174
8	$C \wedge C$	SE STUDY MOERDIJK BRIDGE	176
0	CAS	SE STODT MOERDISK BRIDGE	170
	8.1	INTRODUCTION	176
	8.2	TRAFFIC LOADING	176
	8.3	HEALING	177
	8.4	Lateral wander	178
	8.5	SHIFTING THE TRAFFIC LANES	180
	8.6	PREDICTION OF THE FATIGUE LIFETIME BY NEGLECTING THE STRAIN DEPENDENCY OF	
		THE MIX STIFFNESS	181
	8.6.1		
		method for T=10°C and f=5 Hz	181
	8.6.2	Prediction of the fatigue lifetime for the Moerdijk mix using common	
		method for T=20°C and f=50 Hz	183
	8.6.3	Prediction of the fatigue lifetime for mixes tested by Kolstein using common	
		method	184
	8.7	A PROPOSED PROCEDURE FOR ESTIMATING THE FATIGUE LIFETIME	
	8.7.1	Definition of the procedure	185
	8.7.2		
		temperature of 20°C	186
	8.7.3	·	
		temperature of 20°C	187
	8.7.4	·	
	-	CONCLUSION	

9	CC	DNCLUSIONS AND RECOMMENDATIONS	. 190
		Conclusions	
R	EFEF	RENCES	.194
Α	PPE	NDIX A: SPECIMENS' DIMENSIONS	. 197
Α	PPE	NDIX B: RESULTS FOUR-POINT BENDING TESTS	. 199
		NDIX C: DETERMINATION OF S _{MIX} AS A FUNCTION OF TEMPERATURE OF TIME AND STRAIN LEVEL	
Α	PPE	NDIX D: NOMOGRAPHS	. 222
		NDIX E: DETERMINATION OF THE TENSION AND COMPRESS NGTH AS A FUNCTION OF TEMPERATURE AND LOADING RATE	
Α	PPE	NDIX F: DETERMINATION OF N AS FUNCTION OF ϵ AND S_{MIX}	230
		NDIX G: DETERMINATION OF GDILATION AS A FUNCTION OF STRAIN REMPERATURE	
		NDIX H: DETERMINATION OF $lpha_0$ as a function of strain rate $lpha$	

1 Introduction

Orthotropic steel bridges have a steel deck plate with different elastic properties in the two orthogonal directions. Normally this steel deck plate is surfaced with asphalt. The flexible nature of the structure causes large elastic deformations in both the steel deck plate and the asphalt. Therefore these bridges are often surfaced with a flexible type of asphalt, mastic asphalt. In spite of this flexible type of asphalt it has become clear that the lifetime of asphalt on steel bridges is short compared to normal pavements. On these steel bridges problems, like rutting and cracking, arise in a relative early stadium of lifetime. The next article from a Dutch newspaper shows clearly the problem:

datum: 5 april 2000

bron: ANP

Moerdijkbrug opnieuw op de schop

Financiële strop voor NBM Milieu

MOERDIJK - Een deel van de vorig jaar voor 35 miljoen gulden gerenoveerde Moerdijkbrug moet weer van nieuw asfalt worden voorzien. Twee van de acht rij- en vluchtstroken voldoen na een jaar al niet meer aan de eisen van Rijkswaterstaat. NBM Milieu moet voor de kosten opdraaien.

Het gaat om de vluchtstrook en de meest rechtse strook aan de westkant van de brug, over de volle lengte van een kilometer. Wat de oorzaak van de slechtere kwaliteit van de twee stroken is, is niet duidelijk. Mogelijk heeft het te maken met het gefaseerd onder verschillende omstandigheden uitvoeren van de werkzaamheden, aldus een woordvoerder van Rijkswaterstaat.

Kosten

De kosten voor het opnieuw asfalteren komen voor rekening van NBM Milieu dat de werkzaamheden aan de brug heeft uitgevoerd. Volgens een woordvoerder van NBM Milieu heeft zijn bedrijf de brug nog drie jaar in onderhoud. 'Het asfalt voldoet niet aan het bestek, dus dat moet op onze kosten worden verbeterd', zegt hij.

Over de hoogte van die extra kosten wilde NBM niets zeggen. Hoewel de Moerdijkbrug tijdens het herstel voor het verkeer geopend blijft, zal het verkeer wel hinder ondervinden. De werkzaamheden worden van eind april tot eind mei uitgevoerd.

The interaction between the vehicles, asphalt and bridge structure is not well understood. As a result of this interaction strains of more than 1000 μ m/m have been measured in the asphalt layer, compared with a strain of \approx 200 μ m/m in normal pavements. For the design of asphaltic surfacings on steel bridges elastic theory is used. However, with such high strain levels it is doubtful that the asphalt still behaves linearly.

In the Netherlands there are 86 orthotropic steel bridges. Many of them constitute part of the main highway network, like the Moerdijkbrug and the Van Brienenoordbrug. In the last decades the rush of traffic in the Netherlands became enormous, not only in the peak hours every morning and evening, but also during the rest of the day. Therefore there is very less or actually no time

for maintenance during a day without disturbing the traffic. To avoid this problem road constructions need to be durable, meaning very little maintenance for a very long time. The asphalt surfacings nowadays used on orthotropic steel bridges do not fulfil this demand, because of their short lifetime. Also the short lifetime leads to large costs for maintenance, especially because of the expensive asphalt mixes that are used on this type of bridges. To design asphalt surfaces for orthotropic steel bridges with an increased lifetime a better understanding of the asphalt behaviour on this particular type of bridges is needed. For that purpose the material model developed in the ACRe project can be used successfully.

The main objective of this research is the material characterisation of a typical mastic asphalt mix that is used for surfacing orthotropic steel bridges.

This characterisation consists of:

- Determining the ACRe model parameters by carrying out the uniaxial monotonic tension and compression test
- Determining the relationship between the mix stiffness, loading time and temperature (master curves)
- Determining the fatigue characteristics.

This report is organised as follows: chapter 2 starts with the scope of the research. The objective of the research is presented together with the research questions and the research planning. Chapter 3 shows the main parts of the literature review. In this chapter information about orthotropic steel bridges, mastic asphalt, composite action theories, damage, temperature effect and vibrations of the bridge deck comes up for discussion. Chapter 4 describes the non-linear material model as well as the influence of the different parameters of the material model. Chapter 5 contains an overview of the experimental program. For each part of the experimental program the test conditions and the test set-up are presented. Chapter 6 shows the experimental results after which in chapter 7 the results are analysed. Part of this analysis is the strain dependent behaviour of the mix stiffness of mastic asphalt. With the results from the previous chapters a case study is carried out in chapter 8, in order to predict the fatigue lifetime of the mastic asphalt that was placed on the Moerdijk bridge in June 2000. The conclusions and recommendations follow in chapter 9. Finally, the appendixes will be presented.

2 Scope of this research

2.1 Aim of this research

The life span of mastic asphalt on orthotropic steel bridges is shorter than that of normal pavements. Therefore a better understanding of the mastic asphalt behaviour is needed. The main objective of this research is:

The material characterisation of a typical mastic asphalt mix that is used for surfacing orthotropic steel bridges

In this research the determination of the ACRe model parameters, the master curves and the fatigue characteristics are carried out. This research can be considered as a part of the development of a new design philosophy for asphalt on orthotropic steel bridges. It is believed that such characterisation will lead to a better understanding of the mastic asphalt behaviour, like distress phenomena and the material characteristics that influence them. This knowledge can be used not only for a more successful and efficient design of mastic asphalt on orthotropic steel bridges but also for quality control.

2.2 Research questions

To fulfil the main objective of this research, the following questions have to be answered:

- 1. What is the function of the asphalt on an orthotropic steel bridge?
- 2. What is the function of the different asphalt layers?
- 3. What are the properties of mastic asphalt?
- 4. What is the magnitude of the asphalt strains when they are calculated with the composite action theories?
- 5. What is the relationship between mix stiffness, loading time and temperature?
- 6. What are the fatigue characteristics for the Moerdijk mix?
- 7. What are the values of the different model parameters used in the ACRe model for the mastic asphalt that is used for resurfacing the Moerdijkbridge?
- 8. Are the current design methods for normal pavements applicable for the design of surfacings on orthotropic steel bridges?

The next paragraph consists of the research planning that will be used to answer the subquestions in order to fulfil the main objective.

2.3 Research planning

2.3.1 Literature study

This study contains seven main parts:

- Information about orthotropic steel bridges.
- The properties of mastic asphalt.
- Composite action theories.
- Types of distress for asphalt observed on orthotropic steel bridges.
- Increase of axle loads due to bridge deck vibration.
- Temperature effect on the asphalt strains.
- Literature about the ACRe material model.

2.3.2 Experiments

In this research several experiments are carried out to characterise the mastic asphalt that was used for resurfacing the Moerdijk bridge in June 2000. The experimental program included:

- 1. Density measurements
- 2. Four point bending beam test
 - Determination of the relation between the mix stiffness, loading time and temperature (master curves)
 - Determination of the fatigue characteristic
 - Repeated determination of the master curves and the fatigue characteristics to investigate the effect of healing
 - Determination of the strain dependency of the mix stiffness
- 3. Uniaxial monotonic compression test
- 4. Uniaxial monotonic tension test

2.3.3 Analysis

The results of the three tests will be analysed to obtain the following:

- The relation between stiffness, loading time and temperature (master curves) for mastic asphalt.
- The fatigue characteristics for mastic asphalt.
- The strain dependency of the mix stiffness
- The values of the different model parameters used in the ACRe model for mastic asphalt.

2.3.4 Case study

The results obtained from this experimental program will be applied in a case study for the Moerdijk bridge. In this case study an attempt is made to predict the fatigue life of the mastic asphalt mix which was used for resurfacing the Moerdijk bridge in June 2000.

3 Literature review

3.1 Orthotropic steel bridges

3.1.1 Definition

An orthotropic steel bridge consists of a steel deck plate supported into two perpendicular directions, by 'crossbeams' in the transverse direction and by stiffeners in the longitudinal direction. The load in the crossbeams is transferred into the longitudinal main girders, which form the main support of the bridge. Therefore the elastic properties of the steel deck construction in the two orthogonal directions are different. In other words, the steel deck construction is an orthogonal and anisotropic plate, for short it is called an orthotropic plate. The basic layouts of an orthotropic bridge are shown in figure 3.1.

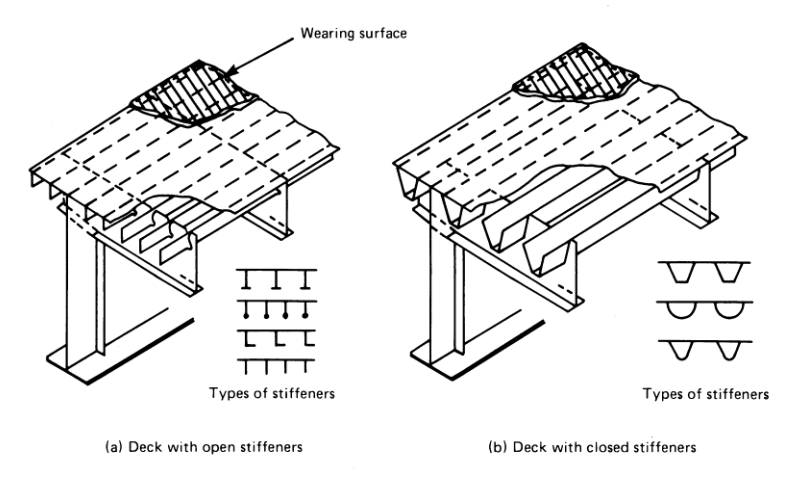


Figure 3.1: Two basic layouts of an orthotropic bridge deck

The deck plate forms the top flange of the bridge deck. There are different types of bridge deck construction, most of them vary in the form of the longitudinal stiffeners. These longitudinal stiffeners can be divided into two types: open stiffeners such as flat bars, angles and bulb sections and closed stiffeners with a trapezoidal, V or rounded form [Gurney, 1992].

3.1.2 History of orthotropic steel bridges

The orthotropic deck was a result of the 'battledeck' floor of the 1930's. This floor consisted of a steel deck plate, supported by longitudinal (normally I-beam) stringers. In their turn, these stringers where supported by cross girders. The cross girders transfer the loads into the longitudinal main girders. The principle of a bridge with a 'battledeck' floor is shown in figure 3.2.

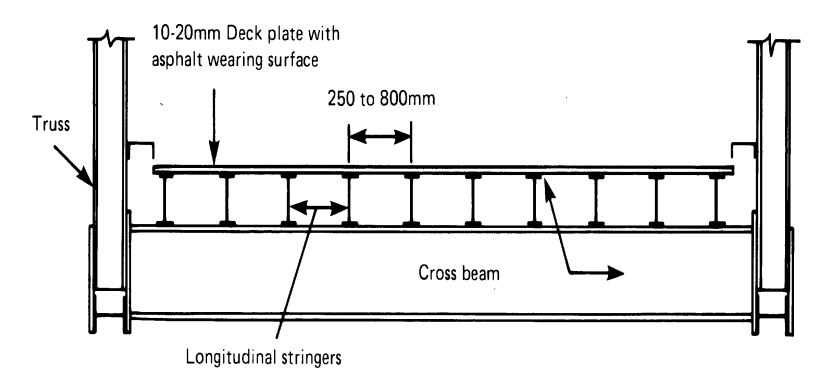


Figure 3.2: Principle of a bridge with a 'battledeck' floor (after Gurney 1992)

In this type of construction the deck plate played no role in strengthening the cross girders. Furthermore, the deck plate had no contribution in strengthening the main longitudinal girders. The main objective of the deck plate in this type of construction is therefore transmission of the wheel loads transversely into the stringers.

The first investigations into surfacing steel deck plates with asphalt mixes were done in 1949 by the English Road Research Laboratory. After a series of field trials it was found that a 1½ inch single course of stone-filled mastic served for five years under heavy traffic loading.

Since that time the experience with asphalt mixes on orthotropic steel decks spread gradually over the rest of Europe, like Germany, Holland and France, especially in Germany where a large number of orthotropic decks were built since World War II. As far is known, the first orthotropic steel bridge was the Kurpfalz bridge over the river Neckar in Mannheim opened in 1950, while the first suspension bridge to have an orthotropic deck was the Cologne-Muelheim Bridge over the Rhine completed in 1951. At first open rib longitudinal stiffeners were used, later the closed stiffeners with a higher torsion stiffness where introduced. The first orthotropic steel bridges in the Netherlands were the Hartel Bridge and the Harmsen Bridge, opened in 1968. Nowadays, there are 86 orthotropic steel bridges in the Netherlands, most of them constitute part of the national road network.

3.1.3 Deck surfacing

3.1.3.1 Introduction

Normally, the steel decks are surfaced with asphalt. This has 4 main objectives [Medani, 2000a]:

- To provide a running surface with suitable skid resistance.
- To provide a flat running surface to compensate for the rough surface of the steel plate.
- To protect the deck plate with a waterproofing layer.
- To reduce the stresses in the steel deck plate.

Because there is no one material that fulfils all these four objectives a functional division can be made, resulting in different functional layers to be applied on a steel bridge deck. In general there are four functional layers, a bonding layer, an isolation layer, an adhesion layer and a wearing course. The different functions of these layers are:

- Bonding layer: to ensure a sufficient strong adhesion between the steel deck plate and the isolation layer.
- Isolation layer: to protect the underlying steel deck against corrosion and to make a flexible transition between the wearing course and the steel deck.
- Adhesion layer: to ensure a sufficient strong adhesion between the isolation layer and the wearing course.
- Wearing course: to take and transfer the loading from traffic to the underlying structure.

The number of asphalt layers to be applied is not necessarily the same as the above mentioned number of functions, because one asphalt layer can fulfil one or more of the functions, resulting in less asphalt layers. Also a further division in functions can be made resulting in more asphalt layers.

3.1.3.2 Requirements for different layers

Brants [1972] defined the general material requirements for the four functional layers. Because a clear distinction between layers is not always possible, some requirements are valid for more layers. The requirements are:

Bonding layer

- Protection against corrosion.
- Sufficient strong adhesion between the overlying asphalt layers and the steel deck, so it has
 to be resistant to shear forces.

According to Kohler and Deters [1974] the bonding layer needs to posses low viscosity to comply with the above-mentioned requirements.

Isolation layer

- Resistance against oil, water and minerals.
- Less susceptibility to weather conditions.
- Sufficient resistance against fatigue.

This layer has to protect the steel from corrosion and to make a flexible transfer of load from the wearing course to the steel deck

Adhesion layer

- Durability.
- Reliability.
- Simple in construction.
- Light weight.
- Economical.

Wearing course:

To ensure a safe and comfortable drive for the road users the requirements are:

- Good skid resistance.
- Even surface.
- Minimum sound levels.
- Minimum vibration.
- Surface run-off or drainage.

For durability of the wearing course the requirements are:

- Resistance against fast deterioration.
- Resistance against oil, water and minerals.
- Less susceptibly to weather conditions.
- High stability.
- Resistance against fatigue.
- Easy to repair.
- Possibility to spread the loads.

3.1.3.3 Materials used in practice for different surfacing layers

In practice the above mentioned requirements have led to the following materials to be used as surfacing layers:

Bonding layer

For this layer bitumen or artificial resin are in common use. Examples are:

- Tar epoxy
- Hot applied rubber bitumen sprayed with grit
- OKTO bonding

It has to be noted that the use of asphalt that contains tar is not allowed for new road structures in the Netherlands since January 2001.

Isolation layer

- Dense mastic layer with poured asphalt as a protective layer over it.
- Mastic coating layer with grit spread over it
 Advantages: high elasticity, good enclosure, good adhesion and sufficient stability to enable immediate transfer of traffic loading.

Adhesion layer

• Bitumen (hot fluid bitumen)

Advantages: immediately after application it is resistant against the influence of

weather and traffic can drive on it after only 10 minutes. Also this layer

needs not to be replaced in case of repairing the toplayers.

Disadvantage: the material tends to diminish the resistance for shearing forces in the

interface at high temperatures.

• Bitumen emulsion (cold fluid bitumen)

Disadvantage: possibility that moisture is trapped when evaporation is not completed

before laying the upper layers. This can lead to certain problems e.g.

formation of blisters.

Artificial resin

Advantage: the layer can serve as isolation layer and protects the steel plate against

corrosion.

Disadvantages: possibility that moisture is trapped when evaporation is not completed

before laying the upper layers. This can lead to certain problems. Also

the application of this adhesion layer requires special skills.

Wearing layer

The most applied materials for this layer are 'rolled or compacted' asphalt (e.g. asphalt concrete and hot rolled asphalt) and poured asphalt (e.g. mastic asphalt). Poured asphalt has some disadvantages compared to 'rolled' asphalt as it is more sensitive to rutting and gives some problems with skid resistance. The stability of the poured asphalt is often improved by the addition of Trinidad-Epurée. This is a natural bitumen and is obtained from an asphalt lake in the island of Trinidad. Furthermore, poured asphalt is more difficult to apply. On the other hand the bonding of the poured asphalt with the underlying layers is higher than that of rolled asphalt. Hence, cracks appear sooner with rolled asphalt. In some countries preference is made for compacted asphalt e.g. France and the USA and in others for poured asphalt e.g. the Netherlands and Germany. In this report is focussed on a type of poured asphalt, namely mastic asphalt.

3.2 Mastic asphalt

3.2.1 Characteristics of mastic asphalt

With regard to the degree of filling three types of asphalt can be distinguished:

Underfilled mixes

In this type of mixes the voids are not filled with mastic (bitumen + filler). The mineral aggregate forms a steady body. There is an open connection between the pores. An example is open asphalt concrete.

Filled mixes

The mineral aggregate forms a steady body, but the voids are nearly totally filled with mastic. There is a small amount of voids, but there is no open connection between them. Examples are dense asphalt concrete and stone mastic asphalt.

Overfilled mixes.

In this mixes there is a remainder of mastic, so the mineral aggregate doesn't form a steady body, but the aggregate is floating in the mastic. In this type of mixes the amount of voids is extremely small. An example is mastic asphalt.

The characteristics of mastic asphalt are:

- The voids are overfilled with mastic.
- Due to the overfilled voids and the absence of a steady body, the asphalt is not compacted.
- Because of the high percentage of fines, mastic asphalt has a poor skid resistance. To improve the skid resistance fine aggregate (grit) are scattered on the surface.
- The stability is not obtained from the mineral body but from a stiff type of bitumen (45/60, 20/30 or a mix from 45/60 and Trinidad-Épurée or modified bitumen) and a large percentage of filler.
- The large amount of mastic (thus the very low air content) render these types of mixes to be extremely impermeable.
- Due to this large mortar stiffness the production and processing take place at relative high temperatures (220-240°C).
- For the production of the mix a normal installation can be used with some special supplies.
- For construction the use of a special spreading machine is required, but because of the small areas normally laid, mastic asphalt is sometimes hand-laid by experienced 'asphalters'.
- Because of the high processing temperature isolated transport is commonly used (figure 3.3).



Figure 3.3: Isolated transport of mastic asphalt

- The thickness of the layers varies between 20 mm and 50 mm [VBW asfalt, 1996; Whiteoak 1990].
- Because of the special deformation properties, mastic asphalt can not be tested with the Marshall test like the other mixes.

3.2.2 Comparison composition mastic asphalt with other Dutch asphalt mixes

Mastic asphalt not only differs from other mixes in the degree of filling but also in composition. At first, the maximum grain size is compared in relation to the application. In table 3.1 the types of warm asphalt and their nominal maximum grain size are shown:

Table 3.1: Warm applied asphalt mixes in the Netherlands

Asphalt	Туре	Nominal maximum grain size [mm]	Application (tc = traffic class)	
GAB	0/16 type 1 16		Top layers tc 2	
	0/16 type 2	16	Top and bottom layers < 50 mm, tc 2 and 3	
	0/32	32	Bottom layers ≥ 50 mm, tc 2 and 3	
STAB	0/16	16	Bottom layers < 50 mm	
	0/22	22	Bottom layers ≥ 50 mm	
OAB	0/11	11	Fill layers 25-45 mm	
	0/16 type 2	16	Inter layers < 50 mm	
	0/16 type 3	16	Inter layers / temporary layers	
	0/22	22	Inter layers > 50 mm	
DAB	0/8	8	Top layers 25 mm, tc 2 and 3	
	0/11	11	Top layers 35 mm, tc 2 and 3	
	0/16	16	Top layers 40 mm, tc 3 and 4	
ZOAB	0/11	11	Top layers 40 mm	
	0/16	16	Top layers 50 mm	
SMA	0/6	6	Top layers 20 mm	
	0/8	8	Top layers 25 mm	
	0/11 type 1	11	Top layers 35 mm	
	0/11 type 2	11	Top layers 35 mm, tc 5	
Mastic Asphalt	-	8	Special applications*	

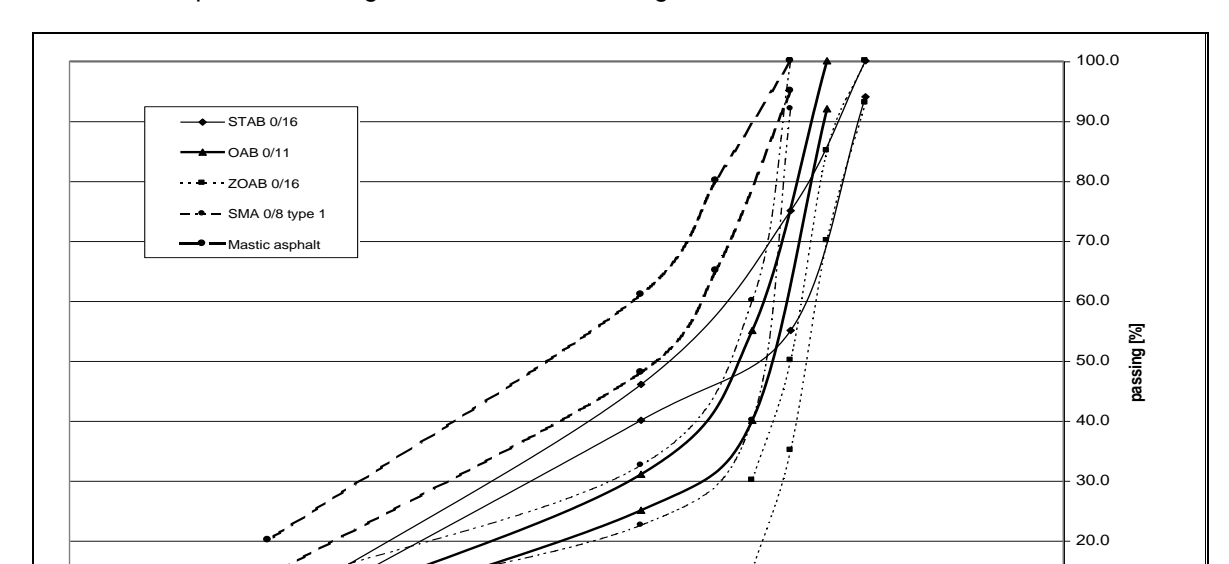
^{*} In the Netherlands mastic asphalt is used for surfacing steel bridge decks, parking decks and industrial floors.

In the Dutch Standaard RAW Bepalingen [CROW, 2000] a subdivision is made in traffic classes, based on the number of 100 kN equivalent axle loads (SAL_{100}) per day for the heaviest loaded lane (table 3.2).

Table 3.2: Traffic classes according to the Standaard RAW Bepalingen

Traffic class	SAL ₁₀₀	Explanation
2	< 500	Extensive loaded pavements
3	< 4000	Intensive loaded pavements
4	> 4000	Very intensive loaded pavements
5	> 500	Intensive loaded pavements with slowly driving and still heavy traffic,
		with a driving speed under 15 km/h.

Between the Dutch asphalt mixes there is not only a difference in maximum grain size, but also in the aggregate gradation.



The Dutch requirements for gradation are shown in figure 3.4.

Figure 3.4: Gradation requirements for different Dutch asphalt mixes

0.01



sieve [mm]

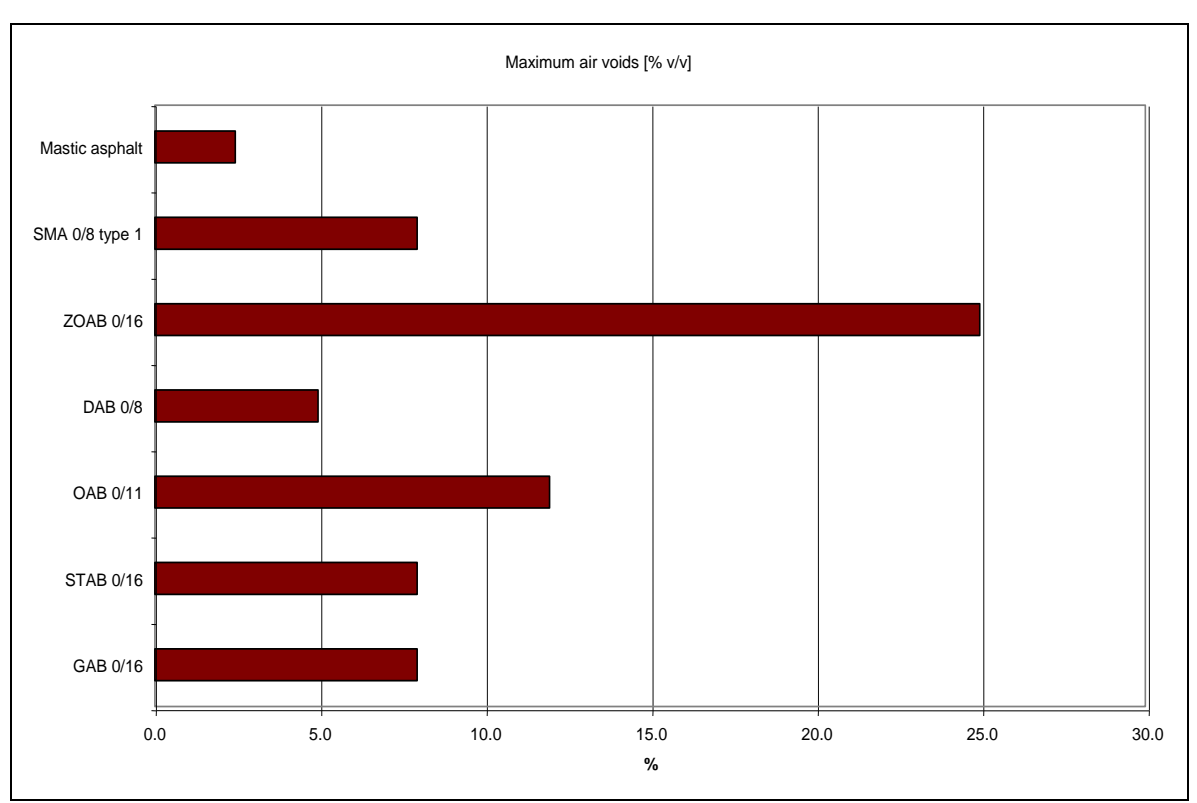


Figure 3.5: Maximum voids for some Dutch asphalt mixes

10.0

100

In figure 3.5 the values are valid for all traffic classes, except the value for DAB 0/8, which is valid for traffic class 2 and 3 (see also table 3.2).

For most of the Dutch asphalt mixes there is also a requirement for the minimum percentage of voids, by means of a maximum degree of filling. However, in the Dutch Standaard RAW Bepalingen [CROW, 2000] gives no maximum degree of filling for mastic asphalt.

The requirements for the percentage of bitumen for some mixes are shown in figure 3.6.

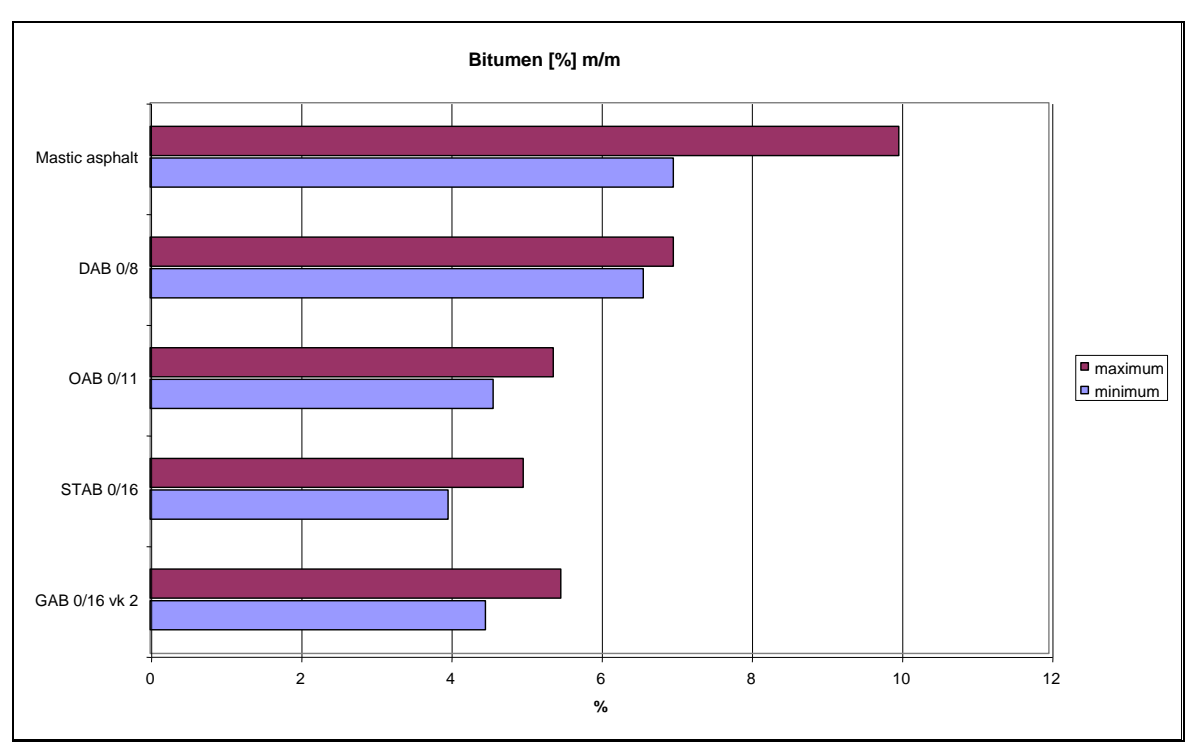


Figure 3.6: Requirements for the percentage bitumen for some mixes

In figure 3.6 the values are valid for all traffic classes, except the value for DAB 0/8, which is valid for traffic class 2 and 3 as well as the value for GAB 0/16, which is valid for traffic class 2. Because mastic asphalt is an overfilled mixture there is a small percentage of air voids and a high percentage of bitumen compared to the other mixes. This difference in composition makes mastic asphalt very suitable for special applications, like surfacing orthotropic steel decks.

3.2.3 The reason that mastic asphalt is often used on orthotropic steel bridges

On an orthotropic steel bridge the longitudinal stiffeners can be considered as stiff points in the structure were only small deformations take place. The largest deformations take place between these stiffeners. These deformations of the steel deck and the asphalt on orthotropic steel bridges are larger than the deformations of a normal pavement on a basecoarse and subgrade. Due to this large deformations a flexible type of asphalt is needed for deck surfacing. Mastic asphalt fulfils this requirement because of its high percentage of mastic (bitumen and filler) and is therefore often used on orthotropic steel bridges.

3.2.4 History of mastic asphalt in the Netherlands

In the Netherlands mastic asphalt was already used before 1940 in floor-, gutter- and tramrail structures [Hardenberg et al., 1985]. In this type of structures mastic asphalt was used because of its durability. Later it was also used on orthotropic steel bridges. Mastic asphalt could resist the

large deformations of the steel deck without fatigue cracking, because of the flexibility of the mix. The composition of the mix was based on experience. Unfortunately, this experience with mastic asphalt wasn't documented.

After 1970 the problems arose very fast, because of a combination of factors:

- The increase of traffic intensity.
- The increase of axle-loads.
- Absence of strong specifications.
- The experience with mastic asphalt disappeared because of retirement of skilled people.
- Changes in production, transport and processing led to a decreasing hardness of the binder, resulting in a mix with a lower stiffness.

So after 1970 the need for other asphalt structures on steel bridges arose. Alternatives, like hotrolled asphalt and modified bitumen mixes were considered. One of the findings is that the deformation of the mastic asphalt was mainly defined by the properties of the binder. This knowledge resulted in the application of another type of bitumen that was less sensible to deformation.

In the Netherlands in 1985 the structure normally consisted of the following parts:

•	Primer layer of thinned bitumen 20/30 on the steel deck	50 μm
•	Bonding layer of rubber-modified bitumen	0.8 kg/m ²
•	Mastic layer based on blown bitumen	6-8 mm
•	Base layer of poured asphalt	20 mm
•	Top layer of poured asphalt modified with Trinidad-Épurée bitumen	22 mm

Chippings, hot rolled

3.2.5 Requirements for mastic asphalt in some countries

Requirements for mastic asphalt differ from one country to the other. The requirements were set according to the experience of individual countries.

3.2.5.1 The Netherlands

In the Netherlands mastic asphalt is used for surfacing steel bridge decks, parking decks and industrial floors. Because of its sensibility to deformations and the high costs it is not used for roads anymore.

In the Netherlands the composition of the mix has to fulfil the requirements shown in table 3.3 [CROW, 2000].

Table 3.3: Requirements	for mastic asphalt	according to the RAW

	Mastic asphalt			
Passing [%]	Desired	min.	max.	
C8	-	95,0	100,0	
C4	75,0	65,0	80,0	
2 mm	56,0	48,0	61,0	
63 μm	17,0	14,0	20,0	
Bitumen percentage	8,5	7,0	10,0	
(on 100 % mineral aggregate)				

The maximum aggregate size is 8 mm. The mix consists of broken stones 2/8, sand type A, filler and bitumen 40/60. Sand type A has aggregates between 2 mm and $63 \mu m$.

The maximum void ratio is 2.5%.

The requirements for penetration and deformation are:

- Penetration 10-40 (*0.1 mm) with the stempel test (300 sec, 5.25 N/mm², 100 mm², 25°C).
- Deformation of 6-10% after 100.000 load repetitions in the wheel track test [NPC, 1996].

The requirements from the Dutch Ministry of Transport, Public Works and Water Management (Rijkswaterstaat) for mastic asphalt on steel bridges are shown in table 3.4 [Kolstein, 1990].

Table 3.4: Requirements from the Dutch Ministry of Transport, Public Works and Water Management for mastic asphalt on steel bridges

	Coarse ma	nstic asphalt	Fine mastic	Tolerance
Passing [%]	Toplayer average Firstlayer average		asphalt average	
C 8	43	-	-	+5
C 5.6	-	38	-	+5
2 mm	40	39	58	+5
0.063 mm	17	23	42	+2
Bitumen (% by mass o	n 100% mineral aggr	egate)		
45/60 + Trinidad	9			+0.5
Épuré				
45/60		9.5		+0.5
85/40			19	+0.5

However some qualitative requirements were specified by NPC in 1996 after an extensive testing program in order to select materials for the Ewijk bridge:

- High resistance against cracking/fatigue (flexural bending test).
- High fracture strength (semi circular bending Test).
- High resistance against permanent deformation (triaxial test, DIN test, wheel track test).
- The top layer must have elastic properties (tough, rubber behaviour) to prevent cracking above the steel longitudinal stiffeners.
- The sub layer must have a high stiffness to prevent permanent deformation and to contribute to the strength of the total structure.

3.2.5.2 Germany

In Germany mastic asphalt is still used for roads, even motorways, because of its durability. It is often used for roads with heavy loads. Therefore they use a mix with over 40% of stone.

In Germany there are 4 main types of mastic asphalt, varying in the maximum grain size (table 3.5):

Table 3.5: Requirements for mastic asphalt in Germany

Mastic asphalt		0/5	0/8	0/11	0/11S
-		(0/5 mm)	(0/8 mm)	(0/11 mm)	(0/11 mm)
Aggregate > 2 mm	% m/m	35-40	40-50	45-55	45-55
Aggregate < 0.09 mm	% m/m	24-34	22-32	20-30	20-30
Bitumen percentage	% m/m	7.0-8.5	6.8-8.0	6.5-8.0	6.5-8.0
Type of bitumen			(B 65) B45		B45 (B25)

Often a bitumen type B65 is used in Germany with a penetration (at 25°C) of 50-70 (0.1 mm).

The requirements for the penetration (40±1°C, 500 mm²) of the four mixes are given in table 3.6:

Table 3.6: Penetration for mastic asphalt (40±1°C, 500 mm²)

Mastic asphalt	Penetration after 30 min [mm]	Penetration in the next 30 min [mm]
0/11 S	1.0 – 3.5	≤ 0.4
0/11	1.0 – 5.0	≤ 0.6
0/8	1.0 – 5.0	≤ 0.6
0/5	1.0 - 5.0	≤ 0.6

The requirements for cracking are:

- In tension no cracking with a force of 400 N in longitudinal and transverse direction (tension test)
- In bending no cracking at ≥3 % strain

In Germany there are also requirements for the bonding layer between the steel and the mastic asphalt:

Ball penetration ≤6 mm at 25°C
 ≤8.5 mm at 40°C

Temperature ring and ball ≥70°C

• After 1 million load repetitions the bonding between the different layers must be still intact (bending test).

This gives an indication of what type of requirements are used in Germany. For the exact test specifications the interested reader is referred to "Technischen Prüfvorschriften für die Prüfung der Dichtungsschichten und der Abdichtungssysteme für Brückenbeläge auf Stahl", edition 1992 (TP-BEL-ST).

3.2.5.3 USA

Table 3.7 shows the requirements for the aggregate gradation in the United States.

Table 3.7: Gradation for mastic asphalt mixes in the USA

Sieve size [mm]	Percent passing	
12.5	95-100	
9.5	80-95	
4.75	58-75	
2.36	43-60	
0.60	20-35	
0.075	7-14	

Some other requirements are:

Minimum density
 Maximum percentage air voids
 3.0 %

Ultimate load value
 As large as possible at ambient laboratory temperature

Expansion coefficient As close to that of steel as possible at ambient

laboratory temperature

Creep percentage at 30 minutes
 Not more than 5 percent at both tension and

compression at ambient laboratory temperature

• Fatigue resistance No cracking, de-bonding or any other form of fatigue

degradation during 8.000.000 cycles under full simulated

wheel load

Also requirements are given for the shear strength between the steel and the asphalt. The bond strength of the surfacing to the corrosion protection layer should be as large as possible, but not less than:

- 2.75 MPa at ambient laboratory temperature.
- 2.75 MPa at 0°C.
- 1.75 MPa at 60°C.

A few general qualitative requirements are:

- High fatigue resistance.
- High bond strength for the bonding layer.
- Skid resistance and resistance against aggregate polishing.
- Sufficient resistance to shoving and rutting under temperature extremes.
- Thickness of surfacing sufficient to provide wheel load distribution and mass for damping of vibrations from wheel loads.

3.2.5.4 England

In England the use of mastic asphalt is limited to special applications, for example heavy loaded roads and to provide a waterproof membrane. Table 3.8 shows the mix gradation in England.

Table 3.8: Gradation for mastic asphalt in England

	Mastic asphalt	
Coarse aggregate	% m/m	30.0
Fine aggregate	% m/m	26.0
Filler	% m/m	32.0
Bitumen	% m/m	12.0
Void content	% v/v	<1.0

Bitumen with a pen of 15-25 (0.1 mm) are used.

3.2.6 Comparison between the composition of mastic asphalt in some countries

At first the gradation for mastic asphalt mixes in some countries is shown in figure 3.7. For Germany type 0/11 is taken for the comparison.

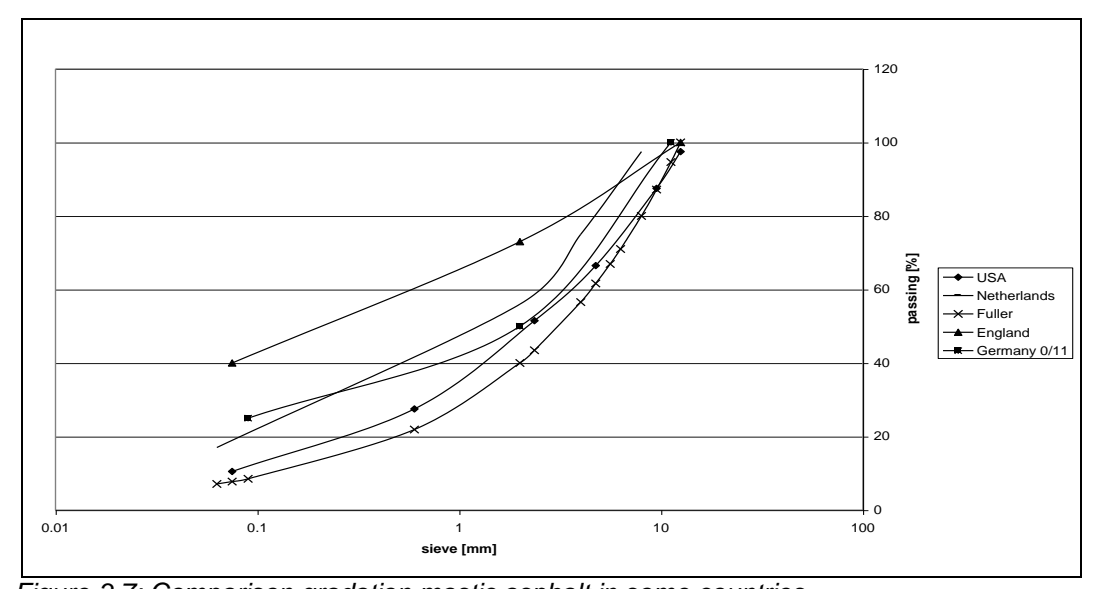


Figure 3.7: Comparison gradation mastic asphalt in some countries

There is not only a difference in composition, but also in maximum grain size, which has an influence on the minimum thickness of the asphalt layer. This maximum grain size for mastic asphalt mixes in some countries is shown in figure 3.8:

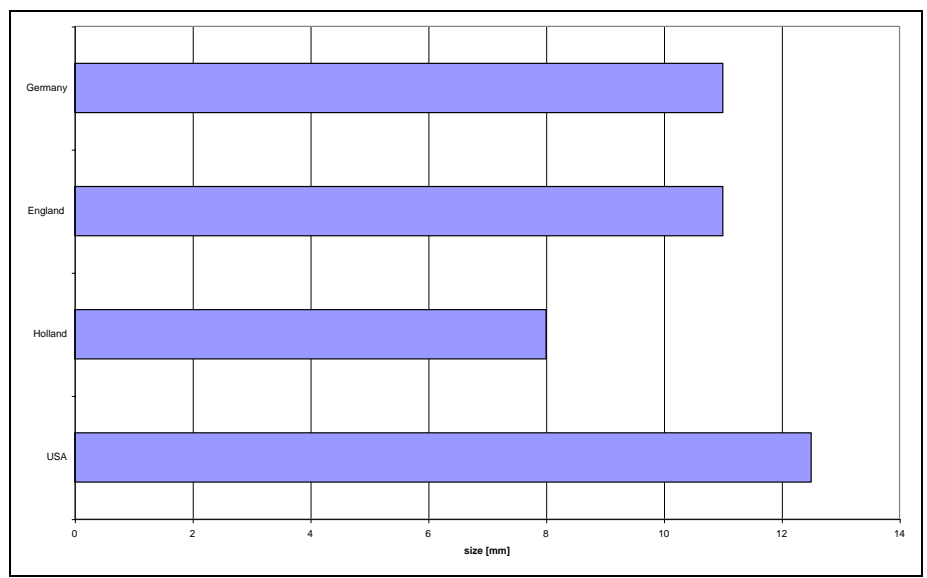


Figure 3.8: Maximum grain size in some countries

In the past a larger maximum grain size was used in mastic asphalt mixes in Holland. However, with larger grain sizes the problem of segregation arose, especially because of the fact that mastic asphalt is not compacted. Segregation is caused by settlement of large grains at the bottom of the asphalt layer (due to gravity) leading to a non-homogeneous mix. To solve this segregation problem it was chosen to divide the mastic asphalt structure in two layers of mastic asphalt and from that moment the mastic asphalt is applied in two layers. The smaller thickness of each layer results in smaller grain sizes to be applied, so from that moment the maximum grain size decreased to 8 mm. The application of smaller maximum grain sizes makes the structure more sensible to rutting. Therefore modifiers are added to the bitumen to make the mix less sensible to rutting.

The maximum voids content for mastic asphalt mixes in some countries is shown in figure 3.9:

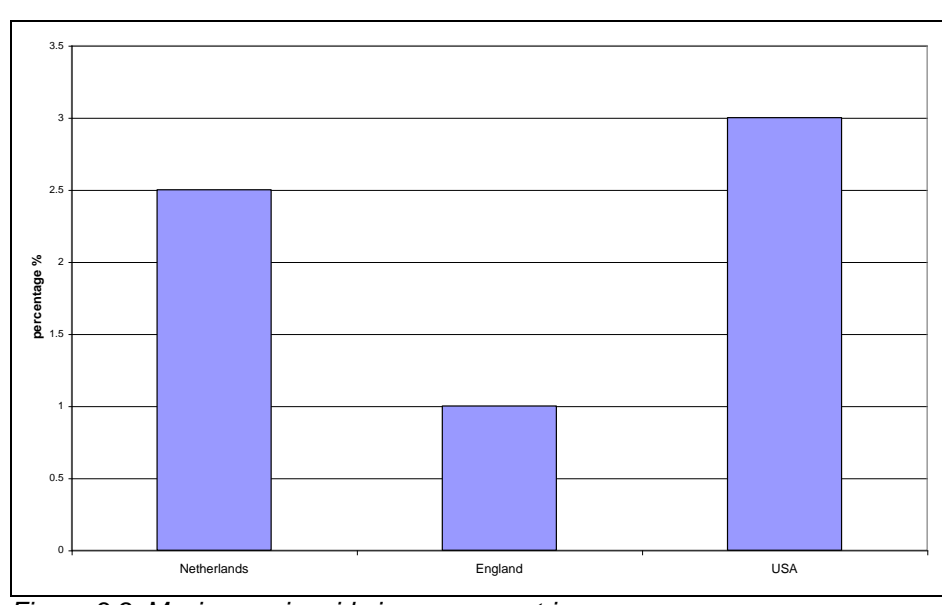


Figure 3.9: Maximum air voids in some countries

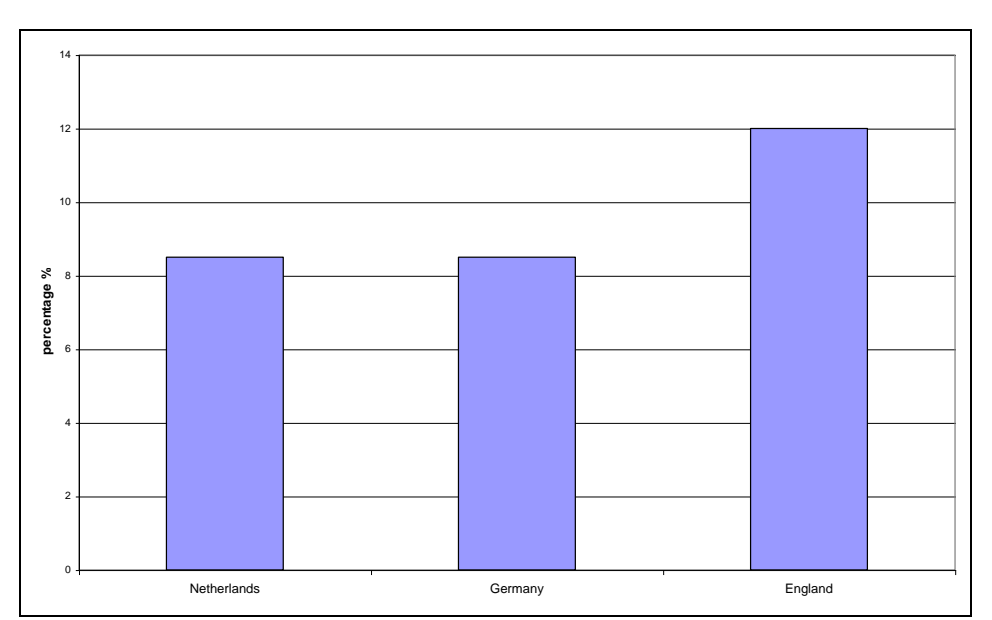


Figure 3.10 shows the maximum percentage of bitumen in mastic asphalt mixes in some countries.

Figure 3.10: Maximum bitumen percentage in some countries

The difference in composition and requirements has led to different cross sections in the different countries.

3.2.7 Typical cross-sections in various countries

The differences in mix composition and requirements have led to different cross-sections of orthotropic steel bridges in some countries. The following figures 3.11-3.17 represent typical cross-sections of orthotropic steel bridges in various countries.

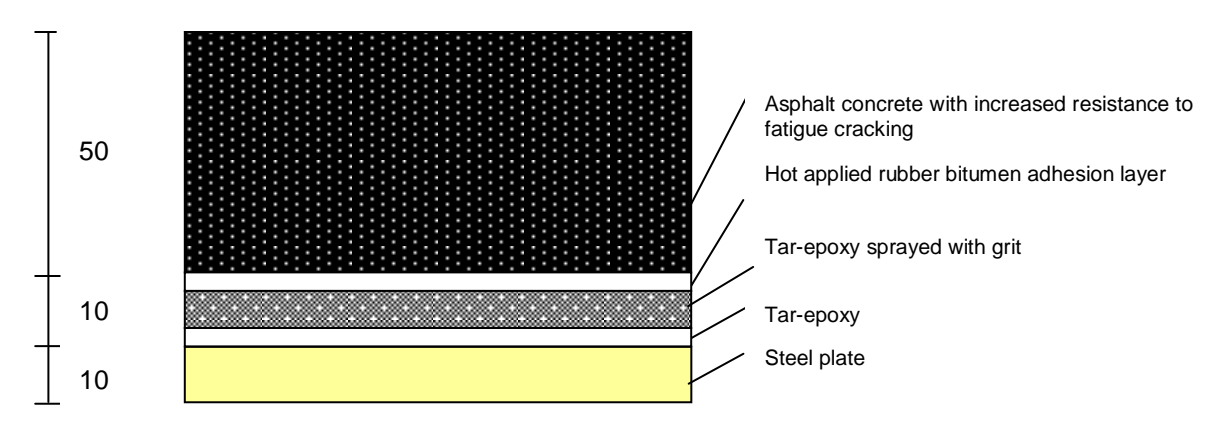


Figure 3.11: Typical cross-section as used in the Netherlands

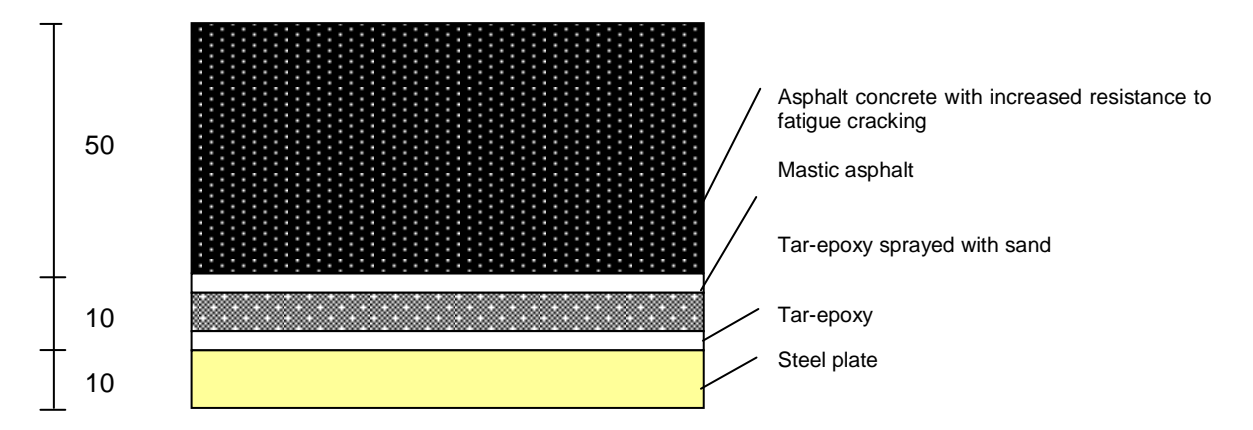


Figure 3.12: Typical cross-section as used in the Netherlands

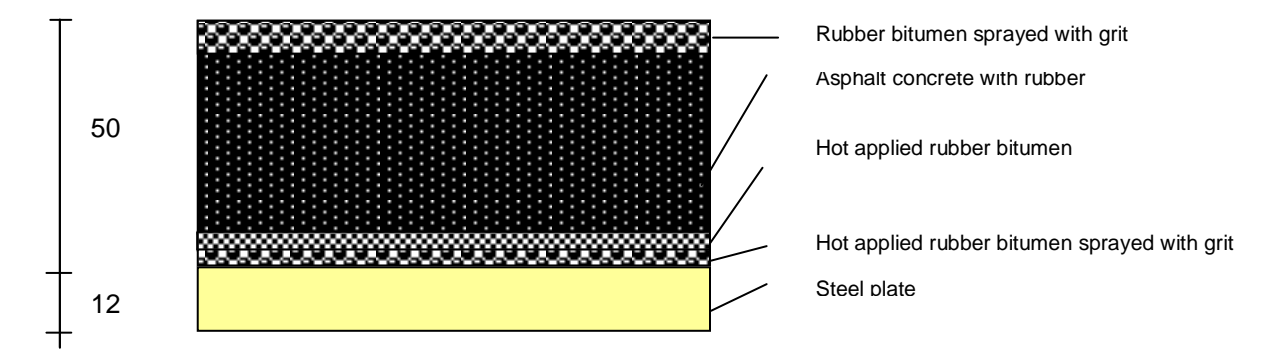


Figure 3.13: Typical cross-section as used the 'Pont de Cornouaille' in France

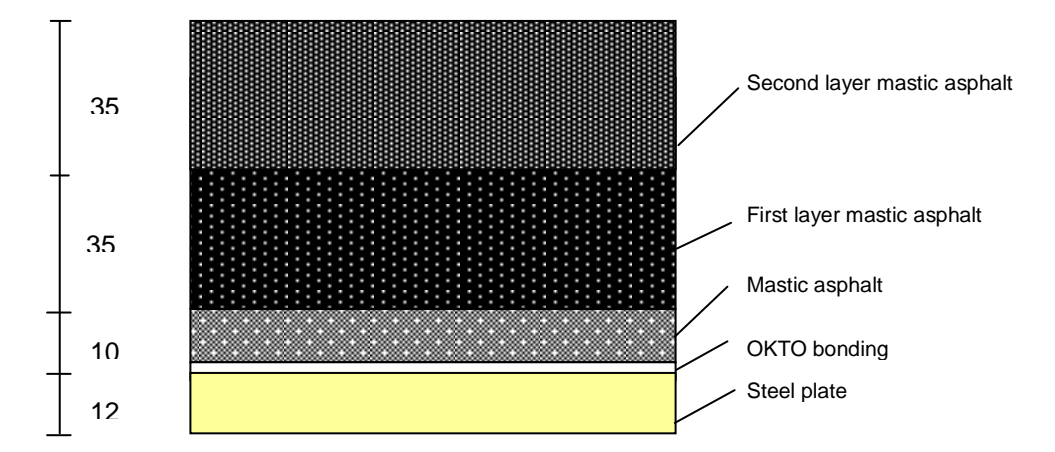


Figure 3.14: Traditional cross-section as used in Germany

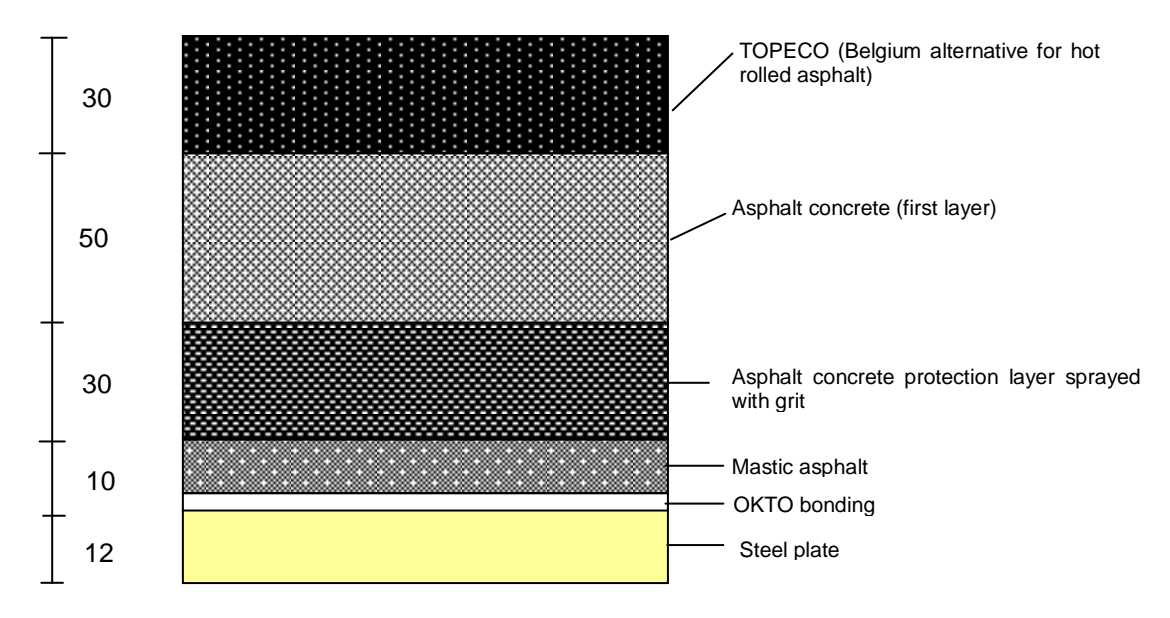


Figure 3.15: Typical cross-section as used in Belgium

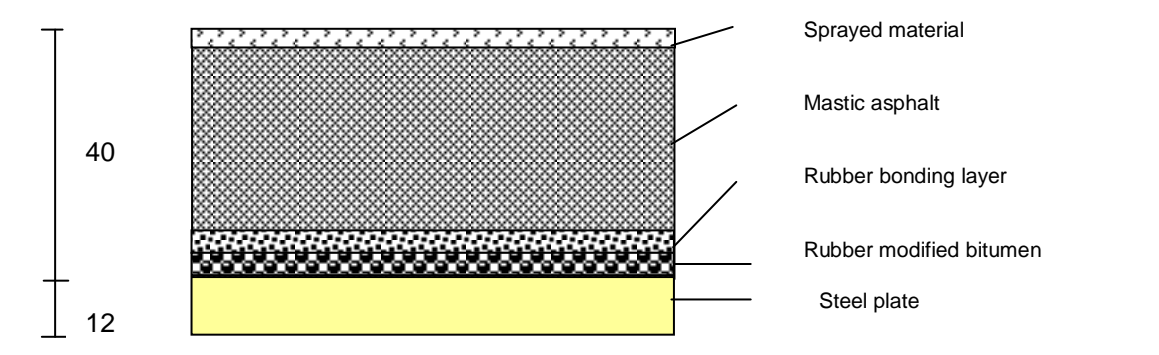


Figure 3.16: Typical cross-section as used in England

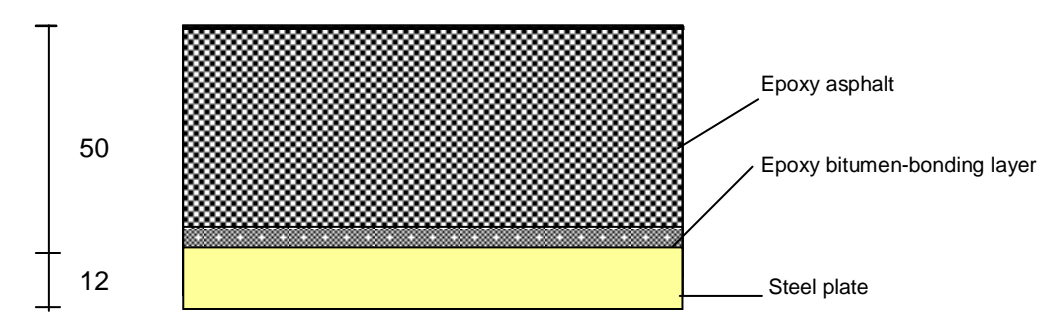


Figure 3.17: Typical cross-section as used in the USA

Note: dimensions are in mm

In Germany sometimes a steel grid is welded on the steel deck plate in order to get a better bond between the steel and the asphalt [Volker 1993].

3.3 Stress reduction in steel deck due to asphalt surfacing

3.3.1 Introduction

It is known that surfacings of a steel orthotropic deck reduce the stresses in the steel structure. Firstly this reduction is a result of the fact that the thickness of the asphalt spreads the loads. The load spreading property of asphalt varies because of its visco-elastic, temperature dependent and ageing behaviour and is therefore often neglected. In the Eurocode 3 [1997] the load spreading through the pavement and the deck is taken at a spread/depth ratio of 1 to 1. De Jong [2000] has shown that the spread/depth ratio is \approx 1:1, but the load spreading starts at approximately the middle section of the asphalt. It seems that the Euro Code assumption overestimates the load spreading.

Secondly the composite action in bending of the asphalt layer with the steel deck causes reduction of stresses. This means that by applying a surface on the steel deck the moment of inertia of the structure increases, resulting in smaller deformations and thus less stresses. The total reduction of stresses due to composite action depends mainly on the bond between the asphalt and the steel deck and the stiffness of the asphalt. When there is no bond between steel and the asphalt, the two layers are effectively separated. When there is complete bond between the two layers, this means that the two layers can be combined as a composite section. Hence resulting in less stresses in the two layers, since the height is of the third order in the equation for the moment of inertia ($I_{zz} = f(h^3)$). However, the two situations mentioned (complete and bond and complete separation) are extreme situations. In practice, the real bond between the two layers is normally intermediate between the two extreme situations and is quite difficult to be determined.

3.3.2 Composite action theories

In this section the different theories for composite action are presented. They are used to calculate the stresses and strains that occur in the mastic asphalt due to bending moment produced by loading. All researchers based their work on linear elastic theory. Furthermore, they have adopted one or both of the following assumptions [Medani 2000a]:

- 1. Linear strain distribution in the asphalt and the steel.
- 2. The slopes of the strain distribution through the depth of the asphalt and steel are equal.

3.3.2.1 Metcalf [1967]

Metcalfs analysis is based on beam theory, in which the beam consists of an asphalt layer and a steel layer. He assumes that the bond between the two layers is 100%, what means no slip and a linear strain distribution throughout the full height of the composite beam.

For determining the asphalt strains Metcalf uses the following relations:

$$t_0 = t_2 \frac{a^2 + n(1+2a)}{2a(a+n)}$$
 Equation 3.1

 t_0 = distance from the neutral axis to the top of the asphalt t_l = thickness of the steel plate t_2 = thickness of the asphalt layer $a = t_2/t_1$ E_1 = elastic modulus of the steel plate E_2 = elastic modulus of the asphalt $n = E_1/E_2$

$$I_o = \frac{bt_2^3}{3} \left[1 + n \frac{1 + 3a + 3a^2}{a^3} \right] - bt_2(\frac{n}{a} + 1)t_0^2$$
 Equation 3.2

 I_0 = moment of inertia b = width of the beam

$$\mathcal{E}_{t} = \frac{Mt_{0}}{E_{2}I_{0}}$$
 Equation 3.3

 ε_t = tensile strain at the top of the asphalt layer M = bending moment

The most important conclusions of his theoretical analysis are:

- An increasing modular ratio E_s/E_a means an increasing deflection at the centre of the beam.
- An increasing modular ratio E_s/E_a means increasing strains in the asphalt layer.
- A greater part of the applied load is carried by the steel plate as the pavement modulus is decreased.

3.3.2.2 Kolstein [1990]

Kolstein considers two extreme situations in his analysis of composite action, namely full adhesion and no adhesion between the steel deck and the asphalt. He also assumes a linear strain distribution in both the steel and the asphalt. Kolstein uses the following relations:

Complete adhesion (100%):

$$z = \frac{nt^2 + h^2 + 2ht}{2nt + 2h}$$
 Equation 3.4

$$\varepsilon_{t} = \frac{M(h+t-z)}{SI}$$
 Equation 3.5

No adhesion (0%):

$$\varepsilon_{t} = \frac{Mh}{2(SI_{1} + EI_{2})}$$
 Equation 3.6

in which:

z = distance from the neutral axis to the bottom of the steel deck

E = elastic modulus of the steel

S = elastic modulus of the asphalt

n = E/S

h = thickness of the asphalt layer

t = thickness of the steel plate

I = moment of inertia of the composite section

 I_1 = moment of inertia of the asphalt section

 I_2 = moment of inertia of the steel section

M = bending moment of the composite section

 ε_t = strain at the top of the asphalt layer

One of his conclusions from his theoretical analysis is that the strain at the top of the asphalt is a function of the asphalt stiffness as shown in figure 3.18:

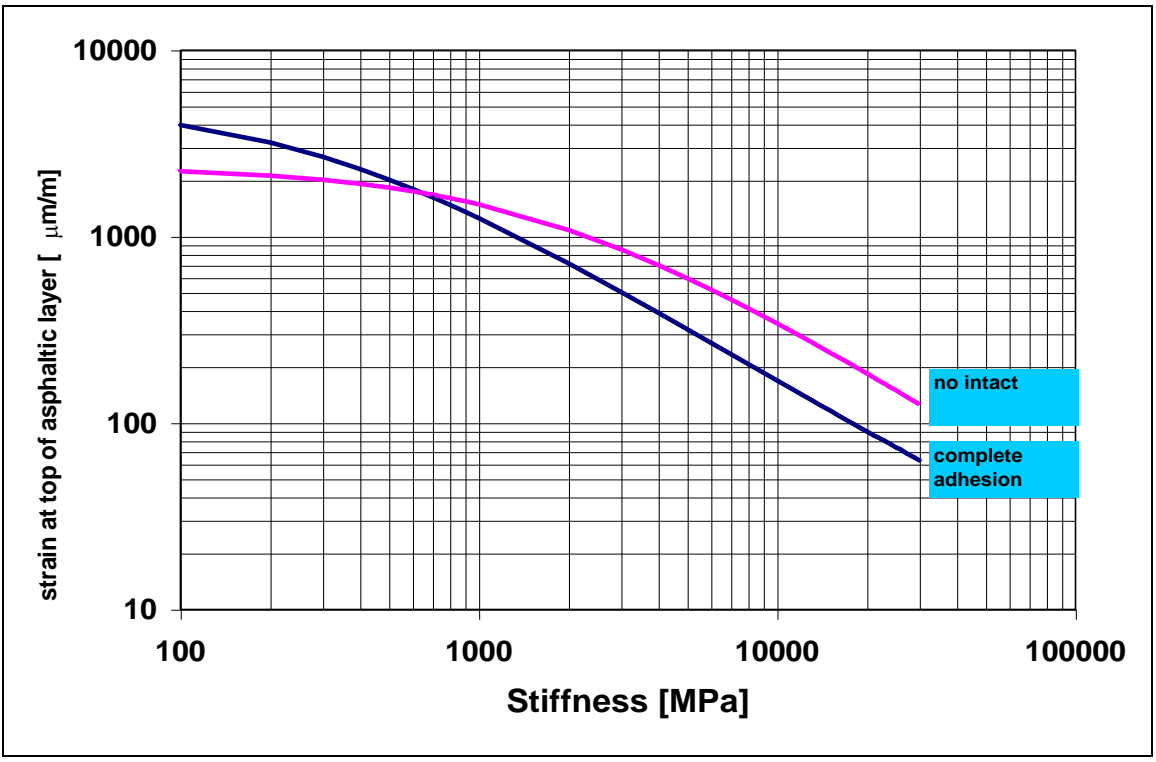


Figure 3.18: Strain at the top of the asphalt layer as a function of the asphalt stiffness

His analysis clearly shows that in case of a large asphalt stiffness and no adhesion the asphalt strains are higher compared to full adhesion, which indicates the importance of the bonding layer between the steel plate and the asphalt. However, when the asphalt stiffness is low and the maximum strain at complete adhesion is considered, the maximum strain reaches the value of $4000~\mu\epsilon$.

3.3.2.3 Cullimore et al. [1983]

Cullimore et al. carried out a theoretical research using stress functions. Throughout the height a linear strain distribution is assumed. The results were compared with the experimental results and showed a quite good agreement.

The theory of Cullimore is based on a two-layer cantilever with an elastic interface. The model in this case is shown in figure 3.19:

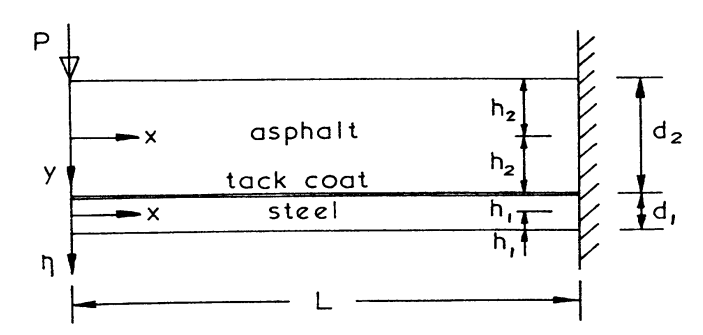


Figure 3.19: Two-layer cantilever with elastic interface in Cullimore's theory

The following relation is used for determining the asphalt strain:

$$\mathcal{E}_{t} = \frac{\alpha}{E} xy + \frac{\gamma}{E} x$$
 Equation 3.7

in which:

$$\alpha = \frac{A_3 B_2 - B_3 A_2}{A_1 B_2 - A_2 B_1}$$
 Equation 3.8

$$\gamma = \frac{1}{Dh_2} (\alpha I_2 + aI_1 + P)$$
 Equation 3.9

and:

$$a = \frac{B_3 A_1 - A_3 B_1}{A_1 B_2 - A_2 B_1}$$
 Equation 3.10

$$A_{1} = -\mu I_{2}(2+3v_{a}) + I_{2}(2+3v_{s}) + \frac{\mu D h_{2}^{2}}{2}(2+v_{a}) + \frac{\mu D L^{2}}{2}$$
 Equation 3.11

$$A_2 = -\mu I_1(2+3\nu_a) + I_1(2+3\nu_s) - \frac{Dh_1^2}{2}(2+\nu_s) - \frac{DL^2}{2}$$
 Equation 3.12

$$A_3 = P[\mu(2+3\nu_a) - (2+3\nu_s)]$$
 Equation 3.13

$$B_{1} = \frac{2E_{s}I_{1}}{k_{i}} + (2 + v_{a})\frac{\mu h_{2}}{2}(\frac{h_{2}^{2}D}{2} + I_{2}) + \frac{L^{2}}{2}(\mu h_{2}D + \frac{\mu I_{2}}{h_{2}} + \frac{I_{1}}{h_{1}}) + (2 + v_{s})\frac{h_{1}}{2}I_{2} \qquad \textit{Equation 3.14}$$

$$B_2 = \frac{2E_sI_1}{k_i} + (2 + v_a)\frac{\mu h_2}{2}I_2 + \frac{L^2}{2}(\frac{\mu I_1}{h_2} + h_1D + \frac{I_1}{h_1}) + (2 + v_s)\frac{h_1}{2}(\frac{h_1^2D}{3} + I_1)$$
 Equation 3.15

$$B_{3} = -P \left[\frac{2E_{s}}{k_{i}} + (2 + v_{a}) \frac{\mu h_{2}}{2} + \frac{L^{2}}{2} (\frac{\mu}{h_{2}} + \frac{1}{h_{1}}) + (2 + v_{s}) \frac{h_{1}}{2} \right]$$
 Equation 3.16

in which:

 ε_t = tensile strain at the top of the asphalt layer

E = elastic modulus of the asphalt layer

 E_s = elastic modulus of the steel

 $\mu = E_s/E = modular ratio$

 k_l =shear stiffness of the interface

 I_1 =moment of inertia of the steel

 I_2 = moment of inertia of the asphalt

x,y = co-ordinates of the point to be considered

 h_1 = half of the height of the steel plate

 h_2 = half of the height of the asphalt layer

 $D = 2(h_1 + h_2)$

 v_a = Poisson's ratio for asphalt

 v_s = Poisson's ratio for steel

L = length of the beam

The theory shows the influence of the stiffness of the bonding layer on the asphalt strains. Cullimore considered a few numerical values to be representative for practical purposes. For the stiffness of the bonding layer he assumed $k_i = 4*10^8$ Pa. However, his assumption for the load (P=1N) which is not comparable to a wheel load.

Two important conclusions of his experimental research are:

- The effect of increasing the stiffness of the bonding layer is insignificant in reducing the maximum tensile stress in the asphalt at temperatures of 35°C.
- At temperatures below the 35°C the strains in the asphalt increased with decreasing stiffness
 of the bonding layer.

3.3.2.4 Nakanishi et al. [2000]

Nakanishi et al. simulates the orthotropic steel bridge using a two-span continuous beam model. The beam model consists of three layers: a steel plate deck, a binder course and a surface course as shown in figure 3.20.

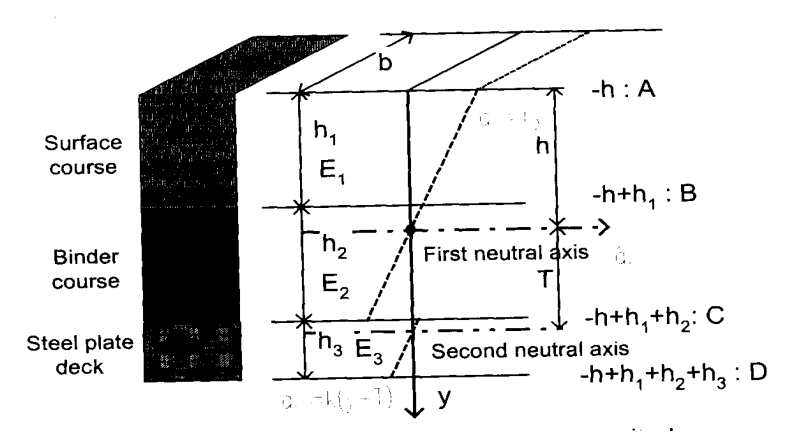


Figure 3.20: Beam considered by Nakanishi

Three assumptions are made:

- Linear strain distribution in both the steel and the asphalt.
- The slopes of the two strain distributions in the steel and the asphalt are the same.
- The binder and the surface coarse are completely bonded.

In the relations from the theoretical analysis the bond between the steel plate and the binder course can be varied. The relations that were determined are:

$$h_0 = \frac{h_1}{2} \left(\frac{1 + 2\alpha\gamma + \alpha\gamma^2}{1 + \alpha\gamma} \right)$$
 Equation 3.17

When the steel and the asphalt are not bonded there are two neutral axes. In that case h_0 is defined as the distance between the neutral axis of the surface and base layer to the top of the asphalt.

The parameters are defined as:

 E_1 = elastic modulus of the surface coarse

 E_2 = elastic modulus of the binder coarse

 E_3 = elastic modulus of the steel plate

 h_1 = thickness of the surface coarse

 h_2 = thickness of the binder coarse

 h_3 = thickness of the steel plate

 $\alpha = E_2/E_1$

 $\gamma = h_2/h_1$

The distance between both neutral axes is dependent on the bond between the steel and the asphalt and can be determined with:

$$T = (1-t)\left\{h_1 + h_2 - h_0 + \frac{h_3}{2}\right\}$$
 Equation 3.18

T = distance between both neutral axes

t = coefficient of bond between the binder course and the steel plate. t=0 is no bonding, t= 1 means complete bondage

The distance from the upper neutral axis to the surface of the asphalt can be determined with:

$$h = \frac{h_1}{2} \left\{ \frac{1 + 2\alpha\gamma + \alpha\gamma^2 + 2\beta\omega + 2\beta\gamma\omega + \beta\omega^2 - 2\beta\omega T / h_1}{1 + \alpha\gamma + \beta\omega} \right\}$$
 Equation 3.19

h = position of the neutral axis in case of a varying coefficient of bond

 $\beta = E_3/E_1$

 $\omega = h_3/h_1$

The formula for h_0 can be seen as a special case of h, namely $h_0 = h(t=0)$. A factor equivalent to the moment of inertia is determined with:

$$J = \frac{b}{3} \{ (B^3 - A^3) + \alpha (C^3 - B^3) + \beta (D^3 - C^3) - 3\beta T (D^2 - C^2) + 3\beta T^2 (D - C) \}$$
 Equation 3.20

J = parameter equivalent to the moment of inertia

A = -h

 $B = -h + h_1$

 $C = -h + h_1 + h_2$

 $D = -h + h_1 + h_2 + h_3$

The strains at the top of the asphalt layer are determined with:

$$\mathcal{E}_{t} = \frac{M}{E_{1}J}A$$
 Equation 3.21

 ε_t = tensile strain at the top of the asphalt layer M = bending moment of the composite section

The main results of the theoretical analysis are:

- Strains at the pavement surface are decreasing when the complex modulus of the asphalt mix increases.
- The surface strain increases when the coefficient of bondage decreases.
- When the coefficient of bond decreases, the shear stress at that bond decreases, but the shear stress increases at other points.
- Not only the strain at failure at low temperatures but also the complex modulus of elasticity of the mixture should be used in design codes.

3.3.2.5 Sedlacek and Bild [1985]

In the German requirements the bearing capacity of the asphalt is not taken into account by assuming that the asphalt stiffness is zero ($E_{asf}=0$). This means that the asphalt takes no stresses. The strains in the asphalt can be calculated by extrapolation of the strains in the deck plate:

$$\mathcal{E}_a = \frac{M}{EI_1} z$$
 Equation 3.22

M = bending moment

 EI_1 = bending stiffness of the steel deck

z = distance between half of the steel deck and the top of the asphalt layer

The bending moment M is calculated with a computer program, using the plate theory. This method should be allowed for dimensioning the steel structure, because of the low asphalt stiffness at high temperatures.

For calculating the asphalt stresses and strains the method mentioned before is not useful, because of their dependency on the modulus of elasticity of the asphalt. Therefore Sedlacek and Bild developed a composite action beam model for the steel plate and the asphalt. The model consists of a beam with a width of 1 cm taken from the steel-asphalt structure and is shown in figure 3.21.

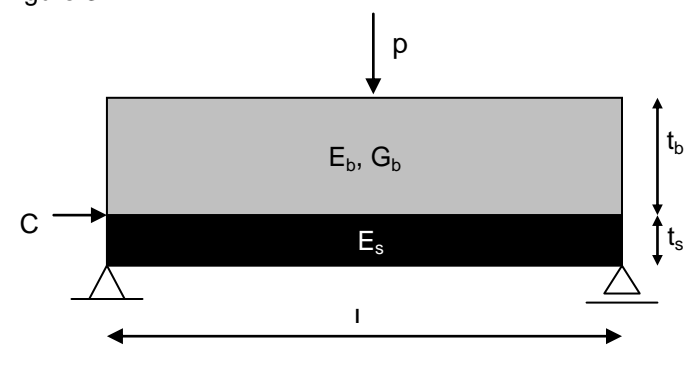


Figure 3.21: Model used by Sedlacek and Bild

 t_b = thickness of the asphalt layer [m]

 t_s = thickness of the steel deck plate [m]

 E_b = Elastic modulus of the asphalt [Pa]

 G_b = Shear stiffness of the asphalt [Pa]

 E_s = Elastic modulus of the steel deck plate [Pa]

C = Elastic modulus of the bonding layer between the asphalt and the steel [Pa]

P = load

L = length of the beam

On the beam a load p is assumed to act at the mid-span. Between the asphalt and the steel there is an elastic bonding layer. Also the shear stiffness of the asphalt layer is taken into account.

The asphalt strains in the model are the sum of three factors:

- Strains due to the bending moment in a fully bonded state.
- Strains due to the deformation of the bonding layer depending on the stiffness of the bonding layer.
- Strains due to the shear deformation of the asphalt depending on the shear stiffness of the asphalt.

Strains due to the bending moment

The strains in the model due to the bending moment are calculated using the method described by Sedlacek [1982].

The next formulas are used:

$$\tau = \frac{t_b}{t_s}$$
 Equation 3.23

$$\varepsilon = \frac{E_b}{E_c}$$
 Equation 3.24

$$k_{1z} = \frac{1}{2}t_s \frac{(1+\tau)\tau\varepsilon}{1+\tau\varepsilon}$$
 Equation 3.25

 k_{1z} = distance between the half of the steel deck plate and the neutral axis [m]

$$A_{zz} = \frac{1}{12} t_s^3 \frac{1 + 4\tau\varepsilon \left(1 + \frac{3}{2}\tau + \tau^2\right) + \tau^4 \varepsilon^2}{1 + \tau\varepsilon}$$
 Equation 3.26

 A_{zz} = factor equivalent to the moment of inertia of the composite beam with width =1 [m^4]

$$z_0 = -\frac{1}{2}t_s \frac{1 + \tau(2 + \tau\varepsilon)}{1 + \tau\varepsilon}$$
 Equation 3.27

 z_0 = distance between the neutral axis and the top of the asphalt layer [m]

$$z_f = -\frac{1}{2}t_s \frac{1 - \tau^2 \varepsilon}{1 + \tau \varepsilon}$$
 Equation 3.28

 z_f = distance between the neutral axis and the bonding layer [m]

$$z_{u} = \frac{1}{2}t_{s} \frac{1 + (2 + \tau)\tau\varepsilon}{1 + \tau\varepsilon}$$
 Equation 3.29

 z_u = distance between the neutral axis and the bottom of the steel deck plate [m]

The strains at the top of the asphalt layer due to the bending moment are calculated using:

$$\mathcal{E}_{a} = \frac{M}{E_{s}A_{zz}} z_{0}$$
 Equation 3.30

 ε_a = asphalt strain at the top of the layer [-] M = bending moment [Nm]

Strains due to the deformation of the bonding layer and the shear deformation of the asphalt For the effect of the bond deformation and the asphalt shear deformation on the asphalt strains an extra analysis has to be made using the method from Roik and Sedlacek [1970].

The effect of the bond deformation and the shear deformation of the asphalt on the asphalt strains is schematically shown in the next figure 3.22.

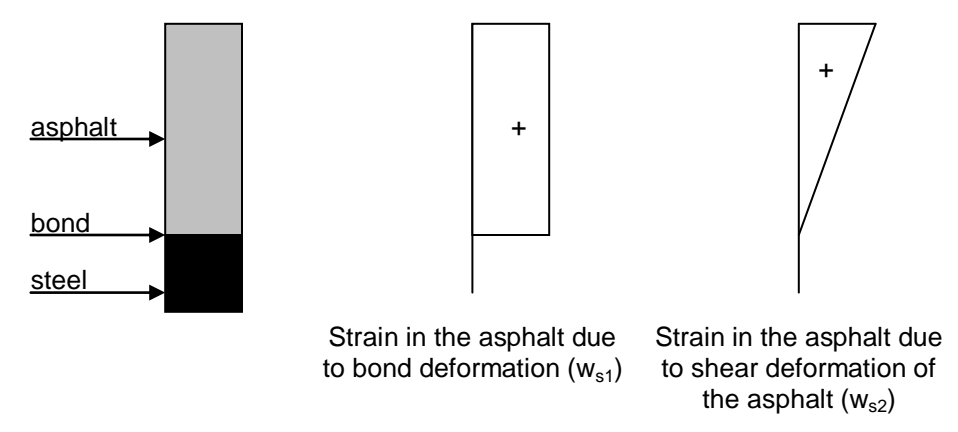


Figure 3.22: Schematic deformations of the asphalt layer due to bond deformation and shear deformation of the asphalt

The ratio between the shear stiffness of the asphalt G_b and the stiffness of the bonding layer C is defined as:

$$\kappa = \frac{G_b}{C}$$
 Equation 3.31

Further four stiffness factors are defined in which the indexes 1 and 2 refer to deformation of the bonding layer respectively shear deformation of the asphalt:

$$A_{ss1} = t_s \tau \varepsilon \frac{\left(1 + \tau^3 \varepsilon\right) + \left(1 - \tau^2 \varepsilon\right) \lambda + \frac{1}{3} \left(1 + \tau \varepsilon\right) \lambda^2}{1 + 4\tau \varepsilon \left(1 + \frac{3}{2}\tau + \tau^2\right) + \tau^4 \varepsilon^2}$$
Equation 3.32

$$A_{ss2} = t_s \tau \varepsilon \frac{\frac{1}{3} (1 + \tau \varepsilon) - (1 - \tau^2 \varepsilon) \frac{\lambda \kappa}{t_s \tau} + (1 + \tau^3 \varepsilon) \left(\frac{\lambda \kappa}{t_s \tau} \right)^2}{1 + 4\tau \varepsilon \left(1 + \frac{3}{2} \tau + \tau^2 \right) + \tau^4 \varepsilon^2}$$
Equation 3.33

$$S_1 = 1 + \frac{\lambda^2 \kappa}{t_* \tau}$$
 Equation 3.34

$$S_2 = \frac{\kappa}{t_s \tau} \left(1 + \frac{\lambda^2 \kappa}{t_s \tau} \right)$$
 Equation 3.35

in which:

$$\lambda = \frac{1}{1 - \tau^2 \varepsilon} \left[-\left(1 + \tau^3 \varepsilon\right) + \frac{1}{3} \left(1 + \tau \varepsilon\right) \frac{t_s \tau}{\kappa} + \sqrt{\left(1 + \tau^3 \varepsilon\right)^2 + \frac{1}{3} \left[1 - 2\tau \varepsilon \left(1 + 3\tau + \tau^2\right) + \tau^4 \varepsilon^2\right] \frac{t_s \tau}{\kappa}} + \left[\frac{1}{3} \left(1 + \tau \varepsilon\right) \frac{t_s \tau}{\kappa} \right]^2 \right]$$
 Equation 3.36

The strains due to deformation of the bonding layer and shear deformation of the asphalt are calculated by solving the following differential equation:

$$E_s A_{ssi} \frac{d^4 v_{si}}{dx^4} - CS_i \frac{d^2 v_{si}}{dx^2} = pr_{si}$$
 Equation 3.37

i = 1 for the deformation of the bonding layer and 2 for the deformation of the asphalt $v_{si} =$ added deformation [m]

p = load[N]

 r_{si} = load factor [-]

$$r_{s1} = \frac{\tau \varepsilon}{t_s} \frac{6(1+\tau) + (3+4\tau+\tau^2 \varepsilon)\lambda}{1+4\tau \varepsilon \left(1+\frac{3}{2}\tau+\tau^2\right) + \tau^4 \varepsilon^2}$$
 Equation 3.38

$$r_{s2} = \frac{\tau \varepsilon}{t_s} \frac{\left(3 + 4\tau + \tau^2 \varepsilon\right) - 6\left(1 + \tau\right) \frac{\lambda \kappa}{t_s \tau}}{1 + 4\tau \varepsilon \left(1 + \frac{3}{2}\tau + \tau^2\right) + \tau^4 \varepsilon^2}$$
Equation 3.39

The differential equation 3.37 is equivalent to the equation of the tensioned bending beam and can be solved using the 2^{nd} order theory [Bouma 1993]. This results in:

$$v_{si} = C_1 e^{\alpha x} + C_2 e^{-\alpha x} + C_3 + C_4 x - \frac{pr_{si}}{2CS_i} x^2$$
 Equation 3.40

with:

$$\alpha^2 = \frac{CS_i}{E_s A_{ssi}}$$
 Equation 3.41

For calculation of the added deformations the second derivative is used:

$$\frac{d^2v_{si}}{dx^2} = \alpha^2C_1e^{\alpha x} + \alpha^2C_2e^{-\alpha x} - \frac{pr_{si}}{CS_i}$$
 Equation 3.42

in which:

$$C_1 = \frac{1 - e^{-\alpha l}}{e^{\alpha l} - e^{-\alpha l}} \frac{p r_{si}}{\alpha^2 CS}$$
 Equation 3.43

$$C_2 = \frac{e^{-\alpha l} - 1}{e^{\alpha l} - e^{-\alpha l}} \frac{p r_{si}}{\alpha^2 C S_s}$$
 Equation 3.44

The moment analogue to the bending moment follows from:

$$M_{si} = -E_s A_{ssi} \frac{d^2 v_{si}}{dx^2}$$
 Equation 3.45

When M_{s1} and M_{s2} are known the strains due to deformation of the bonding layer and shear deformation of the asphalt layer are calculated with:

$$\varepsilon_{si} = \frac{M_{si}}{E_s A_{ssi}} \widetilde{w}_{si}$$
 Equation 3.46

in which:

$$\widetilde{w}_{s1} = w_{s1} + w_{s2}\lambda - \frac{\tau\varepsilon}{1 + \tau\varepsilon} \left(1 + \frac{1}{2}\lambda \right) + r_{s1}z$$
 Equation 3.47

$$\widetilde{w}_{s2} = w_{s2} - w_{s1} \frac{\lambda \kappa}{t_s \tau} - \frac{\tau \varepsilon}{1 + \tau \varepsilon} \left(\frac{1}{2} - \frac{\lambda \kappa}{t_s \tau} \right) + r_{s2} z$$
 Equation 3.48

z = distance to the middle of the steel deck [m] w_{s1} , w_{s2} = basic parameters for asphalt shear- and bond deformation

3.3.3 Comparison between the different composite action theories

3.3.3.1 Introduction

The previous sections showed the different theories for composite action. In this section the theories are compared. For each theory the strains as a result from a certain bending moment are calculated and compared with the strains calculated with the other theories.

It is known that the maximum tensile strain at the top of the asphalt occurs above the longitudinal stiffener when a dual tyre wheel passes as shown in figure 3.23.

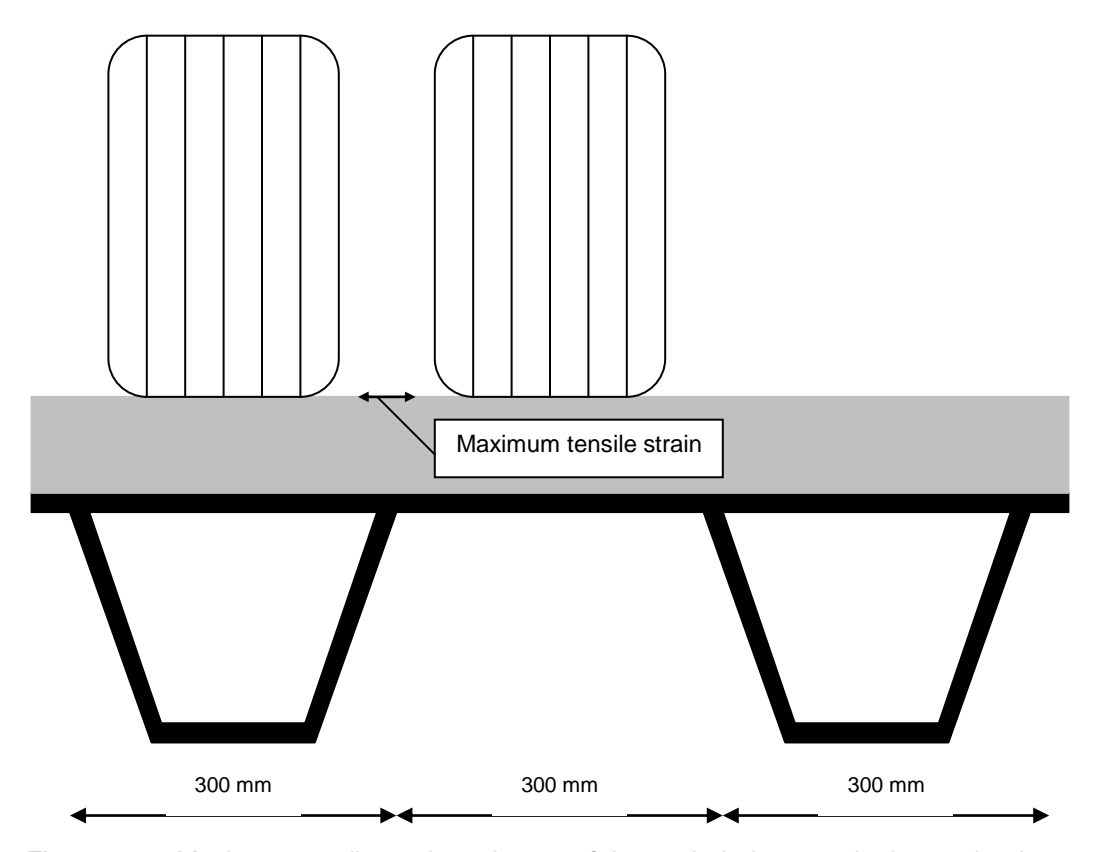


Figure 3.23: Maximum tensile strain at the top of the asphalt due to a dual tyre wheel

In order to calculate the maximum tensile strain with the composite action theories a representative bending moment above the longitudinal stiffener has to be calculated. Therefore the situation from figure 3.23 is simulated with a two-span beam as shown in figure 3.24.

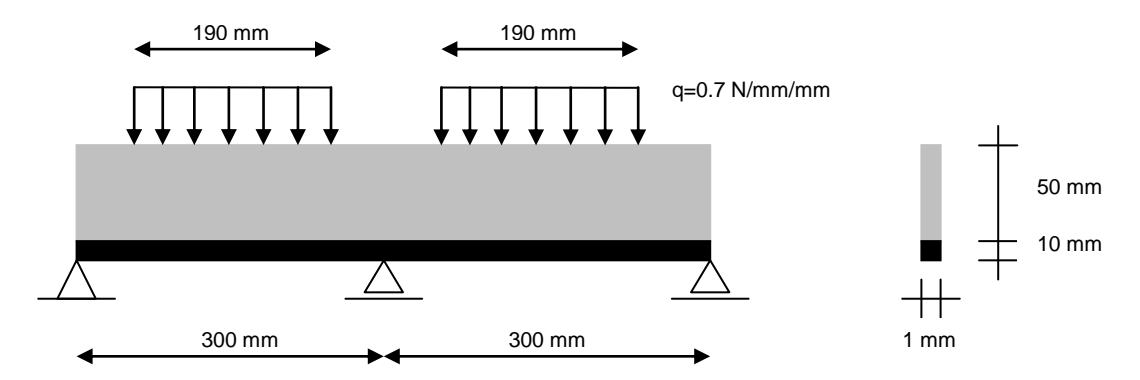


Figure 3.24: Simulation with a two-span beam for calculating the maximum bending moment

The following assumptions are made:

- For the comparison a two-span beam is taken, the distance between the supports is 300 mm, representing the distance between the longitudinal stiffeners. Of coarse this is a simplification of the true behaviour but for a comparison this is allowed, because also all the theories are based on beam-behaviour. The beam consists of a steel plate and an asphalt layer with for some of the theories an elastic interface in between.
- The thickness of the asphalt $h_a = 50$ mm and the steel $h_s = 10$ mm.
- The stiffness of the asphalt Ea = $1*10^{10}$ Pa and the steel Es = $2.1*10^{11}$ Pa.
- Width of the beam b = 1 mm.
- The applied load consists of a dual tyre wheel. The maximum axle load is 100 kN which results in a maximum load of 25 kN per tire. With a contact pressure of 0.7 N/mm² the square contact area is 190x190 mm². This results in two line loads of 0.7 N/mm/mm acting on the beam with a width of 1 mm. In fact the construction is analysed by using two line-loads and not by real wheel loads.

The load configuration as shown in figure 3.24 results in a maximum bending moment above the middle support of 6481 Nmm. With this bending moment the maximum asphalt strain will be calculated by using the different composite action theories.

3.3.3.2 Metcalf

Metcalf only considers the fully bonded state. Using Metcalfs theory the maximum tensile strain above the middle support is $6.58*10^{-4}$ mm/mm.

3.3.3.3 Kolstein

Kolstein considers two extreme situations, namely 0% and 100% bonding. For 100% bonding his theory leads to a strain of 6.58*10⁻⁴ mm/mm, for 0% bonding the strain is 1.33*10⁻³ mm/mm.

3.3.3.4 Cullimore

Cullimore uses a different load model (see figure 3.19). In order to get the same bending moment of 6481 Nmm at the support the load P to be applied on a beam with a length of 300 mm is 21.6 N. Further, in this comparison $v_a = 0.4$ and $v_s = 0.3$ as proposed by Cullimore. In table 3.9 and figure 3.25 the dependency of the asphalt strains on the bonding stiffness is shown.

Table 3.9: Asphalt strains for different values of the bond stiffness according to Cullimore

Bonding stiffness [N/mm ²]	Asphalt strain [mm/mm]
1.00*10 ⁻²	1.33E-03
1.00*10 ⁻¹	1.30E-03
1.00	1.11E-03
1.00*10 ¹	7.62E-04
1.00*10 ²	6.57E-04
1.00*10 ³	6.44E-04
1.00*10 ⁴	6.43E-04

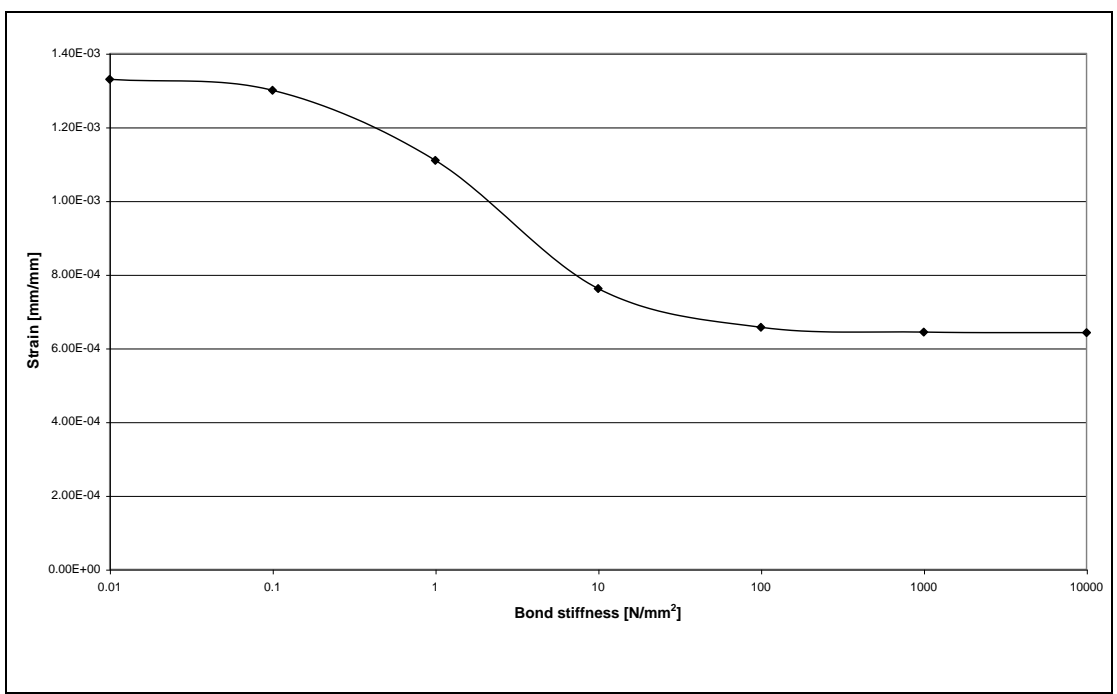


Figure 3.25: Strains in the asphalt as a function of the bonding stiffness according to Cullimore

For 0% bonding the strain reaches the value of 1.33*10⁻³ mm/mm and for 100% bonding the strain is 6.43*10⁻⁴ mm/mm according to Cullimores theory.

3.3.3.5 Nakanishi

Nakanishi considers the asphalt strain as a function of the bond coefficient t. The relation between the asphalt strain and the bond coefficient for a bending moment of 6481 Nmm is shown in table 3.10 and figure 3.26.

Table 3.10: Asphalt strains for different bond coefficients according to Nakanishi

Bond coefficient t	Asphalt strain [mm/mm]
0	1.33E-03
0.1	1.42E-03
0.2	1.42E-03
0.3	1.35E-03
0.4	1.25E-03
0.5	1.13E-03
0.6	1.01E-03
0.7	9.07E-04
0.8	8.12E-04
0.9	7.29E-04
1	6.58E-04

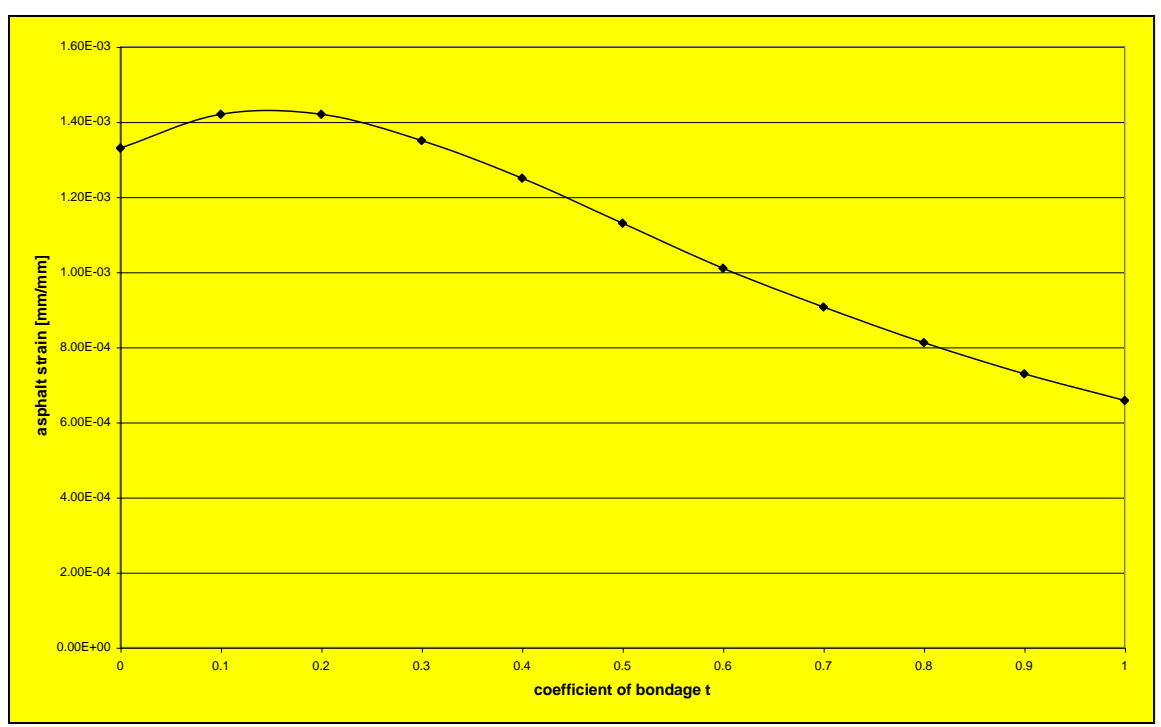


Figure 3.26: Relation between the asphalt strain and the bond coefficient according to Nakanishi

However, according to this theory the maximum strain in the asphalt occurs when the coefficient of bonding is 0.15.

3.3.3.6 Sedlacek and Bild

To compare this theory with the other theories, the bending moment has to be the same. The bending moment used for the comparison is 6481 Nmm. With this bending moment the load p (see figure 3.21) on the beam is 25924 N. The length of the beam is assumed to be 1 meter. Although the fact that the shear stiffness of the asphalt plays a role in this theory, the shear stiffness is set to on $1*10^{10}$ Pa (infinite) to make the comparison possible with the other theories that neglect the shear deformation of the asphalt.

In table 3.11 the values used in this comparison for $w_{\text{s1}},\,w_{\text{s2}}$ and z are shown:

Table 3.11: Values used for w_{s1} , w_{s2} and z

	W _{s1}	W _{s2}	Z
Top of the asphalt layer	1	1	-0.055
Bottom of the asphalt layer	1	0	-0.005
Top of the steel deck	0	0	-0.005
Bottom of the steel deck	0	0	0.005

In table 3.12 and figure 3.27 the dependency of the strains in the asphalt on the bond stiffness is shown for a bending moment of 6481 Nmm.

Table 3.12: Asphalt strains for different values of the bond stiffness and Gb=1*10¹⁰ N/mm²

Bond stiffness [N/mm2]	Asphalt strain [mm/mm]
1.00*10 ⁻²	1.11E-03
1.00*10 ⁻¹	1.07E-03
1.00	8.78E-04
1.00*10 ¹	6.94E-04
1.00*10 ²	6.61E-04
1.00*10 ³	6.58E-04
1.00*10 ⁴	6.58E-04

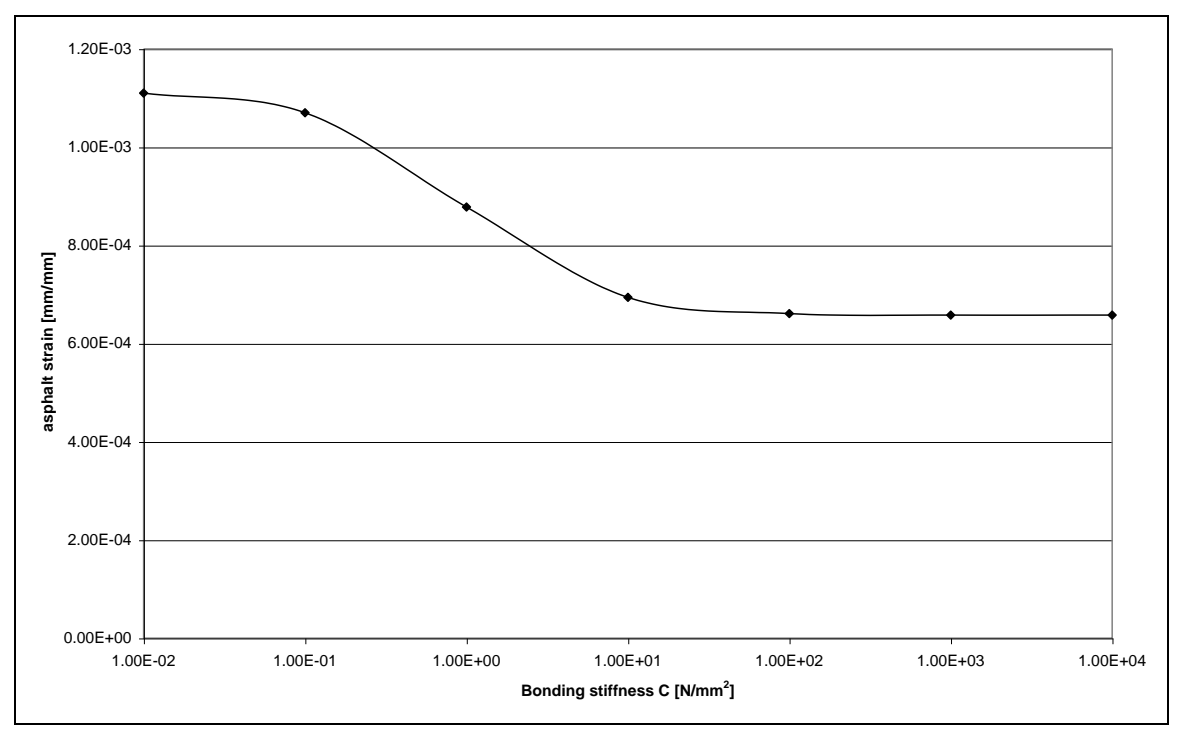


Figure 3.27: Asphalt strains as a function of the bonding stiffness

For a low bonding stiffness the asphalt strain reaches the value of 1.11*10⁻³ mm/mm and for a high bonding stiffness the strain is 6.58*10⁻⁴ mm/mm according to Sedlacek and Bild.

By comparing the above mentioned composite action theories it can be seen that some of the theories use a bond percentage and others use a bonding stiffness. In order to compare the theories it is assumed that 0% bonding is equal to a bonding stiffness of $1.00*10^{-2}$ N/mm² and that 100% bonding is equal to $1.00*10^4$ N/mm².

In table 3.13 the results for the different theories are shown for 0% and 100% bonding.

Table 3.13: Comparison between different composite action theories M=6708 Nmm

Strain [mm/mm]	0% bonding	100% bonding
Metcalf	-	6.58*10 ⁻⁴
Kolstein	1.33*10 ⁻³	6.58*10 ⁻⁴
Cullimore	1.33*10 ⁻³	6.43*10 ⁻⁴
Nakanishi	1.33*10 ⁻³	6.58*10 ⁻⁴
Sedlacek	1.11*10 ⁻³	6.58*10 ⁻⁴

From table 3.13 it is clear that all the theories result in almost the same values of the asphalt strain except Cullimore for 100% bonding and Sedlacek for 0% bonding.

The difference that Cullimore's theory gives for 100% bonding is difficult to explain, but it was noticed that Cullimore's theory is very sensitive to the input.

The difference with Sedlacek's theory is a result from the fact that in this comparison the shear deformation of the asphalt in Sedlacek's theory is neglected. This is done because all the other theories also neglect this phenomenon. When in Sedlacek's theory for 0% bonding the shear stiffness is set to a low value $(1.00*10^{-2} \text{ N/mm}^2)$ the asphalt strain reaches the value of $1.36*10^{-3}$ mm/mm which is comparable with the values of the other theories.

The strain in the asphalt predicted by different theories for an assumed bending moment of 6481 Nmm as function of the bond stiffness is shown in figure 3.28.

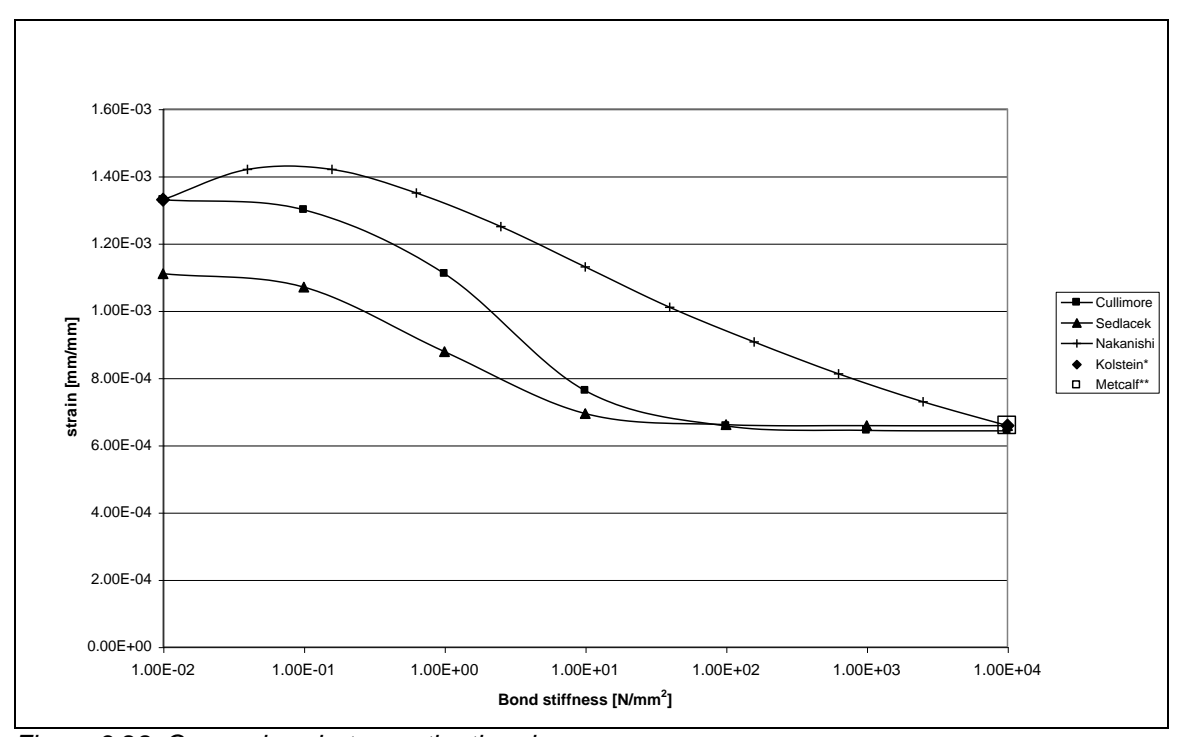


Figure 3.28: Comparison between the theories

- * Kolsteins theory results in only two points, namely (1.00E-02, 1.33E-03) and (1.00E+04, 6.58E-04)
- ** Metcalfs theory gives only one point, namely (1.00E+04, 6.58E-04)

Figure 3.28 shows that different theories for composite action give different results for different values of the bond stiffness. From the comparison it can be concluded that:

- The maximum asphalt strains for a low bonding stiffness are ≈1300 μm/m.
- All the theories are based on linear elasticity.
- The strains/stresses in the steel/asphalt are calculated using a beam model. However, plate theory may be more applicable.
- In all the theories a linear strain distribution is assumed in the asphalt and the steel.
- Nakanishi assumes the same slope of the strain distribution in both the asphalt and the steel.
 This might not be true.
- According to Nakanishi's theory the asphalt strains at ±15% bonding are higher than the strains at 0% bonding.
- For certain conditions the presented theories might be true, but these conditions might not be representative for the real structure.
- For extreme values of the bond (0% and 100% bonding) the theories give the same results, but for values of the bond stiffness between both extremes the theories give different results.

In this comparison use is made of a two-span beam. More reasonable strains can be determined by using a longer beam with more supports, or by using plate theory. The last option makes it all very complex, which makes the use of a finite element program inevitable

3.4 Damage to bridge deck surfacings

3.4.1 Introduction

As mentioned before, the life span of mastic asphalt on orthotropic steel bridges is shorter than that of normal pavements. This problem is not limited to the Netherlands, but has also been reported in other countries, for example the USA and Japan. Some of the problematic bridges are:

Netherlands: Moerdijk bridge, van Brienenoordbrug (figure 3.29), Ewijk bridge



Figure 3.29: Van Brienenoordbrug

USA: George Washington Bridge (figure 3.30)



Figure 3.30: George Washington Bridge

Japan: Seto–Ohashi bridge (figure 3.31)



Figure 3.31: Seto-Ohashi bridge

In this paragraph the main types of distress that occur on these bridges are discussed. De Backer [1978] made an extensive report of damages to bituminous bridge deck surfacings. The report describes the damages based on an inventory of 500 bridges in Belgium.

It is not exactly clear on what type of bridges the damages are established, but the amount of orthotropic steel bridges in Belgium is quite small, so most of the damages described have occurred on concrete bridges. However, these damages also occur on orthotropic steel bridges.

Damages that occur on orthotropic steel bridges include:

- Permanent deformation
- Cracking
- Mounds
- Disintegration
- Loss of bond between the steel deck and the asphalt

3.4.2 Permanent deformation

In general, permanent deformations are caused by exceptionally high and/or repeated stresses (compressive or shear). The most important type of permanent deformation is rutting, which increases with high temperatures. Because mastic asphalt has a large amount of bitumen it is sensitive for rutting.

Kohler and Deter [1974] indicate that heaves occur above and also between the longitudinal stiffeners. The heaves between the longitudinal stiffeners are caused by movement of the pavement, which is caused by traffic moving from the stiffer part of the plate (above the stiffeners) to the weaker parts (between the stiffeners).

Corrugations result from longitudinal forces caused by braking and accelerating vehicles. Sometimes, at high temperatures, the toplayer tends to slide over the bottom layer. This phenomenon was observed on bridges with a high vertical slope in both transversal and longitudinal direction.

3.4.3 Cracking

Cracking is probably the most occurring damage to surfacings on orthotropic steel bridges, both by using mastic asphalt and compacted asphalt. When the cracks reach to the steel deck plate this plate tends to rust, often leading to de-bonding. To prevent that cracks will reflect in the corrosion-protecting layer and reach the steel deck plate a fibre-glass net can be used [Volker 1993].

De Backer [1978] makes a distinction between cracking caused by a strain exceeding the maximum strain in the asphalt after one load cycle and cracking caused by fatigue (more than one load cycle).

The most important cracking occurs above the longitudinal or transverse stiffeners. Often there is a pattern in cracking that follows the distance between the longitudinal stiffeners. Above these stiffeners the strains and stresses are generally high. Especially at low temperatures this is critical because then the asphalt is very stiff.

Kohler and Deter [1974] make a distinction between longitudinal cracks above and between the stiffeners due to bending moments. The cracks between the stiffeners arise at the bottom of the asphalt and will propagate to the surface. The cracks above the stiffeners arise at the surface of the asphalt and propagate to the bottom.

Both types are caused by positive bending moments between the stiffeners, resulting in cracks at the bottom of the pavement that will propagate to the top of the pavement. The cracks between the stiffeners occur often when the bond between the asphalt and steel is weak [de Backer, 1978].

Inspection of the Moerdijk bridge which consists of 10 spans with different steel thicknesses (10-14 mm), showed the following:

- 80% of the cracks were observed in the right lane
- 80% of the cracks were observed in spans where the thickness of the steel plate is 10 mm.

3.4.4 Mounds

This is a local expansion/swell of a waterproof layer (for example mastic asphalt), and occurs when a waterproof layer is laid on a layer that contains water. When asphalt is laid on such a layer, water evaporates forming bubbles and will be seen at the surface as mounds.

3.4.5 Disintegration

This includes ravelling (loss of stone particles from the surface) and potholes. It is caused by cracking, loss of bond and/or a combination of other distress mechanisms. Ravelling can seriously reduce the skid resistance of the pavement and hence, endangers the safety of the road users.

3.4.6 Loss of bond between the steel deck and the asphalt

Experiences in the United States (Dublin Bridge in California), Switzerland (St. Albans Bridge in Basel) and Germany (the Koln-Mulheim bridge) tend to show that once the bond between the steel deck and surfacing is destroyed, the failure of the pavement is merely a matter of time.

3.4.7 Distress mechanisms related to mix parameters

3.4.7.1 Introduction

Sometimes distress is characterised by means of the mechanisms causing the distress. In this paragraph the distress mechanisms and the important mix parameters that influence them are discussed.

For the design of mastic asphalt on orthotropic bridges there are three types of distress of importance, namely permanent deformation, cracking and the loss of bond between the steel and the asphalt. Both other types of distress, mounds and disintegration are mostly dependent on the way of construction and can hardly be influenced by the design. So they are not discussed further in this paragraph.

During lifetime there are factors that have an influence on the distress mechanisms by reducing the pavement strength, for example:

- Ageing of bitumen,
- Weathering of aggregate materials (chemical decomposition caused by oxygen, water, heat and/or solar radiation).
- Strength reduction of bituminous materials because of low viscosity at high temperatures.

Most damage occurs as a combination of several distress mechanisms.

3.4.7.2 Permanent deformation

Permanent deformation can be a result of:

- Exceptionally high and/or repeated stresses (compressive or shear).
- Bleeding because of deformation of bituminous materials with too high bitumen content and too low voids content (typical characteristics for mastic asphalt).

The most important type of permanent deformation is rutting. It is caused by:

- Post-compaction of the asphalt
- The flow of the asphalt

Laboratory tests are carried out to determine the relation between the number of load repetitions and the permanent deformation ϵ_p for asphalt. The permanent deformation ϵ_p is dependent on several parameters:

$$\varepsilon_p = f(\varepsilon_e, N, V_a, f_{reg})$$

 ϵ_{p} : permanent strain ϵ_{e} : elastic strain

N : number of load repetitions

V_a: void content

f_{req}: loading frequency [Hz]

For mix design the elastic strain and the voids content are important. The elastic strain indicates that the stiffness modulus of the asphalt is of importance. Because mastic asphalt is an overfilled mixture the mix stiffness is mainly influenced by the bitumen stiffness. Further also the mineral aggregate contributes to the material stiffness.

Important mix parameters

- Bitumen stiffness.
- Gradation, grain shape and maximum grain size.
- Void content.
- Bitumen content.

3.4.7.3 Cracking

Types of cracking:

- Fatigue cracking of pavement materials due to repeated stresses (shear and/or tensile) induced by traffic, environment and poor construction. This type of cracking can occur at the top or at the bottom of the asphaltic layer.
- Cracking due to exceptionally high stresses, induced by heavy traffic or freezing, exceeding the material's tensile or shear strength.
- Crack propagation because of high tensile stress intensities at the tips of a previously initiated crack.

Most important on orthotropic steel bridges is the fatigue cracking. Fatigue is the gradual decrease of the pavement strength caused by repeated stress cycles. The result of this decreasing pavement strength is cracking. The main factors influencing cracking are [Medani 2000al:

- the pavement's strength (mainly the structural thickness, material strength and stiffness)
- the traffic loading (number and magnitude of wheel loads)
- the climate and weather conditions (solar radiation, temperature, temperature gradients and moisture regimes that influence the traffic induced stresses, but independently also cause ageing)

There are different fatigue damage models that are used in asphalt road engineering. One of them is the Wöhler fatigue model. This model uses a relation between the number of load applications to failure and the strain at the bottom of the asphalt layer:

$$N = k_1 \left(\frac{1}{\varepsilon}\right)^n$$
 Equation 3.49

N: number of load applications to failure ε : strain at the bottom of the asphalt layer

 k_1 , n: material dependent constants

This relation is often used to get an indication of the fatigue resistance of the mix. Very important in this case is the flexibility of the mix, which is dependent on the void and bitumen content.

Important mix parameters

- Bitumen content
- Void content
- Mix stiffness

3.4.7.4 Loss of bond

Some reasons for the loss of bond between the steel deck and the asphalt are:

- Loss of bond can already occur during construction due to the rather high temperature of the asphalt mix (≅ 220°C). This leads to an increasing temperature of the steel plate and may result in high strains at the topside. The severity of the problem is dramatically increased when the deck plate can not deform freely, resulting in high compressive stresses.
- High shear stresses between the pavement and the steel deck as a result of braking and
 accelerating traffic can also lead to loss of bond according to Fondriest [1969]. When the
 bridge is not horizontal (both in the longitudinal and transverse direction) the shear forces are
 increasing, which has an even more destructive influence on the bond. Speculations were
 made, particularly by the German road authorities, that the vibrations of the deck as a result
 of fast moving traffic also weaken the bond.
- It was noticed that separation between the deck and the pavement also occurs on places were no traffic is driving. This is partly explained by the fact that not only the traffic weakens the bond but also the different thermal expansion of both the steel and the asphalt. This may lead to high strains and as a result weakening of the bond.

Important bond parameters

Shear stiffness of the bond

It can be seen that different types of distress are caused by different mechanisms. Unfortunately, it is not as simple as one can assign a specific mechanism for each distress type. There can also be considerable interaction between the different distress types e.g. the unevenness of the surface can cause high dynamic loads which will in turn results in faster cracking of the pavement. Also ravelling can be the origin of potholes [Groenendijk, 1998].

It is shown that the shear stiffness of the bond is an important parameter in relation to the asphalt strains and thus on the distress mechanisms. This shear stiffness is dependent on the temperature. The temperature effect on the shear stiffness of the bond and the asphalt strains is described in the next paragraph.

3.5 Temperature effect

Sedlacek and Bild [1985] carried out a parametric study of the temperature effect on the composite section. The change of temperature can lead to stresses and strains in both the asphalt and the steel because of the different expanding coefficients of both materials. In this study a one-span beam with a length of 300 mm and a width of 10 mm was used.

Because of the rather complicated visco-elastic behaviour of the asphalt this study was only concentrated on pure elastic behaviour. In other words, on short-time temperature changing and the behaviour of the asphalt at low temperatures. A fast temperature reduction of 1°C was used. The coefficients of expansion for the asphalt and the steel that were assumed:

 $\begin{array}{ll} \text{Mastic asphalt:} & \alpha_\text{T} = 6^* 10^{\text{-}4} \, \text{K}^{\text{-}1} \\ \text{Steel:} & \alpha_\text{T} = 1.2^* 10^{\text{-}5} \, \text{K}^{\text{-}1} \\ \end{array}$

The maximum strain at the bottom of the asphalt arises when the bonding layer is weak:

$$\varepsilon_{\text{max}} = \alpha_{\text{T}} * \Delta \text{T} = 6*10^{-4} * (-1) = -600 \ \mu\text{m/m}.$$

A high bonding stiffness results in strains that are about 1/20 to 1/5 of the maximum strain. The strain due to the change in temperature is clearly influenced by the stiffness of the bonding layer. In figure 3.32 the relation between the strain at the bottom of the asphalt (ϵ_{bu}), the bonding stiffness (C) and the ratio E_{asf}/E_{steel} is shown.

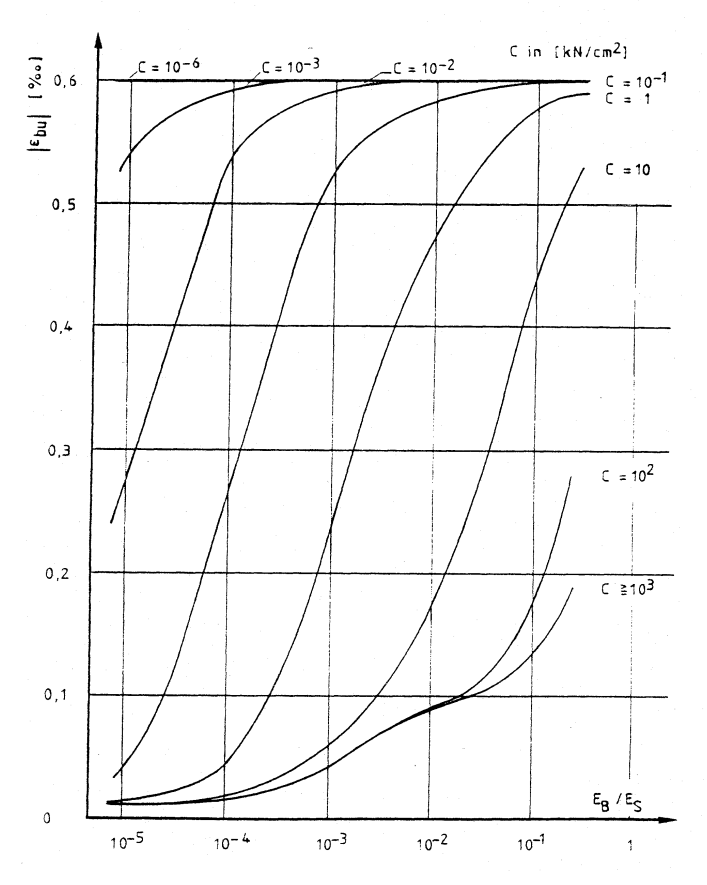


Figure 3.32: Strains at the bottom of the asphalt related to the bonding stiffness C and East/Esteel

The high strains that are a result of a temperature change of only 1°C show that the temperature effects cannot be neglected.

Besides the temperature there is another important phenomenon that cannot be neglected, namely the vibration of the bridge deck.

3.6 Vibration of the bridge deck

3.6.1 Dynamic axle loads on pavements on a subgrade

For pavements on a subgrade it is known that dynamic axle loads can be up to 40% higher than the static ones [Divine, 1997]. The dynamic axle loads depend on the suspension type, static axle load, speed of travel and longitudinal profile of the road. The dynamic loads are generated within two frequency ranges:

- Frequencies between 1.5 and 4 Hz corresponding with body bouncing.
- Frequencies between 8 and 15 Hz corresponding with axle bouncing.

Very little is known about the interaction between the loads and the pavement and the effects of dynamic loads on pavements. The more interested reader is referred to Huurman [1997], who investigated the effect of dynamic axle loads on concrete block pavements. However, most design codes are based on a "safety factor" that is multiplied with the static loads to deal with the effect of dynamic loads.

3.6.2 Vibration of the bridge deck

For pavements on bridges it seems that vibrations play even a more important role, because on bridges not only the vehicles are vibrating, but also the bridge itself. The dynamic response of bridges depends on:

- The bridge damping.
- The bridge natural frequencies.
- The road and bridge profile.
- The vehicle mass.
- Frequencies of the vehicles dynamic wheel loads.
- The number of vehicles simultaneously on the bridge.

The damping of a bridge is dependent on the mass, an increasing mass leads to an increasing damping. For a bridge this means that two contradictory interests play a role since the mass of a bridge is often minimised in the design. The natural frequency of bridges is dependent on the span of the bridge:

- Short span bridges (L=8-15 m) have a natural frequency of 8-15 Hz.
- Short-medium span bridges (L=15-30 m) have a natural frequency of 4-8 Hz.
- Medium-span bridges (L=30-60 m) have a natural frequency of 2-4 Hz.
- Long-span bridges (L=60-80 m) have a natural frequency of 1.5-1.8 Hz.

When the frequency of the wheel loads is close to the natural frequency of the bridge (frequency matching) this can lead to problems, like increased dynamic responses. For very short bridges (<8 m) vibrations play a less important role. In that case vehicles are longer than the bridge and no true interaction takes place. Very long bridges (>100 m) have such a low natural frequency that only the summed effects of several vehicle vibrations can lead to dynamic responses.

3.6.3 The effect of vibrations on the pavement

3.6.3.1 Axle loads on pavements on a subgrade

To get an indication of the effect of bridge vibrations two models are compared in this paragraph. a two-mass spring system representing the axle load on pavement on a subgrade and a more extensive two-mass spring system representing the axle load on the bridge.

The axle load on a pavement on a subgrade can be simulated with a two-mass spring system (figure 3.33).

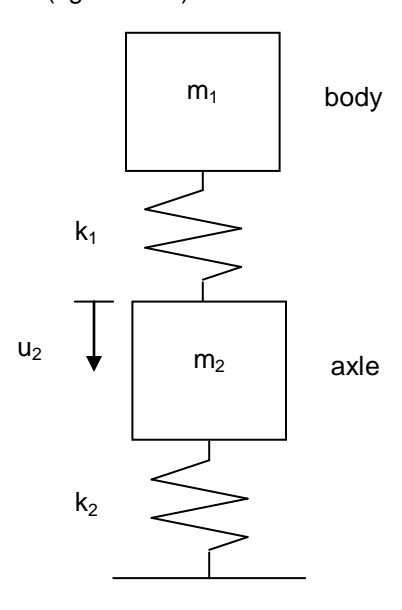


Figure 3.33: Model of an axle load on a pavement on a subgrade

The force in spring 1 represents the dynamic load of the body on the axle and the force in spring 2 represents the dynamic load on the pavement. To describe the behaviour of the model, mass 2 (axle) is displaced over a distance x_2 and released at t=0, representing the axle displacement due to an unevenness in the road. The model is described by the following formulae [Dieterman, 1997]:

$$\begin{bmatrix} m_1 & 0 \\ 0 & m_2 \end{bmatrix} \begin{bmatrix} \ddot{x}_1 \\ \ddot{x}_2 \end{bmatrix} + \begin{bmatrix} k_{11} & k_{12} \\ k_{21} & k_{22} \end{bmatrix} \begin{bmatrix} x_1 \\ x_2 \end{bmatrix} = \begin{bmatrix} F_1 \\ F_2 \end{bmatrix}$$
 Equation 3.50

In which:

$$\begin{aligned} k_{11} &= k_1 \\ k_{12} &= -k_1 \\ k_{21} &= -k_1 \\ k_{22} &= k_1 + k_2 \end{aligned}$$

In this case F_1 and F_2 are zero, which means there is only a general solution:

$$\begin{bmatrix} x_1(t) \\ x_2(t) \end{bmatrix} = A_1 \begin{bmatrix} 1 \\ R_1 \end{bmatrix} \sin(\omega_1 t + \phi_1) + A_2 \begin{bmatrix} 1 \\ R_2 \end{bmatrix} \sin(\omega_2 t + \phi_2)$$
 Equation 3.51

The natural frequencies ω_1 and ω_2 follow from:

$$\left(\omega^{2}\right)_{1/2} = \frac{\omega_{11}^{2} + \omega_{22}^{2}}{2} \pm \left[\left(\frac{\omega_{22}^{2} - \omega_{11}^{2}}{2}\right)^{2} + \left(\omega_{12}\right)^{4}\right]^{\frac{1}{2}}$$
 Equation 3.52

in which:

$$(\omega_{11})^2 = \frac{k_{11}}{m_1}$$
 Equation 3.53

$$(\omega_{22})^2 = \frac{k_{22}}{m_2}$$
 Equation 3.54

$$(\omega_{12})^2 = \frac{k_{12}k_{21}}{m_1m_2}$$
 Equation 3.55

R₁ and R₂ follow from:

$$R_{1} = \frac{-\omega_{1}^{2} m_{1} + k_{11}}{-k_{12}}$$
 Equation 3.56

$$R_2 = \frac{-\omega_2^2 m_1 + k_{11}}{-k_{12}}$$
 Equation 3.57

 A_1 , A_2 , ϕ_1 and ϕ_2 follow from:

$$A_{1} = \left[u_{1}^{2}(0) + \dot{u}_{1}^{2}(0)/\omega_{1}^{2}\right]^{1/2}$$
 Equation 3.58

$$A_2 = \left[u_2^2(0) + \dot{u}_2^2(0)/\omega_2^2\right]^{1/2}$$
 Equation 3.59

$$\tan \phi_1 = \omega_1 u_1(0) / \dot{u}_1(0)$$
 Equation 3.60

$$\tan \phi_2 = \omega_2 u_2(0) / \dot{u}_2(0)$$
 Equation 3.61

in which:

$$u_1(0) = \frac{R_2 x_1(0) - x_2(0)}{R_2 - R_1}$$
 Equation 3.62

$$u_2(0) = \frac{-R_1 x_1(0) + x_2(0)}{R_2 - R_1}$$
 Equation 3.63

$$\dot{u}_1(0) = \frac{R_2 \dot{x}_1(0) - \dot{x}_2(0)}{R_2 - R_1}$$
 Equation 3.64

$$\dot{u}_{2}(0) = \frac{-R_{1}\dot{x}_{1}(0) + \dot{x}_{2}(0)}{R_{2} - R_{1}}$$
 Equation 3.65

In these formulae $x_1(0)$, $x_2(0)$, $\dot{x}_1(0)$ and $\dot{x}_2(0)$ are the start conditions at t=0.

The force in spring 1, i.e. the force of the bouncing body on the axle, is:

$$F_{s1}(t) = -k_1[x_1(t) - x_2(t)]$$
 Equation 3.66

The force in spring 2, i.e. the force on the pavement, is:

$$F_{s2}(t) = -k_2 x_2(t)$$
 Equation 3.67

Knowing this force due to the axle displacement at t=0, the model can also be simplified to a one-mass spring system with a harmonic force (figure 3.34), representing the force $F_{s1}(t)$ of the bouncing body on the axle.

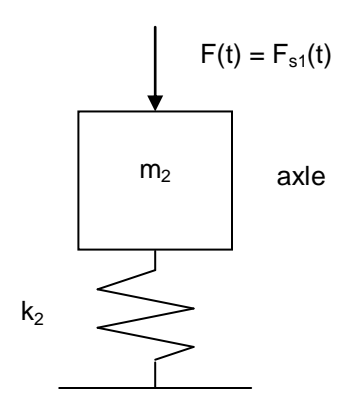


Figure 3.34: Simplified model of the axle load on a pavement on a subgrade

Due to the fact that the force $F_{s1}(t)$ is a force in which the natural movement of the axle is already included, only the particular solution has to be determined of this simplified model. In that case the results are the same as the results of the original model (figure 3.33). This knowledge will be used in the next paragraph to reduce the number of masses in the model.

3.6.3.2 Axle loads on pavements on a undamped bridge

The axle load on a pavement on a bridge can be simulated with a three-mass spring system (figure 3.35). In this case the pavement is not a static element.

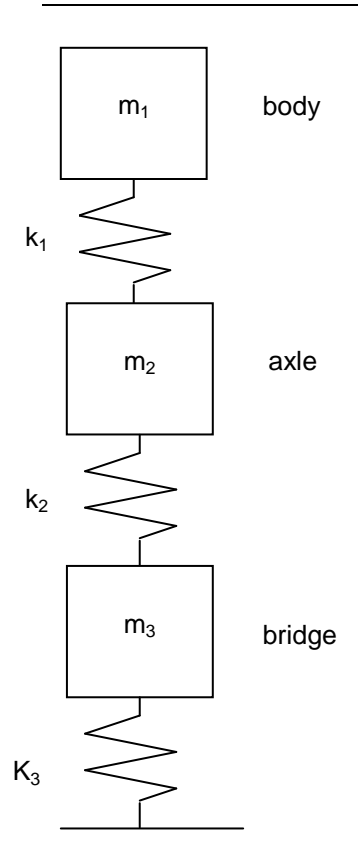


Figure 3.35: Model of an axle load on a pavement on a bridge

In the previous paragraph it was shown that this model can be simplified into a two-mass spring system with a harmonic force on the axle representing the body bouncing as shown in figure 3.36.

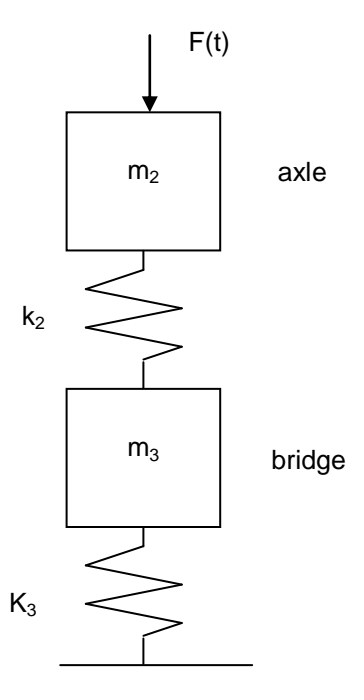


Figure 3.36: Simplified model of an axle load on a pavement on a bridge

For the force F(t) the equation for $F_{s1}(t)$ (equation 3.66) can be taken as representing the force of a moving body on the axle due to a certain axle displacement at t=0. This force is the sum of two cosines. This simplified model is described with:

$$\begin{bmatrix} m_2 & 0 \\ 0 & m_3 \end{bmatrix} \begin{bmatrix} \ddot{x}_2 \\ \ddot{x}_3 \end{bmatrix} + \begin{bmatrix} k_{11} & k_{12} \\ k_{21} & k_{22} \\ \end{bmatrix} \begin{bmatrix} x_2 \\ x_3 \end{bmatrix} = \begin{bmatrix} F(t) \\ 0 \end{bmatrix}$$
 Equation 3.68

in which:

$$\begin{aligned} k_{11} &= k_2 \\ k_{12} &= -k_2 \\ k_{21} &= -k_2 \\ k_{22} &= k_2 + k_3 \end{aligned}$$

Again, only the particular solution is determined because the homogeneous solution is part of the force F(t). In this case there are two particular solutions. The movement of the axle and the bridge is described with:

$$\begin{bmatrix} x_2(t) \\ x_3(t) \end{bmatrix} = \begin{bmatrix} x_2 a \\ x_3 a \end{bmatrix} \cos(\omega_3 t) + \begin{bmatrix} x_2 b \\ x_3 b \end{bmatrix} \cos(\omega_4 t)$$
 Equation 3.69

 ω_3 and ω_4 are the frequencies of load F(t). Further:

$$x_{2}a = \frac{-\omega_{3}^{2}m_{3} + k_{22}}{\omega_{3}^{4}m_{2}m_{3} - \omega_{3}^{2}(m_{3}k_{11} + m_{2}k_{22}) + k_{11}k_{22} - k_{12}k_{21}}F_{2}a$$
 Equation 3.70

$$x_2b = \frac{-\omega_4^2 m_3 + k_{22}}{\omega_4^4 m_2 m_3 - \omega_4^2 (m_3 k_{11} + m_2 k_{22}) + k_{11} k_{22} - k_{12} k_{21}} F_2 b$$
 Equation 3.71

$$x_{3}a = \frac{k_{21}}{\omega_{3}^{4}m_{2}m_{3} - \omega_{3}^{2}(m_{3}k_{11} + m_{2}k_{22}) + k_{11}k_{22} - k_{12}k_{21}}F_{2}a$$
 Equation 3.72

$$x_3b = \frac{k_{21}}{\omega_4^4 m_2 m_3 - \omega_4^2 (m_3 k_{11} + m_2 k_{22}) + k_{11} k_{22} - k_{12} k_{21}} F_2 b$$
 Equation 3.73

in which:

$$F_2 a = A_1 (1 - R_1)$$
 Equation 3.74

$$F_2 b = A_2 (1 - R_2)$$
 Equation 3.75

3.6.3.3 Axle loads on pavements on a damped bridge

For a damped bridge the model changes as shown figure 3.37.

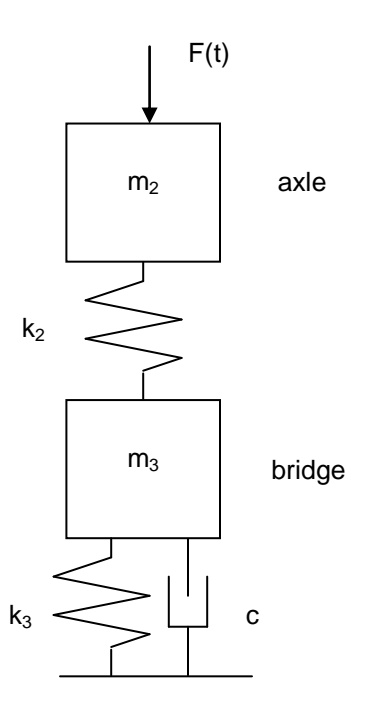


Figure 3.37: Simplified model of an axle load on a pavement on a damped bridge

The model is described with the following differential equations:

$$\begin{bmatrix} m_2 & 0 \\ 0 & m_3 \end{bmatrix} \begin{bmatrix} \ddot{x}_2 \\ \ddot{x}_3 \end{bmatrix} + \begin{bmatrix} c_{11} & c_{12} \\ c_{21} & c_{22} \end{bmatrix} \begin{bmatrix} \dot{x}_2 \\ \dot{x}_3 \end{bmatrix} + \begin{bmatrix} k_{11} & k_{12} \\ k_{21} & k_{22} \end{bmatrix} \begin{bmatrix} x_2 \\ x_3 \end{bmatrix} = \begin{bmatrix} F(t) \\ 0 \end{bmatrix}$$
 Equation 3.76

In vector notation this results in:

$$M \ddot{\underline{x}} + C \dot{\underline{x}} + K \underline{x} = \underline{F}(t)$$
 Equation 3.77

For the force F(t) on the axle, the equation for $F_{s1}(t)$ (equation 3.66) can be taken which represents the force of a moving body on the axle due to a certain axle displacement at t=0 which can be a result of an unevenness in the road profile. This unevenness can be for example the joint between the bridge and the approach of the bridge, which is often of poor quality due to the difference in settlement.

For the solution of this model a different approach is used, the modal analysis, as described by Spijkers [1996]. This analysis assumes that the response can be determined with eigenvectors that are determined on the basis of the undamped system:

$$\underline{x}(t) = \sum_{i=1}^{n} \hat{\underline{x}}_{i} u_{i}(t) = E\underline{u}(t)$$
 Equation 3.78

In this case, with two degrees of freedom, there are two eigenvectors, namely:

$$\hat{\underline{x}}_1 = \begin{bmatrix} 1 \\ R_1 \end{bmatrix}$$
 and $\hat{\underline{x}}_2 = \begin{bmatrix} 1 \\ R_2 \end{bmatrix}$

R₁ and R₂ can be determined as described with the equations 3.56 and 3.57.

It is assumed that the solution is the sum of synchronic movements. Substitution of 3.78 in 3.77 results in:

$$ME\ddot{u} + CE\dot{u} + KE\underline{u} = \underline{F}(t)$$
 Equation 3.79

Pre-multiplication with E^T results in:

$$E^{T}ME\ddot{u} + E^{T}CE\dot{u} + E^{T}KE\underline{u} = E^{T}\underline{F}(t)$$
 Equation 3.80

This can also be written as:

$$M^*\ddot{\underline{u}} + C^*\dot{\underline{u}} + K^*\underline{u} = E^T\underline{F}(t)$$
 Equation 3.81

It is known that the eigenvectors are orthogonal to M and K, i.e. M^* and K^* are diagonal matrices. However, C^* is not always a diagonal matrix. This is called non-proportional damping, which means that the system of differential equations is not uncoupled. In this case C^* is the diagonal matrix:

$$C = \begin{bmatrix} 0 & 0 \\ 0 & c \end{bmatrix}$$

$$E = \begin{bmatrix} 1 & 1 \\ R_1 & R_2 \end{bmatrix}$$

$$E^T = \begin{bmatrix} 1 & R_1 \\ 1 & R_2 \end{bmatrix}$$

$$C^* = E^T C E = \begin{bmatrix} 0 & 0 \\ 0 & R_2^2 c \end{bmatrix}$$
 Equation 3.82

This special case of the damped system, in which the modal damping matrix C^* is diagonal, is called a proportional damped system and allows the use of the modal analysis. The system is harmonically loaded and the response is the sum of the homogeneous and the particular solutions, but due to damping the homogeneous solution disappears in time. Here only the particular solutions are described, presenting the "steady state" behaviour.

The response to the following harmonic load $\underline{F}(t) = \hat{\underline{F}} \cos \Omega t$ can be written as a harmonic function with the same frequency and a phase angle ϕ_i :

$$u_i(t) = \hat{u}_i \cos(\Omega t - \varphi_i)$$
 Equation 3.83

in which:

$$\hat{u}_{i} = \frac{1}{\sqrt{\left(1 - \left(\frac{\Omega}{w_{i}}\right)^{2}\right)^{2} + \left(2\xi_{i}\frac{\Omega}{\omega_{i}}\right)^{2}}} \frac{1}{\omega_{i}^{2}} \frac{\hat{x}_{i}^{T}\hat{F}}{\hat{x}_{i}^{T}M\hat{x}_{i}}$$
Equation 3.84

$$\tan \varphi_i = \frac{2\xi_i \frac{\Omega}{\omega_i}}{1 - \left(\frac{\Omega}{\omega_i}\right)^2}$$
 Equation 3.85

The movements of the axle and the bridge are described with:

$$\underline{x}(t) = \begin{bmatrix} x_2(t) \\ x_3(t) \end{bmatrix} = \sum_{i=1}^n \hat{\underline{x}}_i \frac{1}{\sqrt{\left(1 - \left(\frac{\Omega}{w_i}\right)^2\right)^2 + \left(2\xi_i \frac{\Omega}{\omega_i}\right)^2}} \frac{1}{2\pi i} \frac{\hat{\underline{x}}_i^T \hat{\underline{F}}}{\hat{\underline{x}}_i^T M \hat{\underline{x}}_i} \cos(\Omega t - \varphi_i)$$
Equation 3.86

The damping ratio ξ_i determines the damping of both the degrees of freedom:

$$\xi_i = \frac{c}{c_{kr}} = \frac{c_i}{2\sqrt{k_i m_i}}$$
 Equation 3.87

3.6.3.4 Comparison between axle loads on a subgrade and on a bridge

To compare the axle loads on a subgrade with the axle loads on a undamped and damped bridge the following vehicle parameters are chosen representing the rear axle of a DAF truck with a maximum static axle load of 100 kN [Huurman, 1997]:

- $M_1 = M_{body}$: 8894 kg • $M_2 = M_{axle}$: 1300 kg • K_1 : $7*10^5$ N/m • $E_1 = E_{body}$: 0
- K₂: 4*10⁶ N/m

• $\xi_2 = \xi_{\text{avio}}$: 0

To schematise the bridge into a mass spring system the next formulae are used:

$$k = \frac{48EI}{L^3}$$
 Equation 3.88

$$M_{bridge} = \frac{\rho AL}{2}$$
 Equation 3.89

For a bridge with a width of 12 meters and a length of 25 meters the following parameters are determined:

M₃ = M_{bridge}: 3.1*10⁴ kg
 K₃: 7.6*10⁶ N/m

• $\xi_3 = \xi_{\text{bridge}}$: 0.02

A medium span bridge is chosen because of the following reasons:

- On short span bridges no real interaction between vehicle and bridge takes place.
- On long span bridges the vehicle movement is often already damped before the vehicle reaches the critical place on the bridge.

For most of the steel structures the damping ratio is smaller than 0.01, what means that the structures are under damped [Dieterman, 1997]. Medium to long span bridges have damping values of ξ =0.008-0.02 and for short span bridges the range is ξ =0.01-0.05 [Divine, 1997].

The axle loads in these models depend on the displacement of the axle at t=0, representing the axle displacement due to an unevenness in the road. In figure 3.38 $F_{\text{axle}}/F_{\text{static}}$ as a function of the axle displacement $u_{\text{axle}}(0)$ is shown for both axle loads on a subgrade and on a bridge.

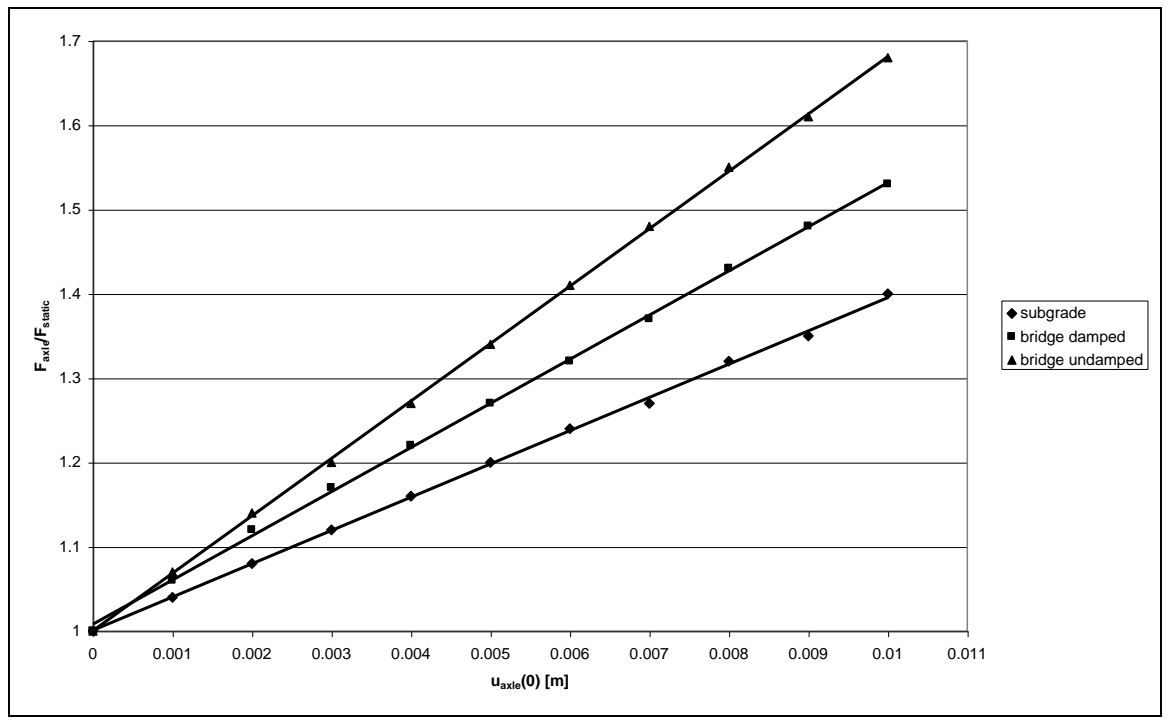


Figure 3.38: F_{axle}/F_{static} as a function of the axle displacement $u_{axle}(0)$

It can be seen that the dynamic axle loads on a bridge are higher than the axle loads on a subgrade. This is a result of the fact that due to interaction between the vehicle and the bridge the axle displacements and thus the axle loads are increasing. Figure 3.38 shows that on a subgrade the maximum axle loads can be 1.40 times the static load, on a damped bridge 1.53 times the static load, which means a 13% higher value. The figure also shows clearly the effect of damping.

The static displacement at the midspan of the bridge used in this model can be calculated with:

$$w = \frac{FL^3}{48FI}$$
 Equation 3.90

For this bridge this leads to a static displacement of 13.2 mm. The vibration of the bridge leads to an additional displacement of 0.5 mm when $u_{\text{axle}}(0)$ =0.01 m, an increment of 4%. The total displacement at the midspan becomes 13.7 mm.

To get an indication of the dependency of the dynamic axle load on different bridge types, the maximum axle loads as a function of the bridge natural frequency are shown in figure 3.39 for $u_{axle}(0)$ =-0.01 for both the damped and the undamped bridge.

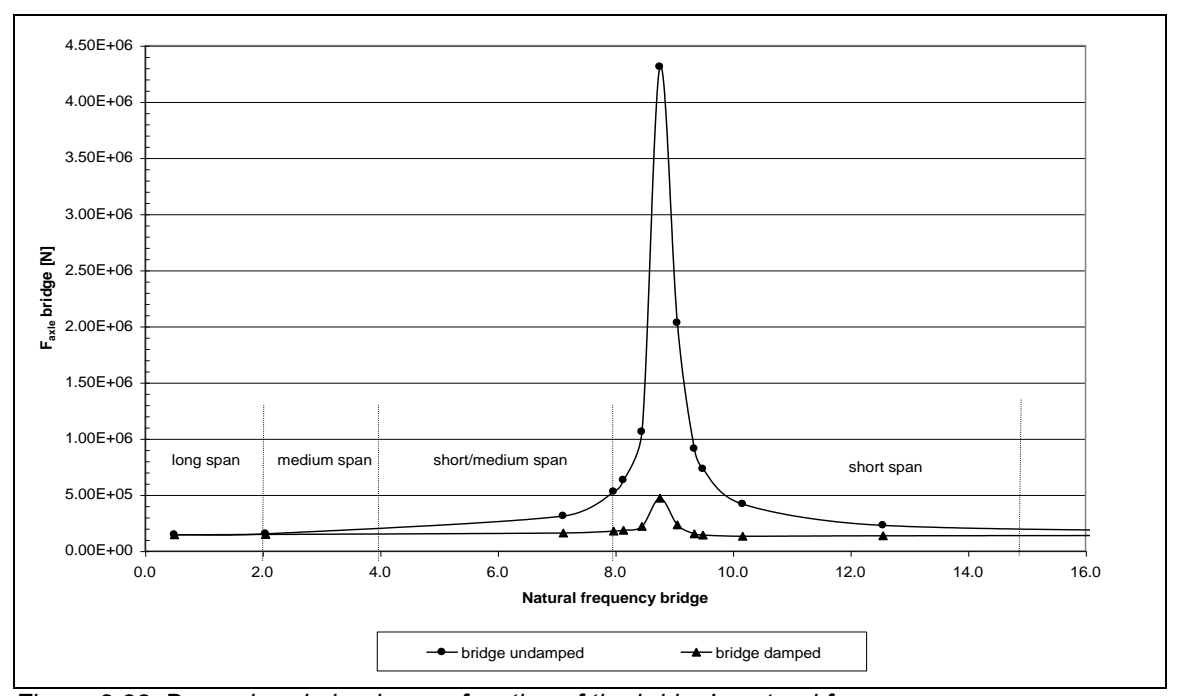


Figure 3.39: Dynamic axle loads as a function of the bridge's natural frequency

Several conclusions can be drawn from figure 3.39. At first, it shows that when the bridge's natural frequency is close to the natural frequency of the axle load (in this case 8.8 Hz) the axle loads reach very high values due to frequency matching. For this particular type of axle it can be seen that the impact on short span bridges is highest. Secondly, is can be seen that the axle loads for a certain range of bridge natural frequencies can reach extreme high values. In practice this is impossible because in that certain frequency range the damping of the whole system plays a role, so not only the damping of the bridge but also that of the vehicle. Also in the model the spring between the axle and the bridge can take tension forces, which is not possible in practice.

According to the fact that the bridge deck is not a static element, it seems that a vibrating bridge deck has effects on the pavement. Comparing the model for pavements on a subgrade with the model for pavements on a bridge the following conclusions can be made:

- Vibration of the deck could lead to increasing strains in the pavement due to an increasing impact of the dynamic axle loads compared to pavements on a subgrade, because of the interaction between the bridge deck and the vehicle. For fatigue cracking there is an exponential relation to the axle load, for permanent deformation there is a power relationship. When these dynamic loads on bridges reach to a higher value it might lead to non-linear behaviour of the pavement.
- Vibration of the deck could lead to a faster alternation between tensile and compressive strains in the pavement compared to pavements on a subgrade. This alternation might have influence on the fatigue behaviour.
- As mentioned before, speculations were made that vibrations could lead to weakening of the bond between the steel and the asphalt. Weakening of the bond leads to a faster deterioration of the pavement.

4 Material modelling

4.1 Introduction

It has been shown, in previous sections, that different countries have different requirements for mastic asphalt. It has also been shown that different countries use different materials of different thickness. Despite this fact, several problems are encountered in many countries. It seems that the reported problems are not associated only with inferiority of surfacing materials, but rather with a poor understanding of the behaviour of asphalt when placed on the structure.

Therefore it is believed that a non-linear material model, which can describe the rather complicated response of the asphaltic surfacings on orthotropic steel decks, is needed [Medani, 2000b]. This belief is supported by the following facts:

- Practice has shown that the existing linear models for estimation of strains in the asphalt have limited success in predicting the behaviour of the surfacings.
- The strain level in the asphalt is quite high. It is doubtful that, under such circumstances, the material will still behave linearly.
- The nature of loading in bridges is cyclic. This means that even if the stress level in the asphalt is less than the apparent strength of the material, the repetition of loading can lead to failure. The monotonic envelope shown in figure 4.1 acts as a limiting surface for the cyclic degradation mechanism. This means that during cyclic loading plastic strain accumulates, so the state of stress gradually approaches the monotonic envelope. When it touches this envelope, the material starts to degrade rapidly. Furthermore, the flexibility of the structure (vibration of the bridges) can enhance the distress process.

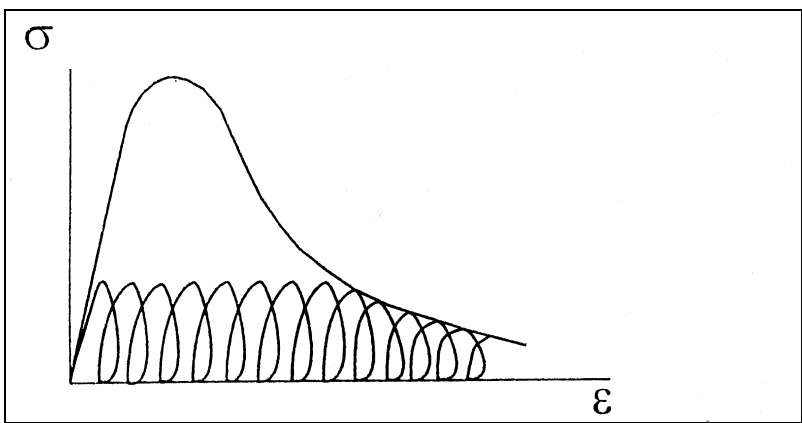


Figure 4.1: The monotonic envelope, after Medani (2000b)

- The effect of temperature changes could lead to non-linear behaviour of the asphalt.
- The vibration of the bridges and the geometry of the structure can also lead to a non-linear response of surfacing materials.
- In linear models a distinction between the response of the material in tension and compression is not possible. This implies that linear models can not correctly differentiate the modes of damage.

In the next paragraph a non-linear elastic material model will be described that can be used to describe the rather complicated asphalt behaviour. For this description use is made of parts from Erkens et al. [1998].

4.2 The material model

A model that can be used successfully to describe the non-linear asphalt behaviour is the so-called Asphalt Concrete Response (ACRe) material model. It is based on the model originally proposed by Desai [1986] and modified by Scarpas [1997]. The model describes the flow function, indicating the transition from linear elastic to inelastic (plastic) behaviour. It is defined in stress invariant space as:

$$f_D = \frac{J_2}{p_a^2} - F_b \times F_c = 0$$
 Equation 4.1

in which:

$$F_b = \left[-\alpha \left(\frac{I_1 - R}{p_a} \right)^n + \gamma \left(\frac{I_1 - R}{p_a} \right)^2 \right]$$
 Equation 4.2

$$F_c = (1 - \beta \cos 3\theta)^{-1/2}$$
 Equation 4.3

$$\cos 3\theta = 3\frac{\sqrt{3}}{2}\frac{J_3}{J_2^{\frac{3}{2}}}$$
 Equation 4.4

where:

 I_1, J_2 and J_3 are stress invariants defined as:

$$I_1 = \sigma_1 + \sigma_2 + \sigma_3$$
 Equation 4.5

$$J_{2} = \frac{1}{2} \left[(\sigma_{1} - \sigma_{2})^{2} + (\sigma_{2} - \sigma_{3})^{2} + (\sigma_{1} - \sigma_{3})^{2} \right]$$
 Equation 4.6

$$J_{3} = (\sigma_{xx} - p)(\sigma_{yy} - p)(\sigma_{zz} - p) + 2\tau_{xy}\tau_{yz}\tau_{xz} - \sigma_{xx}\tau_{yz}^{2} - \sigma_{yy}\tau_{xz}^{2} - \sigma_{zz}\tau_{xy}^{2}$$
 Equation 4.7

$$p = \frac{\sigma_{xx} + \sigma_{yy} + \sigma_{zz}}{3}$$
 Equation 4.8

and:

 σ_1 , σ_2 , σ_3 : principal stresses ρ_a : atmospheric pressure

 α , β , γ , n, θ and R : model parameters depending on material characteristics

p : isotropic stress

The function f_D indicates either the material response to a certain stress condition is elastic (f_D <0) or inelastic (f_D = 0). Elastic response means that no damage appears and inelastic response indicates the material starts to flow and thus damages. In the inelastic phase permanent deformations are introduced due to the formation of cracks and the reorientation of grains in the material.

The flow function can be plotted in the I_1 - $\sqrt{J_2}$ plane to get a two-dimensional picture. See figure 4.2.

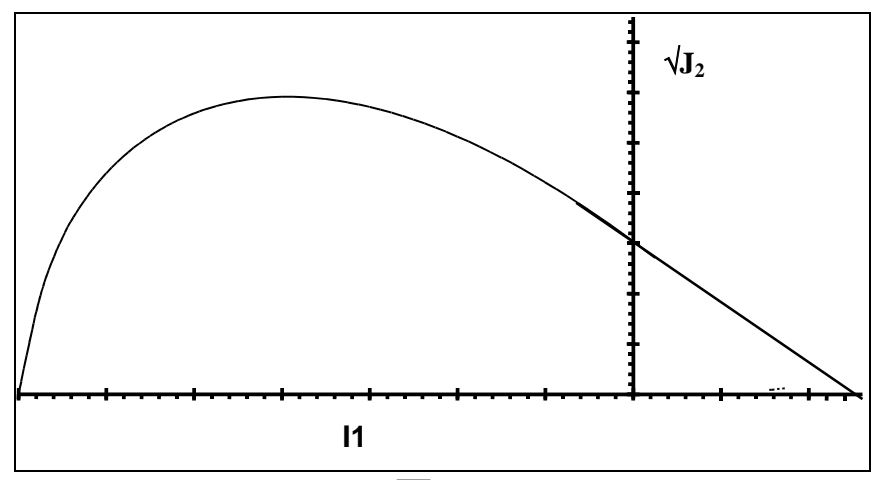


Figure 4.2: Flow surface in $I_1 / \sqrt{J_2}$ plane

The flow function in this plot is called the viscous flow surface and fulfils the stress conditions: $f_D = 0$. This condition means the material starts to flow. Elastic response means that the certain stress condition lies inside the flow surface, $f_D < 0$.

The flow surface is not a steady surface but it can grow due to hardening. This means that the stresses can still increase until peak strength. At peak strength the growth of the flow surface has reached a critical limit. At that moment the hardening stops and softening will start, meaning deteriorating of the material. In the following figure 4.3 the schematic material response in the ACRe model is shown:

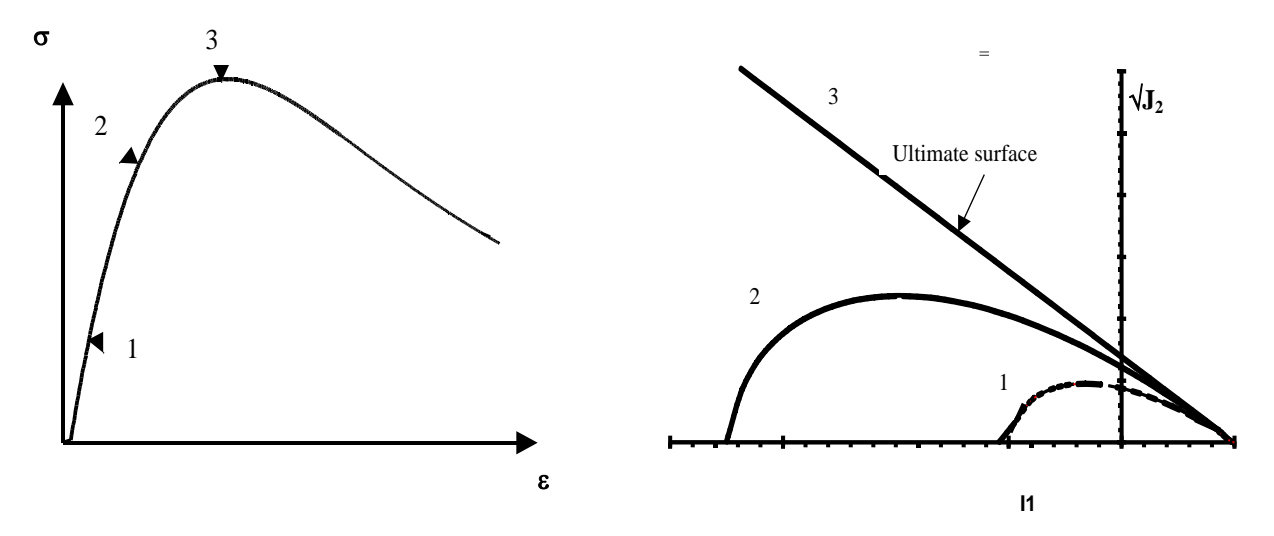


Figure 4.3: Schematic material response in ACRe model

Until point 1 the response is linear elastic. Then in point 1 and flow surface 1 the hardening phase starts and the flow surface grows. The material can resist increasing stresses, but permanent deformations are introduced. Point 2 and flow surface 2 are in the hardening phase. The flow surface grows until the critical limit, the ultimate surface, indicated as flow surface 3 and point 3 in figure 4.3 above. At that moment the material has reached its peak strength and softening starts. The deformation becomes inhomogeneous and a shear band may develop [Sitters, 1998].

4.3 Influence of the model parameters

The model parameters α , β , γ , n, θ and R all have their own specific influence on the model. In this paragraph their influence will be explained.

Influence of α

"The model parameter α determines the size of the flow surface, the size increases with decreasing α so this parameter controls the hardening of the material. For elastic states of stress it retains its original value, but as soon as non-linear states of stress occur, α decreases until α =0 at peak stress, when the hardening stops (figure 4.4).

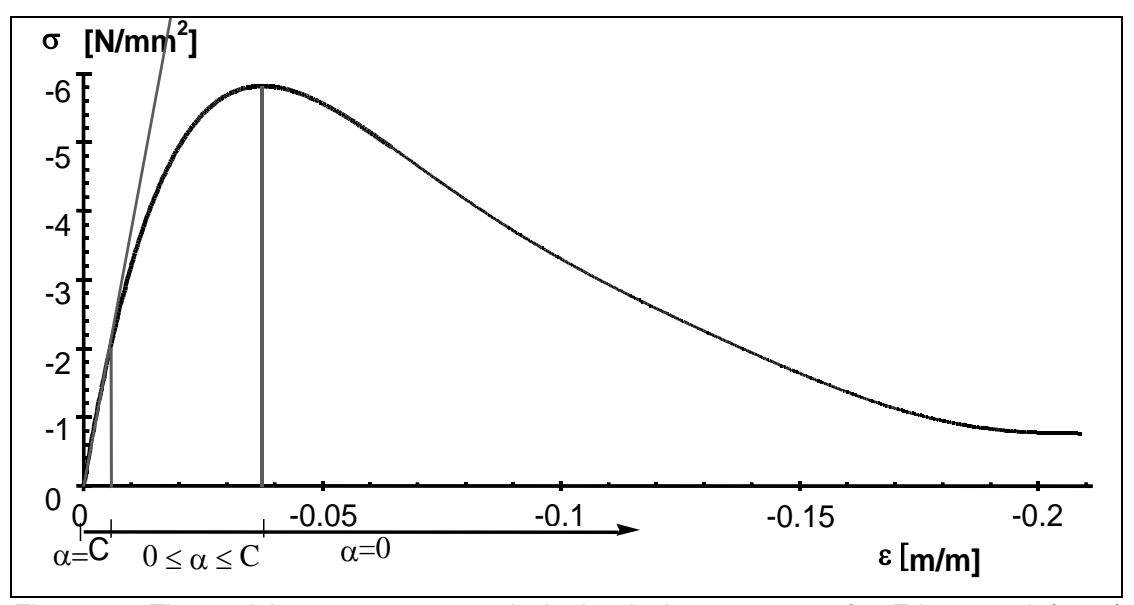


Figure 4.4: The model parameter α controls the hardening response, after Erkens et al. (1998)

The influence of α on the size of the flow surface is shown in figure 4.5. At peak stress, for α =0, the surface reduces to a straight line at the I₁ - $\sqrt{J_2}$ surface" [Erkens et al., 1998, 50, 51].

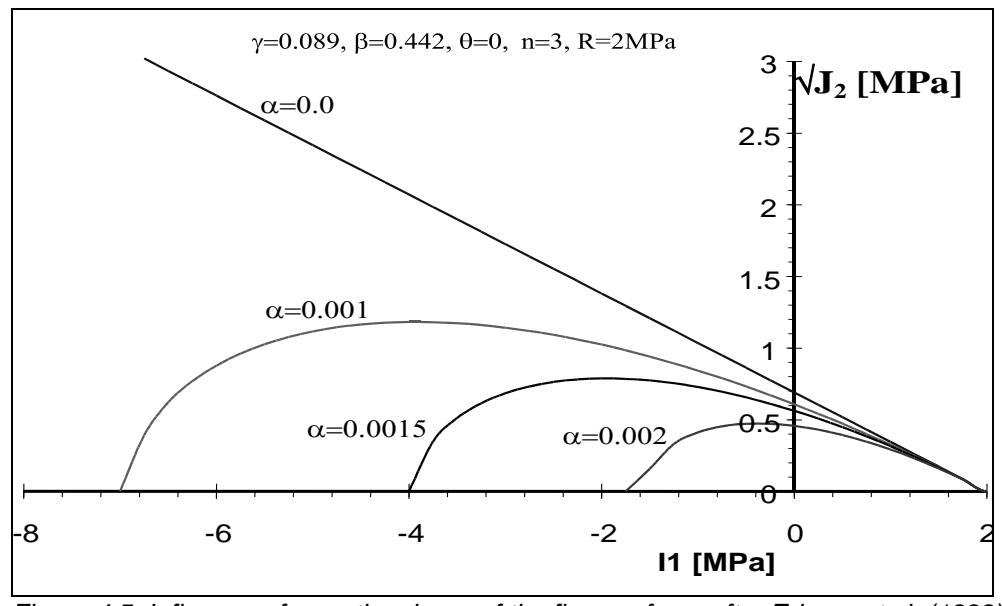


Figure 4.5: Influence of α on the shape of the flow surface, after Erkens et al. (1998)

Influence of β and θ

"The model parameter β determines the shape of the model on the π -plane¹. For β =0 it is circular and with increasing β it becomes triangular. Since cos(3 θ) is 1 for uniaxial states of stress, the square root term in equation 4.3 reduces to: $\sqrt{(1-\beta)}$. The effect of uniaxiality on θ is:

$$\cos(3\theta) = 1 \Rightarrow \theta = 0 + k\frac{2}{3}\pi \Rightarrow \theta = \left(0, \frac{2}{3}\pi \text{ or } \frac{4}{3}\pi\right) + 2k\pi$$
 with k=1,2,3.... Equation 4.9

These values of θ correspond to the position of the σ_1 , σ_2 and σ_3 axes on the π -plane¹, indicating that uniaxial test results are related to a state of stress where two principal stresses are zero and the third is not. The shape of the cross section is determined by the multiaxial state of stress (figure 4.6)" [Erkens et al., 1998, 53].

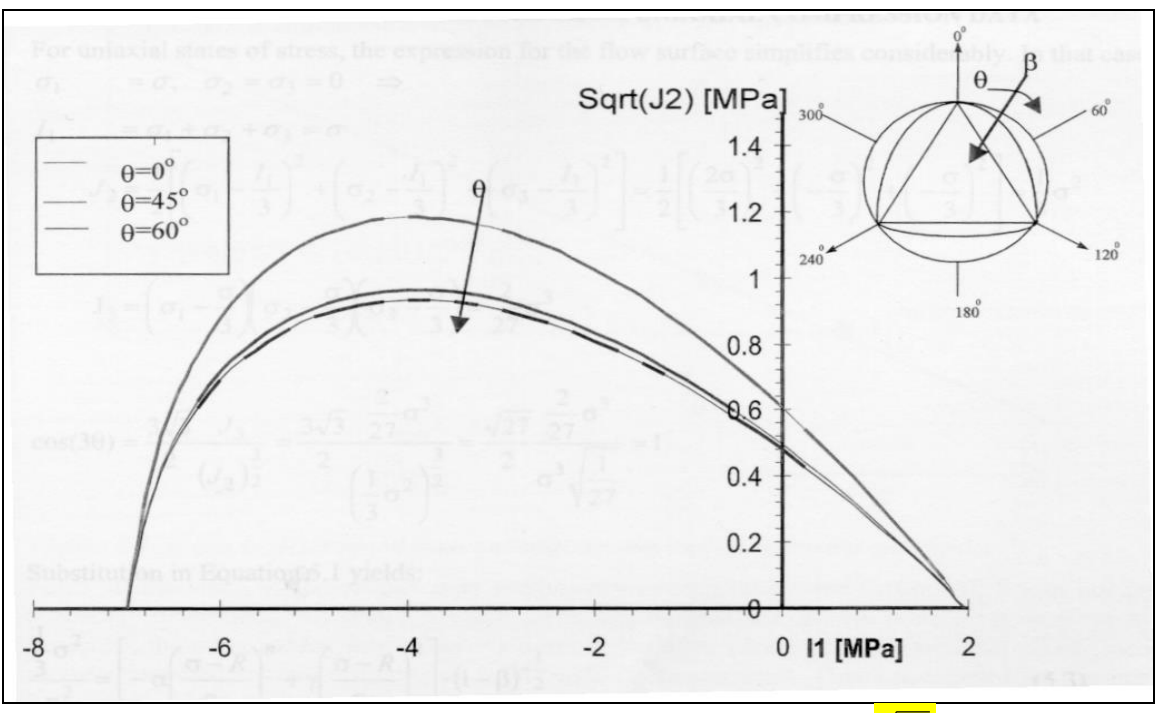


Figure 4.6: Influence of β and θ on the flow surface plotted in the I_1 - $\sqrt{J_2}$ and π -plane, after Erkens et al. (1998)

_

¹ The π -plane is the plane perpendicular to the isotropic stress axis ($\sigma_1 = \sigma_2 = \sigma_3$) which passes through the origin in the principal stress space. Any state of stress can be described by cylinder co-ordinates using its projection on the π -plane. These co-ordinates are the distance from the original point to its projection along the isotropic stress axis ($\xi = l_1/3$), the distance from the origin to the projection ($r = \sqrt{(2J_2)}$) and the angle between r and the σ_1 axis (θ). The advantage of this representation of the state of stress is that it immediately separates the influence of the isotropic stresses, which cause volume changes, and the deviatoric stresses, which cause distortion.

Influence of γ

"The model parameter γ determines the slope of the (ultimate) surface, the slope increases with increasing γ . It is stress-state independent (does not change during a test), but it can vary as a function of, for example, temperature and loading rate (figure 4.7) [Erkens et al., 1998, 52].

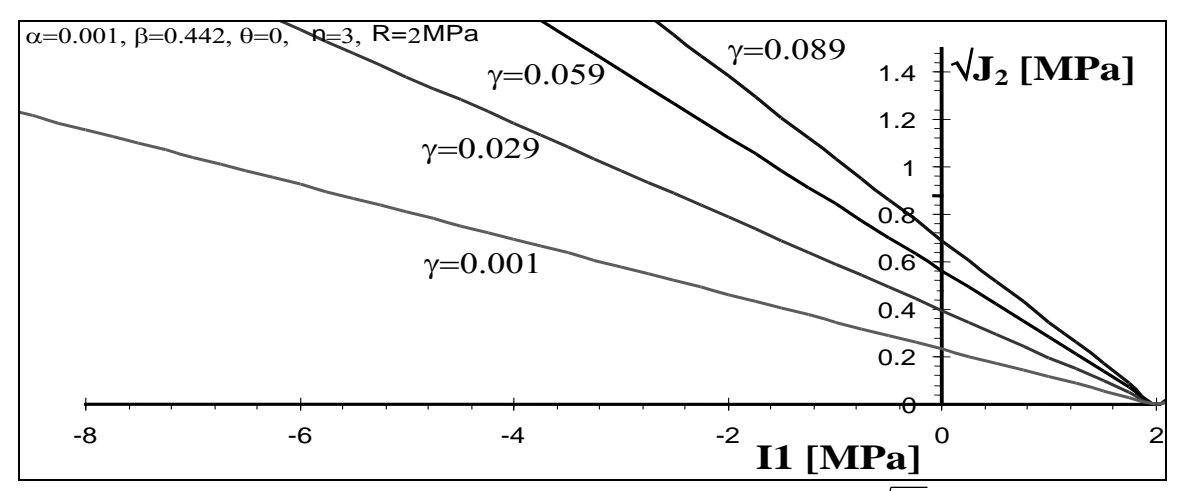


Figure 4.7: Influence of γ on the shape of the flow surface, plotted in I1 - $\sqrt{J_2}$ space, after Erkens et al. (1998)

Influence of n

"The model parameter n determines the apex of the surface, it expresses the state of stress after which the material starts to dilate. The apex is defined as that point of the flow surface where the tangent is a horizontal line ($\delta f/\delta l_1=0$, see figure 4.8), indicating a fully deviatoric state of stress" [Erkens et al., 1998, 52, 53].

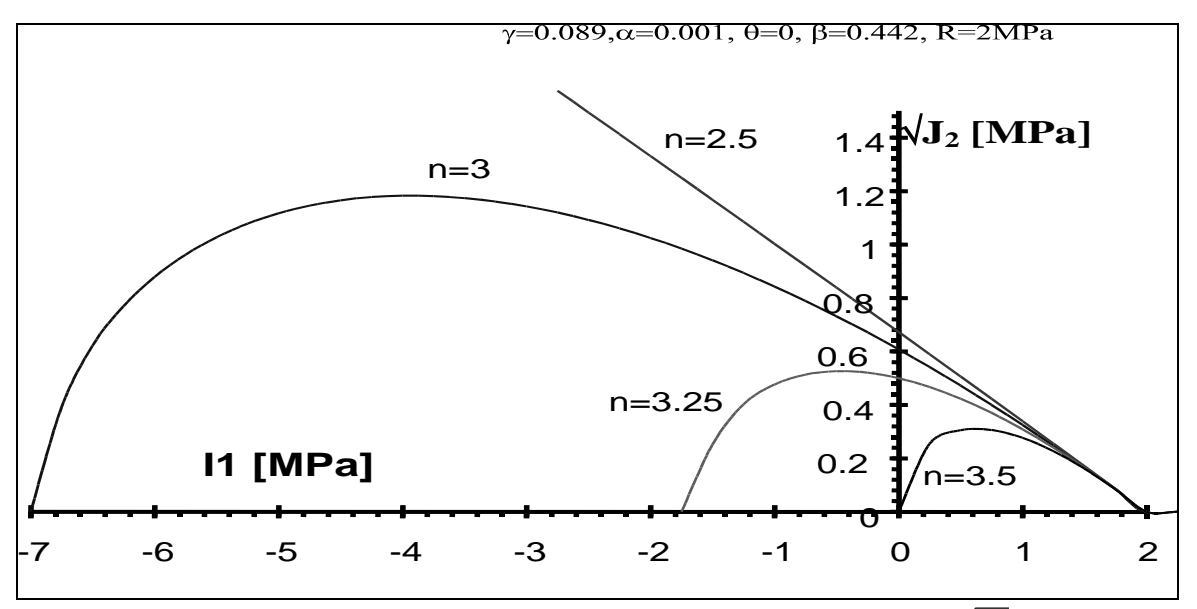


Figure 4.8: Influence of n on the shape of the flow surface, plotted in the I_1 - $\sqrt{J_2}$ space, after Erkens et al. (1998)

The stress conditions at the start of dilation can be determined when a plot is made of the axial versus the volumetric strain and a plot of the axial strain versus axial stress. The material starts to dilate at minimum volumetric strain.

Influence of R

"R is the three dimensional tensile strength, which is an indication of cohesion. For cohesionless materials R=0, which means that that only states of stress for which $I_1 \le 0$ are possible within that material. For increasing R values, the flow surface moves in the direction of the positive I_1 axis (figure 4.9)" [Erkens et al., 1998, 54].

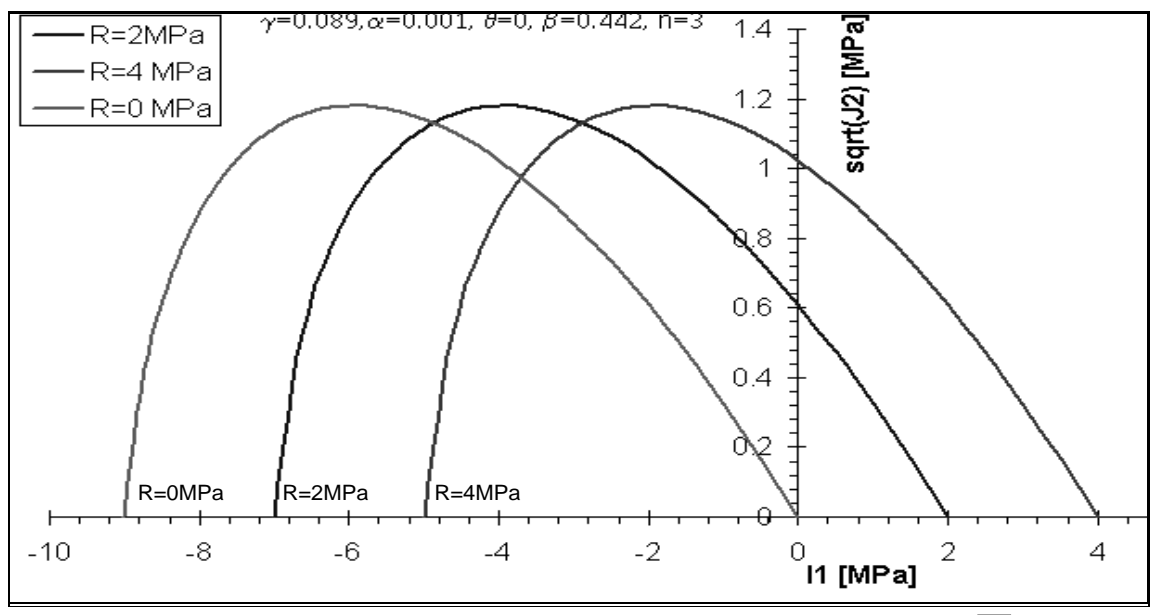


Figure 4.9: Influence of R on the shape of the flow surface plotted in the I_1 - $\sqrt{J_2}$ space, after Erkens et al. (1998)

4.4 Tests to determine the model parameters

To determine the parameters for the ACRe-model, a couple of tests were specified [Scarpas et al., 1997]. These tests are:

- Uniaxial monotonic compression test
- Uniaxial monotonic tension test
- Four point shear test

To get a clear relation between the state of stress and the material response, tests are needed in which the state of stress is uniform throughout the specimen. For this reason triaxial tests can be used, but these tests have the disadvantage that they are rather expensive in relation to the area of response. Therefore uniaxial tension and compression tests were chosen to be the basic tests for parameter determination. By using these tests not all the parameters can be determined. For example, these tests give no information about the parameter β . Therefore additional multi-axial testing is required, the four point shear test. When these tests can not be done, β is often assumed to be zero.

In this research only the uniaxial monotonic compression and uniaxial monotonic tension tests are carried out. The shear test set up was under development at the moment of writing this thesis, so it could not be used in this project. Therefore β is assumed to be zero.

5 Experimental program

5.1 Introduction

An experimental program has been designed to characterise the mastic asphalt mix which was used for resurfacing the Moerdijk bridge in June 2000. This asphalt mix will be referred to as the "Moerdijk mix". The experimental program included:

- 1. Density measurements.
- 2. Four point bending beam test for:
 - Determination of the master curves,
 - · Determination of the fatigue characteristics.
- 3. Uniaxial monotonic compression test.
- 4. Uniaxial monotonic tension test.

After the determination of the master curves and the fatigue characteristics of the mix the dependency of the mix stiffness on the strain became obvious. Therefore, an additional testing program to investigate this phenomenon has been designed. This additional testing program included four point bending beam tests at different strain levels, temperatures and loading frequencies. Because of the fact that there were no sufficient specimens to carry out the program, it has been decided to get specimens from slabs that had been obtained while surfacing the Lintrack test bridge at the TU Delft. This asphalt mix is referred to as the "Lintrack mix".

It has also been decided to retest the specimens from the Moerdijk mix 2.5 months after the first series of fatigue tests, to determine the master curves and fatigue characteristics again.

5.2 Mix composition

Both the Moerdijk mix and the Lintrack mix have the same mix composition. The mastic asphalt mix consists of stone 2/8 and 2/6 in the ratio 1:1, river sand and fine sand in the ratio 2:3, weak limestone filler and SBS modified bitumen with a pen of 90. The mix composition is shown in table 5.1:

Table 5.1: Mix composition

Materials		Percentage %m/m	
Passing	Retained	targeted	Tolerance
C11.2	C8	0	+2.0
C8	2 mm	52.0	±5.0
2 mm	63 μm	26.0	±5.0
63 μm	·	22.0	±2.0
Bitumen on 100	0% (by mass)	8.8	±0.5

5.3 Specimen preparation

While resurfacing the Moerdijk bridge, which took place in June 2000, three slabs of dimensions ≈600x600x70 mm³ have been obtained (see figure 5.1).



Figure 5.1: Preparation of the slabs

From these slabs the following specimens have been obtained:

• 8 beams for the determination of master curves and the fatigue characteristics using the four-point bending test. The beams have been sawn from the slabs in the following way. First the edges of the slab have been cut off. After that the beams have been sawn at their desired length of 450mm. Next the top and bottom of each beam has been cut off in order to avoid edge effects and to give the specimens dimensions of ≈450x50x50mm (length x width x height). Table 5.2 shows the average dimensions of each specimen. The height, width and length of the beams have been measured at four positions (see appendix A). From these four values the average has been taken.

Table 5.2: Average	dimensions of the	he specimens t	for the four	-point bendina test

Specimen	Height [mm]	Width [mm]	Length [mm]
1	50.6	52.8	450
2	51.0	52.9	449
3	51.6	52.2	449
4	51.4	52.6	450
5	51.0	53.0	450
6	50.8	53.1	450
7	50.9	52.8	450
8	50.9	52.9	450
Average	51.0	52.8	449.8
STDEV	0.3	0.3	0.5
Variation [%]	0.6	0.5	0.1

• 13 cores for the tension and 13 cores for the compression tests. First beams were sawn from the slabs with a width of approximately 100mm. From each beam 10 cores were horizontally drilled, with a height of 100 mm and a diameter of 50 mm. After drilling some of the cores were polished to a height of approximately 90mm and some to 100mm to get parallel surfaces. Table 5.3 shows the average dimensions of the specimens for the compression tests. At four positions the dimensions have been measured after which the average has been taken. Appendix A shows the results from the four measurements.

Table 5.3: Dimensions of the specimens for the monotonic compression test

Specimen	Height [mm]	Diameter [mm]
M4-3	90.1	49.8
M11-4	100.1	49.8
M5-3	90.1	49.8
M4-4	89.9	50.0
M3-10	89.8	49.8
M2-5	90.2	49.9
M11-3	100.2	50.0
M6-4	99.6	49.7
M7-4	100.1	50.1
M9-2	100.3	49.8
M10-2	100.3	49.8
M10-10	100.3	49.8
M6-6	100.1	49.8
Average	96.2	49.9
STDEV	5.1	0.1
Variation [%]	5.3	0.2

The height shows a quite large variation because specimens are tested with a height of approximately 100mm and specimen with a height of approximately 90mm. This difference is a result of additional polishing to some of the specimen.

The dimensions of the specimens for the tension tests have been measured at four positions after which the average is taken. Table 5.4 shows the average results. Appendix A shows the results for the four measurements.

Table 5.4: Dimensions of the specimens for the monotonic tension test

Specimen	Height [mm]	Diameter [mm]
M11-5*	89.4	49.9
M2-1*	89.1	49.8
M11-8	90.9	49.6
M2-3	89.0	49.8
M3-9	90.3	50.0
M3-1	90.0	50.0
M1-10*	89.3	49.7
M3-7	90.2	49.6
M5-2	90.1	49.9
M3-4	90.0	49.9
M2-4	90.0	49.7
M4-7	90.0	49.9
M1-3	90.0	49.5
Average	89.9	49.8
STDEV	0.53	0.16
Variation [%]	0.59	0.32

In table 5.4 three specimen are marked with *. On these specimens 2 PVC rings (h=8 mm) were glued to prevent the specimen from cracking in the glue layer between the steel cap and the specimen. These PVC rings reduced the height of the specimens by 16 mm.

While surfacing the Lintrack test bridge several slabs have been casted. 46 beams have been sawn from four of the slabs in the same way as described for the beams of the Moerdijk mix. However, these beams have dimension of \approx 420x50x50mm (length x width x height). These beams have been used for the determination of the strain dependent behaviour of the mix stiffness.

Table 5.5 shows the average dimensions of the specimens. The height, width and length of the beams have been measured at four positions (see appendix A). From these four values the average has been taken.

Table 5.5: Dimensions of the specimens for determining the stress dependent behaviour

	s of the specimens for		
Specimen	Height [mm]	Width [mm]	Length [mm]
ML/4pb/1/1	50.5	50.4	420
ML/4pb/1/2	50.4	50.1	420
ML/4pb/1/3	50.4	50.7	420
ML/4pb/1/4	50.5	50.6	421
ML/4pb/1/5	50.4	51.1	422
ML/4pb/1/6	50.6	52.5	421
ML/4pb/1/7	52.6	50.5	422
ML/4pb/1/8	50.7	50.6	421
ML/4pb/1/9	50.6	51.0	422
ML/4pb/1/10	50.4	51.1	421
ML/4pb/2/1	49.6	52.1	420
ML/4pb/2/2	49.4	50.5	420
ML/4pb/2/3	49.2	49.0	420
ML/4pb/2/4	49.2	53.8	420
ML/4pb/2/5	49.2	55.0	420
ML/4pb/2/6	49.5	56.5	420
ML/4pb/2/7	49.3	51.9	420
ML/4pb/2/8	49.2	52.7	420
ML/4pb/2/9	49.1	52.5	421
ML/4pb/2/10	49.2	51.0	421
ML/4pb/3/1	50.5	50.5	421
ML/4pb/3/2	50.5	50.4	422
ML/4pb/3/3	50.6	50.7	422
ML/4pb/3/4	50.2	50.6	422
ML/4pb/3/5	49.9	49.8	422
ML/4pb/3/6	49.7	49.6	422
ML/4pb/3/7	50.2	49.2	422
ML/4pb/3/8	50.4	49.6	422
ML/4pb/3/9	50.6	49.9	422
ML/4pb/3/10	50.7	50.5	422
ML/4pb/4/1	50.3	50.5	420
ML/4pb/4/2	50.7	50.8	421
ML/4pb/4/3	50.7	50.4	421
ML/4pb/4/4	50.7	51.0	421
ML/4pb/4/5	50.7	50.4	421
ML/4pb/4/6	50.8	50.2	422
ML/4pb/4/7	50.6	49.9	422
ML/4pb/4/8	50.7	50.1	421
ML/4pb/4/9	50.4	49.8	422
ML/4pb/4/10	50.6	50.9	421
Average	50.2	51.0	421.1
STDEV	0.7	1.5	0.8
Variation [%]	1.4	2.9	0.2

Before testing the beams and cores have been stored at 13°C in a box filled with a bed of sand to avoid deformations of specimens.

5.4 Density measurements

The density of all the asphalt specimens were determined according to the Dutch Standard [CROW, 2000] using the "weighing under-water procedure" described briefly as follows:

- 1. Obtain the dry weight of the specimen (m_{dry})
- 2. Soak the specimen in water for at least 3 minutes
- 3. Obtain the weight of the specimen under water (m_{under})
- 4. Remove the suspended water particles using a wet towel and then obtain the weight (m_{wet})
- 5. Measure the water temperature.

The density of the specimen (ρ_{sp}) can be determined by using:

$$ho_{sp} = rac{m_{dry}.
ho_w}{m_{wet} - m_{under}}$$
 Equation 5.1

where:

 $\rho_{sp} = \text{specimen density } [kg/m^3]$ $m_{dry} = \text{dry mass specimen } [g]$ $m_{wet} = \text{wet mass specimen } [g]$ $m_{under} = \text{mass specimen under water } [g]$ $\rho_w = \text{density of water } [kg/m^3]$

The density of the mix (ρ_{mix}), for $m_s+m_z+m_f+m_d=100\%$, is calculated with:

$$\rho_{mix} = \frac{100}{\frac{m_s}{\rho_s} + \frac{m_z}{\rho_z} + \frac{m_f}{\rho_f} + \frac{m_b}{\rho_b}}$$
 Equation 5.2

in which:

 m_s = mass percentage stone [%m/m]

 m_z = mass percentage sand [%m/m]

 m_f = mass percentage filler [%m/m]

 m_b = mass percentage bitumen [%m/m]

 ρ_s = density of the stone [kg/m³]

 ρ_z = density of the sand [kg/m³]

 ρ_f = density of the filler [kg/m³]

 ρ_b = density of the bitumen [kg/m³]

With the specimen density and the mix density the percentage of air voids in the specimen is calculated with:

$$V_a = rac{
ho_{mix} -
ho_{sp}}{
ho_{mix}}$$
 Equation 5.3

where:

 V_a = percentage voids [%] ρ_{mix} = density of the mix [kg/m³] ρ_{sp} = density of the specimen [kg/m³] The filler, bitumen, sand and stone content for the mix without voids is calculated with:

$$V_f = \frac{m_f}{\rho_f} \times \rho_{mix}$$
 Equation 5.4

$$V_b = \frac{m_b}{\rho_b} \times \rho_{mix}$$
 Equation 5.5

$$V_z = \frac{m_z}{\rho_z} \times \rho_{mix}$$
 Equation 5.6

$$V_s = \frac{m_s}{\rho_s} \times \rho_{mix}$$
 Equation 5.7

in which:

 V_f = Filler content in the mix without voids [%V/V]

 V_b = Bitumen content in the mix without voids [%V/V]

 V_z = Sand content in the mix without voids [%V/V]

 V_s = Stone content in the mix without voids [%V/V]

The contents in the mix inclusive voids are calculated with:

$$V_f' = \frac{m_f}{\rho_f} \times \rho_{sp}$$
 Equation 5.8

$$V_b^{'} = \frac{m_b}{\rho_b} \times \rho_{sp}$$
 Equation 5.9

$$V_z' = \frac{m_z}{\rho_z} \times \rho_{sp}$$
 Equation 5.10

$$V_s' = \frac{m_s}{\rho_s} \times \rho_{sp}$$
 Equation 5.11

in which:

 V_f' = Filler content in the mix with voids [%V/V]

 V_b ' = Bitumen content in the mix with voids [%V/V]

 V_z ' = Sand content in the mix with voids [%V/V]

 V_s ' = Stone content in the mix with voids [%V/V]

The void content in the mineral aggregate without bitumen is calculated with:

$$V_a^{'} = V_a + V_b^{'}$$
 Equation 5.12

in which:

 $V_a' = \text{Void content in the mineral aggregate without bitumen } [\%\text{V/V}]$

The degree of filling is determined with:

$$D_f = 100 \times \frac{V_b'}{V'}$$
 Equation 5.13

in which:

 D_f = Degree of filling [%]

The results of the density measurements are shown in the tables 6.2-6.5 in chapter 6.

5.5 Four point bending test

5.5.1 Test set up

Figure 5.2 shows the Universal Testing Machine (UTM) testing equipment, manufactured by the Industrial Process Controls Limited (IPC) in Melbourne, Australia. The mechanism allows for free translation and rotation of the clamps. Pneumatic actuators at the ends of the beam center it laterally and clamp it. The load is applied through the piston rods to the beam specimen, 400 mm long with a width and depth not exceeding 63.5 mm. The pneumatic testing machine is capable of applying loads in the form of sine or haversine waves for 0.1-2 s duration with 0-10 s rest periods. Servo-motor driven clamps secure the beam at four points. Adjustable stops nuts installed on the loading rods prevent the beam from bending below the initial horizontal position during the rest period. The dynamic deflection of the beam at the midspan is measured with a linear variable differential transformer (LVDT). The repeated flexure apparatus is enclosed in a controlled temperature cabinet.

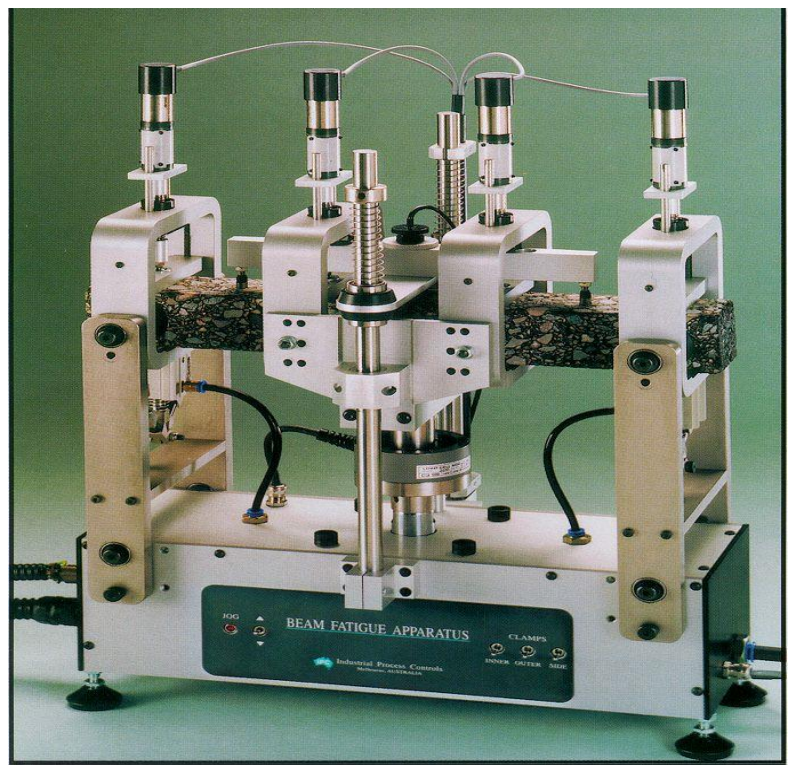


Figure 5.2: The four point bending beam fatigue testing equipment

5.5.2 Survey of the four point bending testing program

For the first and repeated determination of master curves and fatigue characteristics 8 specimens of the Moerdijk mix were used. For the repeated determination of master curves two strain levels were used, namely 80 μ m/m to investigate the effect of healing and 800 μ m/m to investigate the strain dependency of the mix stiffness. Figure 5.3 shows a survey of the four point bending tests that were carried out on the Moerdijk mix.

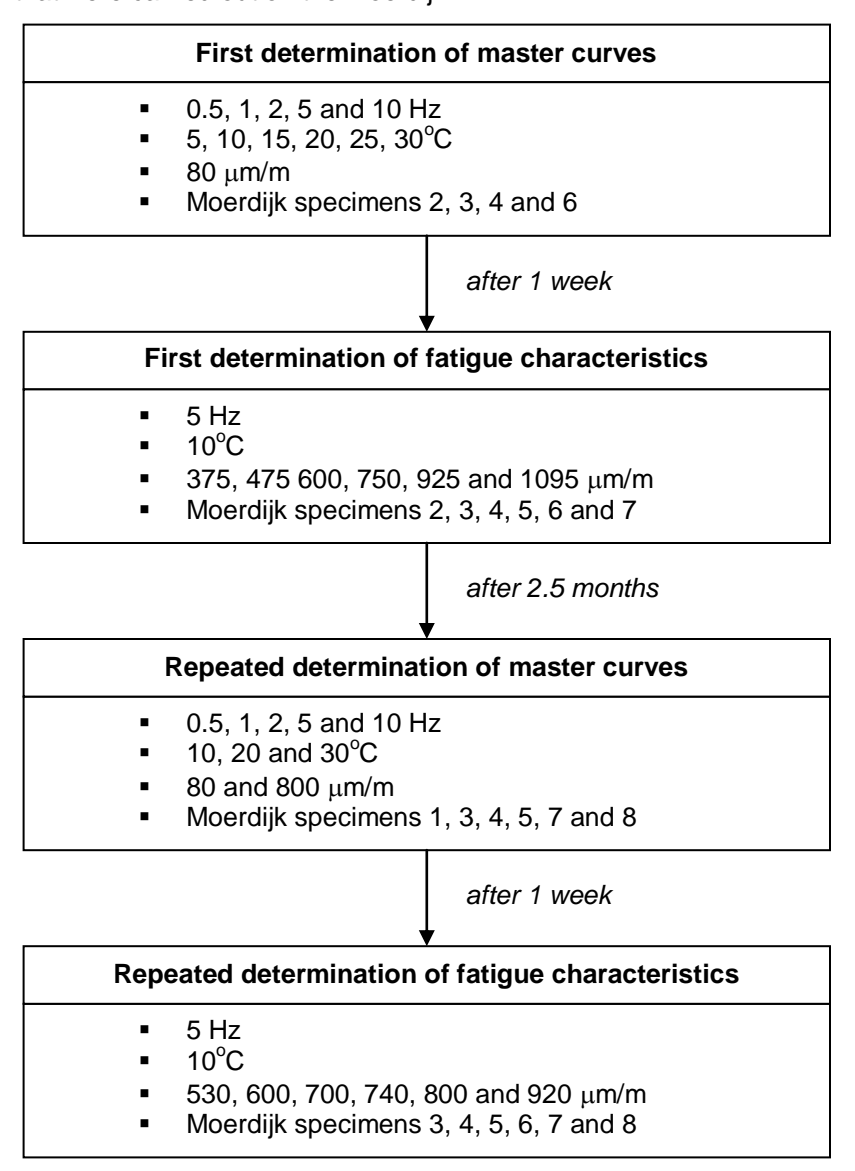


Figure 5.3: Survey of the four-point bending testing program carried out on the Moerdijk mix

From the repeated determination of master curves the strain dependency of the mix stiffness became obvious. However, due to a lack of specimens the repeated determination of master curves took place at only 3 temperatures, namely 10, 20 and 30°C. Therefore it was decided to carry out a more extensive testing program to investigate the strain dependency of the mix stiffness. For this program use is made of specimen from the Lintrack mix.

Figure 5.4 shows an overview of the four point bending testing program on the Lintrack mix.

Determination of the strain dependency of the mix stiffness

- 0.5, 1, 2, 5 and 10 Hz
- 5, 12.5, 20, 27.5, 35 and 42.5°C
- 80, 200, 600 and 1000 μm/m
- 46 Lintrack specimens

Figure 5.4: Survey of the four-point bending testing program carried out on the Lintrack mix

5.5.3 Input for the four point bending fatigue testing machine

5.5.3.1 Test conditions for the first determination of master curves

The test conditions that were used for determining the master curves are:

Type of test: displacement controlled
Frequencies: 0.5, 1, 2, 5 and 10 Hz
Temperatures: 5, 10, 15, 20, 25 and 30°C

Strain: 80 μm/m
Loading wave: sine
Poisson's ratio: 0.3

- Specimen nrs: 2, 3, 4 and 6

The stiffness is measured after 100 pulses. The results of the first determination of master curves are shown in paragraph 6.2.2.

5.5.3.2 Test conditions for the repeated determination of master curves

After 2.5 months it was decided to determine the master curves again at two strain levels, namely 80 and 800 μ m/m. Therefore the specimens are used that were tested before in the fatigue test. The test conditions are:

Type of test: displacement controlled
 Frequencies: 0.5, 1, 2, 5 and 10 Hz
 Temperatures: 10, 20 and 30°C
 Strain amplitude 80 and 800 μm/m

Loading wave: sinePoisson's ratio: 0.3

- Specimen nrs: 1, 3, 4, 5, 7 and 8

The stiffness is also measured after 100 pulses. Paragraph 6.2.3 contains the results from the repeated determination of master curves.

5.5.3.3 Test conditions for the first determination of the fatigue behaviour

The test conditions that were used for determining the fatigue behaviour are:

- Type of test: displacement controlled

Frequency: 5 HzTemperatures: 10°C

- Strain amplitude: 375, 475, 600, 750, 925 and 1095 μm/m

Loading wave: sinePoisson's ratio: 0.3

- Specimen nrs: 2, 3, 4, 5, 6 and 7

The number of load repetitions to failure is determined when the initial stiffness is halved. Paragraph 6.3.1 contains the results from the first determination of the fatigue characteristics.

5.5.3.4 Test conditions for the repeated determination of the fatigue behaviour

After the repeated determination of the master curves it was decided to repeat the fatigue tests also, one week after the repeated determination of master curves. The test conditions are:

- Type of test: displacement controlled

Frequency: 5 HzTemperatures: 10°C

- Strain amplitude: 530, 600, 700, 740, 800 and 920 μm/m

- Loading wave: sine

Poisson's ratio: 0.3
 Specimen nrs: 3, 4, 5, 6, 7 and 8

The number of load repetitions to failure is determined when the initial stiffness is halved. The results from the repeated determination of the fatigue characteristics are shown in paragraph 6.3.2.

5.5.3.5 Test conditions for the determination of the strain dependency of the mix stiffness

After the first series of fatigue tests the strain dependency of the mix stiffness became obvious. Therefore it was decided to determine the strain dependency of the mix stiffness by additional testing. The test conditions of this additional testing are:

Type of test: Displacement controlled
 Frequencies 0.5, 1, 2, 5 and 10 Hz

- Temperatures 5, 12.5, 20, 27.5, 35 and 42.5°C - Strain amplitudes: 80, 200, 600 and 1000 μm/m

- Loading wave: sine wave

- Specimen nrs: ML/4pb/1/1-Ml/4pb/1/10

ML/4pb/2/1-Ml/4pb/2/10 ML/4pb/3/1-Ml/4pb/3/10 ML/4pb/4/1-Ml/4pb/4/6

The stiffness is also measured after 100 pulses.

5.5.4 Output for the four point bending fatigue testing machine

The following tabulated data is calculated and displayed on the screen and written in a file:

- Test loading time (hours, minutes and seconds)
- Applied load
- Beam deflection
- Tensile stress and strain
- Core and skin temperature of a dummy specimen
- Phase angle
- Loading cycle count
- Flexural stiffness
- Modulus of elasticity
- Dissipated energy
- Cumulative dissipated energy

5.5.5 Data calculations in the four point bending test

The calculations performed by the computer are based on the equations displayed in this paragraph.

The maximum tensile stress is calculated with:

$$\sigma_{t} = 3000 \frac{aP}{wh^{2}}$$
 Equation 5.14

Where:

 σ_t : maximum tensile stress [kPa]

a: distance between reaction and load clamps (typically 118.5 mm)

P: peak force [N]
w: beam width [mm]
h: beam height [mm]

The maximum tensile strain is calculated with:

$$\varepsilon_t = \frac{12\delta h}{23a^2}$$
 Equation 5.15

Where:

ε_t: maximum tensile strain [mm/mm]

δ: peak deflection at centre of beam [mm]

Flexural stiffness:

$$S = \frac{\sigma_{t}}{1000\varepsilon_{t}}$$
 Equation 5.16

Where:

S: flexural stiffness [MPa]

Modulus of elasticity:

$$E = \frac{Pa}{\delta wh} \left[\frac{23a^2}{4h^2} + k(1+v) \right]$$
 Equation 5.17

Where:

E: modulus of elasticity [MPa]

k: actual shear stress divided by average shear stress (assumed 1.5 N/mm²)

v: oisson's ratio

The results obtained by means of the four point bending test are reported in chapter 6.

5.6 Optimisation of the tension and compression experimental program

5.6.1 Introduction

For the determination of the effects of more than one variable a researcher usually designs a simple comparative experiment to determine the effects of the different variables. This procedure is extremely insufficient. For example in this experimental program the range of interest for temperatures is 0-40°C and for the deformation rate 0.01-10 mm/s. Using the normal procedure this means that tests are done at 3 temperatures (0, 20 and 40°C) and 4 loading rates (0.01, 0.1, 1.0 and 10 mm/s). To get representative results each combination is repeated 4 times. For this example this means that the number of tests to be carried out is 3x4x4=48. However, with a properly designed experiment, the same or better information can be obtained with as few as 13 trials. This means much less testing and a saving of specimens of 73%. To achieve this, use is made of a "central composite rotatable design" [Robinson, 2000].

5.6.2 Procedure for the central rotatable design

The central rotatable experimental design technique was chosen. The procedure is described below.

- 1. At first the range of interest is determined. For the compression test the range of interest for the speed is 0.01-10 mm/s and for the temperature 0-40°C. The tension tests are carried out in a temperature range of 0-43.6°C and a speed range of 0.01-5 mm/s.
- 2. The general design of the trials to be conducted is expressed in coded terms in table 5.6 below:

Table 5.6: Coded test conditions

Trial	V_{coded}	T_{coded}
1	-1	-1
2	+1	-1
3	-1	+1
4 5	+1	+1
5	-ψ	0
6	–ψ +ψ	0
7	0	-ψ
8	0	-ψ +ψ
9	0	0
10	0	0
11	0	0
12	0	0
13	0	0

The test conditions are also shown in a graphical form (figure 5.5).

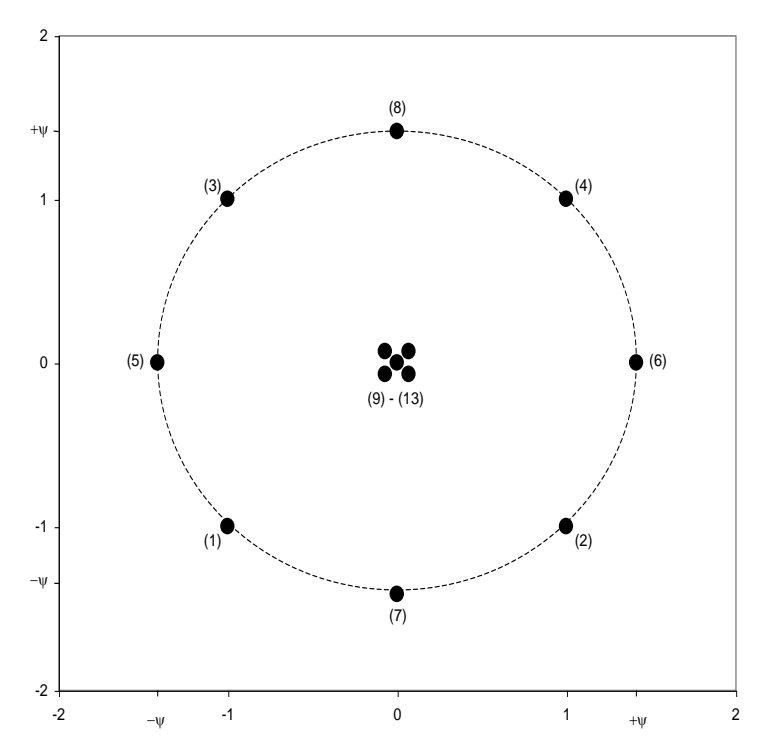


Figure 5.5: Coded test conditions for the central composite rotatable design

This figure shows that 5 tests are repeated in the centre of the range of interest (trials 9-13) and further there are 8 tests at rotatable positions around this centre.

3. Any value may be used for ψ , and there may be any number of replicated points in the centre. However, the experimental design will have special properties (rotatable design) if the value of ψ is set at 1.4142. It is recommended by Robinson [2000] to use 5 central points with 2 variables. In that case the trials 9-13 all have the same distance to the 5 centre points, which results in measurements that are evenly spread over the range of interest. Trials 5-8 are called star points of the design and trials 9-13 are called centre points. To scale the coded terms of table 5.6 into values within the range of interest, ψ =1.4142 is set equal to half the ranges of the variables and the scaling factors for the compression tests follow from:

$$1.4142V_{scaling} = (V_{\text{max}} - V_{\text{min}}) \times \frac{1}{2}$$
 Equation 5.18

$$1.4142T_{scaling} = (T_{\text{max}} - T_{\text{min}}) \times \frac{1}{2}$$
 Equation 5.19

in which:

 $\begin{array}{lll} \textit{V}_{\textit{scaling}} & : & \text{Scaling factor for the loading rate} \\ \textit{T}_{\textit{scaling}} & : & \text{Scaling factor for the temperature} \\ \textit{V}_{\textit{min}} : & : & \text{Minimum loading rate [mm/s]} \\ \textit{V}_{\textit{max}} & : & \text{Maximum loading rate [mm/s]} \\ \textit{T}_{\textit{min}} & : & \text{Minimum test temperature [°C]} \\ \textit{T}_{\textit{max}} & : & \text{Maximum test temperature [°C]} \\ \end{array}$

Finally the experimental values of the loading speed V and the temperature T follow from:

$$V = V_{coded} \times V_{scaling} + \frac{1}{2} \times \left(V_{\max} + V_{\min}\right)$$
 Equation 5.20
$$T = T_{coded} \times T_{scaling} + \frac{1}{2} \times \left(T_{\max} + T_{\min}\right)$$

5.7 Uniaxial monotonic compression test

5.7.1 Compression test set up

"The compression test set-up consists of a 3D-space frame in which an MTS 150kN hydraulic actuator is mounted. The actuator is connected rigidly to the upper loading plate. The frame itself is placed on an elastically supported concrete block. On the lower part of the frame a pedestal is constructed to which the bottom plate is connected. The bottom and top plate are kept parallel by means of three massive (Φ 16 mm) bars which are connected to the bottom plate and pass through linear bearings in the top plate. A cabinet is placed within the frame, which allows the tests to be performed at specific temperatures. Inside the temperature cabinet are the transducers, which register the radial and axial deformations of the specimen, as well as the applied force [Erkens, 1998, 18]". A picture from the compression test set-up inside the temperature cabinet with an inserted specimen is shown in figure 5.6.



Figure 5.6: Picture from the compression test set-up inside the temperature cabinet

The axial deformation is registered by means of three displacement transducers (LVDT's). The radial deformation is measured by means of two circumferential measurement systems. An extensometer measures the first part of the radial deformation, a string measures the second part. Figure 5.7 shows a close-up from a specimen inserted in the compression test set-up. At the left side of the picture one of the LVDT's can be seen. Also very clear are the two circumferential measurement systems, namely the extensometer (chain) and the string. The picture also shows the friction reduction system on top and under the specimen.



Figure 5.7: Close-up from a specimen inserted in the compression test set-up

The force is measured by means of a load cell, which is positioned between the top plate and the actuator. An external MTS 418.91 controller is used to improve a deformation-rate-controlled test. The measurements systems are connected to a PC-based data acquisition system, which produces a single ASCII output file for each test.

5.7.2 Specimen preparation for the compression test

To determine the response of a specimen, the combination of the state of stress to which it is subjected and the material characteristics are of importance. The material characteristics can be obtained from the observed response and the state of stress. However, the true state of stress can be completely different from the intended state of stress. For the uniaxial monotonic compression test the intended state of stress is pure uniaxial compression. For the compression test it is therefore very important that the top and bottom surfaces of the specimen are parallel, otherwise shear forces might be introduced. To obtain parallel surfaces all the specimens are polished.

Friction between the specimen and the loading plates can have a significant disturbing effect on the state of stress in the specimen. During a test the specimen deforms in the radial as well as the axial direction. Friction between specimen and loading plates leads to confinement for the bottom and top of the specimen and results in the barrel-shape of specimens. This shape is an indication of undesirable non-uniaxial states of stress. To avoid this problem a friction reduction system is used for the compression test. This system consists of two thin (0.5mm) corrosion resistant steel plates. A thin layer of soap is applied to the steel plates, after which a plastic foil is added. Next a second layer of soap is added on the plastic foil. For the compression test the specimen is placed between two of these metal-soap-plastic-soap sandwiches.

The third part of the specimen preparation consists of gluing three little hooks halfway the heights of the specimens. These hooks guide the string that measures the radial displacement.

After preparation the specimens were placed in a temperature controlled unit at the designated test temperature for at least 24 hours before testing. After that the specimen including the friction reduction system is placed in the temperature cabinet.

5.7.3 Input for the compression test

5.7.3.1 Computer input for the compression test

The following data may be used as an input:

- Date
- Specimen identification
- Specimen height and diameter [mm]
- Temperature [°C]
- Loading rate [mm/s]
- Number of scans per second [Hz]
- Calculation factor for the force and the displacement

5.7.3.2 Test conditions for the uniaxial monotonic compression test

Uniaxial compression tests are performed under displacement controlled conditions by applying a monotonically increasing deformation (constant deformation rate) until complete annihilation of the strength. The test conditions for the compression tests are determined by using the central composite rotatable design, described in paragraph 5.6. Table 5.7 shows the test conditions for the compression test:

Table 5.7: Test conditions compression test

Specimen	Loading rate [mm/s]	Temperature [°C]
1	1.473	5.9
2	8.537	5.9
3	1.473	34.1
4	8.537	34.1
5	0.01	20.0
6	10	20.0
7	5.005	0
8	5.005	40.0
9	5.005	20.0
10	5.005	20.0
11	5.005	20.0
12	5.005	20.0
13	5.005	20.0

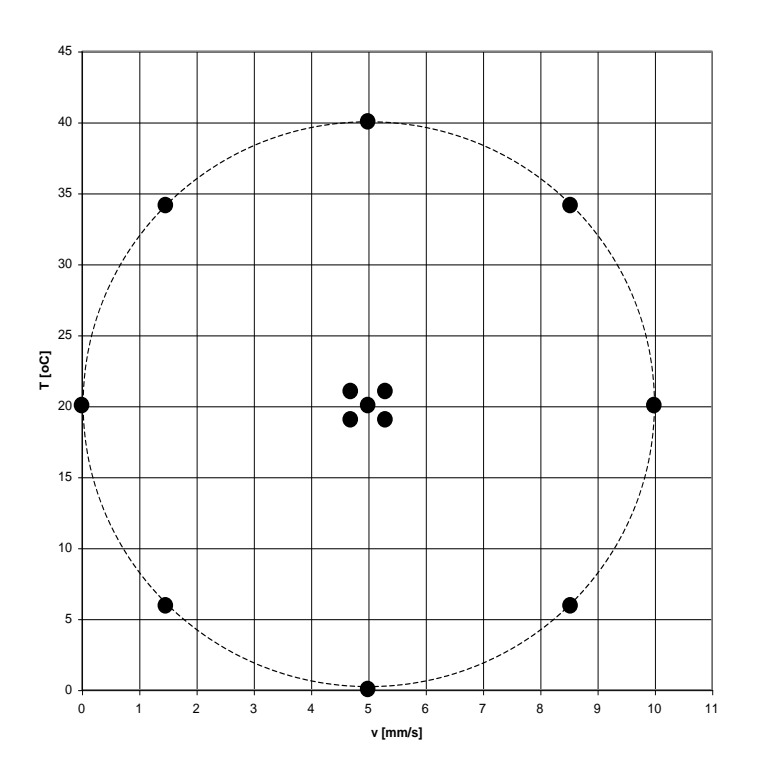


Figure 5.8 shows the test combinations when they are plotted in a chart.

Figure 5.8: Test conditions for the monotonic compression test

5.7.4 Output from the compression test

The following data is written in a file:

- Date of the test
- Specimen identification
- Temperature
- Loading rate
- Calculation factors for the force and the displacement
- The number of scans per second [Hz]
- Force [V]
- Displacement of the hydraulic ramp [V]
- Displacement of the three LVDT's [V]
- Displacement of the extensometer [V]
- Displacement of the string [V]

The results will be discussed in chapter 6.

5.8 Uniaxial monotonic tension test

5.8.1 Tension test set up

The tension test set-up consists of a closed temperature cabinet with a 50kN hydraulic actuator inside. The actuator is connected rigidly to the bottom of the temperature chamber. In the temperature cabinet the specimen is placed in a rigid framework that can resists the high forces that occur during the test without deforming. In the test set-up the specimen is placed between

three hinges to ensure that the specimen is subjected to pure uniaxial tension. There are two hinges above and one under the specimen to avoid bending moments in the specimen.

The force is measured by means of a load cell, which is positioned between the two hinges above the specimen. An internal 407 MTS controller is used to improve a deformation-rate-controlled test.

The axial deformation is registered by means of three displacement transducers (LVDT's). These LVDT's are fixed in a steel ring that is placed around the steel cap at the bottom of the specimen. On top of the specimen the three LVDT's touch a second steel ring which is placed around the steel cap on top of the specimen.

A close-up from the tension test set-up with an inserted specimen is shown in figure 5.9.

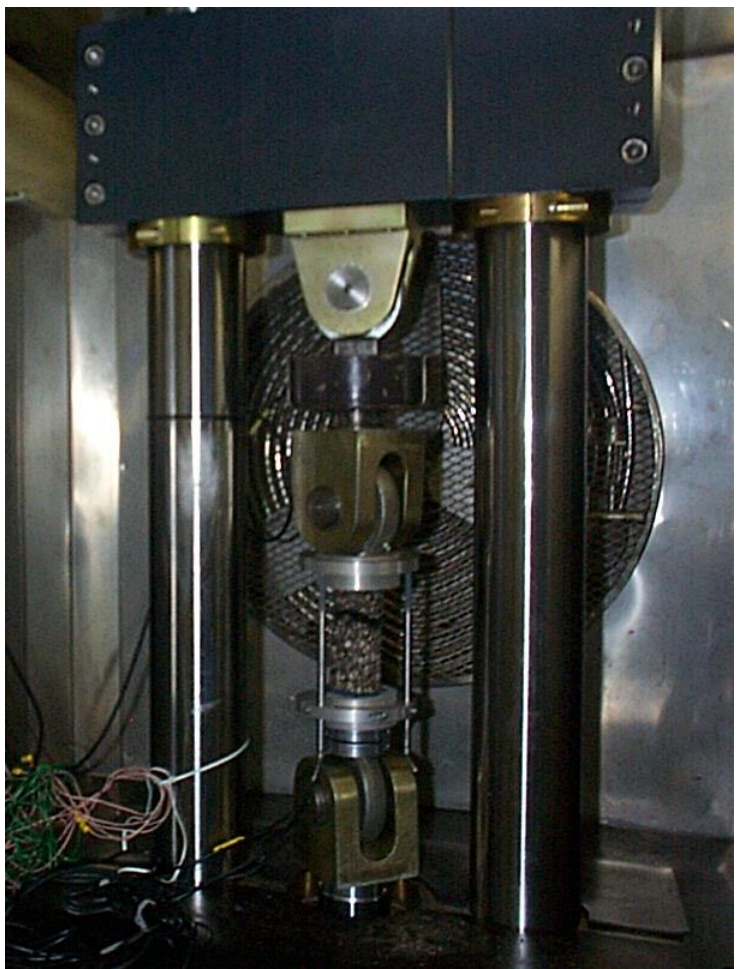


Figure 5.9: Test set up for the uniaxial monotonic tension test

The measurements systems are connected to a PC-based data acquisition system, which produces a single ASCII output file for each test.

5.8.2 Specimen preparation for the tension test

The cores for the tension test needed special preparation before testing took place. Two steel caps had to be glued at the top and bottom surface of the specimen before the specimen could be placed in the tension test set up. The steel caps are 30 mm thick and have a diameter of 80 mm. The caps have to be glued parallel to each other to ensure pure tension during the test. When the caps are not parallel bending moments are introduced during the test which is unacceptable.

The set up for gluing the caps parallel on the specimen is shown in figure 5.10.



Figure 5.10: Set-up for gluing the caps parallel on the specimen

For the tests at 0°C and 6.4°C special PVC rings (height 80 mm) are glued around the specimen at the cap, in order to prevent that the specimen cracks between the cap and the asphalt i.e. in the glue layer. The glue that is used consists of two components, ARALDITE SW 404 and HY 2404, which is mixed in the ratio 10:1.

After gluing the specimen stays in the set-up for at least two hours. After 24 hours the glue will harden and the specimen can be placed in a temperature chamber.

5.8.3 Input for the tension test

5.8.3.1 Computer input for the tension test

The following data may be inserted before the test:

- Date
- Specimen identification
- Specimen height and diameter [mm]
- Temperature [°C]
- Loading rate [mm/s]
- Number of scans per second [Hz]
- Calculation factor for the force and the displacement

5.8.3.2 Test conditions for the uniaxial monotonic tension test

Uniaxial tension tests are performed under displacement controlled conditions by applying a monotonically increasing deformation (constant deformation rate) till failure. When the central composite rotatable design is used for the tension tests, the following test conditions are obtained (table 5.8):

Table 5.8: Test conditions tension test

Specimen	Loading rate [mm/s]	Temperature [°C]
1	0.741	6.4
2	4.269	6.4
3	0.741	37.2
4	4.269	37.2
5	0.01	21.8
6	5	21.8
7	2.505	0
8	2.505	43.6
9	2.505	21.8
10	2.505	21.8
11	2.505	21.8
12	2.505	21.8
13	2.505	21.8

The rotatibility of the procedure becomes clear again when the test conditions are plotted in a chart (figure 5.11):

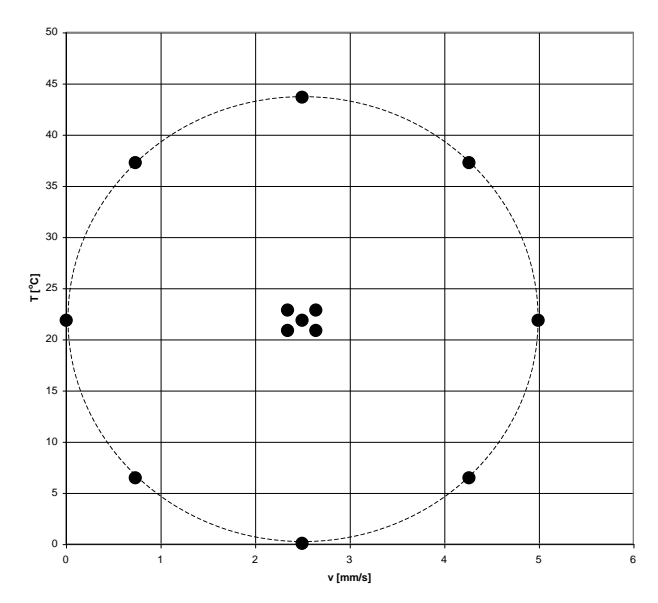


Figure 5.11: Test conditions for the monotonic tension test

5.8.4 Output from the tension test

The following data is written in a file:

- Date of the test
- Specimen identification
- Temperature
- Loading rate
- Calculation factors for the force and the displacement
- The number of scans per second [Hz]
- Force [V]
- Displacement of the hydraulic ramp [V]
- Displacement of the three LVDT's [V]

The results will be discussed in chapter 6.

6 Experimental results

6.1 Density measurements

6.1.1 Introduction

In this section the results of the density measurements are presented. For the density calculations the densities of the filler, sand, stone and bitumen are assumed as shown in table 6.1. These assumptions were made for both the Moerdijk and the Lintrack mix.

Table 6.1: Assumed densities

Туре	Grain size [mm]	Density [kg/m³]
Filler	<63 μm	2775
Sand	63 μm <z<2 mm<="" td=""><td>2650</td></z<2>	2650
Stone	2 mm <s<8 mm<="" td=""><td>2700</td></s<8>	2700
Bitumen	-	1020

For each specimen the density and the void content (V_a) , bitumen content (V_b) , filler content (V_f) , sand content (V_z) and stone content (V_s) is calculated. Finally the degree of filling (D_f) is determined.

6.1.2 Mix composition of the specimen for the four point bending test

6.1.2.1 Moerdijk mix

8 beams were used to determine the master curves and the fatigue behaviour. The mix composition of these 8 beams is shown in table 6.2.

Table 6.2: Mix composition of the specimens for the four-point bending test

Specimen	$ ho_{\rm sp}$ [kg/m 3]	V _a [%]	V _b ' [%]	V _f ' [%]	V _z ' [%]	V _s ' [%]	D _f [%]
opecimen	$p_{\sf sp}$ [kg/III]	v _{a [70]}	v _b [/0]	V f [/0]	V _Z [/0]	V _S [/0]	D _f [/0]
1	2357.37	1.14	18.69	17.18	21.26	41.73	94.2
2	2351.27	1.40	18.64	17.13	21.20	41.62	93.0
3	2355.04	1.24	18.67	17.16	21.24	41.69	93.8
4	2357.29	1.15	18.69	17.18	21.26	41.73	94.2
5	2355.60	1.22	18.68	17.16	21.24	41.70	93.9
6	2357.29	1.15	18.69	17.18	21.26	41.73	94.2
7	2356.59	1.17	18.69	17.17	21.25	41.72	94.1
8	2354.69	1.25	18.67	17.16	21.23	41.68	93.7
Average	2355.64	1.21	18.68	17.16	21.24	41.70	93.90
STDEV	2.06	0.09	0.02	0.02	0.02	0.04	0.41
Variation [%]	0.09	7.11	0.09	0.09	0.09	0.09	0.44

Where:

 ρ_{sp} : Specimen density [kg/m³] V_a : Percentage voids [%]

 V_{b}' : Bitumen content in the mix with voids [%V/V] : Filler content in the mix with voids [%V/V] V_{z}' : Sand content in the mix with voids [%V/V] : Stone content in the mix with voids [%V/V]

D_f: Degree of filling [%]

From table 6.2 it becomes clear that both the standard deviation and the variation of the mix composition is very small for the eight specimens. The density varies between 2351 kg/m³ and 2357 kg/m³ and the voids content between 1.14% and 1.40%. The variation in bitumen, filler, sand and stone content as well as degree of filling is so small that they are nearly constant for the eight specimens. Because the mix composition is comparable for the eight specimens the behaviour during testing will also be comparable. Therefore also the results of the tests can be compared after testing.

6.1.2.2 Lintrack mix

From the Lintrack mix 36 specimen are used in the four-point bending test to determine the strain dependent behaviour of the mix stiffness. Table 6.3 shows the results of the density measurements and calculations.

Table 6.3: Mix composition of the specimens for determining the stress dependent behaviour

Specimen	$ ho_{ m sp}$ [kg/m 3]	V _a [%]	V _b ' [%]	V _f ' [%]	V _z ' [%]	V _s ' [%]	D _f [%]
ML/4pb/1/1	2343.5	1.73	18.58	17.08	21.13	41.48	91.50
ML/4pb/1/2	2349.4	1.48	18.63	17.00	21.19	41.59	92.66
ML/4pb/1/3	2348.0	1.53	18.62	17.12	21.17	41.56	92.39
ML/4pb/1/4	2346.5	1.60	18.61	17.10	21.16	41.54	92.09
ML/4pb/1/5	2348.1	1.53	18.62	17.10	21.17	41.56	92.39
ML/4pb/1/6	2347.9	1.54	18.62	17.11	21.17	41.56	92.36
ML/4pb/1/7	2352.3	1.35	18.65	17.14	21.21	41.64	93.24
ML/4pb/1/8	2346.5	1.60	18.61	17.10	21.16	41.54	92.08
ML/4pb/1/9	2346.6	1.59	18.61	17.10	21.16	41.54	92.11
ML/4pb/1/10	2343.7	1.72	18.58	17.08	21.13	41.49	91.54
ML/4pb/2/1	2339.4	1.89	18.55	17.05	21.10	41.41	90.74
ML/4pb/2/2	2338.6	1.93	18.54	17.04	21.09	41.40	90.57
ML/4pb/2/3	2341.3	1.82	18.57	17.06	21.11	41.44	91.09
ML/4pb/2/4	2340.5	1.85	18.56	17.05	21.11	41.43	90.94
ML/4pb/2/5	2343.0	1.75	18.58	17.07	21.13	41.47	91.41
ML/4pb/2/6	2333.2	2.15	18.50	17.00	21.04	41.30	89.57
ML/4pb/2/7	2335.7	2.05	18.52	17.02	21.06	41.35	90.03
ML/4pb/2/8	2340.6	1.84	18.56	17.06	21.11	41.43	90.96
ML/4pb/2/9	2342.3	1.78	18.57	17.07	21.12	41.46	91.27
ML/4pb/2/10	2341.2	1.82	18.56	17.06	21.11	41.44	91.06
ML/4pb/3/1	2332.1	2.20	18.49	16.99	21.03	41.28	89.36
ML/4pb/3/2	2325.2	2.49	18.44	16.94	20.97	41.16	88.10
ML/4pb/3/3	2327.5	2.39	18.46	16.96	20.99	41.20	88.52
ML/4pb/3/4	2328.8	2.34	18.47	16.97	21.00	41.22	88.74
ML/4pb/3/5	2329.3	2.32	18.47	16.97	21.00	41.23	88.84
ML/4pb/3/6	2328.9	2.34	18.47	16.97	21.00	41.22	88.77
ML/4pb/3/7	2333.2	2.16	18.50	17.00	21.04	41.30	89.56
ML/4pb/3/8	2326.1	2.45	18.45	16.95	20.98	41.18	88.26
ML/4pb/3/9	2324.4	2.53	18.43	16.94	20.96	41.15	87.95
ML/4pb/3/10	2320.2	2.70	18.40	16.91	20.92	41.07	87.20
ML/4pb/4/1	2323.1	2.58	18.42	16.93	20.95	41.12	87.71
ML/4pb/4/2	2325.4	2.48	18.44	16.94	20.97	41.16	88.14
ML/4pb/4/3	2328.4	2.36	18.46	16.97	21.00	41.22	88.68
ML/4pb/4/4	2325.4	2.48	18.44	16.94	20.97	41.16	88.14
ML/4pb/4/5	2326.2	2.45	18.45	16.95	20.98	41.18	88.27
ML/4pb/4/6	2326.0	2.46	18.44	16.95	20.97	41.17	88.23
Average	2336.1	2.0	18.5	17.0	21.1	41.4	90.1
STDEV	9.3	0.4	0.1	0.1	0.1	0.2	1.7
Variation [%]	0.4	19.1	0.4	0.4	0.4	0.4	1.9

The variation in density, bitumen, filler, sand and stone content and degree of filling is negligible for the 46 specimens. Only the coefficient of variation for the percentage air voids is quite high. A closer look to the percentage air voids of the different specimens shows that the first 20 specimens (ML/4pb/1/1-ML/4pb/2/10) have a void content between 1% and 2%. The final 16 specimens (ML/4pb/3/1-ML/4pb/4/6) have a void content between 2% and 3%. This difference can be explained by the fact that the first 20 specimen have a higher density (ρ_{sp} =2330-2350 kg/m³) than the final 16 specimen (ρ_{sp} =2320-2335 kg/m³). This difference can be explained by the fact that the last 16 specimens are sawn from two different asphalt slabs. Probably the preparation of these slabs was different from the preparation of the first two slabs from which the first 20 specimens were obtained. The slabs were prepared manually and the asphalt was not condensed, so some variation is to be expected.

6.1.3 Mix composition of the specimen for the monotonic compression test

For the compression test 13 cylindrical specimens are used. Table 6.4 shows the results for the density measurements and calculations.

Table 6.4: Mix composition of the specimens for the monotonic compression test

Specimen	$\rho_{\rm sp}$ [kg/m ³]	V _a [%]	V _b ' [%]	V _f ' [%]	V _z ' [%]	V _s ' [%]	D _f [%]
M4-3	2354.09	1.28	18.67	17.15	21.23	41.67	93.58
M11-4	2351.38	1.39	18.65	17.13	21.20	41.62	93.05
M5-3	2349.41	1.48	18.63	17.12	21.19	41.59	92.66
M4-4	2350.47	1.43	18.64	17.13	21.20	41.61	92.87
M3-10	2355.06	1.24	18.67	17.16	21.24	41.69	93.78
M2-5	2345.27	1.65	18.60	17.09	21.15	41.51	91.85
M11-3	2354.25	1.27	18.67	17.15	21.23	41.67	93.62
M6-4	2353.01	1.33	18.66	17.15	21.22	41.65	93.37
M7-4	2351.20	1.40	18.64	17.13	21.20	41.62	93.01
M9-2	2349.49	1.47	18.63	17.12	21.19	41.59	92.67
M10-2	2356.28	1.19	18.68	17.17	21.25	41.71	94.02
M10-10	2358.53	1.09	18.70	17.19	21.27	41.75	94.48
M6-6	2345.29	1.65	18.60	17.09	21.15	41.52	91.86
Average	2351.83	1.37	18.65	17.14	21.21	41.63	93.14
STDEV	3.95	0.17	0.03	0.03	0.04	0.07	0.78
Variation [%]	0.17	12.08	0.16	0.17	0.17	0.17	0.84

Table 6.4 shows that the variation and standard deviation for the density, bitumen, filler, sand and stone content as well as the degree of filling is very small. The variation in voids content is somewhat higher. This is to be expected since the slab is prepared manually and the asphalt is not compacted, which leads to variation in the density. The variation in density is linear related to the voids content, an increasing density means a decreasing voids content.

6.1.4 Mix composition of the specimen for the monotonic tension test

For the tension test use is made of 13 cylindrical specimens. Table 6.5 shows the results of the density measurements and calculations.

T-11-0 - M'	'(' (()					
I ania h h' iviiv com	nacitian at the	s enacimane ti	or tno	manatania	tancian '	tact.
Table 6.5: Mix com	<i>DUSILIUI I UI LII</i>	, 300011110113 1	01 1110		LUISIUII	ισοι

Specimen	$ ho_{ m sp}$ [kg/m 3]	V _a [%]	V _b ' [%]	V _f ' [%]	V _z ' [%]	V _s ' [%]	D _f [%]
M11-5	2353.68	1.30	18.66	17.15	21.22	41.66	93.50
M2-1	2354.09	1.28	18.67	17.15	21.23	41.67	93.58
M11-8	2346.08	1.62	18.60	17.10	21.16	41.53	92.01
M2-3	2350.81	1.42	18.64	17.13	21.20	41.61	92.93
M3-9	2348.58	1.51	18.62	17.11	21.18	41.57	92.50
M3-1	2354.77	1.25	18.67	17.16	21.23	41.68	93.72
M1-10	2350.50	1.43	18.64	17.13	21.20	41.61	92.87
M3-7	2346.04	1.62	18.60	17.09	21.16	41.53	92.00
M5-2	2347.34	1.56	18.61	17.10	21.17	41.55	92.25
M3-4	2352.01	1.37	18.65	17.14	21.21	41.63	93.17
M2-4	2351.99	1.37	18.65	17.14	21.21	41.63	93.17
M4-7	2351.99	1.37	18.65	17.14	21.21	41.63	93.17
M1-3	2339.20	1.90	18.55	17.05	21.09	41.41	90.69
Average	2349.78	1.46	18.63	17.12	21.19	41.59	92.74
STDEV	4.30	0.18	0.03	0.03	0.04	0.07	0.84
Variation [%]	0.18	12.27	0.18	0.18	0.18	0.18	0.90

The variation and standard deviation for the density, bitumen, filler, sand and stone content as well as the degree of filling is very small for the specimen of the monotonic tension test. The variation in voids content is somewhat higher, which was also the case for the specimen for the monotonic compression test. The variation in voids content is to be expected since the slab was prepared manually and the asphalt is not compacted, which leads to variation in density and thus in voids content. A comparison between table 6.4 and 6.5 shows that the mix composition of the specimens for the compression tests is almost the same as the mix composition of the specimens for the tension tests. This is important since both tests are used to determine the model parameters for the ACRe material model.

6.2 Master curves

6.2.1 Determination of the master curves

Typically the stiffness modulus of asphaltic mixes increases with decreasing temperature and increasing loading frequency. By shifting the stiffness modulus versus loading time relationship for various temperatures horizontally with respect to the curve chosen as reference, a complete modulus-time behaviour curve at a constant, arbitrary chosen, reference temperature T_r can be assembled. This curve is referred to as 'the master curve'.

The software from the four-point bending testing machine gives two stiffness values, namely the flexural stiffness and the elastic modulus. Normally, for road engineering the elastic modulus is used, because for the determination of this value the effects of shear stresses are taken into account. However, in this report the flexural stiffness is used for the determination of all the master curves. The difference between the flexural stiffness and the elastic modulus is analysed in paragraph 6.5.

The technique of the determination of the master curve is based on the principle of time-temperature correspondence, or thermorheological simplicity, which uses the equivalence between frequency and temperature for the stiffness of bituminous mixes (equation 6.1).

$$\log f_{fict} - \log f = \log \alpha_{T}$$

Equation 6.1

where:

f_{fict}: the frequency where the master curve should be read (Hz).

f : loading frequency (Hz).

 α_t : shifting factor.

The shifting factor α_t can be determined in different ways, two of them are described here:

1) by means of an Arrhenius type equation.

2) by means of the Williams-Landel-Ferry (WLF) equation.

Method 1: Arrhenius type equation

A commonly used formula for the shift factor is an Arrhenius type equation [Francken et al. 1988, Jacobs 1995, Lytton et al. 1993].

$$\log \alpha_{\scriptscriptstyle T} = C \cdot \left(\frac{1}{T} - \frac{1}{T_{\scriptscriptstyle ref}}\right) = \log e \cdot \frac{\Delta H}{R} \left(\frac{1}{T} - \frac{1}{T_{\scriptscriptstyle ref}}\right)$$
 Equation 6.2

where:

T = the experimental temperature (K) T_{ref} = the reference temperature (K)

C = a constant (K)

 ΔH = activation energy (J/mol)

R = ideal gas constant, 8.314 J/(mol.K)

In literature, different values were reported for the constant C:

- 1) C=10920 K, Francken et al. [1988].
- C=13060 K, Lytton et al. [1993].
- 3) C=7680 K, Jacobs [1995].

It is emphasized here that all these researchers implicitly assume the constant C and the activation energy ΔH to be independent of temperature. From the thermodynamical background of ΔH this seems rather unlikely. Saygeh [1967] has reported that the activation energy decreases with temperature, from 310 kJ/mol at 253 K to 117 kJ/mol at 313 K.

Method 2: Williams-Landel-Ferry equation

Another formula for the calculation of the shift factor is the Williams-Landel-Ferry (WLF) equation [Williams et al. 1955]:

$$\log f_{\text{fict}} - \log f = \log \alpha_T = -\frac{C_1.(T - T_{\text{ref}})}{C_2 + T - T_{\text{ref}}}$$
 Equation 6.3

where:

f_{fict} = the frequency where the master curve should be read (Hz)

f = loading frequency (Hz) C₁,C₂ = empirical constants

and other variables as previously defined.

According to Sayegh [1967] C_1 = 9.5 and C_2 =95. It has also been reported by Lytton et al. [1993] that C_1 =19 and C_2 = 92.

From the above literature survey on the shift factor it is evident that there is no common agreement on which formula to use, and on the values of the corresponding parameters, which also might vary between different bituminous mixes. Therefore it was decided to use both methods with different parameters and to compare them.

6.2.2 Results from the first determination of the master curves

Table 6.6 shows the stiffness of mastic asphalt at different temperatures and frequencies that was measured with the four-point bending test. An overview of the results from all the measurements is shown in appendix B.

Table 6.6: Stiffness of mastic asphalt at different temperatures and frequencies

freq [Hz]	t [s]	5°C	10°C	15°C	20°C	25°C	30°C
0.5	2	4816	2399	1137	584	421	314
1	1	5967	3197	1559	851	497	332
2	0.5	7258	4106	2059	1083	644	418
5	0.2	8871	5493	3070	1734	935	515
10	0.1	10394	6785	4018	2236	1351	791

The figures 6.1-6.5 show the master curves determined with the different methods for T=15°C.

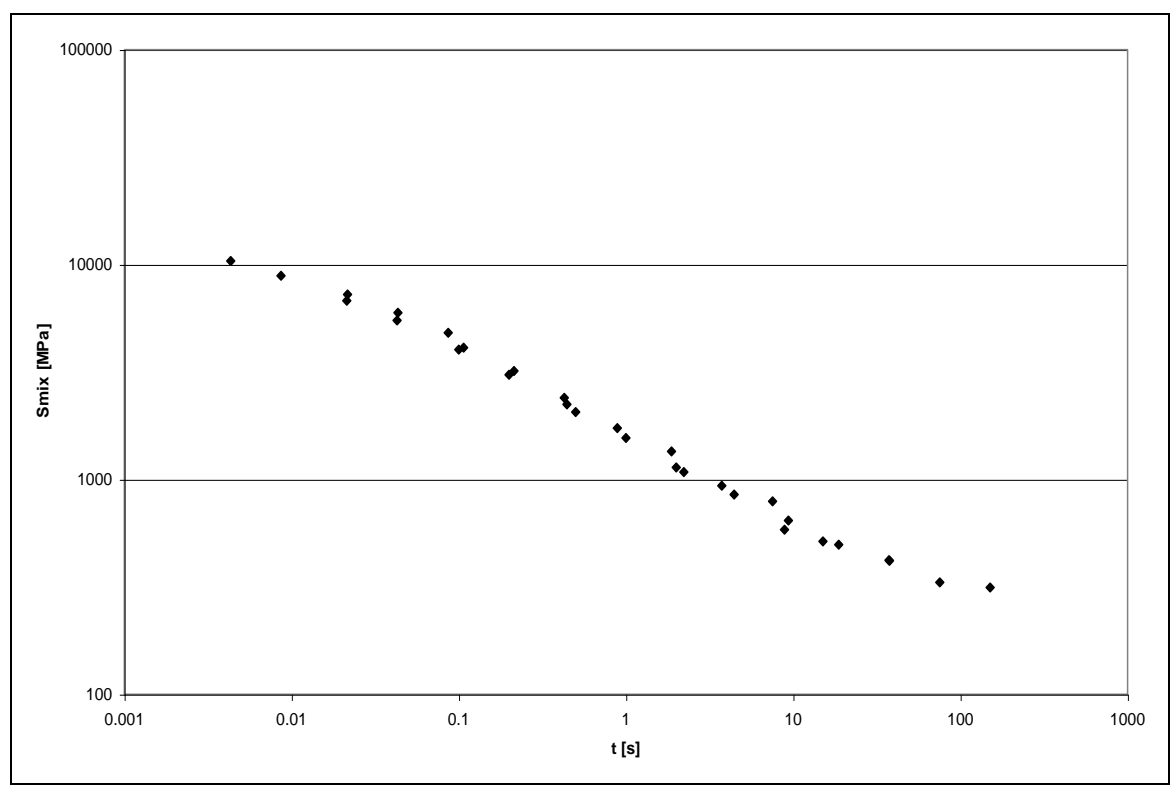


Figure 6.1: Master curve for mastic asphalt at T=15°C using Arrhenius-equation with Francken et al. [1988] constants

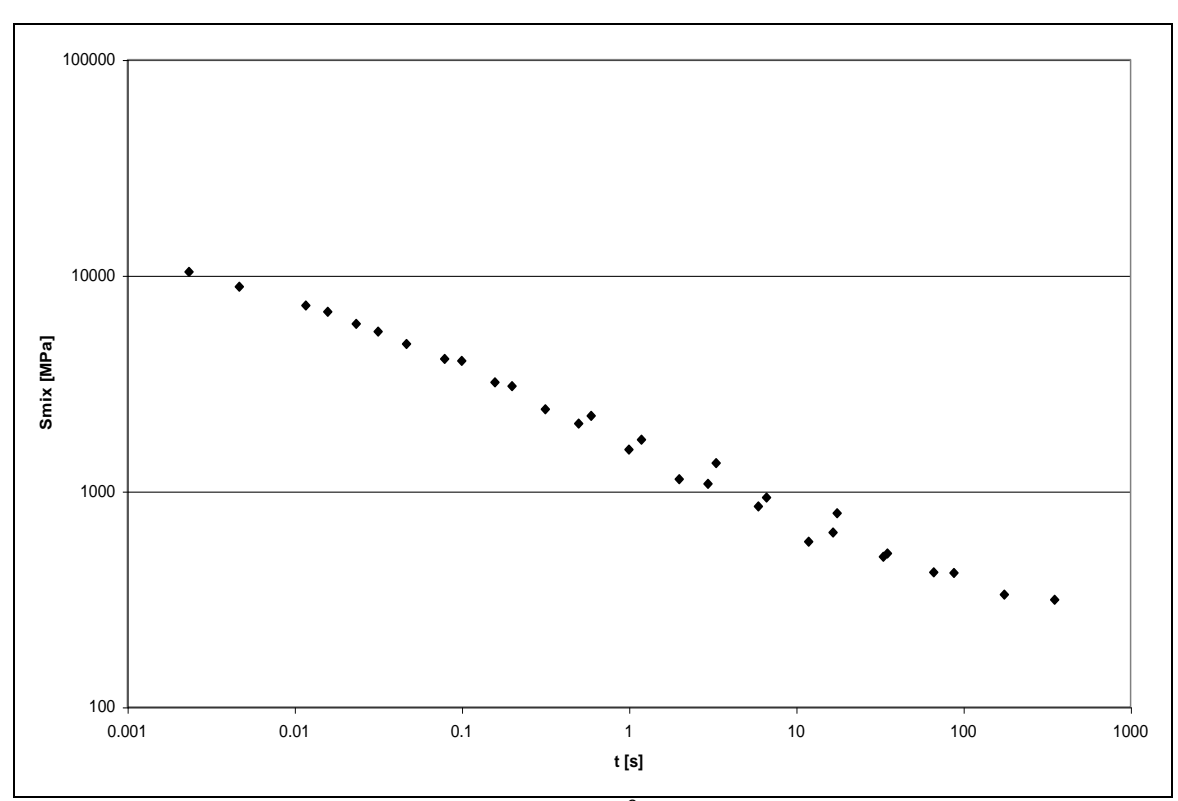


Figure 6.2: Master curve for mastic asphalt at T=15°C using Arrhenius-equation with Lytton et al. [1993] constants

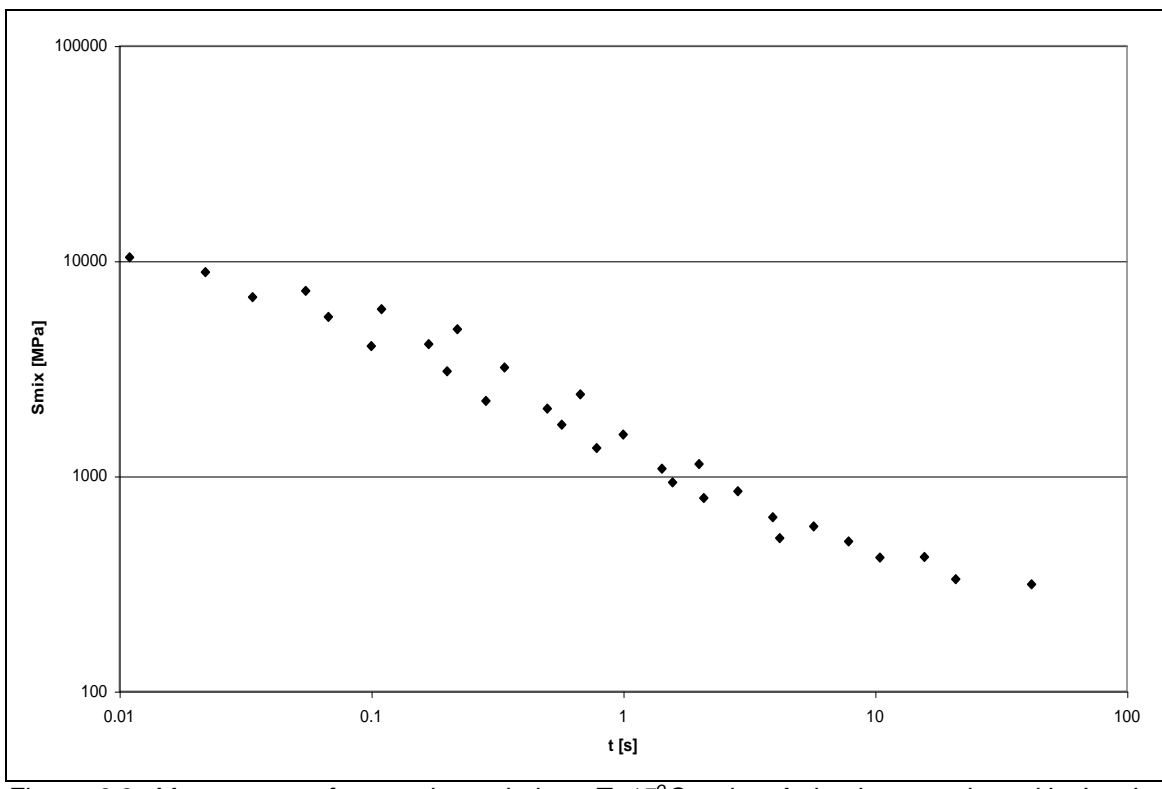


Figure 6.3: Master curve for mastic asphalt at T=15°C using Arrhenius-equation with Jacobs [1995] constants

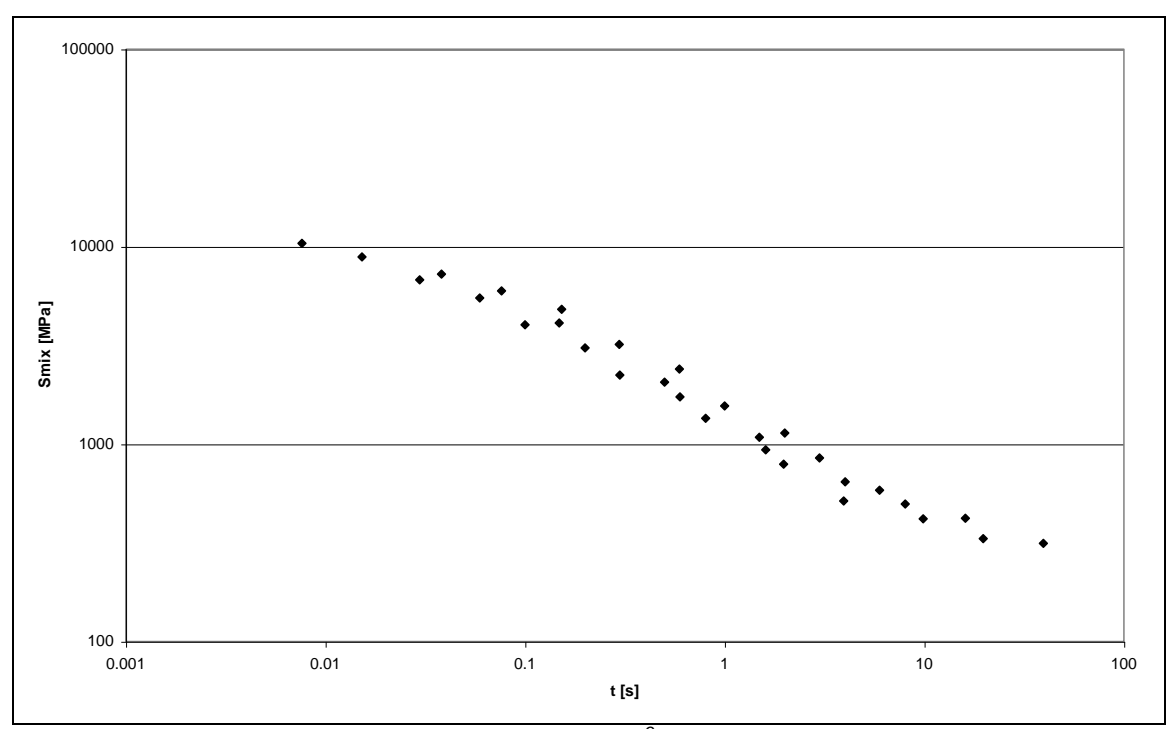


Figure 6.4: Master curve for mastic asphalt at T=15°C after Williams et al. [1955] with Sayegh [1968] constants

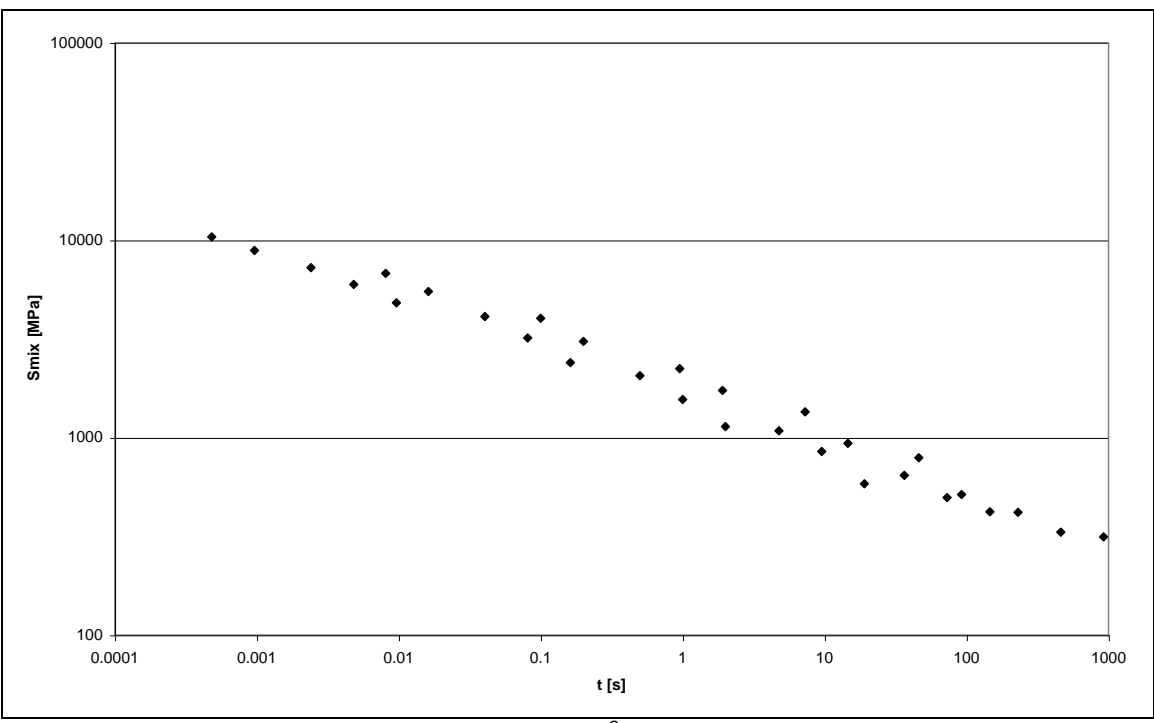


Figure 6.5: Master curve for mastic asphalt at T=15°C after Williams et al. [1955] with Lytton et al. [1993] constants

It is clear that different techniques and methods for the determination of the master curves give different results. This is expected because there are no universal values for the constants and they vary for different mixes. The Arrhenius type equation with the constant of Francken et al. [1988] gives the best results for mastic asphalt.

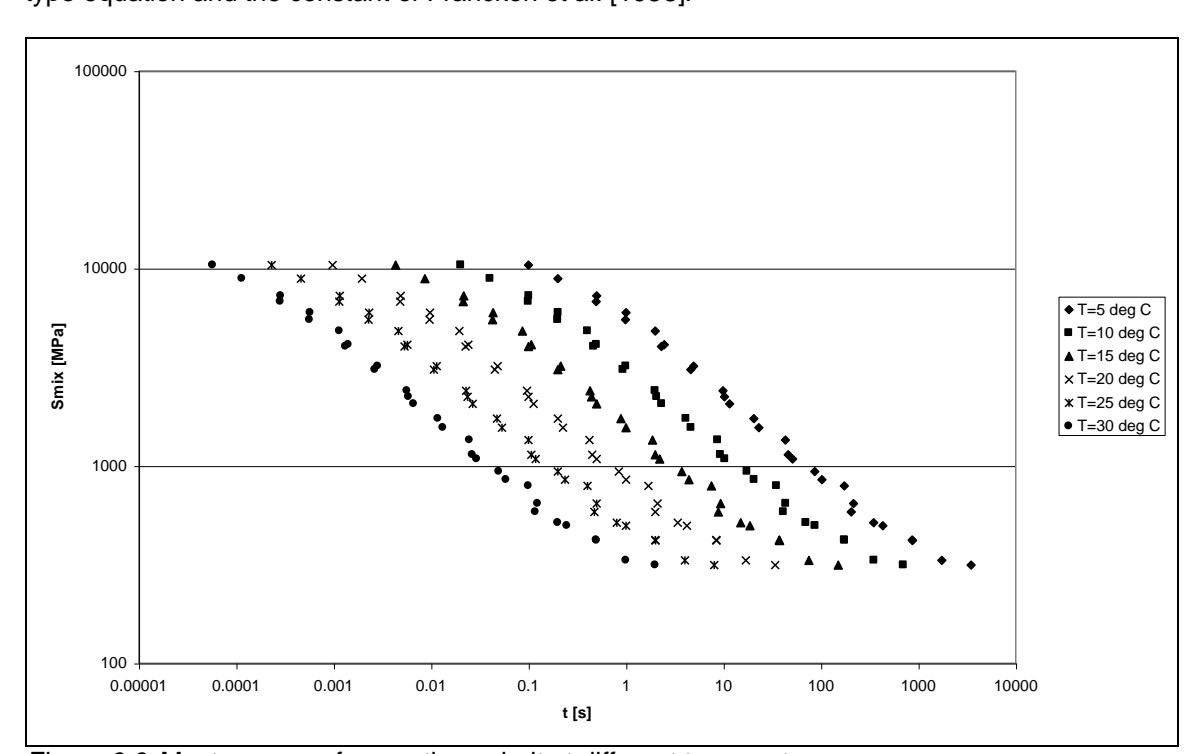


Figure 6.6 shows the master curves for the different temperatures determined with the Arrhenius type equation and the constant of Francken et al. [1988].

Figure 6.6: Master curves for mastic asphalt at different temperatures

In paragraph 7.1 the master curves are analysed.

6.2.3 Results from the repeated determination of master curves

Two and a half months after the first series of fatigue tests the master curves are determined again at strain levels of 80 and 800 μ m/m. In these tests the same specimens were used as the specimens that were used before in the fatigue tests. The tables 6.7 and 6.8 show the stiffness of mastic asphalt at different temperatures and frequencies from the repeated four-point bending tests. An overview of the results from all the measurements is shown in appendix B.

Table 6.7: Stiffness of mastic asphalt at ε =80 μ m/m

Table 6.7: Sumfees of mastic deprial at e-ee pringm							
freq [Hz]	t [s]	10°C	20°C	30°C			
0.5	2	2224	602	262			
1	1	2886	757	350			
2	0.5	3713	1068	384			
5	0.2	5129	1615	490			
10	0.1	6264	2099	707			

Table 6.8: Stiffness of mastic asphalt at ε =800 μ m/m

Tubic C.C.	Table 6.6. Guillies of mastic asphalt at ε =000 μ m/m					
freq [Hz]	t [s]	10°C	20°C	30°C		
0.5	2	1098	263	83		
1	1	1520	374	110		
2	0.5	2132	540	159		
5	0.2	3490	1095	346		
10	0.1	5162	1429	471		

10000 1000 ♦T=10, eps=80 Smix [MPa] ■ T=20, eps=80 ▲T=30, eps=80 ×T=10, eps=800 **X**T=20, eps=800 ● T=30, eps=800 100 0.0001 0.001 0.01 0.1 1 10 100 1000

With these results the master curves were created using the Arrhenius type equation and the C-value of 10920. Figure 6.7 shows the new master curves for both the strain levels.

Figure 6.7: New master curves after repeated testing at ε =80 and 800 μ m/m

t [s]

An analysis of the master curves is presented in paragraph 7.1.

6.3 Fatigue results

6.3.1 Results from the first fatigue test

Table 6.9 shows the results from the first fatigue test.

Table 6.9: Results from fatigue testing at 10°C and 5Hz

Strain [μm/m]	Load repetitions [-]	Dissipated energy [MPa]	Phase angle [°]
375	3600000	3607.006	-
475	934900	1248.319	40.3
600	152630	300.082	46.9
750	28140	76.463	46.6
925	5430	25.331	47.5
1095	4270	24.367	67.4

The fatigue behaviour is analysed in paragraph 7.2.

6.3.2 Results from the repeated fatigue test

Table 6.10 shows the fatigue results after repetition of the test. The tests were repeated after 2.5 months.

Table 6.10: Results from repeated fatigue testing at 10°C and 5Hz

Strain [μm/m]	Load repetitions [-]	Dissipated energy [MPa]	Phase angle [°]
530	1515530	2201.430	37.50
600	231970	437.027	36.8
700	91040	215.853	32.30
740	55070	149.81	38.6
800	11390	39.906	37.7
920	5770	25.999	43.4

In paragraph 7.2 the analysis of the fatigue behaviour is presented.

6.4 Strain dependency of the mix stiffness

Additional testing is carried out to study the dependency of the mix stiffness on the strain. For this additional testing use is made of specimen that were prepared when the test bridge for LINTRACK at the TU Delft was surfaced.

To test the strain dependency of the mix stiffness the master curves were determined at four different strain levels, six different temperatures and 5 different frequencies. The strain levels at which the tests were performed are 80 μ m/m, 200 μ m/m, 600 μ m/m and 1000 μ m/m. The mix stiffness for different strain levels, temperatures and frequencies is shown in the tables 6.11-6.14. An overview of the results from all the measurements is shown in appendix B.

Table 6.11: Mix stiffness of mastic asphalt at ε =80 μ m/m

freq [Hz]	t [s]	5°C	12.5°C	20°C	27.5°C	35°C	<i>4</i> 2.5°C
0.5	2	4129	1832	759	367	275	214
1	1	5104	2430	971	484	333	259
2	0.5	6143	3201	1300	573	393	261
5	0.2	7675	4261	1890	850	414	301
10	0.1	8973	5511	2298	1113	572	385

Table 6.12: Mix stiffness of mastic asphalt at ε =200 μ m/m

freq [Hz]	t [s]	5°C	12.5°C	20°C	27.5°C	35°C	<i>42.5</i> °C
0.5	2	3607	1496	539	265	166	121
1	1	4518	1962	728	319	182	136
2	0.5	5613	2701	1000	412	213	143
5	0.2	7283	4006	1673	708	285	158
10	0.1	8730	5187	2228	984	455	302

Table 6.13: Mix stiffness of mastic asphalt at ε =600 μ m/m

freq [Hz]	t [s]	5°C	12.5°C	20°C	27.5°C	35°C	<i>42.5</i> °C
0.5	2	2786	930	367	149	84	60
1	1	3629	1287	500	197	102	62
2	0.5	4706	1786	728	271	125	77
5	0.2	6681	2796	1312	490	295	207
10	0.1	8601	3903	1792	793	456	295

Table 6.14: Mix stiffness of mastic asphalt at ε =1000 μ m/m

	and or minimum control of made adjusted at a mode printing						
freq [Hz]	t [s]	5°C	12.5°C	20°C	27.5°C	35°C	<i>42.5</i> °C
0.5	2	2113	720	279	115	56	42
1	1	2851	1006	399	151	70	51
2	0.5	3945	1418	588	241	129	90
5	0.2	6339	2296	921	469	306	-
10	0.1	8259	3435	1446	703	437	-

Table 6.14 shows that there are two results missing at a temperature of 42.5°C. At this high temperature the specimens became so flexible that no measurements were possible at frequencies of 5 and 10Hz, because in that case the vibration of the specimen caused resonance of the testing machine.

From the results the master curves were determined using the constant from Francken. The figures 6.8-6.11 show the master curves for the four different strain levels.

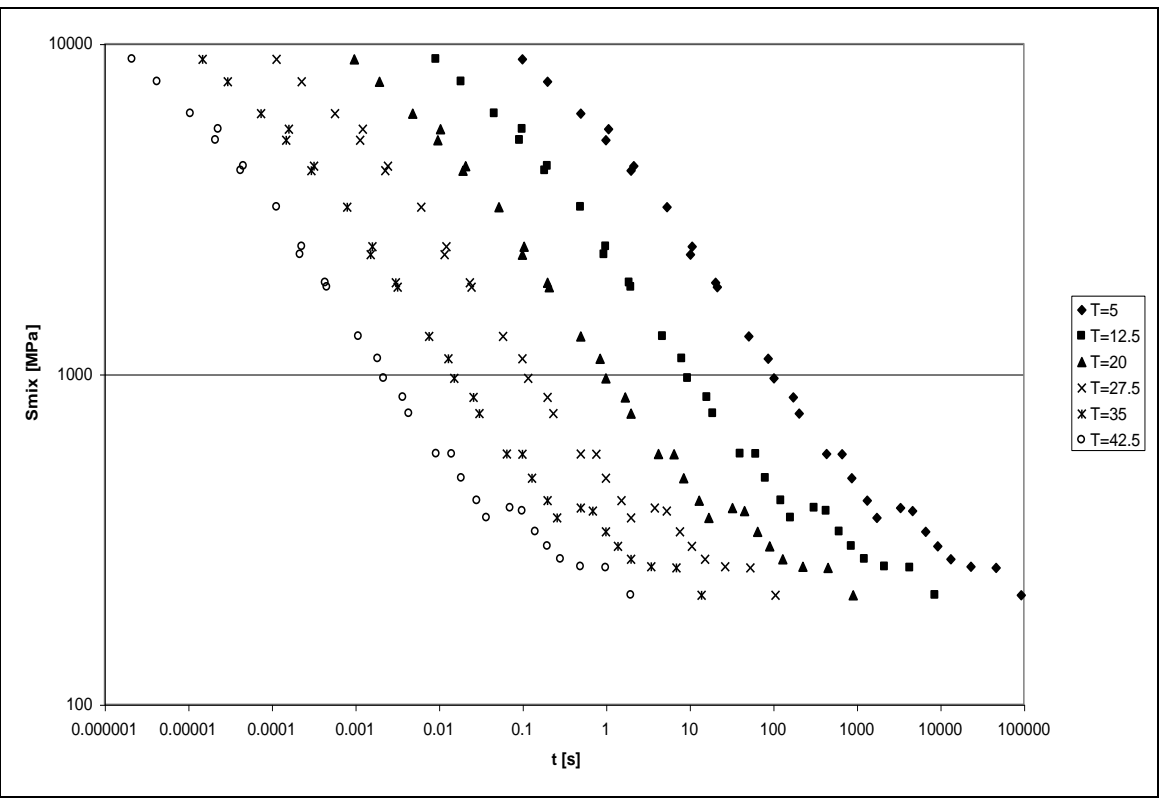


Figure 6.8: Master curves at ε=80 μm/m

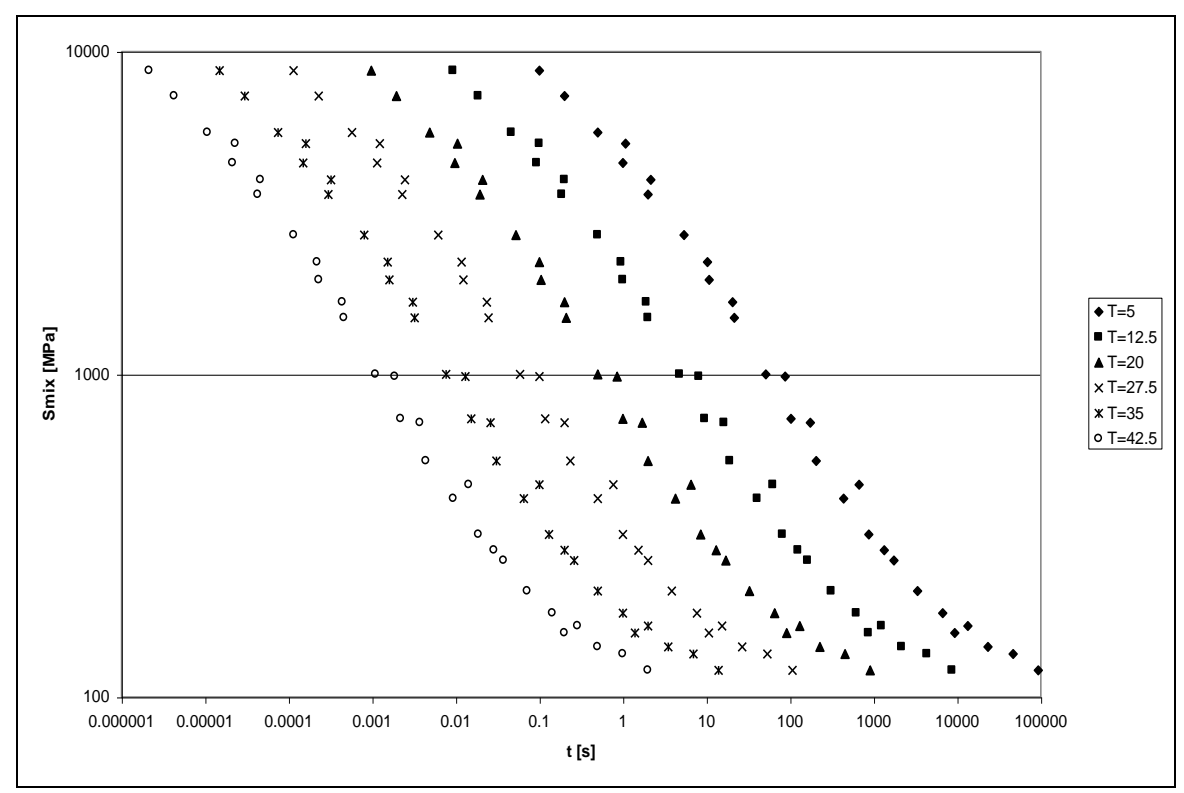


Figure 6.9: Master curves at ε =200 μ m/m

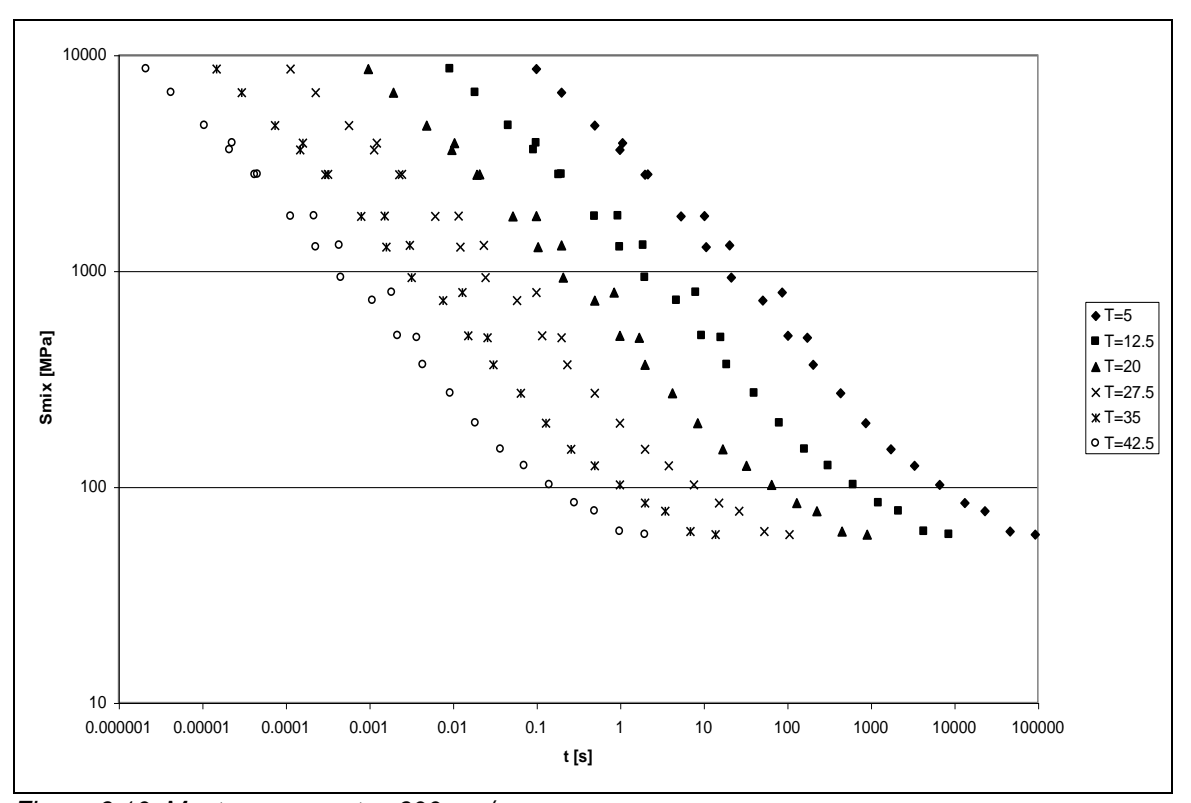


Figure 6.10: Master curves at ε=600 μm/m

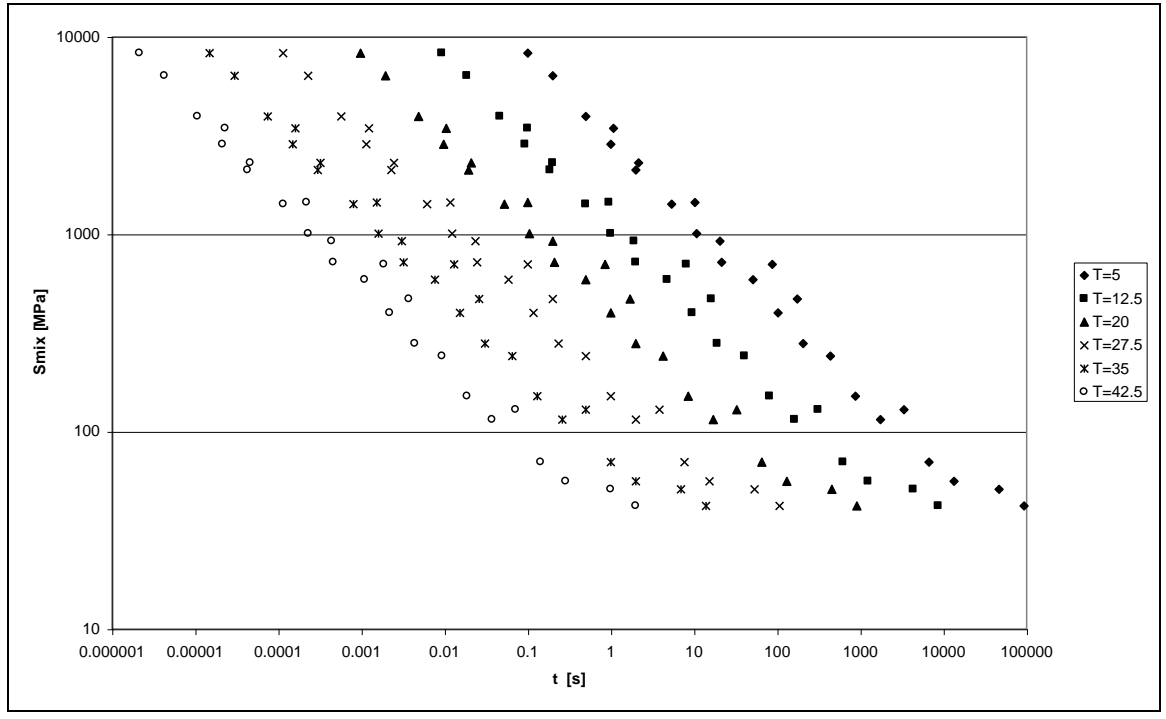


Figure 6.11: Master curves at ε =1000 μ m/m

For an analysis of the strain dependency of the mix stiffness the reader is referred to paragraph 7.3.

6.5 The difference between the elastic modulus and the flexural stiffness

For the determination of master curves the flexural stiffness was used. However, for road engineering the elastic modulus is normally used. The relation between the flexural stiffness and the elastic modulus is obtained by comparing equation 5.16 and 5.17. When equation 5.16 is rewritten by using equation 5.14 and equation 5.15 the flexural stiffness becomes:

$$S = \frac{23a^3P}{4\delta wh^3}$$
 Equation 6.4

in which:

S: flexural stiffness [MPa]

a : distance between reaction and load clamps (typically 118.5 mm)

P : peak force [N]

 δ : peak deflection at centre of beam [mm]

w : beam width [mm]h : beam height [mm]

Combining this equation with equation 5.17 the relation between the flexural stiffness and the elastic modulus becomes:

$$E = S + \frac{Pa}{\delta wh} [k(1+v)]$$
 Equation 6.5

in which:

E : elastic modulus [MPa]

k: actual shear stress divided by the average shear stress (assumed 1.5 N/mm²)

 υ : Poisson's ratio

The second term in equation 6.5 is included to take the shear stresses into account. Each beam has a width and a height op approximately 50 mm and for the Poisson's ratio a value of 0.3 is used. Equation 6.5 becomes:

$$E = S + 0.09243 \frac{P}{S}$$
 Equation 6.6

From this equation it becomes clear that the elastic modulus is higher than the flexural stiffness. This means that in all cases the stiffness is underestimated. The difference is determined by the ratio P/δ , which is dependent on the test conditions. The following can be noticed about P:

- an increasing strain level leads to an increasing P
- an increasing temperature leads to a decreasing P
- an increasing frequency leads to an increasing P

For δ the following can be noticed:

an increasing strain level leads to an increasing δ

The difference between the elastic modulus is analysed for the extreme test conditions, namely for frequencies of 0.5 Hz and 10 Hz and for temperatures of 5°C and 42.5°C. Table 6.15 shows the differences for 80 μ m/m, 200 μ m/m, 600 μ m/m and 1000 μ m/m.

Table 6.15: Difference between the flexural stiffness (S) and the elastic modulus (E)

		80 μ	.m/m	ر 200	ւm/m	600 յ	ւm/m	1000	μ m/m
		0.5 Hz	10 Hz						
5°C	S [MPa]	4062	8870	3639	8823	2873	9356	2107	8748
	E [MPa]	4312	9416	3863	9364	3050	9932	2237	9289
	Diff. [%]	5.8	5.8	5.8	5.8	5.8	5.8	5.8	5.8
42.5°C	S [MPa]	222	327	134	298	60	278	42	451*
	E [MPa]	235	347	142	316	63	295	45	479*
	Diff. [%]	5.5	5.8	5.6	5.7	4.8	5.8	6.7	5.8*

^{*} no measurements were carried out at T=42.5°C and 10 Hz so the values for T=35°C and 10 Hz were used

From table 6.15 it becomes clear that the difference between the elastic modulus and the flexural stiffness is almost constant. By using the flexural stiffness instead of the elastic modulus the stiffness is underestimated by approximately 6%.

6.6 Uniaxial monotonic compression test

Table 6.16 shows the results from the uniaxial monotonic compression test.

T / / O / O A / ·				
Table 6.16: Maximum	anmaraeeinn etraee	e tar maetic aenhal:	t tor dittarant tamnarati	irae and etrain ratae
Table U. TU. Maxilliulli	JUHIDI GOSIUH SU GOS	ว เบเ เมลงแบ ลงมมลม	i ioi uiileieiii leiiibeiali	ii co anu onani i alco

Specimen	Height [mm]	Loading speed [mm/s]	Strain rate [1/s]	T [°C]	f _c [MPa]
M5-3	90.1	1.5	1.68E-02	5.9	-16.96
M4-3	90.1	8.8	9.75E-02	5.9	-24.22
M4-4	88.8	1.5	1.70E-02	34.1	-2.58
M3-10	89.8	8.8	9.78E-02	34.1	-4.71
M10-10	100.3	0.0	9.97E-05	20.0	-1.80
M10-2	100.3	10.3	1.03E-01	20.0	-9.70
M11-4	100.1	5.9	5.86E-02	0	-30.12
M2-5	90.2	5.1	5.68E-02	40.0	-2.65
M11-3	100.2	5.1	5.12E-02	20.0	-8.01
M6-4	99.6	5.1	5.15E-02	20.0	-8.46
M7-4	100.1	5.1	5.12E-02	20.0	-7.97
M9-2	100.3	5.1	5.11E-02	20.0	-8.38
M6-6	100.1	5.1	5.12E-02	20.0	-7.98

From the output data the stress-strain figures are constructed. Figure 6.12 shows the stress-strain figure for the 13 compression tests.

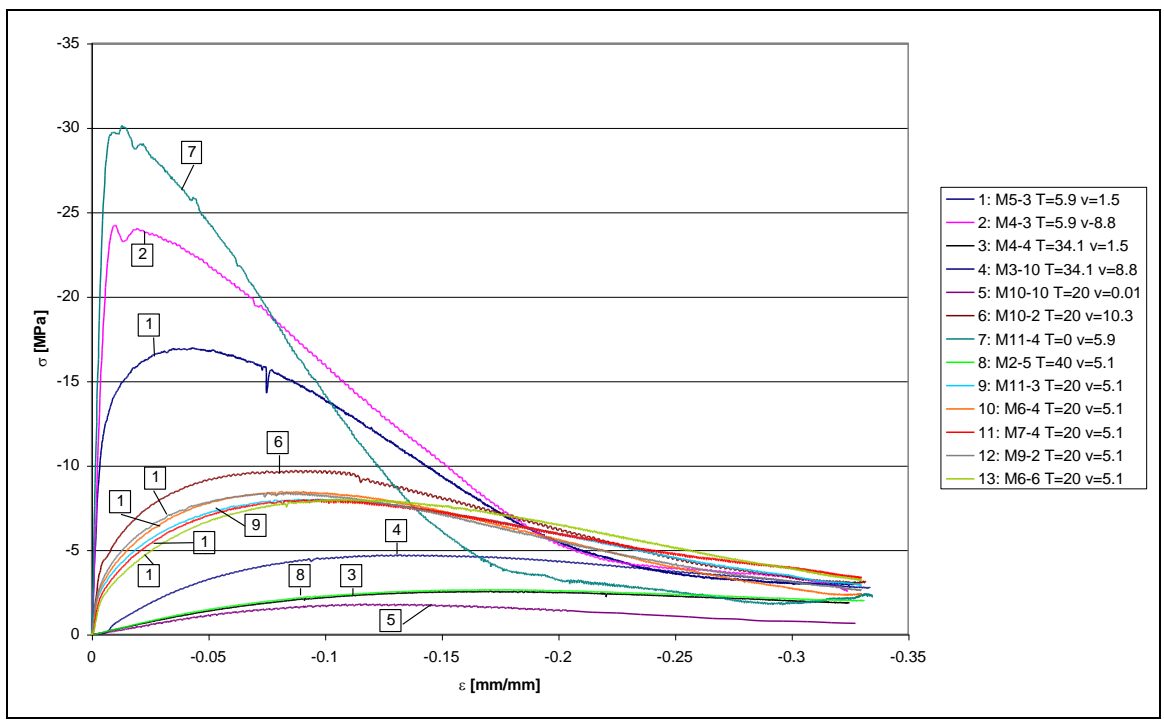


Figure 6.12: Stress-strain relation at different temperatures and deformation rates for the compression test

Figure 6.12 shows clearly the increasing compressive strength with increasing deformation rate and decreasing temperature as to be expected. Further the strain at the peak stress decreases with increasing deformation rate and decreasing temperature, which means that under these conditions the material behaves more brittle.

During the compression test also the radial deformation has been measured. Figure 6.13 shows the stress as a function of the axial as well as the radial strain. For the 5 measurements at $T=20^{\circ}\text{C}$ and the strain rate of 0.051 s⁻¹ the average has been taken.

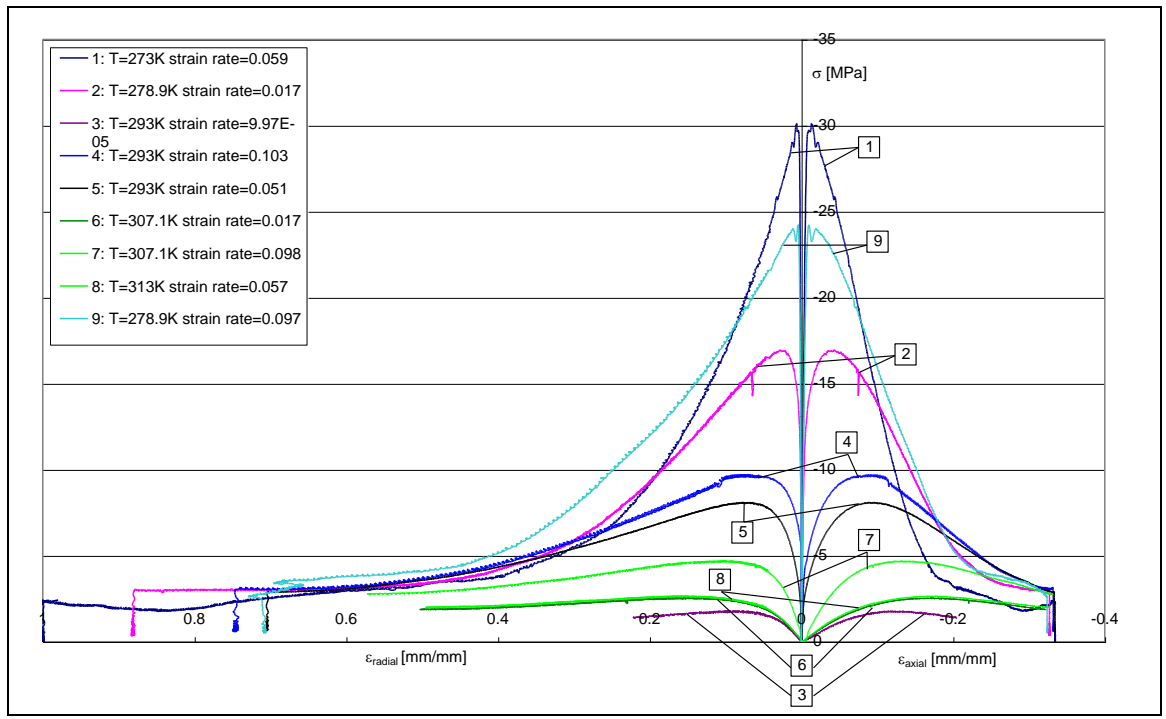


Figure 6.13: Radial and axial strain versus stress

From the results it can be seen that the measured deformation rates are somewhat different from the deformation rates that were intended. The difference is shown in table 6.17.

Table 6.17: Difference between the intended and measured deformation rate

Specimen	v _{intended} [mm/s]	v _{measured} [mm/s]	Difference [%]
M5-3	1.473	1.514	2.8
M4-3	8.537	8.782	2.9
M4-4	1.473	1.513	2.7
M3-10	8.537	8.783	2.9
M10-10	0.010	0.010	0.0
M10-2	10.000	10.321	3.2
M11-4	5.005	5.862	17.1
M2-5	5.005	5.127	2.4
M11-3	5.005	5.126	2.4
M6-4	5.005	5.133	2.6
M7-4	5.005	5.128	2.5
M9-2	5.005	5.124	2.4
M6-6	5.005	5.130	2.5

Except for specimen M11-4 the difference is negligible. The difference of 17% between the intended and measured loading speed can be explained by the fact that this specimen is tested at 0°C. At this temperature the mix stiffness is very high and the specimen behaves very brittle. This brittle behaviour leads to such a short test duration that it becomes impossible for the displacement controller to reach the intended deformation rate.

For this experimental program use is made of a central composite rotatable design, which means that only the tests at the five centre points are repeated.

Table 6.18 shows the average compressive strength for these five points, as well as the standard deviation and the coefficient of variation.

Table 6.18: Average, standard deviation and coefficient of variation for the compressive strength of the five centre points for T=20°C and v=5.005 mm/s

Specimen	f _c [MPa]
M11-3	-8.01
M6-4	-8.46
M7-4	-7.97
M9-2	-8.38
M6-6	-7.98
Average	-8.16
STDEV	0.24
Variation [%]	2.93

From table 6.18 it becomes clear that both the standard deviation and the coefficient of variation are very small. This indicates that repetition of tests at certain constant test conditions is not necessary. However, the values in table 6.18 are results from average test conditions. At extreme test conditions (high and low temperatures, high and low loading rates) the standard deviation and the variation are expected to increase. Table 6.19 shows the standard deviation and the variation for extreme test conditions for the compression tests carried out by Erkens [1998].

Table 6.19: STDEV and variation for tests at extreme conditions carried out by Erkens [1998]

T [°C]	v [mm/s]	Average f _c [MPa]	STDEV	Coefficient of variation [%]				
30	0.1	-1.9	0.1	5				
15	0.1	-5.7	0.3	5				
0	0.1	-21.6	0.4	2				
30	10	-7.5	0.8	11				
15	10	-22.3	0.6	3				
0	10	-56.7	1.3	2				

From table 6.19 it becomes clear that the coefficient of variation varies between 2% and 5% for a low loading rate of 0.1 mm/s, which is quite small. For a high loading rate of 10 mm/s the variation is still small for low temperatures. For 30°C the variation becomes 11%, which is still reasonable for such an extreme test condition. From table 6.19 it can be concluded that for previous compression tests both the coefficient of variation and the standard deviation are quite small, which means that the central composite rotatable design, without repetition of tests, seems reasonable for the compression tests. The analysis of the compression tests is presented in paragraph 7.4.

6.7 Uniaxial monotonic tension test

Table 6.20 shows the results for the uniaxial monotonic tension test.

Table 6.20: Maximum	tanaian atraa	a for different :	tomporaturas au	nd deformation rates
I ADIE O.ZU. IVIAXIIIIUIII	tension sues.	s ioi uillelelit i	lennberalures ar	iu ueioiiialioii iales

	· · · · · · · · · · · · · · · · · · ·						
Specimen	Height [mm]	v [mm/s]	strain rate [1/s]	T [°C]	f _⊤ [MPa]		
11-5	73.4	0.742	1.01E-02	6.4	5.91		
2-1	73.1	2.561	3.50E-02	6.4	10.80		
11-8	90.9	0.74	8.14E-03	37.2	0.47		
2-3	89.0	4.268	4.80E-02	37.2	0.83		
3-9	90.3	0.01	1.11E-04	21.8	0.46		
3-1	90.0	5.00	5.56E-02	21.8	3.20		
1-10	73.3	1.260	1.72E-02	0	10.49		
3-7	90.2	2.498	2.77E-02	43.6	0.47		
5-2	90.1	2.505	2.78E-02	21.8	2.42		
3-4	90.0	2.505	2.78E-02	21.8	2.40		
2-4	90.0	2.500	2.78E-02	21.8	2.22		
4-7	90.0	2.497	2.77E-02	21.8	2.37		
1-3	90.0	2.499	2.78E-02	21.8	2.22		

From the output data the stress-strain figures are constructed, they are shown in figure 6.14.

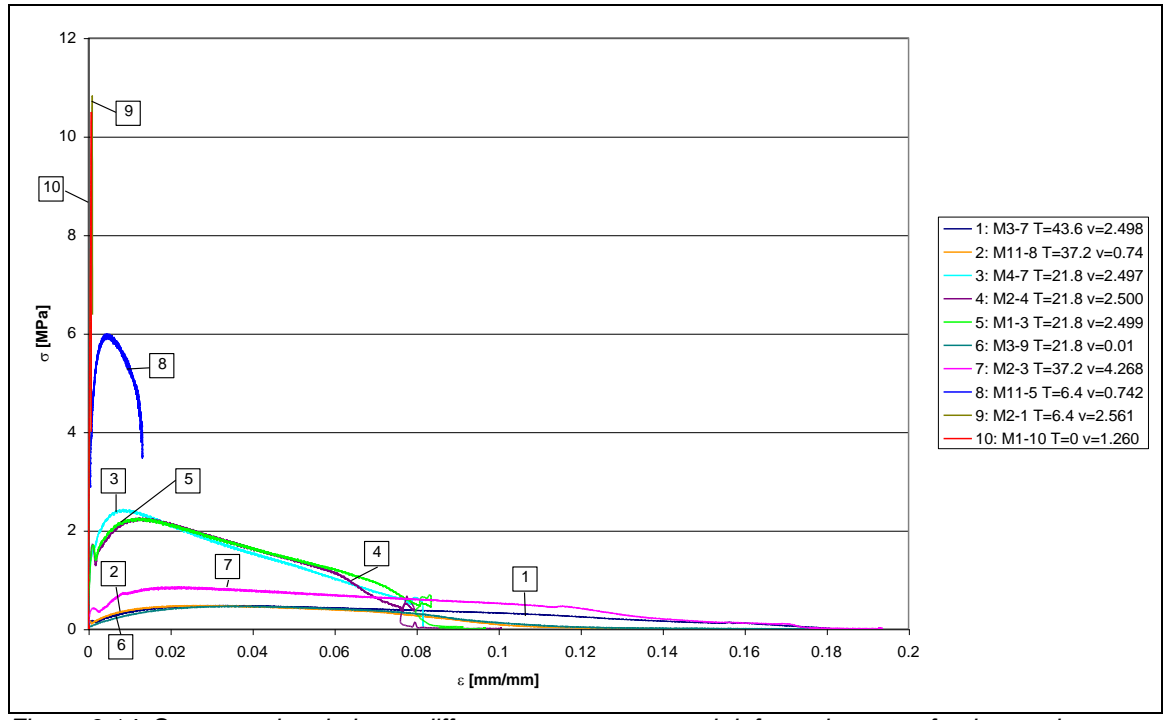


Figure 6.14: Stress-strain relation at different temperatures and deformation rates for the tension test

In figure 6.14 only 10 lines are shown because for 3 tests no output data was generated due to technical problems. For these tests the maximum tensile strength was obtained from the scope. After analysis of the 10 test results it was found that the maximum peak stress that is determined from the scope is very well comparable with the peak stress determined with the output data as it should be.

The figure with tension results also clearly shows the increase in compressive strength with increasing deformation rate and decreasing temperature. Further the strain at the peak stress

decreases with increasing deformation rate and decreasing temperature, which means that the material behaves more brittle under these conditions.

For some of the tension tests the measured deformation rate is different from the intended deformation rate, as shown in table 6.21.

Table 6.21: Difference between the intended and measured deformation rate

Specimen	v _{intended} [mm/s]	v _{measured} [mm/s]	Difference [%]
M11-5	0.741	0.742	0.13
M2-1	4.269	2.561	-40.01
M11-8	0.741	0.74	-0.13
M2-3	4.269	4.268	-0.02
M3-9	0.01	0.01	0.00
M3-1	5.000	5.000	0.00
M1-10	2.505	1.260	-49.70
M3-7	2.505	2.498	-0.28
M5-2	2.505	2.505	0.00
M3-4	2.505	2.505	0.00
M2-4	2.505	2.500	-0.20
M4-7	2.505	2.497	-0.32
M1-3	2.505	2.499	-0.24

The table shows that for two specimens, M2-1 and M1-10, there is a large difference between the intended and measured deformation rate. These specimens were both tested at low temperatures (T=0 and 6.4°C) and high deformation rates. In that situation the stiffness of the specimen is so high that the material behaves very brittle. This results in a very short duration of the test until peak stress. In this short time the displacement controller is not able to reach the intended deformation rate.

For the tension tests only the five centre points were repeated according to the central composite rotatable design. Table 6.22 shows the average, standard deviation and coefficient of variation for the tension strength for these five centre points.

Table 6.22: Average, standard deviation and coefficient of variation for the tensile strength of the five centre points for T=21.8°C and v=2.505 mm/s

Specimen	f_t [MPa]
M5-2	2.42
M3-4	2.40
M2-4	2.22
M4-7	2.37
M1-3	2.22
Average	2.33
STDEV	0.10
Variation [%]	4.16

It shows that for the tension tests also the standard deviation and coefficient of variation are very small for average test conditions. In this case no information is available from previous tension tests at extreme tests conditions, but it is expected that the variation and standard deviation at these conditions will have the same small magnitude as for the compression tests. This indicates that the central composite rotatable design, without repetition of tests, seems reasonable for the tension tests. The tension tests are analysed in paragraph 7.5.

7 Analysis of test results

7.1 Master curves

7.1.1 Introduction

In this section first the master curves, i.e. the relationship between the mix stiffness S_{mix} , the loading time t and temperature T, are described. Secondly, the master curves from the first and repeated test are compared. Thirdly, the stiffness behaviour of the Moerdijk mix is compared with the stiffness behaviour of some different mastic asphalt mixes. The mastic asphalt mixes that are included in this comparison are: mastic asphalt mix tested by the 'Dienst Weg- en Waterbouwkunde' (DWW), which is referred to as "GIET-DWW", as well as 4 modified mixes tested by Kolstein [1989]. In these mixtures modified bitumen were used. The 4 mixtures are shown in table 7.1.

Table 7.1: Mixes involved in the comparison tested by Kolstein

Mix	Type of bitumen
REFBL0	Bitumen 45/60 + Trinidad Epuré
STYL0	Styrelf 1360
SEAL1	Sealoflex
EVAL2	Bitumen 45/60 + Eva 18-150

In these codes L stands for a laboratory mixture and REF for reference material. In the reference material Trinidad Epuré is added to the bitumen, which is a natural bitumen obtained from an asphalt lake in the island of Trinidad.

The STYL0, SEAL1 and EVAL2 mixes are all polymer modified. In STYL0 styrene is added to the bitumen and in EVAL2 the elastomer Ethyl Vinyl Acetate. The positive effects of adding polymers to the bitumen are:

- decreasing temperature sensibility
- increasing resistance against permanent deformation
- · increasing capability for elastic recovery
- increasing resistance against fatigue (repeated strains)
- increasing strength (force at break) [Hopman, 1989]

Finally a comparison is made between the stiffness behaviour of the Moerdijk mix and the stiffness behaviour of some different types of asphalt mixes. These mixes are:

ZOK: Porous synthetic wearing coarse (ZOK) tested at TU Delft

ZOAB-DWW: Porous asphalt concrete (ZOAB) tested at the Road and Hydraulic

Engineering Division of the Dutch Ministry of Transport (DWW)

GAB: Gravel Asphalt Concrete tested at DWW

7.1.2 Determining S_{mix} as a function of T and t for the first determination of master curves

The master curves for the Moerdijk mix (figure 6.6) are described best with a logarithmic equation in the form of:

$$\log(S_{mix}) = a_0 + a_1 \log t + a_2 (\log t)^2 + a_3 (\log t)^3$$
 Equation 7.1

in which:

S_{mix}: stiffness of the mix [MPa]

t: loading time [s] a_i: regression constants

Table 7.2 shows the regression constants for mastic asphalt determined for the different temperatures.

Table 7.2: Regression constants for the formula describing the master curves for the first fatigue test

T [°C]	$a_{\rm o}$	a ₁	a_2	a_3	R^2
5	3.7570	-0.3423	-0.0725	0.0192	0.9977
10	3.4909	-0.4153	-0.0326	0.0192	0.9977
15	3.2039	-0.4331	0.0060	0.0192	0.9977
20	2.9314	-0.4012	0.0433	0.0192	0.9977
25	2.7021	-0.3246	0.0793	0.0192	0.9977
30	2.5391	-0.2076	0.1141	0.0192	0.9977

7.1.3 Determining S_{mix} as a function of T and t for the repeated determination of master curves

The master curves from figure 6.7 are described best with a logarithmic equation in the form of:

$$\log(S_{mix}) = a_0 + a_1 \log t + a_2 (\log t)^2 + a_3 (\log t)^3$$
 Equation 7.2

in which:

S_{mix}: stiffness of the mix [MPa]

t: loading time [s] a_i: regression constants

Table 7.3 and 7.4 show the regression constants for the master curves of figure 6.7.

Table 7.3: Regression constants for the master curves at ε =80 μ m/m

T [°C]	a _o	a ₁	a_2	a_3	R^2
10	3.4568	-0.3984	-0.0380	0.0186	0.9982
20	2.9088	-0.4016	0.0355	0.0186	0.9982
30	2.5032	-0.2297	0.1042	0.0186	0.9982

Table 7.4: Regression constants for the master curves at ε =800 μ m/m

T [°C]	a _o	a ₁	a_2	a ₃	R^2
10	3.2152	-0.4397	0.0334	-0.0145	0.9833
20	2.6610	-0.4270	-0.0238	-0.0145	0.9833
30	2.0729	-0.5513	-0.0773	-0.0145	0.9833

7.1.4 Comparison between the first and repeated determination of master curves

After this repeated testing the new stiffness at a strain level of 80 μ m/m is compared with the old stiffness that was determined 2.5 months earlier for the same strain level. This comparison is shown in the tables 7.5-7.7 for the different temperatures.

Table 7.5: Comparison first and repeated stiffness at 80 μ m/m and T=10°C

Frequency [Hz]	First stiffness [MPa]	Repeated stiffness [MPa]	Difference [%]
0.5	2399	2224	-7.3
1	3197	2886	-9.7
2	4106	3713	-9.6
5	5493	5129	-6.6
10	6785	6264	-7.7

Table 7.6: Comparison first and repeated stiffness at 80 μm/m and T=20°C

Frequency [Hz]	First stiffness [MPa]	Repeated stiffness [MPa]	Difference [%]
0.5	584	602	3.1
1	851	757	-11.0
2	1083	1068	-1.4
5	1734	1615	-6.9
10	2236	2099	-6.1

Table 7.7: Comparison first and repeated stiffness at 80 μm/m and T=30°C

Table Titt Compan	rable 1111 Companies in mot and repeated commede at 60 pm m and 1 co c					
Frequency [Hz]	First stiffness [MPa]	Repeated stiffness [MPa]	Difference [%]			
0.5	314	262	-16.6			
1	332	350	5.4			
2	418	384	-8.1			
5	515	490	-4.9			
10	791	707	-10.6			

It shows that, although the specimens are tested before in the fatigue test (loaded until the stiffness decreased to half of the initial stiffness), the stiffness has increased again in the 2.5 months of rest. The result is a rather small difference (averagely the difference is –6.5%) between the first and the repeated stiffness. This phenomenon is a result of healing of the material. Healing can be defined as the self-restoring capacity of the mix. This means that a mix can sustain less load repetitions if the test specimens are subjected to a repeated cyclic loading than they can sustain if between the load cycles rest periods are introduced [Molenaar, 1994]. Healing is highly dependent on the bitumen content and the degree of filling of a mix, as well as the hardness of the bitumen. An increasing bitumen content leads to an increasing healing capacity of the mix. Due to the high bitumen content of mastic asphalt a good healing behaviour is to be expected, which is in accordance with the test results.

Figures 7.1-7.3 show the master curves for both the first and repeated measurements at a strain level of 80 μ m/m.

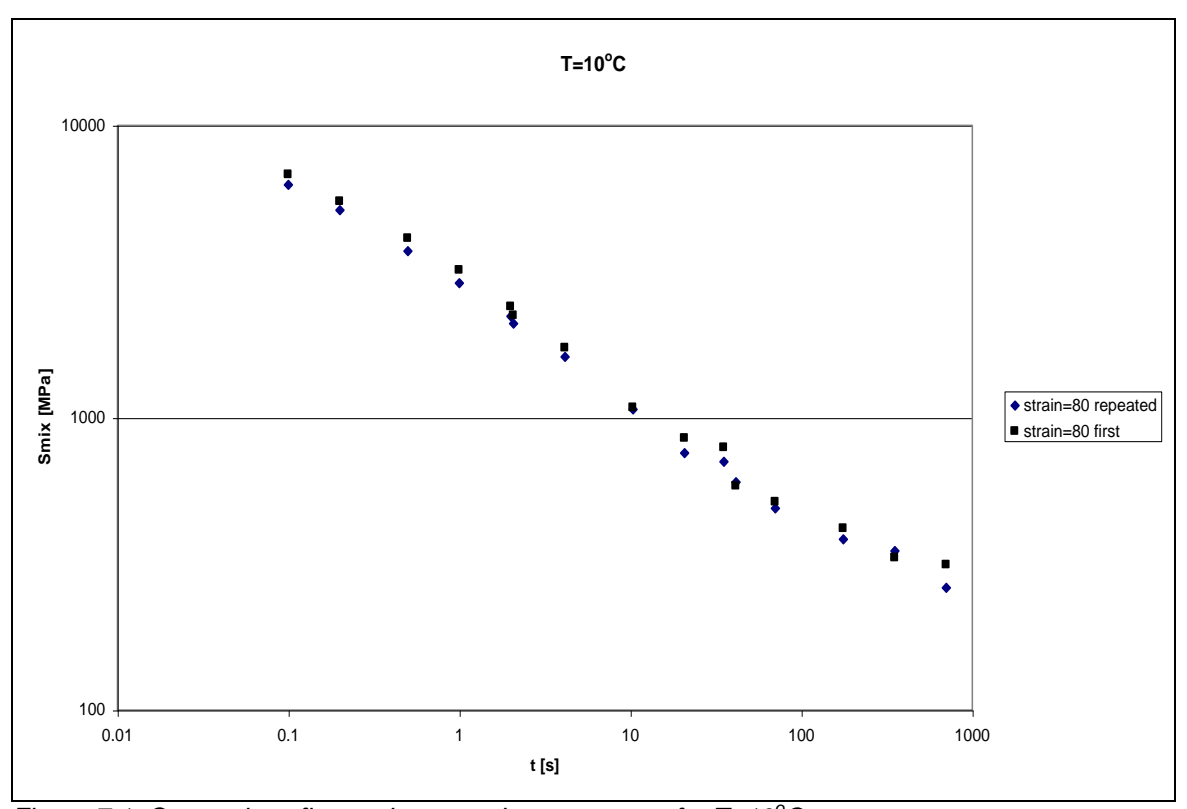


Figure 7.1: Comparison first and repeated master curve for T=10°C

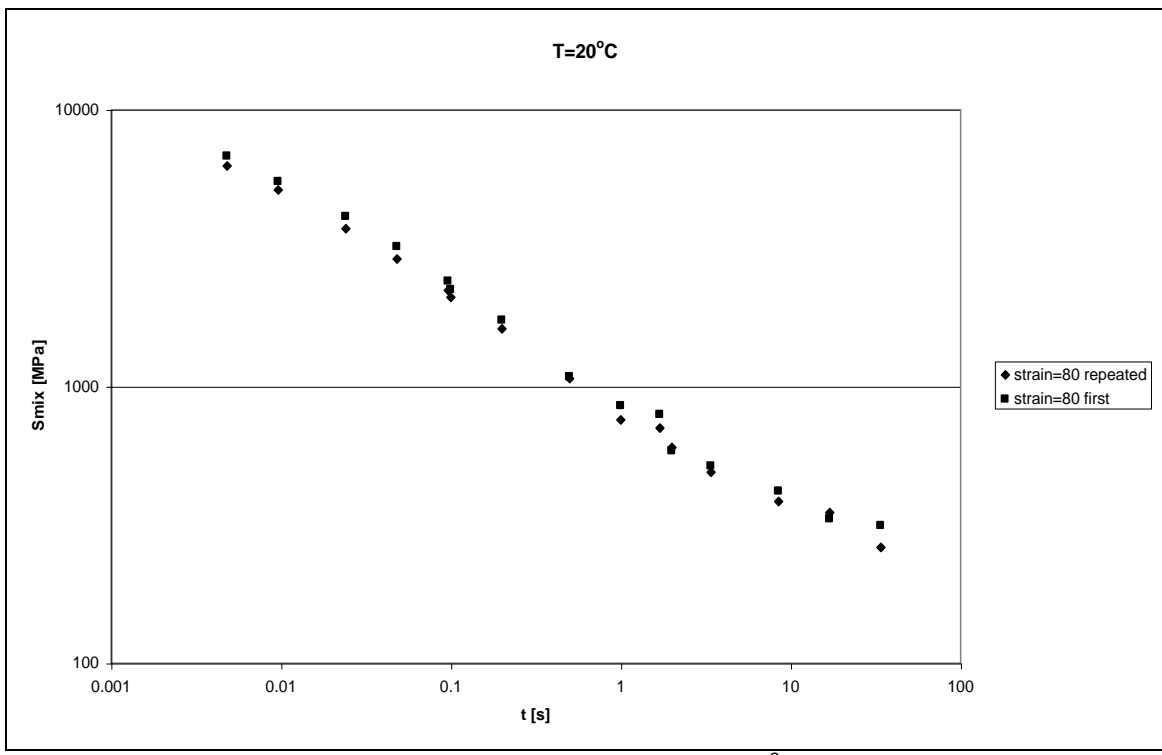


Figure 7.2: Comparison first and repeated master curve for T=20°C

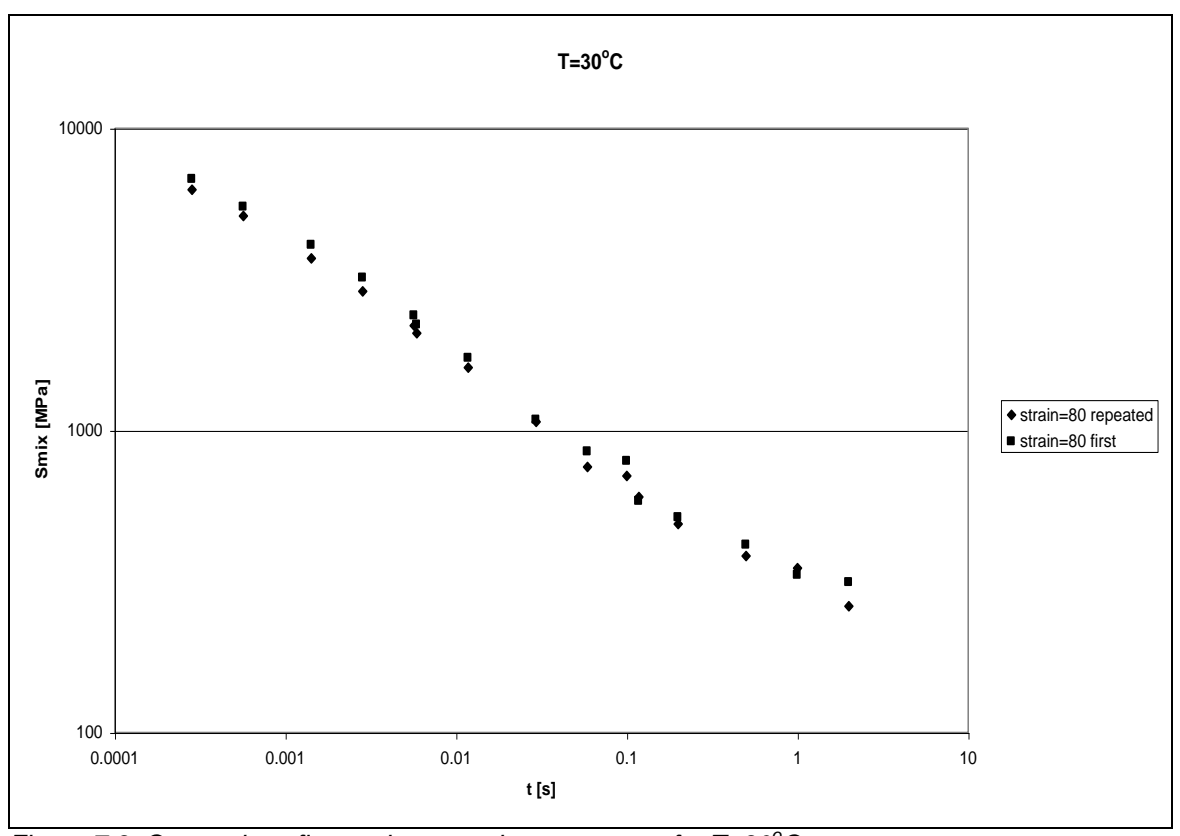


Figure 7.3: Comparison first and repeated master curve for T=30°C

From these figures the small difference between the first and the repeated stiffness measurements at a strain level of 80 μ m/m becomes very clear.

7.1.5 Comparison of the stiffness behaviour of some different mastic asphalt mixes

Kolstein [1989] determined the stiffness at temperatures of -10°C, 0°C, 10°C and 20°C and at loading frequencies of 1, 3, 5, 7, 9, 20 and 30 Hz. The strain amplitude in the tests was 80 μ m/m. DWW tested the GIET-DWW at temperatures of -10°C, -5°C, 0°C, 5°C, 10°C, 15°C and 20°C and at frequencies of 5.9, 9.8, 19.5, 25.4, 29.3, 35.2, 39.1, 50.8 and 58.6 Hz. The strain amplitude in the tests was 80 μ m/m.

The data from Kolstein, DWW and the Moerdijk mix are used to create the master curves at a temperature of 20°C (see figure 7.4). To create all these master curves the equation from Francken [1988] was used.

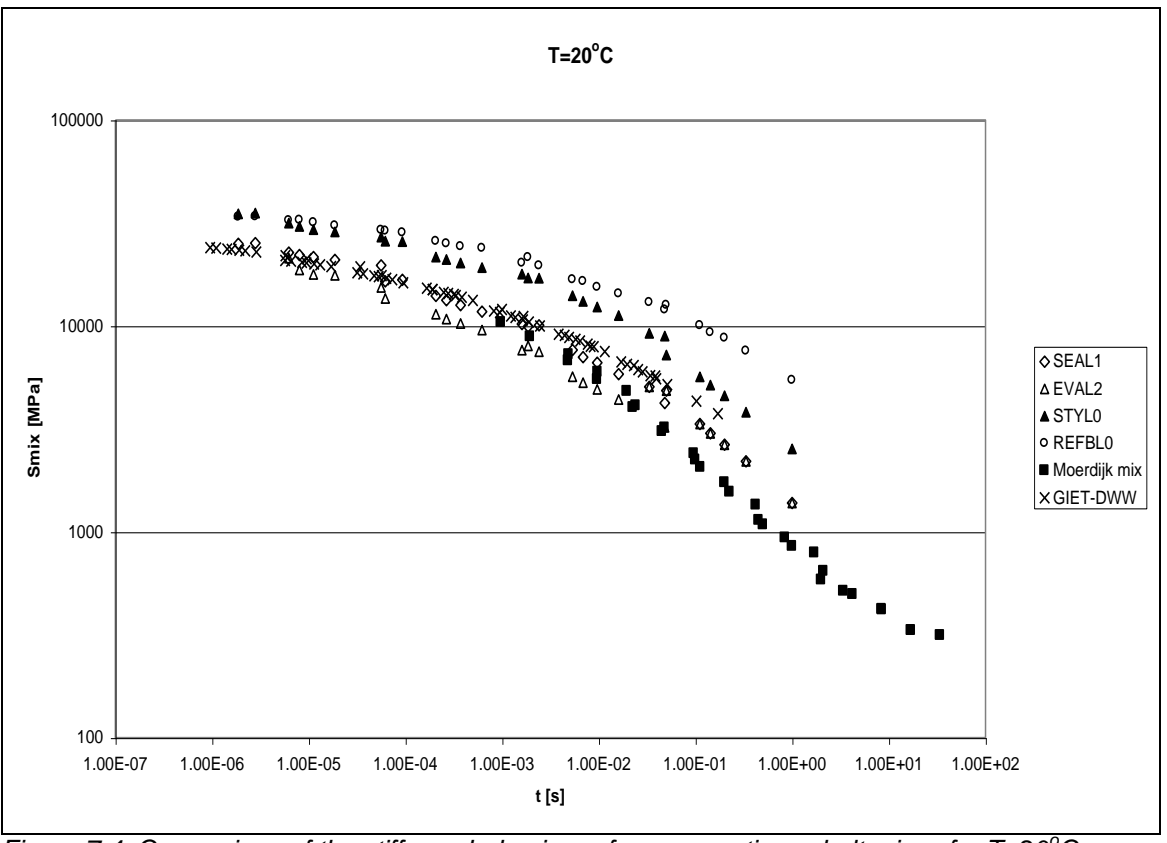


Figure 7.4: Comparison of the stiffness behaviour of some mastic asphalt mixes for T=20°C

This figure shows that the stiffness behaviour of the Moerdijk mix is comparable with the stiffness of EVAL2, GIET-DWW and SEAL1 for loading times near 0.01 s. At this loading time the stiffness of STYL0 and REFBL0 is higher than that of the Moerdijk mix. For loading times higher than 0.01 s the difference between the stiffness of the mixes increases. For t=1.0 s all mixes have a higher stiffness than the Moerdijk mix. This means that for fast moving traffic the stiffness of the Moerdijk mix is comparable to that of EVAL2, GIET-DWW and SEAL1, but in that case the stiffness is smaller than that of STYL0 and REFBL0. For low traffic speeds the stiffness of the Moerdijk mix is smaller than that of the other mixes.

7.1.6 Stiffness behaviour of mastic asphalt compared to some other types of asphalt mixes

Also a comparison can be made between mastic asphalt and some other types of asphalt mixtures. To create the master curves for ZOK and ZOAB-DWW test data from four-point bending tests are used. For the GAB the next relation, determined by Sassen [1991], is used:

$$\log S_{mix} = 3.59939 - 0.373735(\log t) - 0.069368(\log t)^2 - 0.00522(\log t)^3$$
 Equation 7.3

Again the master curves for a temperature of 20°C were created (figure 7.5).

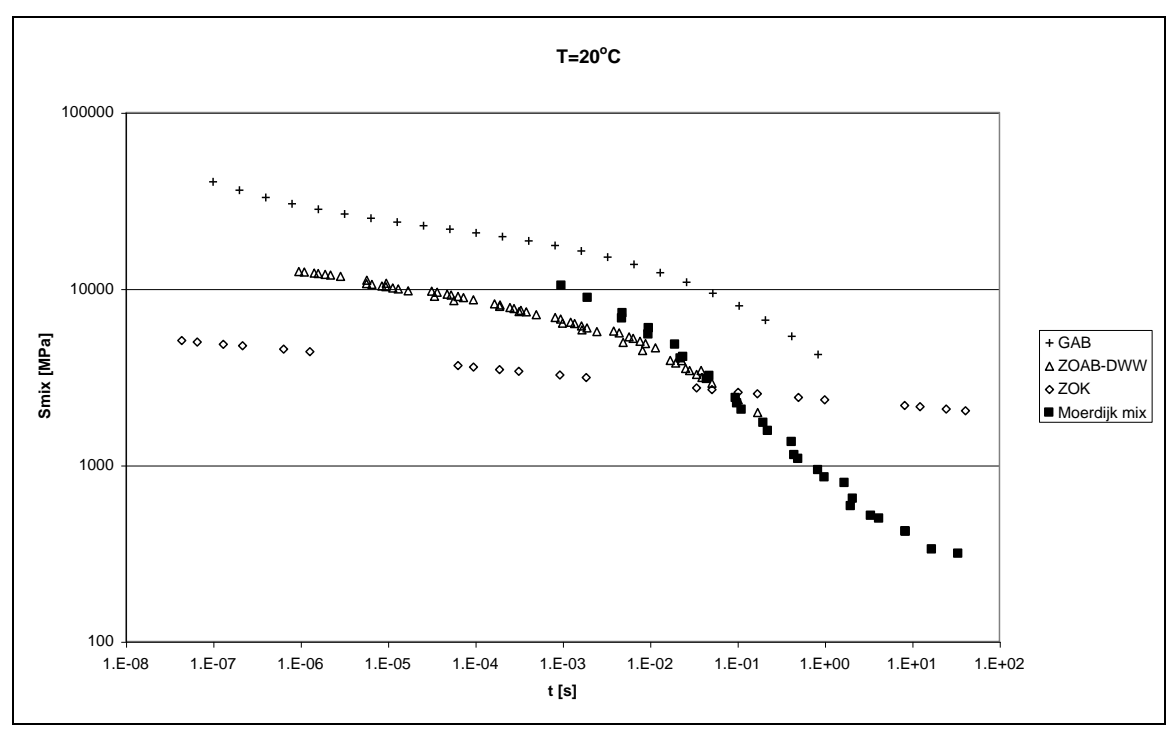


Figure 7.5: Master curves for some different types of asphalt mixes

From figure 7.5 it becomes clear that the stiffness behaviour of mastic asphalt is comparable to the stiffness behaviour of ZOAB-DWW for loading times between 0.001 and 0.1 s. For other loading times no comparison can be made because the master curves are valid in different ranges of loading times. Figure 7.5 also shows that the stiffness of GAB is higher than that of the other mixes.

The master curve of ZOK is totally different from the other master curves. These master curves show an increasing dependency of the stiffness on the loading time for increasing loading times. However, the master curve for ZOK is a straight line in the whole range of loading times. The slope of the line is very small, which means that the stiffness of ZOK hardly varies with loading time. This results in a less stiff behaviour of the material in situations of traffic driving with high speed. In situations of slow driving traffic the stiffness is considerably higher.

7.2 Fatigue characteristics

7.2.1 Introduction

The fatigue behaviour of an asphalt mix is an important characteristic that is used for road engineering. First the fatigue behaviour of the first fatigue test is analysed. Secondly the repeated fatigue test is analysed, after which both fatigue tests are compared.

Further the fatigue behaviour of the modified Moerdijk mix is compared to that of other mixes. At first it is compared to the fatigue behaviour of four modified mastic asphalt mixes that were tested by Kolstein [1989]. Further it is compared to the fatigue behaviour of GAB and DAB 0/8. To create the fatigue line of GAB the relation determined by Wattimena [1991] is used. This is a result of four point bending tests carried out by the Netherlands Pavement Consultants. The fatigue line of DAB 0/8 is a result of tests at the Road and Hydraulic Engineering Division (DWW) carried out by Pronk [1998].

7.2.2 First fatigue test

7.2.2.1 Characterisation of fatigue parameters using the Wöhler approach

The Wöhler approach is a relationship between the number of strain applications to failure and the flexural tensile strain, which occurs at the bottom of the test specimen written as:

$$N_f = k_1 \left(\frac{1}{\varepsilon}\right)^n$$
 Equation 7.4

where:

 N_f : number of strain applications to failure

 ε :flexural tensile strain at the bottom of test specimens [μ m/m]

 k_1 , n: factors, depending on the composition and properties of the asphalt mix

The Wöhler relationship can be rewritten as:

$$\log N_f = \log k_1 - n \log \varepsilon$$
 Equation 7.5

It should be noted in this context that N_f is defined as the number of load repetitions at which the stiffness has decreased to half of the initial flexural stiffness value, since the fatigue tests were carried out in a displacement-controlled mode. The values of k_1 and n are determined by regression analysis. For mastic asphalt the parameters are:

 $log k_1=23.903$ n=6.7363 $R^2=0.987$

Figure 7.6 shows the fatigue characteristics for the Moerdijk mix using the Wöhler approach.

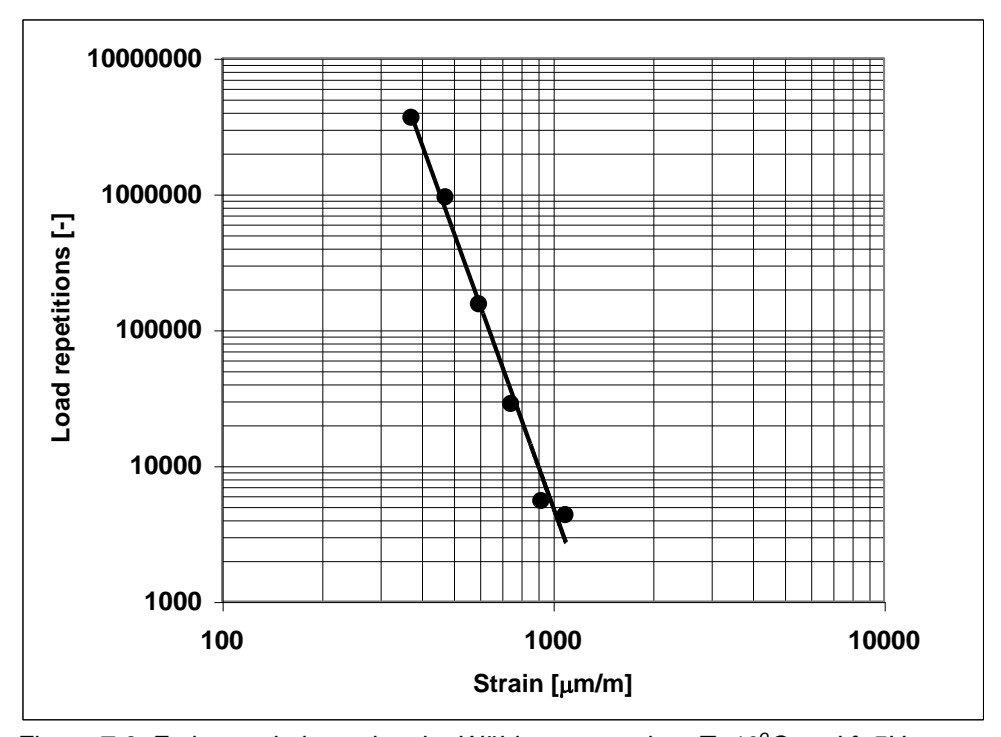


Figure 7.6: Fatigue relation using the Wöhler approach at T=10°C and f=5Hz

7.2.2.2 Characterisation of fatigue parameters using the energy approach

The dissipated energy is an alternative approach to fatigue characterisation. In this characterisation the number of load repetitions is related to the dissipated energy. Van Dijk [1975] showed that the total energy dissipated per volume to fatigue failure can be written as:

$$W_f = B_f N_f^z$$
 Equation 7.6

where:

 W_f : total amount of dissipated energy per volume [J/m³]

: number of load repetitions to fatigue failure

 B_f , z: constants

Equation 7.6 can be rewritten as:

$$\log W_f = \log B_f + z \log N_f$$
 Equation 7.7

The values of B_t , and z are determined by regression analysis.

B=0.0394 z=0.753 $R^2 = 0.9979$

The value of z is comparable with the value of 0.7 reported by Van Dijk and Visser [1977] for several mixes. Furthermore, the value of B_f is different from the value of 0.012 reported by van Dijk and Visser [1977]. The higher value of B_f for mastic asphalt indicates that more energy is dissipated for the same number of load repetitions, meaning a better fatigue resistance.

Figure 7.7 shows the fatigue characteristics of the Moerdijk mix using the energy approach.

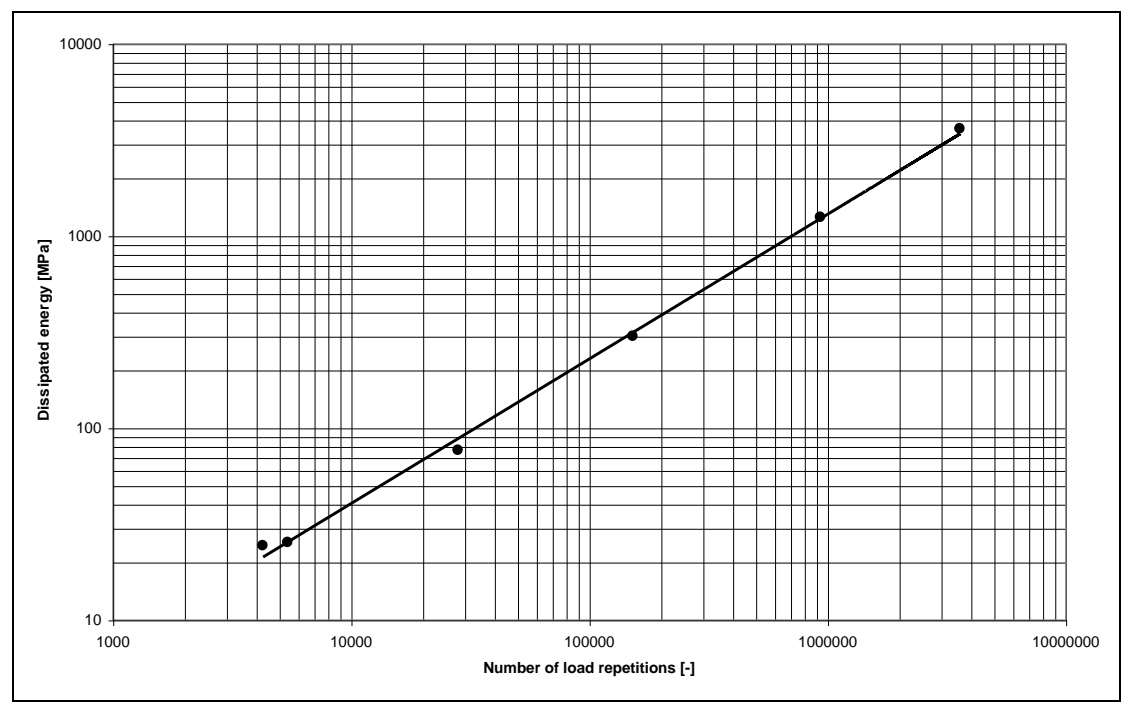


Figure 7.7: Fatigue characteristics of the Moerdijk mix using the energy approach

7.2.2.3 Relationship between the strain, the mix stiffness and the number of load repetitions

The fatigue behaviour of mastic asphalt can be presented in a different way, when also the mix stiffness is involved. Table 7.8 shows the values of the strain, number of load repetitions and the stiffness, that were measured during the first fatigue tests on the Moerdijk mix.

Table 7.8: Results from the first fatigue test on the Moerdijk mix

Strain [μm/m]	Load repetitions [-]	Initial stiffness [MPa]
375	3600000	4679
475	934900	4444
600	152630	4083
750	28140	3443
925	5430	3820
1095	4270	3174

Regression analysis with the data in table 7.8 resulted in the following relation between the number of load repetitions, the strain and the mix stiffness:

$$\log N = a_1 - n_1 \log \varepsilon - n_2 \log S_{mix}$$

Equation 7.8

in which:

N : number of load repetitions [-]

 ε : strain [μ m/m]

 S_{mix} : initial mix stiffness [MPa]

 a_1 : 33.377 n_1 : 7.439 n_2 : 2.086

The output from the regression analysis that was carried out to obtain equation 7.8 is shown in appendix F. By using equation 7.8 a new fatigue chart is obtained as shown in figure 7.8.

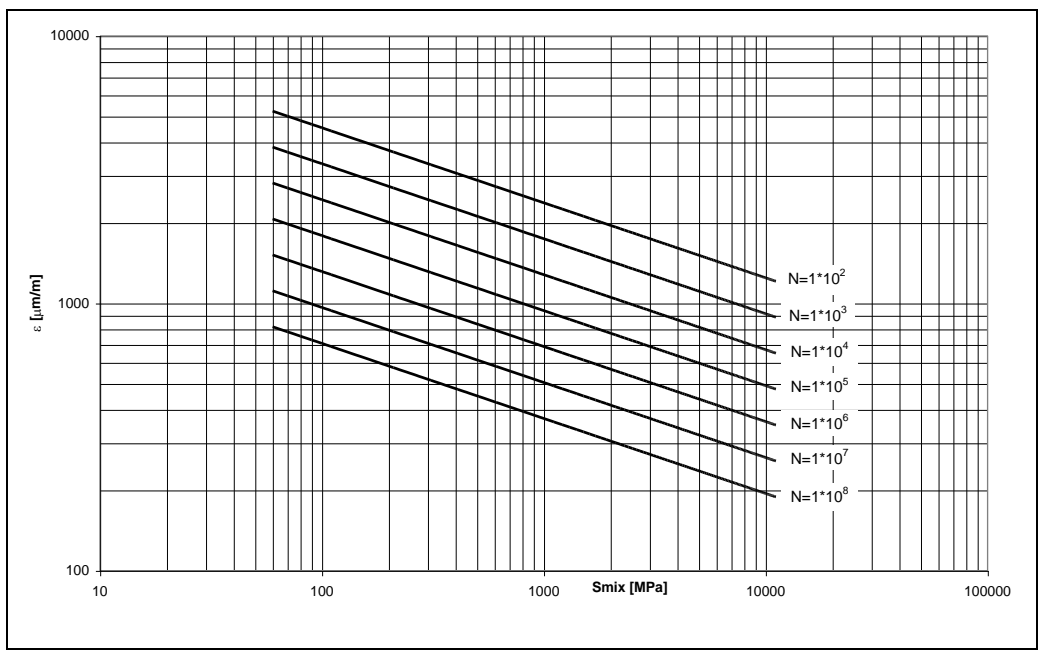


Figure 7.8: Relation between the number of load repetitions, the stiffness and the strain

7.2.3 Repeated fatigue test

7.2.3.1 Characterisation of fatigue parameters using the Wöhler approach

After repetition of the fatigue test the parameters used in equation 7.5 are determined for the repeated fatigue line:

Log k_1 =33.477 n=10.06 R^2 =0.969

Figure 7.19 shows the fatigue characteristics after repeating the test by using the Wöhler approach.

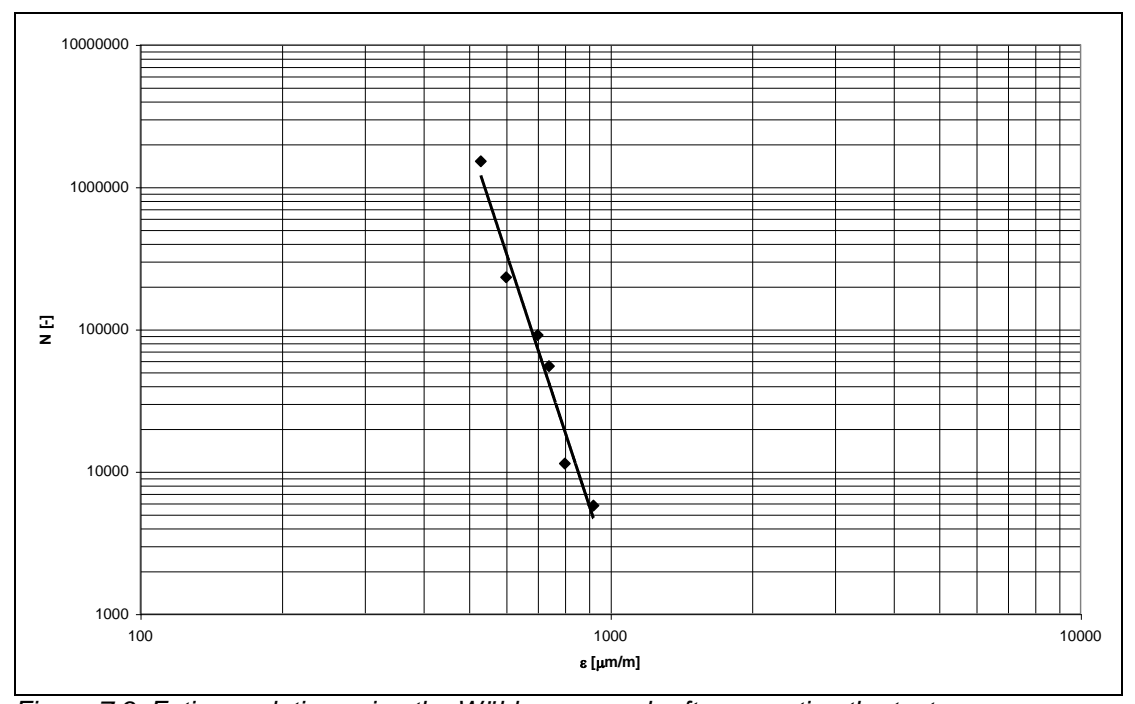


Figure 7.9: Fatigue relation using the Wöhler approach after repeating the test

7.2.3.2 Characterisation of fatigue parameters using the energy approach

After repetition of the test the values of B_f , and z in equation 7.7 are determined by regression analysis for the repeated test.

B = 0.024 z = 0.7992 $R^2 = 0.9989$

The value of z is again comparable with the value of 0.7 reported by Van Dijk and Visser [1977]. Furthermore, the value of B_f is of the same order of magnitude to the value of 0.012 reported by van Dijk and Visser [1977].

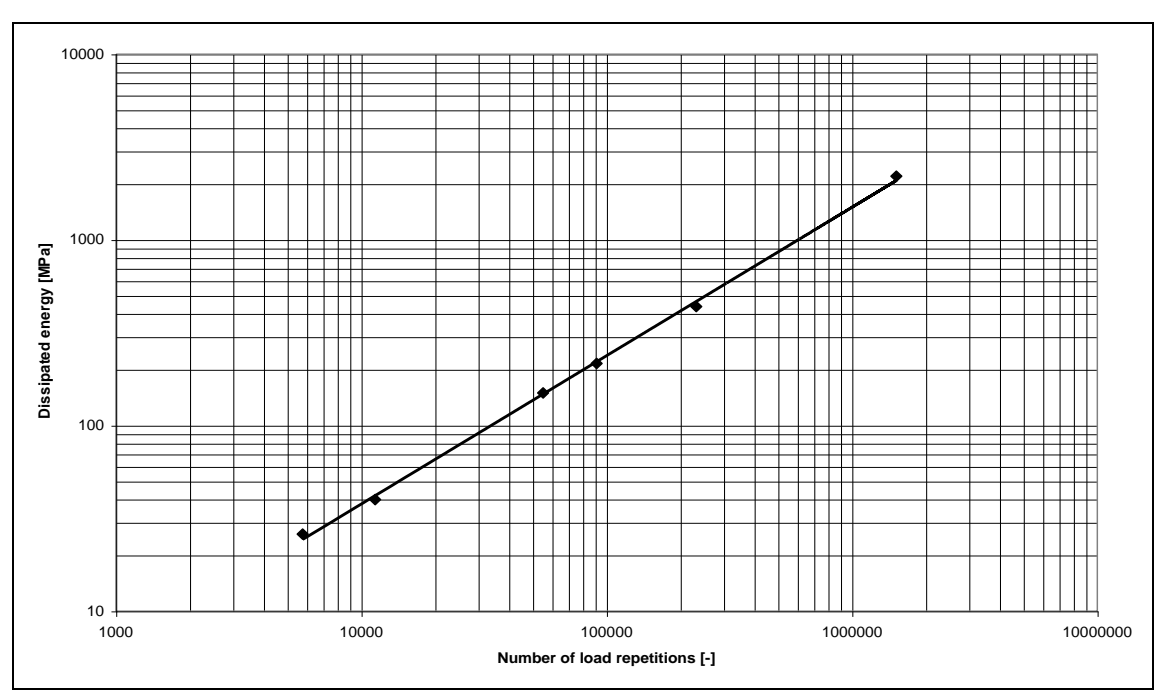


Figure 7.10 shows the fatigue characteristics of the tested mix using the energy approach.

Figure 7.10: Fatigue characteristics of the mix using the energy approach after repeating the test

7.2.4 Comparison between the first and repeated fatigue test for the Moerdijk mix

In order to investigate the influence of healing it was decided to repeat the fatigue test on the Moerdijk mix after 2.5 months after the repetition of the determination of the master curves. Both the fatigue line of the first test and the fatigue line of the repeated test are shown in figure 7.11.

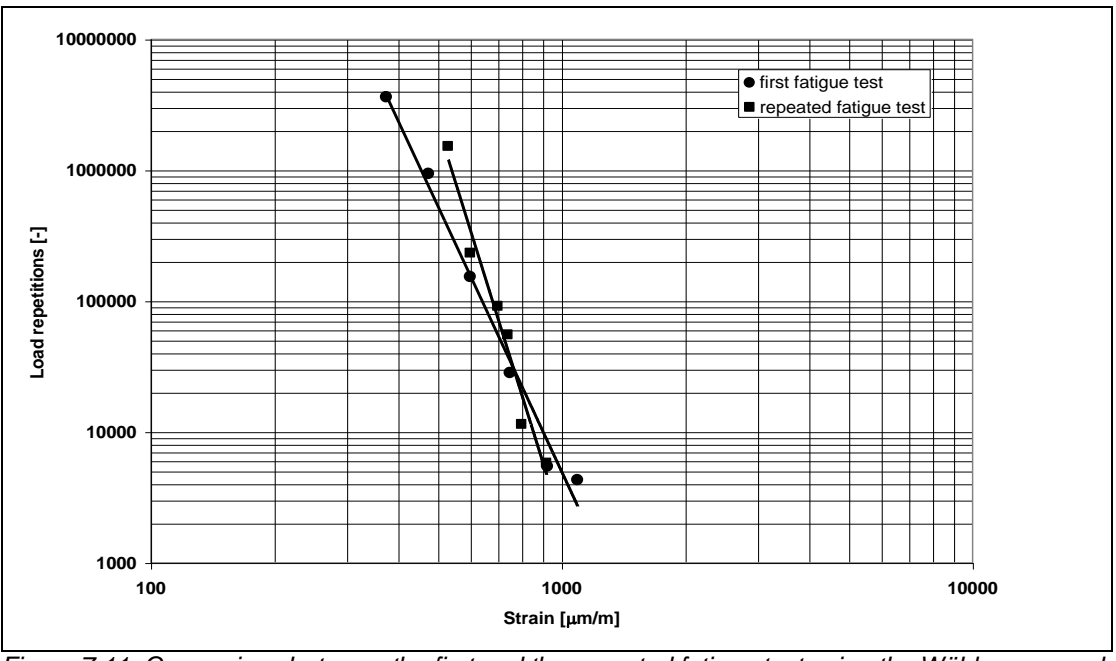


Figure 7.11: Comparison between the first and the repeated fatigue test using the Wöhler approach

Both fatigue lines cross at a strain level of 760 μ m/m and the number of load repetitions is approximately 31350. The figure shows that the slope of the fatigue line has increased after repetition of the test. This corresponds to a somewhat more brittle behaviour of the specimen. The effect is that the material becomes more sensible to high strain levels and behaves better under lower strain levels.

The reason for this might be the ageing of the bitumen during the two and a half months of storage, in spite of the fact that the specimens were stored in a temperature controlled room at 13°C between both tests. Further the healing of the material plays an important role.

Figure 7.12 shows the comparison between the first and repeated fatigue test using the energy approach.

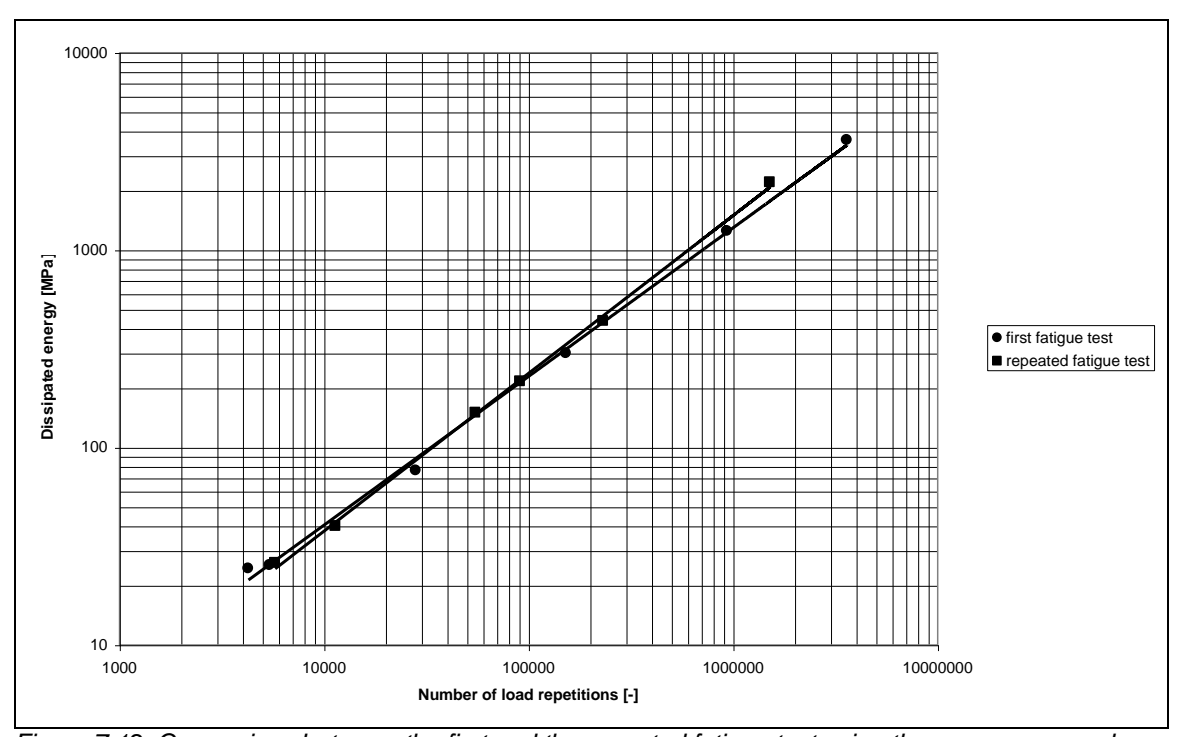


Figure 7.12: Comparison between the first and the repeated fatigue test using the energy approach

Again the fatigue lines cross each other. Using the energy approach the intersection point is N=45700 and E=127 MPa. Comparing the number of load repetitions at the intersection point for the Wöhler and the energy approach shows that the value is higher for the second approach. However, the trend for both approaches is the same, the fatigue behaviour of the material after repetition of the test becomes better for lower strain levels (corresponding to high values of N) and becomes worse for higher strain levels (corresponding to low values of N).

7.2.5 Fatigue behaviour of the Moerdijk mix compared to some modified mastic asphalt mixes

Figure 7.13 shows the fatigue behaviour of the Moerdijk mix and the fatigue behaviour of four modified mastic asphalt mixes, namely REFBL0 (bitumen 45/60 + Trinidad-Épurée), STYL0 (Styrelf 1360), SEAL1 (Sealoflex) and EVAL2 (Bitumen 45/60 + Eva 18-150). It has to be noted that the fatigue lines of these four modified mixes are valid for T=20°C and f=30 Hz, while the fatigue line of the Moerdijk mix is determined at T=10°C and f=5 Hz. Nevertheless these lines are

comparable, because the stiffness of the mixes at these different temperatures and frequencies is comparable.

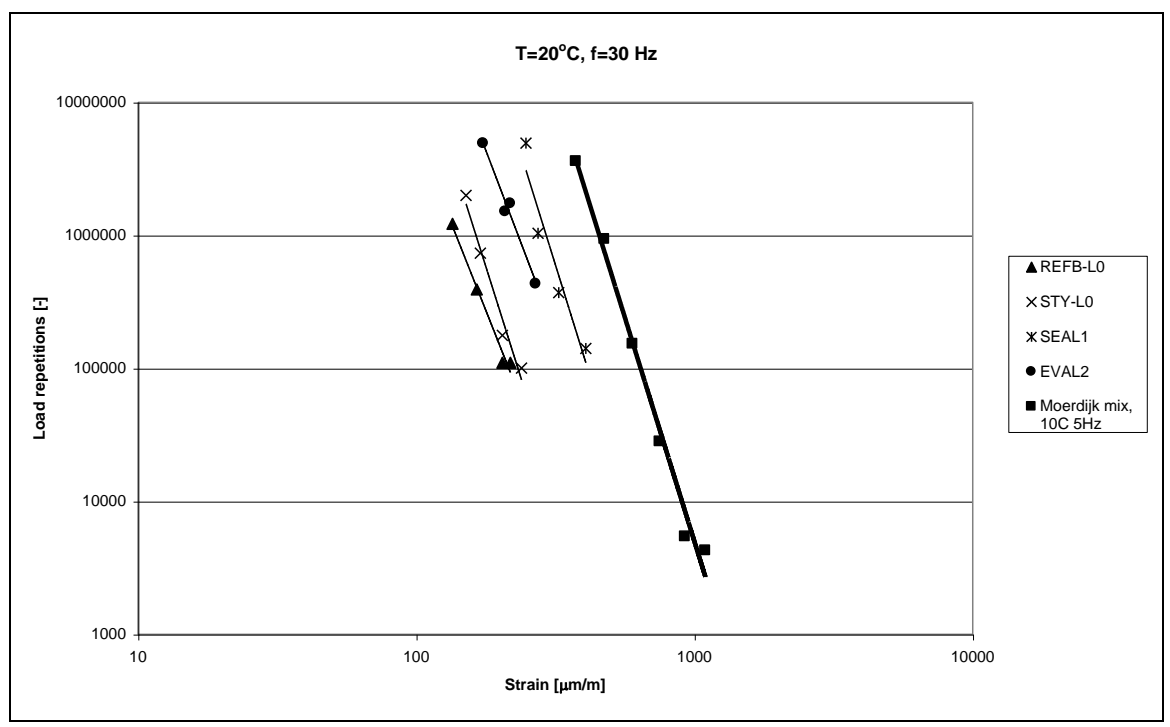


Figure 7.13: Fatigue behaviour of different mastic asphalt mixes

Figure 7.13 shows that the fatigue behaviour of the Moerdijk mix is better than that of the other mixes. The figure also shows that the strain range in which the Moerdijk mix is tested is larger than the range in which the other mixes are tested. The modified mixes are tested within a very small strain range and at quite low strain levels. The validity of these lines is therefore questionable because of the high strains ($\pm 1300~\mu m/m$) that may occur in the asphalt on orthotropic steel bridges.

7.2.6 Fatigue behaviour of the Moerdijk mix compared to some other mixes

Figure 7.14 shows the fatigue behaviour of the Moerdijk mix, GAB and DAB 0/8. For the GAB the relation is used that is determined by Wattimena [1991]. This relationship is:

$$\log N = 12.40 - 3.63 \log \varepsilon$$

In this relation ε is in μ m/m.

For the DAB the relation determined by Pronk [1998] is used:

$$\log N = 14.69 - 4.06 \log \varepsilon$$
 Equation 7.10

In this relation ε is in μ m/m.

The relations from Wattimena and Pronk are determined at T=20°C and f=30 Hz, the fatigue line of the Moerdijk mix is valid for T=10°C and f=5 Hz. However the results are comparable because at these different conditions the stiffness of the mixes is approximately the same.

Equation 7.9

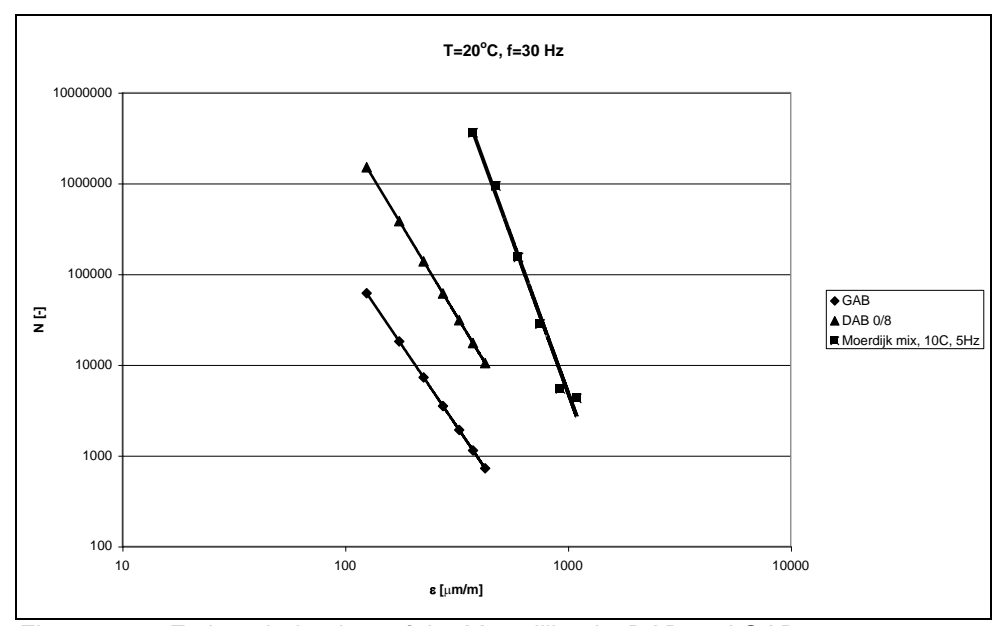


Figure 7.14: Fatigue behaviour of the Moerdijk mix, DAB and GAB

Figure 7.14 shows that the fatigue behaviour of the Moerdijk mix is better than the fatigue behaviour of GAB and DAB tested by Wattimena and Pronk. It should be noted that the range of strains in which the Moerdijk mix was tested differs considerably from the range in which the GAB and the DAB were tested. This is attributed to the fact that for orthotropic steel bridges higher strain levels are of interest. Under these high strain conditions the behaviour of the material may be different, which might have led to the differences in figure 7.14 between the mixes.

7.2.7 Fatigue behaviour of the Moerdijk mix compared to the SPDM

Additional fatigue information is obtained by comparing the fatigue behaviour of the Moerdijk mix with the F1 and F2 SPDM lines, using the Shell pavement Design Manual [SPDM 1978]. To use this manual the average initial stiffness from the first fatigue tests is taken, which is 3941 MPa. The corresponding SPDM F1 and F2 fatigue characteristics were determined by using charts M3 and M4 from the SPDM, see figure 7.15.

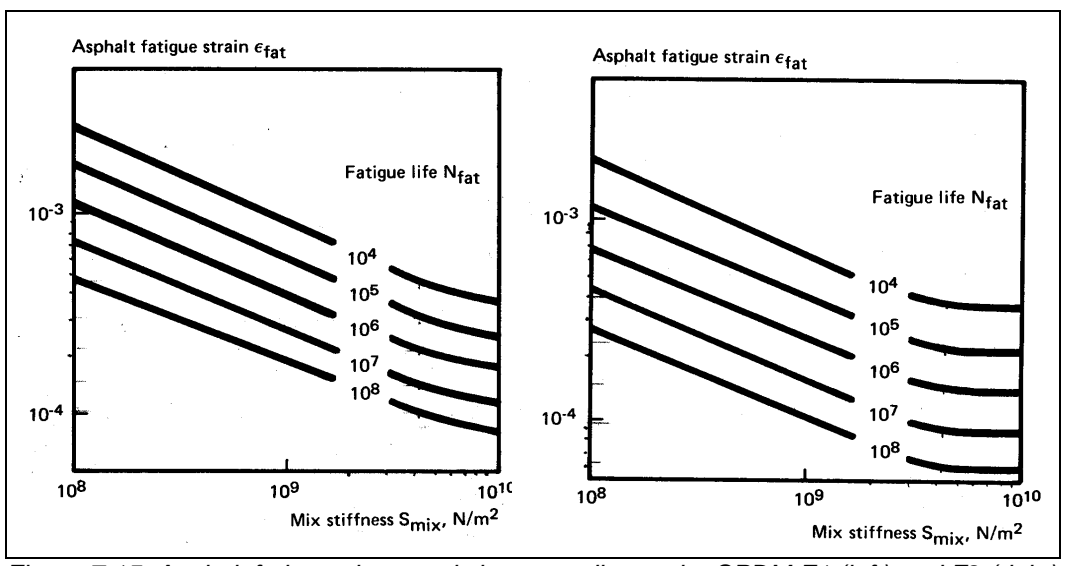


Figure 7.15: Asphalt fatigue characteristics according to the SPDM F1 (left) and F2 (right)

The SPDM F1 and F2 characteristics are shown in table 7.9.

Table 7.9: Load repetitions according to SPDM for the average Moerdijk mix stiffness

	Corresponding strain [μm/m]			
N	SPDM F1	SPDM F2		
1.00E+04	500	420		
1.00E+05	340	240		
1.00E+06	220	160		
1.00E+07	145	90		
1.00E+08	100	60		

According to the design manual the following can be used as a rough guide:

F1: Many base course mixes with moderate bitumen and voids contents

F2: Many base course mixes with relatively higher voids contents

For the comparison this means that F1 can be compared best with the Moerdijk mix fatigue line since this mix has a very small voids content. With the data of table 7.9 the fatigue line of the Moerdijk mix can be compared to the SPDM F1 and F2 fatigue lines. This comparison is shown in figure 7.16.

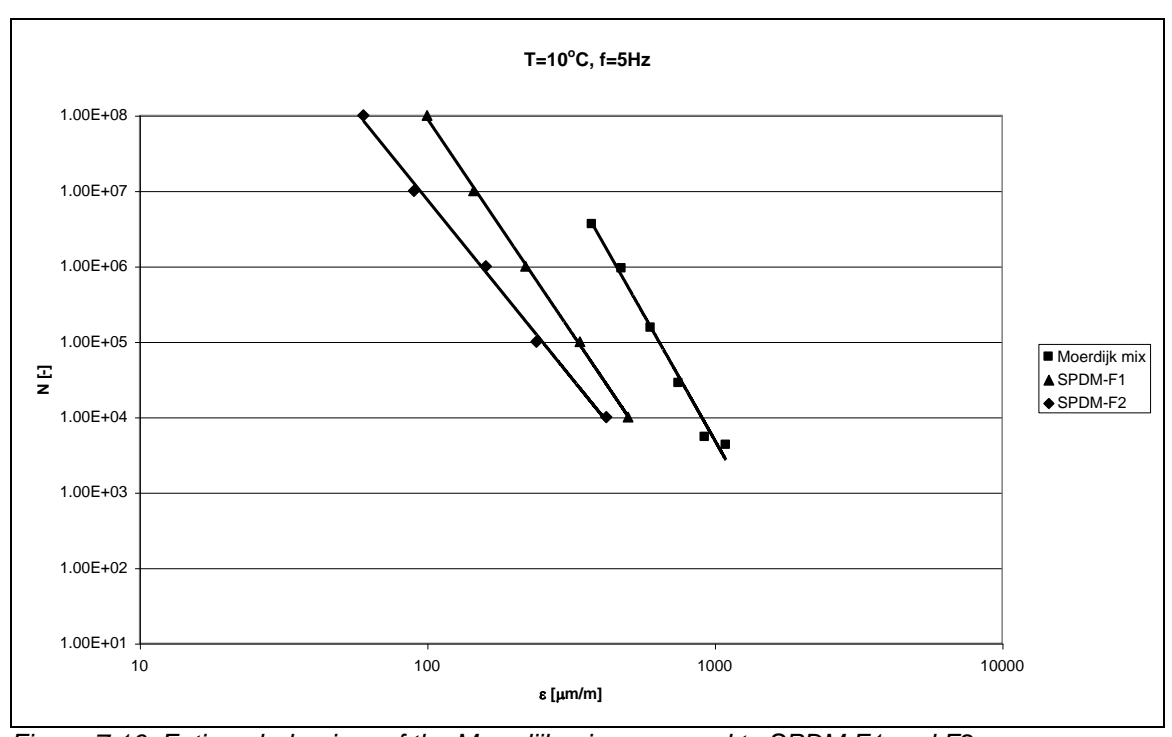


Figure 7.16: Fatigue behaviour of the Moerdijk mix compared to SPDM F1 and F2

From this figure it can be seen that the Moerdijk mix is rather fatigue resistant compared to the Shell F1 and F2 fatigue line. It should be noted that the F1 and F2 fatigue line are valid for average mix types. Therefore some difference may be expected because mastic asphalt is a special type of asphalt with special properties that differs considerably from the average types of asphalt.

The procedure for the development of the fatigue charts F1 and F2 by Shell is based on the energy approach.

Equation 7.6 was related to the limiting strain, by using the dissipated energy per cycle per unit volume:

$$W = \pi \sigma \varepsilon \sin \varphi$$
 Equation 7.11

where:

 σ : stress amplitude ε : strain amplitude

If the dissipated energy per cycle is constant, the relation between the total amount of dissipated energy W_f and the dissipated energy per cycle is:

$$W_f = N_f \times W_{in}$$
 Equation 7.12

in which:

 W_f : total amount of dissipated energy per volume N_f : number of load repetitions to fatigue failure

 W_{in} : initial dissipated energy per cycle = $\pi \cdot \sigma_0 \cdot \varepsilon_0 \cdot \sin \varphi_0$ $\sigma_0, \varepsilon_0, \phi_0$: stress, strain and phase angle at the beginning of the test.

However, the dissipated energy per cycle decreases during a constant displacement fatigue test and increases in a constant load fatigue test due to the change of σ , ϵ and ϕ_0 . Therefore equation 7.12 changes in:

$$W_f = N_f \times W_{in} / \psi$$
 Equation 7.13

where:

ψ : factor taking into account the variation in dissipated energy per cycle during the test

For a displacement controlled test ψ is larger than 1 and in a load controlled test ψ is smaller than 1.

Combination of equation 7.6 and 7.13 results in:

$$\frac{N_f \cdot \pi \cdot \sigma_0 \cdot \varepsilon_0 \cdot \sin \varphi_0}{\psi} = B_f N_f^z$$
 Equation 7.14

Rewriting equation 7.14 results in the relation between the strain, S_{mix} and N:

$$arepsilon_0 = \sqrt{\frac{B_f \psi}{\pi S_{mix} \sin \varphi_0}} \cdot N^{(z-1)/2}$$
 Equation 7.15

It has been observed that the variation of Z is very small for common mixes and can be taken as constant for practical purposes ($Z\approx0.7$). By taking a B_f value representing a good fatigue behaviour and a B_f value representing a worse fatigue behaviour different charts can be developed. On this procedure the design charts F1 and F2 are based [Molenaar, 1994].

7.2.8 Relationship between the mix stiffness and the number of load repetitions in a fatigue test

A typical experimental relationship between the mix stiffness and the number of load repetitions is shown in figure 7.17.

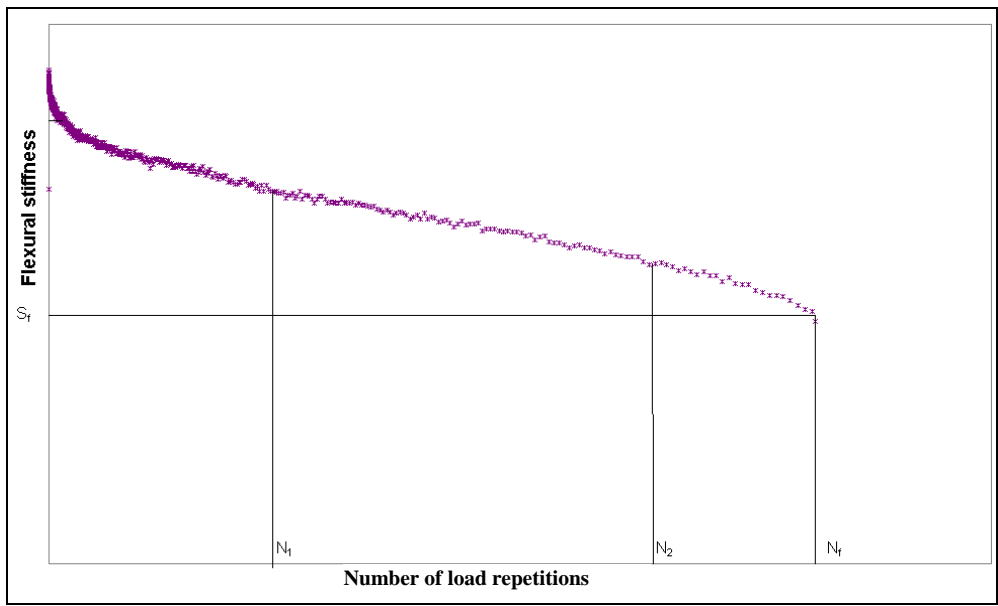


Figure 7.17: A typical relationship between the stiffness and the number of cycles in a straincontrolled four point bending test

Three parts can be distinguished:

- 1. Part I: At the beginning of the test a sharp decrease of the stiffness modulus may be observed. According to Ullidtz et al. [1997] this might probably be due to the visco-elastic characteristics of the asphalt where the dissipation energy will cause an increase of the temperature in the beam until the heat flow has reached a steady state.
- 2. Part II: In the second part the rate of the stiffness loss is almost constant (from N₁ to N₂).
- 3. Part III: A sharp decrease of the stiffness may also be observed. This part seems to be associated with the development of macrocracks (from N_2 to N_f).

The similarity between these three parts and the three stages which can be distinguished [e.g. Ewalds and Wanhil, 1986] in the fracture mechanics approach is obvious. The three stages are:

- 1. The initiation phase: development of hairline or micro cracks,
- 2. The propagation phase: development of macro cracks out of microcracks,
- 3. The disintegration phase, being the propagation of the macro cracks, leading to collapse and initial failure of the material. In this phase unstable crack growth can be observed.

From the analysis of the fatigue data of the Moerdijk mix the following remarks can be made:

 Part III was reached in none of the specimens. The reason is that the stiffness was halved, and thus the test was terminated, before the initiation of this part. This may suggest that researchers should think of another more fundamental definition of failure instead of the arbitrary chosen criteria, which considers the specimen is failed when the initial flexural stiffness is halved. • Table 7.10 shows the ratio N_1/N_f for the six fatigue tests that were carried out.

Table 7.10: Ratio N₁/N_f

Specimen	Strain level [µm/m]	N_f	N_1	N_1/N_f
FM2	1095	4270	-	-
FM3	600	152630	41000	0.27
FM4	375	3600000	675000	0.19
FM5	750	28140	8250	0.29
FM6	925	5430	-	-
FM7	475	934900	200000	0.21

- The value of the ratio of N_1 (which defines the end of Part I) to N_f (i.e. the number of cycles to failure) was found to be 0.19-0.29 for low values of the strain. For higher values of the strain level the ratio of N_1 to N_f can not be determined because then the stiffness decreases so fast that half of the stiffness is reached before N_1 is reached.
 - It has been demonstrated by a large number of researchers [Jenq and Perng, 1991; Ramsamooj, 1991] that the characterisation of fatigue by these three stages is only valid if the plastic deformation is limited, especially if asphaltic materials are studied. This may explain the fact that for high strain levels no N_1 value can be defined, because for high strain levels (in this case $\approx 1000 \ \mu m/m$) the plastic deformations are considerable.
- Comparison of the ratio N₁/N_f with values determined by Medani [1999] shows that his values are in approximately the same range (0.18-0.26).

7.3 Dependency of the mix stiffness on the strain

7.3.1 Introduction

For determining the master curves for asphalt mixes used for pavement layers on a subgrade the initial stiffness is determined normally after few load repetitions, say 100, at a low strain level of 80 $\mu\text{m/m}$. This strain level is representative for the strains that occur in pavements on a subgrade. However, on orthotropic steel bridges this strain level can be up to 1300 $\mu\text{m/m}$. These high strain levels might have an influence on the mix stiffness. In this section the strain dependency of the mix stiffness is investigated.

7.3.2 Strain dependency of some asphalt mixes

Also during fatigue testing at different strain levels the initial stiffness is determined after 100 load repetitions. By using the data from the first series of 4-point bending tests figure 7.18 is created, showing the relationship between the strain level and the mix stiffness for the Moerdiik mix.

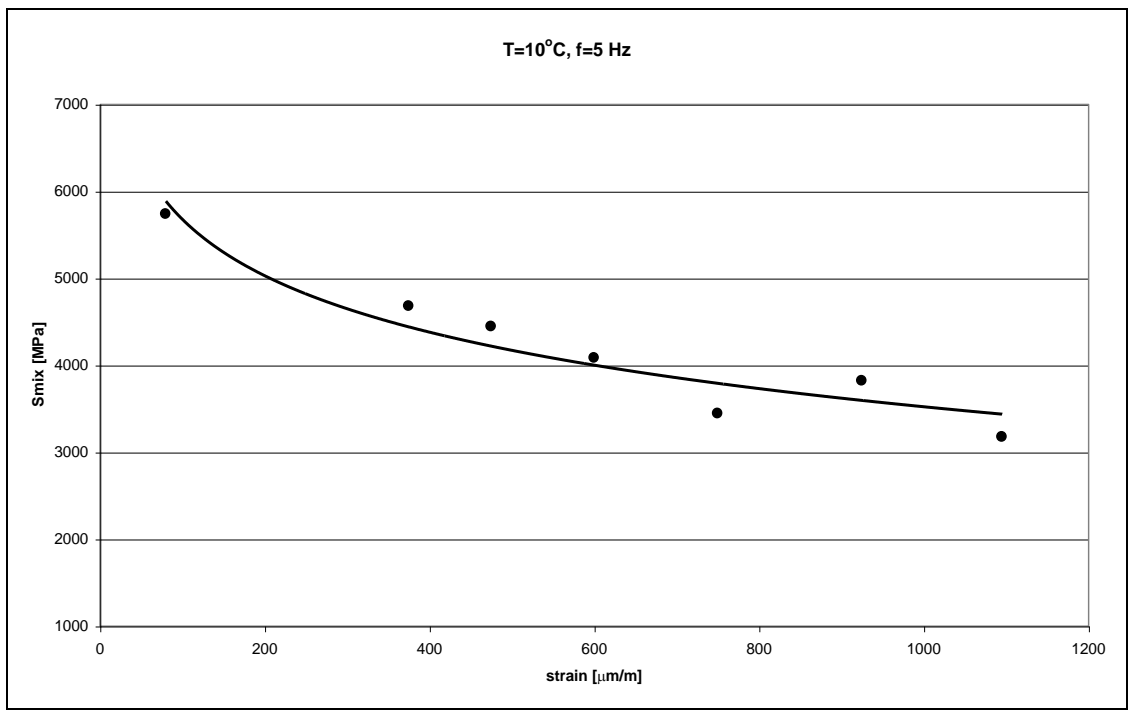


Figure 7.18: Relation between the mix stiffness and strain

This figure shows clearly that the mix stiffness decreases with increasing strain level, which indicates the stress-dependent behaviour of the material. This phenomenon can also be observed for other asphalt mixes. Figure 7.19 shows the relationship between the mix stiffness and the strain for some modified mastic asphalt mixes that have been tested by Kolstein.

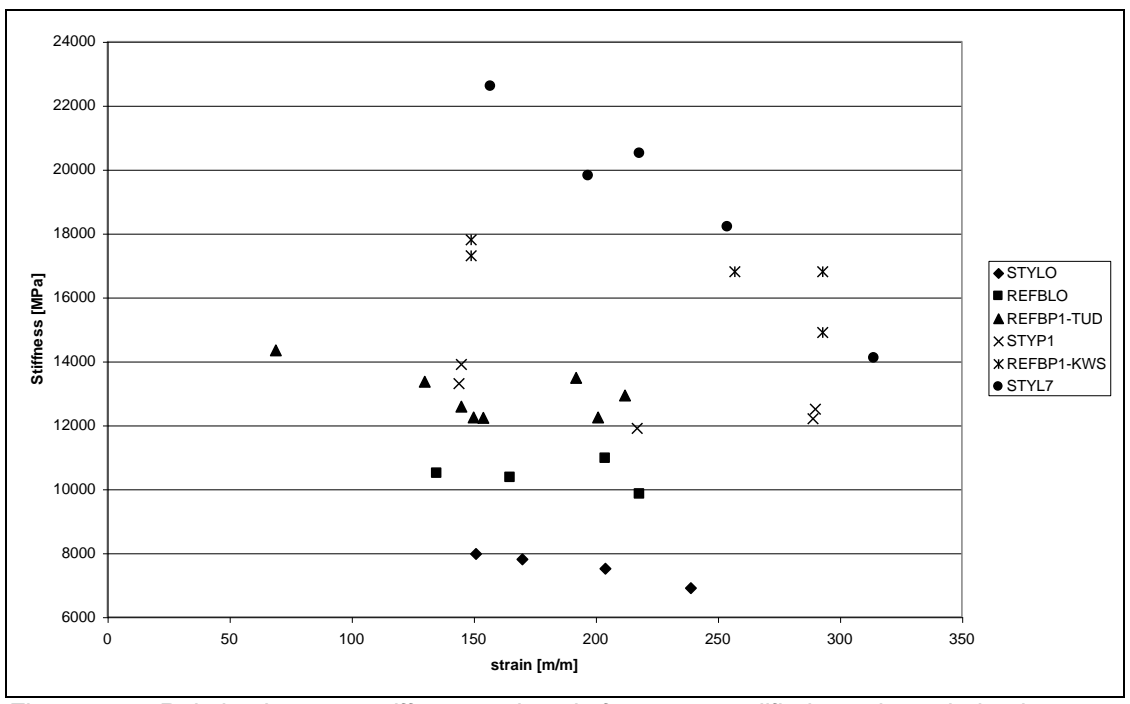


Figure 7.19: Relation between stiffness and strain for some modified mastic asphalt mixes

It has to be noted again that Kolstein tested at very small strain levels. The influence of the strain on the mix stiffness might be increasing with increasing strain level.

Considering the data from the Strategic Highway Research Program (SHRP) [1994] more or less the same trend can be observed for some of the asphalt mixes that were tested in this program. Figure 7.20 shows the relation between the mix stiffness and the strain for some of the mixes tested in the SHRP-program.

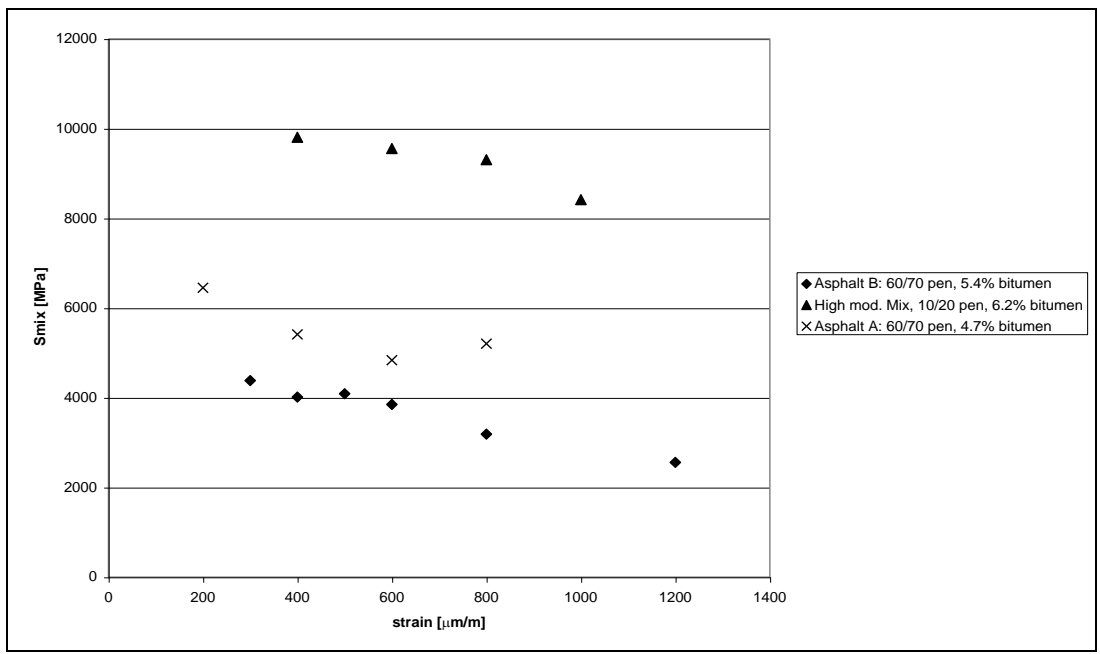


Figure 7.20: Relation between the stiffness and the strain for mixes tested in the SHRP program

Also some mixes tested at the TU Delft show a certain relation between the mix stiffness and the strain as shown in figure 7.21.

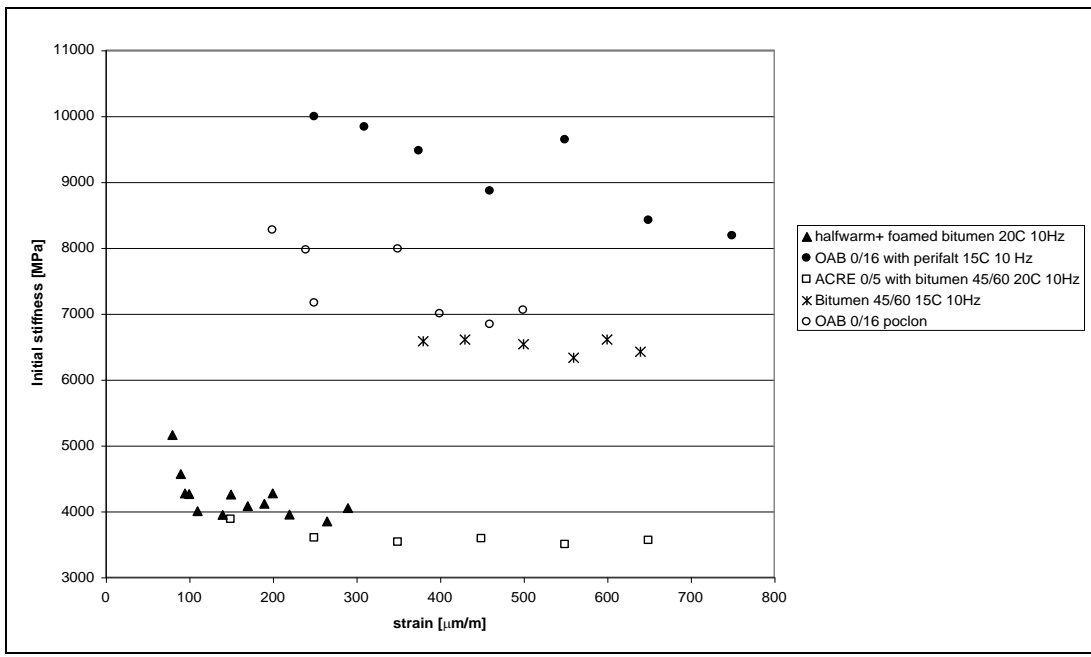


Figure 7.21: Relation between the stiffness and the strain for some mixes tested at TU Delft

7.3.3 Comparison between master curves at 80 μ m/m and 800 μ m/m for the Moerdijk mix

The figures 7.18-7.21 all show the trend of a decreasing mix stiffness for an increasing strain level. Because of the high strain levels ($\pm 1300~\mu\text{m/m}$) that were measured on bridges, this means that the stiffness determined at the low strain levels ($80~\mu\text{m/m}$) is not representative for mastic asphalt on steel bridges. Therefore it was chosen to repeat the four-point bending test at two strain levels, $80~\mu\text{m/m}$ and $800~\mu\text{m/m}$ and at three temperatures, 10°C , 20°C and 30°C . For the repetitions the same specimens were used that were tested before, some of them were also tested at high strain levels for fatigue testing. These specimens were stored at a temperature of 13°C for 2.5 months. The measurements at the strain level of $80~\mu\text{m/m}$ can be seen as reference measurements. The figures 7.22-7.24 show the comparison between the master curve at $80~\mu\text{m/m}$ and $800~\mu\text{m/m}$ for three temperatures.

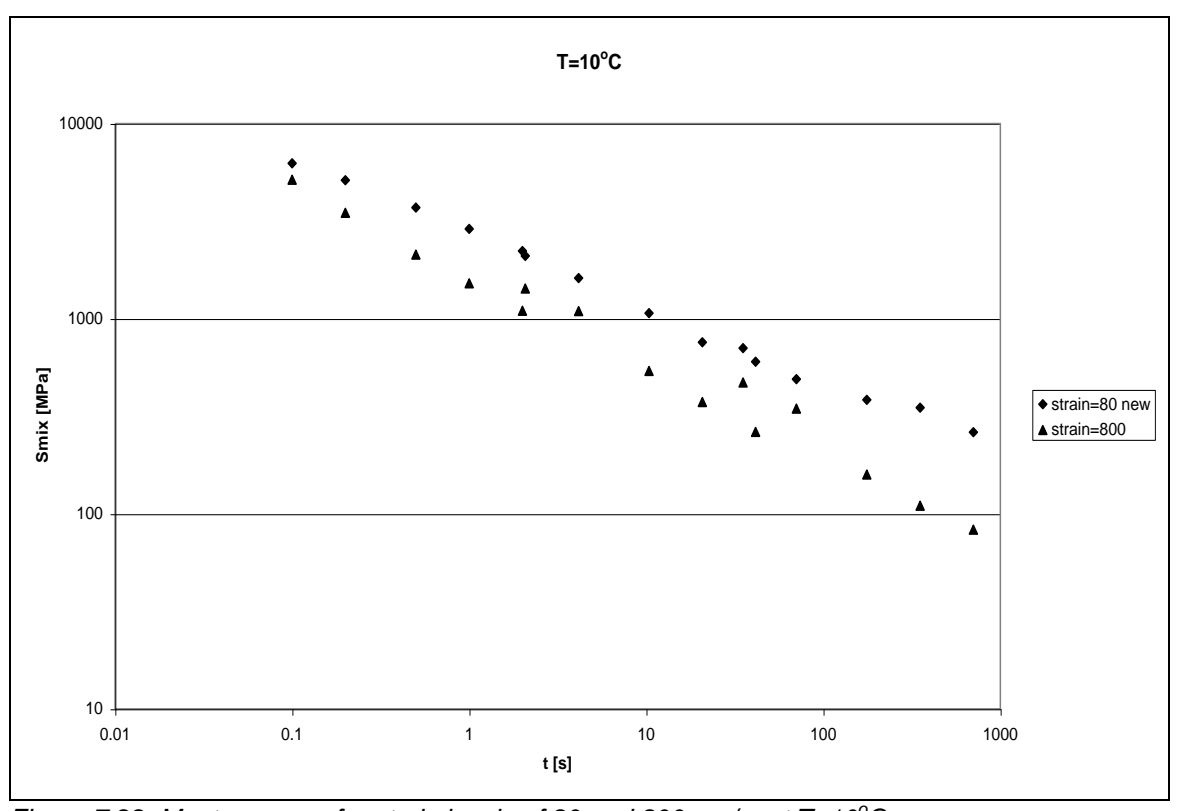


Figure 7.22: Master curves for strain levels of 80 and 800 μm/m at T=10°C

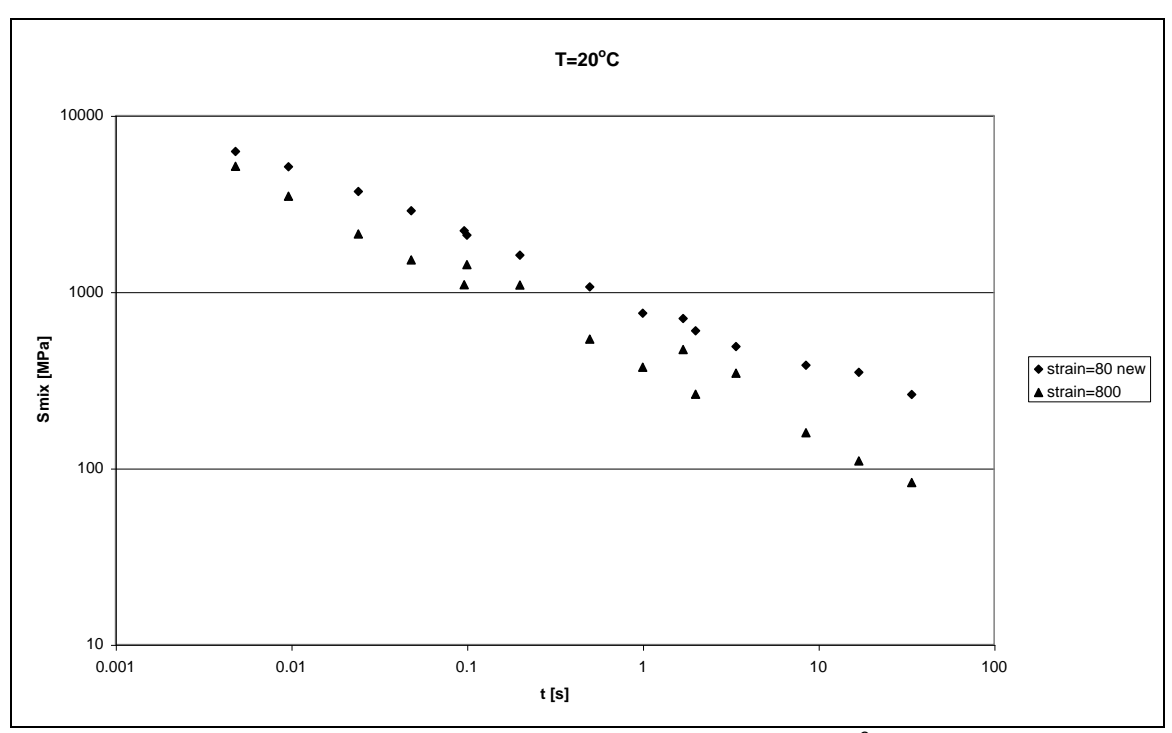


Figure 7.23: Master curves for strain levels of 80 and 800 μm/m at T=20°C

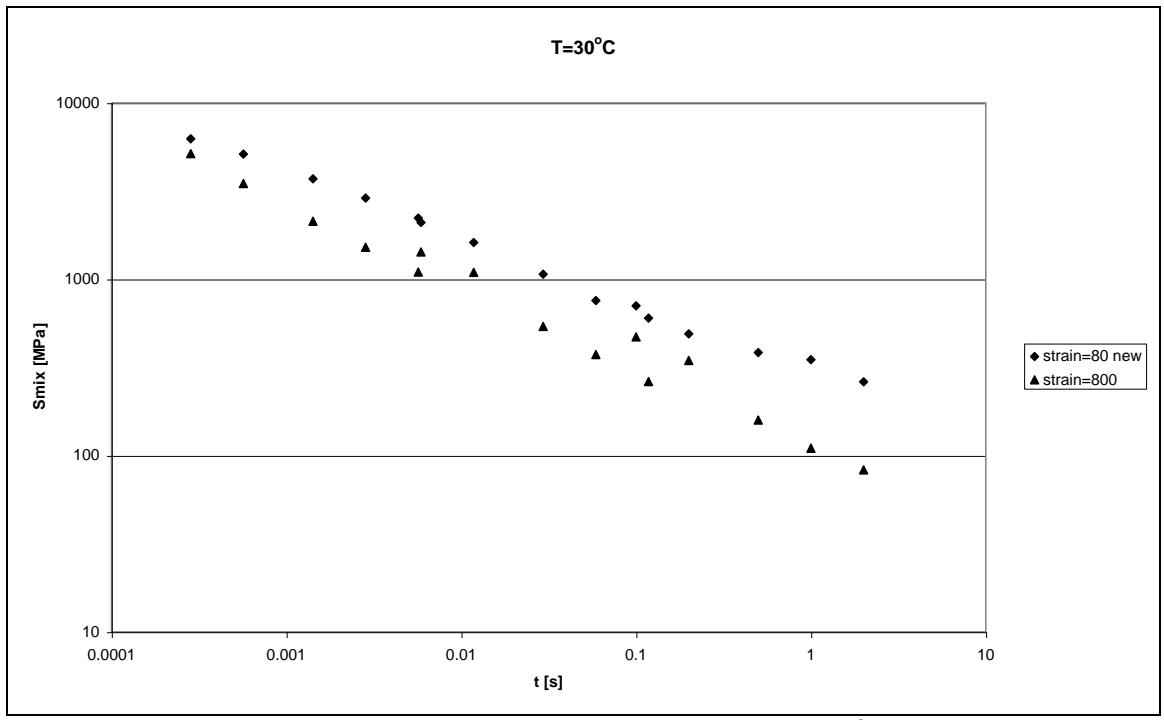


Figure 7.24: Master curves for strain levels of 80 and 800 μm/m at T=30°C

For the master curve at a strain of 800 μ m/m it can be seen that there are four outlying points and two gaps. This is a result of the fact that the modulus testing is only done at three temperatures. Additional testing at T=15°C and T=25°C would have given a smoother master curve with smaller gaps.

7.3.4 Determination of a shift-factor for the Moerdijk mix

The figures in the previous paragraph also show that for the three temperatures there is a shift between the mix stiffness determined at ϵ =80 μ m/m and ϵ =800 μ m/m. To determine this shift-factor the shift-factor is defined as:

$$SHIFT_{80\rightarrow800} = \frac{S_{mix}(\varepsilon = 800)}{S_{mix}(\varepsilon = 80)}$$
 Equation 7.16

This shift-factor is a function of both temperature and loading time. Analysis of the data has lead to the following function for the shift-factor:

$$SHIFT_{80\to800} = -0.0428 \ln(t) - 0.0126T + 0.7224$$

This relation is valid for loading times between 0.01 s and 1 s and temperatures between 10° C and 30° C. Table 7.11 shows the comparison between the mix stiffness at ϵ =800 μ m/m that is measured and the one that is predicted with the shift-factor.

Table 7.11: Comparison between S_{mix} measured and S_{mix} predicted with the shift-factor

T [°C]	t [s]	S _{mix} measured [MPa]	S _{mix} with shift-factor [MPa]	Difference [%]
10	0.1000	5162	4353	-16
10	0.2000	3490	3412	-2
10	0.5000	2132	2325	9
10	1.0000	1520	1721	13
10	2.0747	1098	1186	8
10	10.3733	540	530	-2
10	35.2345	374	314	-16
10	70.4691	263	203	-23
10	176.1726	159	144	-9
10	352.3453	110	121	10
10	704.6906	83	83	0
20	0.0048	5162	4377	-15
20	0.0096	3490	3432	-2
20	0.0241	2132	2339	10
20	0.0482	1520	1732	14
20	0.1000	1098	1194	9
20	0.5000	540	534	-1
20	1.6983	374	317	-15
20	3.3966	263	205	-22
20	8.4916	159	145	-9
20	16.9832	110	122	11
20	33.9665	83	84	1
30	0.0003	5162	4347	-16
30	0.0006	3490	3407	-2
30	0.0014	2132	2321	9
30	0.0028	1520	1718	13
30	0.0059	1098	1184	8
30	0.0294	540	529	-2
30	0.1000	374	313	-16
30	0.2000	263	203	-23
30	0.5000	159	144	-10
30	1.0000	110	121	10
30	2.0000	83	82	-1

This table shows that the difference between the measured and predicted stiffness varies between 1% and 23%. The average of the absolute value of the differences is 9.9%. It has to be noted that the determined shift-factor is valid only for shifting the master curve from ϵ =80 μ m/m to ϵ =800 μ m/m. To shift the master curve at ϵ =80 μ m/m to an arbitrarily strain level, the shift-factor becomes a function of loading time, temperature as well as the strain:

$$SHIFT_{80 \to \varepsilon}(\varepsilon, t, T) = \frac{S_{mix}(\varepsilon, t, T)}{S_{mix}(80, t, T)}$$
 Equation 7.17

Additional testing was carried out to determine this strain dependent behaviour of mastic asphalt. These tests are described in section

7.3.5 Strain dependency of the LINTRACK mix stiffness

After additional testing the master curves for the LINTRACK mix were created for different strain levels. When these master curves are combined in one figure the influence of the strain becomes obvious. This is shown in the figures 7.25-7.30. In each of the figures the master curves at different strain levels are shown for a constant temperature.

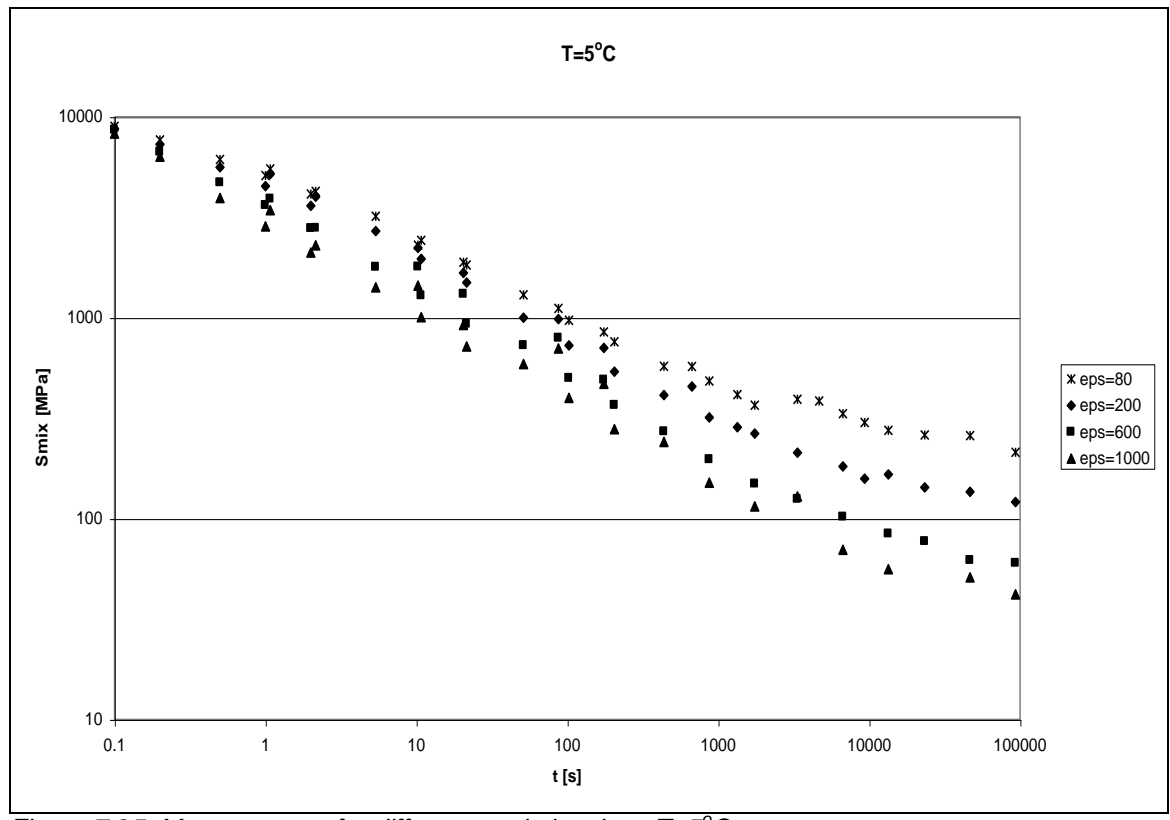


Figure 7.25: Master curves for different strain levels at T=5°C

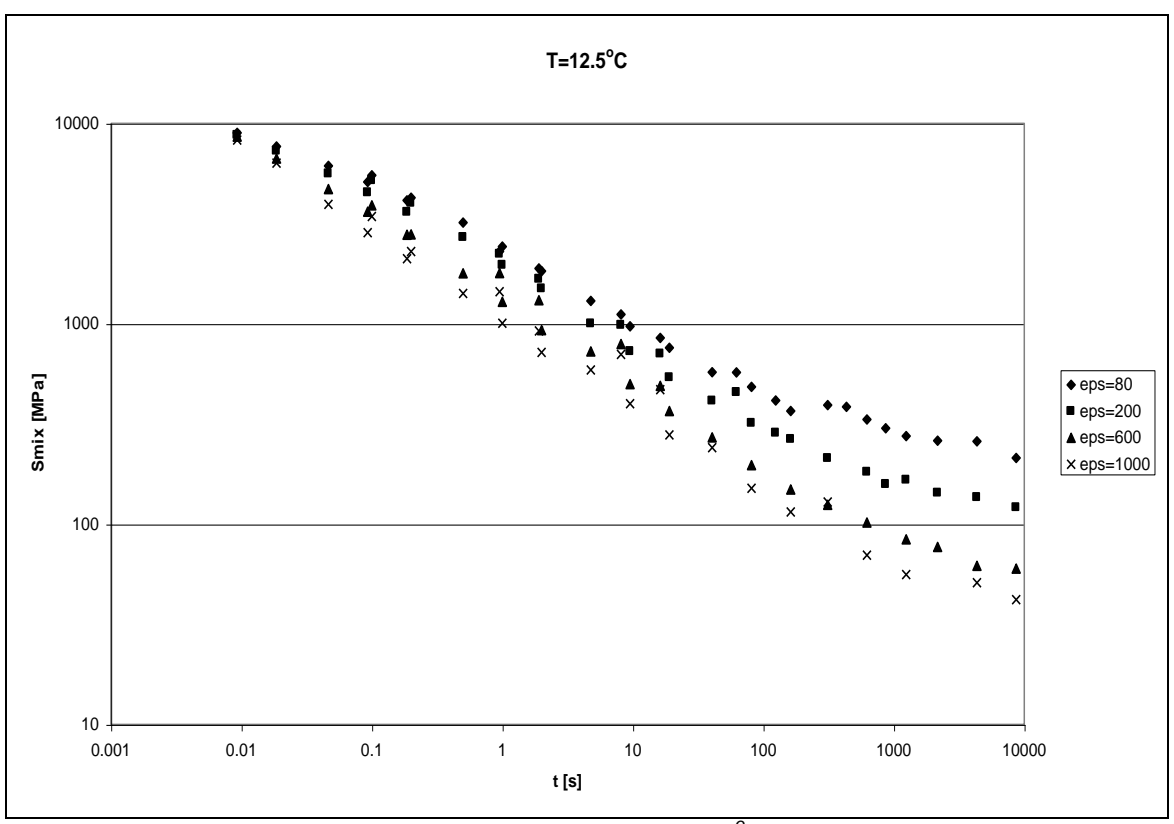


Figure 7.26: Master curves for different strain levels at T=12.5°C

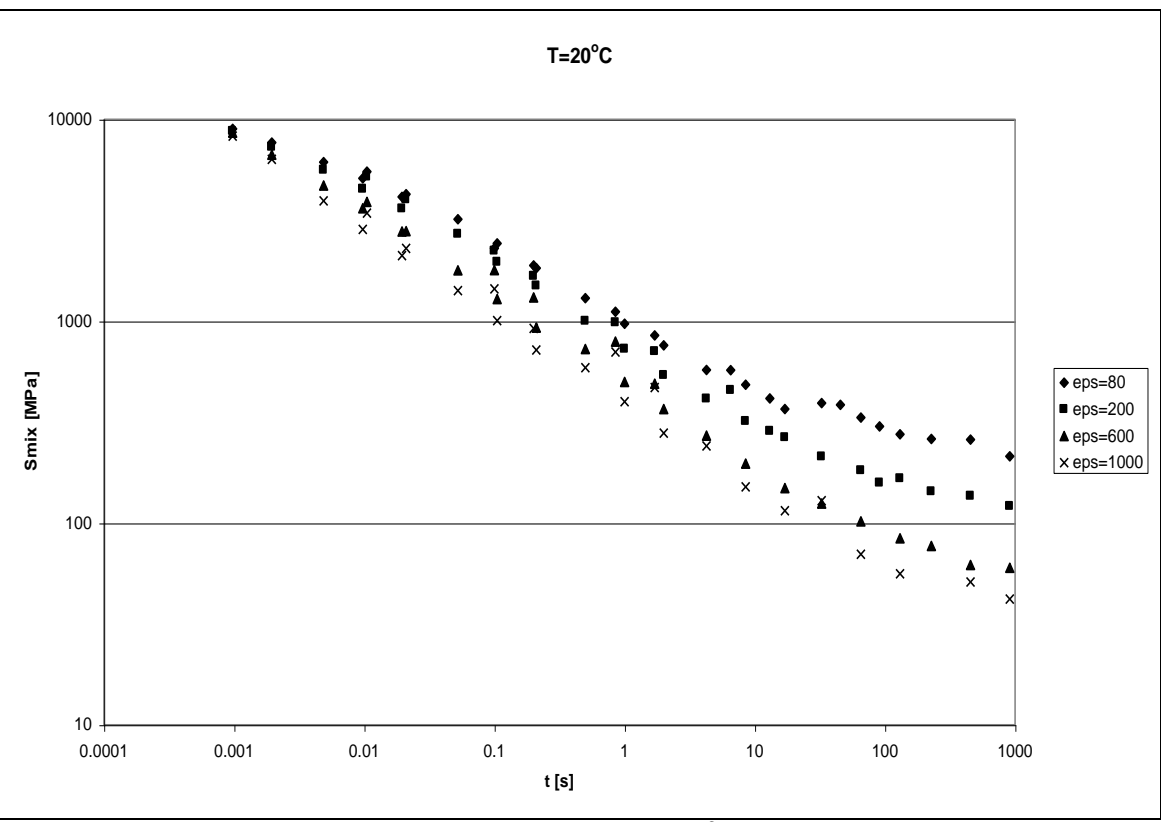


Figure 7.27: Master curves for different strain levels at T=20°C

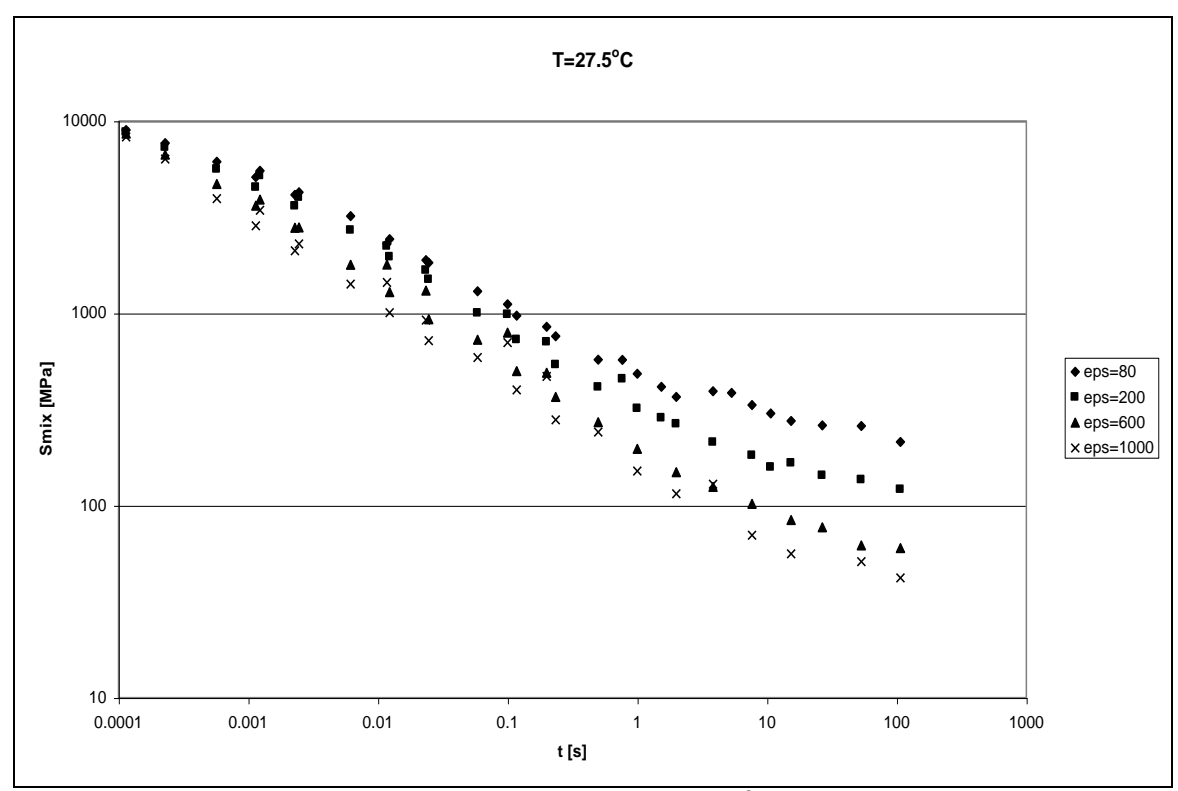


Figure 7.28: Master curves for different strain levels at T=27.5°C

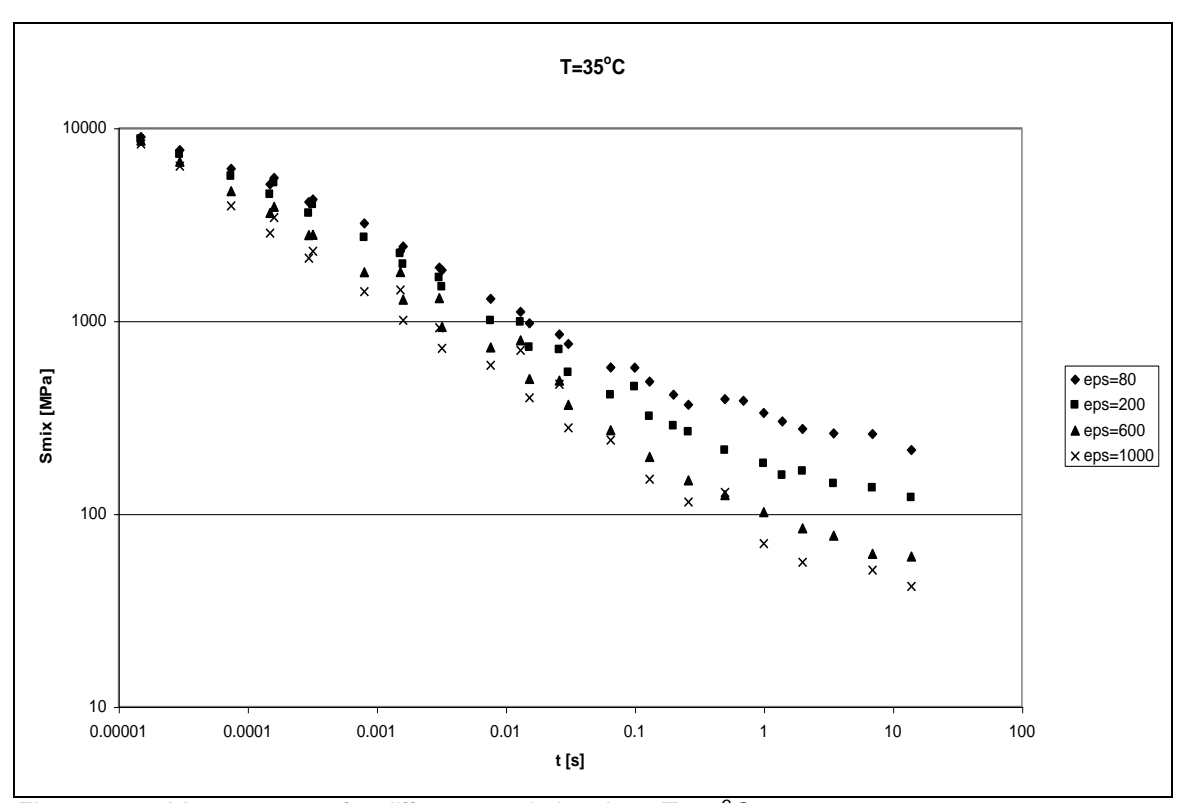


Figure 7.29: Master curves for different strain levels at T=35°C

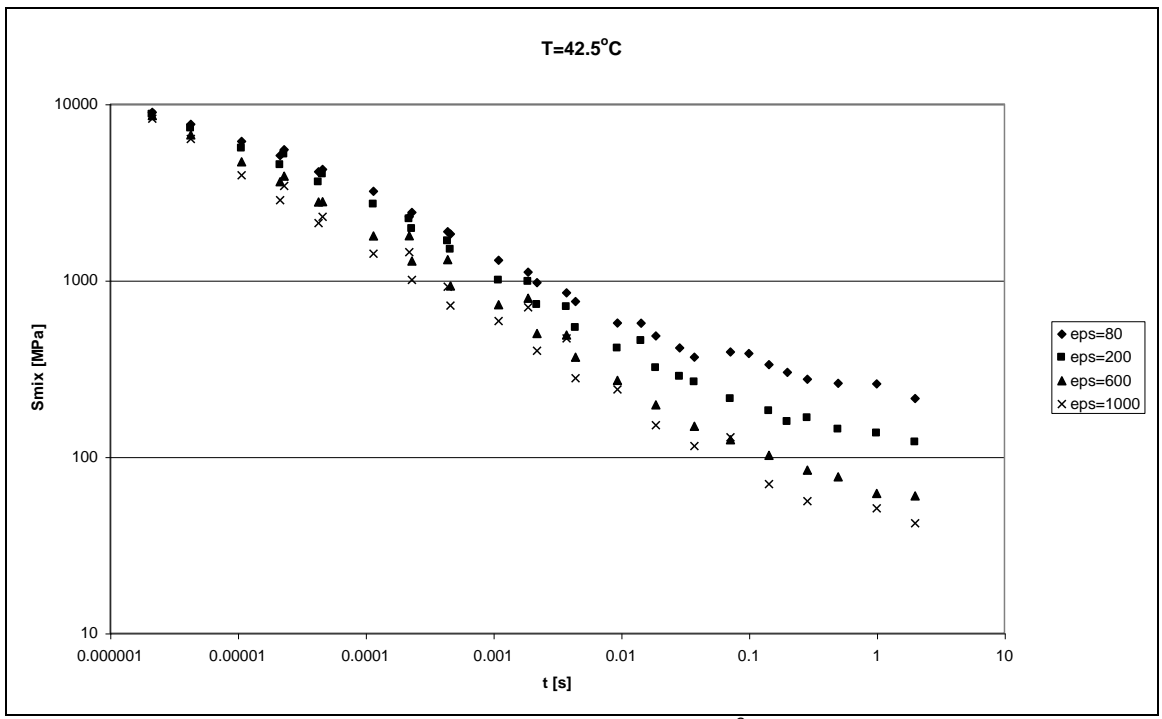


Figure 7.30: Master curves for different strain levels at T=42.5°C

All the figures show that for increasing loading time the difference in mix stiffness for the different strain levels is increasing. This means that the strain dependency is increasing with increasing loading times. This behaviour leads to sensibility of the mix to traffic congestion, especially at high temperatures. The maximum difference at high loading times between the mix stiffness at 80 μ m/m and 1000 μ m/m can be a factor 5.

7.3.6 The mix stiffness as a function of loading time and temperature

The separate master curves in the figures 7.25-7.30 are described best with the following equation:

$$\log(S_{mix}) = a_0 + a_1 \log t + a_2 (\log t)^2 + a_3 (\log t)^3$$
 Equation 7.18

in which:

S_{mix}: stiffness of the mix [MPa]

t: loading time [s] a; regression constants

The tables 7.12-7.15 show the regression constants for the master curves.

Table 7.12: Regression constants for the master curves at ε =80 μ m/m

T [°C]	a _o	a ₁	a_2	a_3	R^2
5.0	3.7151	-0.3003	-0.0453	0.0104	0.9969
12.5	3.3685	-0.3605	-0.0130	0.0104	0.9969
20.0	3.0129	-0.3558	0.0177	0.0104	0.9969
27.5	2.7057	-0.2957	0.0469	0.0104	0.9969
35.0	2.4880	-0.1882	0.0746	0.0104	0.9969
42.5	2.3887	-0.0401	0.1010	0.0104	0.9969

Table 7.13: Regression constants for the master curves at ε =200 μ m/m

T [°C]	$a_{ m o}$	a ₁	a_2	a_3	R^2	
5.0	3.6872	-0.3125	-0.0640	0.0126	0.9971	
12.5	3.3104	-0.4045	-0.0250	0.0126	0.9971	
20.0	2.9022	-0.4173	+0.0119	0.0126	0.9971	
27.5	2.5345	-0.3624	+0.0471	0.0126	0.9971	
35.0	2.2595	-0.2494	+0.0805	0.0126	0.9971	
42.5	2.1140	-0.0869	+0.1124	0.0126	0.9971	

Table 7.14: Regression constants for the master curves at ε =600 μ m/m

T [°C]	a_{o}	a ₁	a_2	a_3	R^2
5.0	3.5889	-0.3709	-0.0483	0.0098	0.9952
12.5	3.1656	-0.4392	-0.0179	0.0098	0.9952
20.0	2.7277	-0.4459	+0.0110	0.0098	0.9952
27.5	2.3304	-0.3999	+0.0385	0.0098	0.9952
35.0	2.0135	-0.3087	+0.0646	0.0098	0.9952
42.5	1.8051	-0.1789	+0.0894	0.0098	0.9952

Table 7.15: Regression constants for the master curves at ε =1000 μ m/m

T [°C]	$a_{ m o}$	a ₁	a ₂	a ₃	R^2
5.0	3.5057	-0.4096	-0.0232	0.0057	0.9896
12.5	3.0646	-0.4393	-0.0055	0.0057	0.9896
20.0	2.6346	-0.4338	0.0112	0.0057	0.9896
27.5	2.2453	-0.3982	0.0271	0.0057	0.9896
35.0	1.9181	-0.3369	0.0422	0.0057	0.9896
42.5	1.6675	-0.2537	0.0566	0.0057	0.9896

It is clear that the mix stiffness is not only dependent on loading time and temperature, but also on the strain level.

7.3.7 The mix stiffness as a function of strain, temperature and loading time

With the computer program TableCurve2D the relationship between the mix stiffness, ϵ , t, T was determined. For each master curve the point (t, S_{mix})=(1*10⁻¹⁰, 16000) is added, to make sure that the determined function has a stiffness that reaches asymptotic to the maximum value of 16000. The TableCurve program only determines the relation between two variables, so first the relation is determined for each master curve separately. Each master curve is described best with:

$$\log S_{mix} = w + \frac{x}{\left(1 + e^{\frac{-(\log t - y)}{z}}\right)}$$
 Equation 7.19

The parameters w, x, y and z for each master curve are shown in the tables 7.16-7.19.

Table 7.16: Parameters for the master curves at ε =80 μ m/m

T [°C]	W	Х	У	Z
5.0	2.25	1.94	1.42	-1.25
12.5	2.25	1.94	0.39	-1.25
20.0	2.25	1.94	-0.59	-1.25
27.5	2.25	1.94	-1.52	-1.25
35.0	2.25	1.95	-2.41	-1.26
42.5	2.25	1.95	-3.26	-1.26

Table 7.17: Parameters for the master curves at ε =200 μ m/m

				10 = 00 pt
T [°C]	W	х	У	Z
5.0	1.89	2.30	1.67	-1.33
12.5	1.89	2.31	0.64	-1.33
20.0	1.89	2.31	-0.34	-1.33
27.5	1.89	2.31	-1.27	-1.33
35.0	1.89	2.31	-2.16	-1.33
42.5	1.89	2.32	-3.01	-1.34

Table 7.18: Parameters for the master curves at ε =600 μ m/m

T [°C]	W	Х	У	Z
5.0	1.49	2.73	1.74	-1.45
12.5	1.49	2.73	0.70	-1.45
20.0	1.49	2.73	-0.28	-1.45
27.5	1.49	2.74	-1.21	-1.46
35.0	1.48	2.75	-2.09	-1.46
42.5	1.48	2.76	-2.94	-1.47

Table 7.19: Parameters for the master curves at ε =1000 μ m/m

T [°C]	W	Х	У	Z
5.0	1.28	2.96	1.75	-1.57
12.5	1.28	2.96	0.71	-1.58
20.0	1.28	2.97	-0.27	-1.58
27.5	1.27	2.98	-1.20	-1.59
35.0	1.27	3.00	-2.09	-1.60
42.5	1.25	3.02	-2.94	-1.62

From these tables it becomes clear that w, x and z are constant for each strain level and that y varies with strain level and temperature, so:

$$w = f(\varepsilon)$$

$$x = f(\varepsilon)$$

$$y = f(\varepsilon, T)$$

$$z = f(\varepsilon)$$

The next step that is carried out is the determination of w, x, y and z. Therefore also use is made of TableCurve2D, which has resulted in the following relations:

$$w = a \log \varepsilon + b$$
 Equation 7.20

$$x = c + d(\log \varepsilon)^2$$
 Equation 7.21

$$y = -fT - g - \frac{h}{\varepsilon^{1.5}}$$
 Equation 7.22

$$z = i + j\sqrt{\varepsilon}$$
 Equation 7.23

Filling in these relations in the total relation results in a function describing the mix stiffness as a function of loading time, temperature and strain:

$$\log S_{mix}(\varepsilon, t, T) = a \log \varepsilon + b + \frac{c + d(\log \varepsilon)^{2}}{1 + e^{\left(\frac{-(\log t + fT + g + h\varepsilon^{-1.5})}{i + j\varepsilon^{0.5}}\right)}}$$
 Equation 7.24

in which:

 S_{mix} : mix stiffness [MPa] ε : strain [μ m/m] t: loading time [s] T: temperature [$^{\circ}$ C]

The constants a-j are determined by regression analysis:

a :-0.886 b :3.937 c :1.273 d :0.191 f :0.125 g :-2.297 h :238.048 i :-1.125 j :-0.014

The relation is valid within the following ranges:

80 μ m/m $\leq \varepsilon \leq 1000 \mu$ m/m

 $0^{\circ}\text{C} \le T \le 45^{\circ}\text{C}$

 $0.01s \le t \le 1s$

The range of the loading times corresponds to speeds between 108 km/h and 1 km/h. Appendix C shows the complete derivation of equation 7.24 as well as the significance of the function, by comparing the measured with the predicted stiffness for each master curve.

Equation 7.24 has been used to make graphs representing the dependency of the mix stiffness on the strain level. Four loading times are chosen to be representative, namely, 0.01, 0.02, 0.1 and 1.0s. The speeds to which these loading times correspond are calculated with:

$$v = \frac{3.6D}{t}$$
 Equation 7.25

in which:

v : speed [km/h]

D: diameter of the contact area of a wide base tyre [0.3m]

t : loading time [s]

The speeds that correspond to the four loading times are shown in table 7.20.

Table 7.20: Relation between loading time and speed

t [s]	Speed [km/h]
0.01	108
0.02	54
0.1	11
1.0	1

The speed of 54 km/h corresponds to the speed used in Shell design manuals.

The figures 7.31-7.34 show the stiffness as a function of strain level for these loading times and several temperatures between 0 and 45° C.

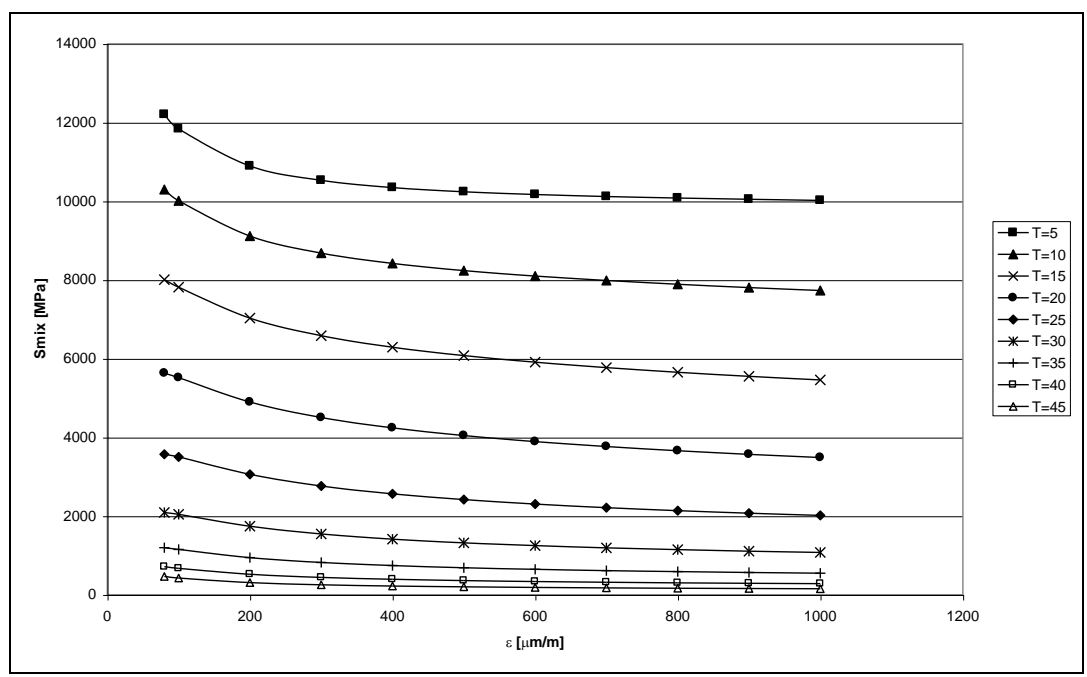


Figure 7.31: Strain dependency of the mix stiffness for t=0.01s

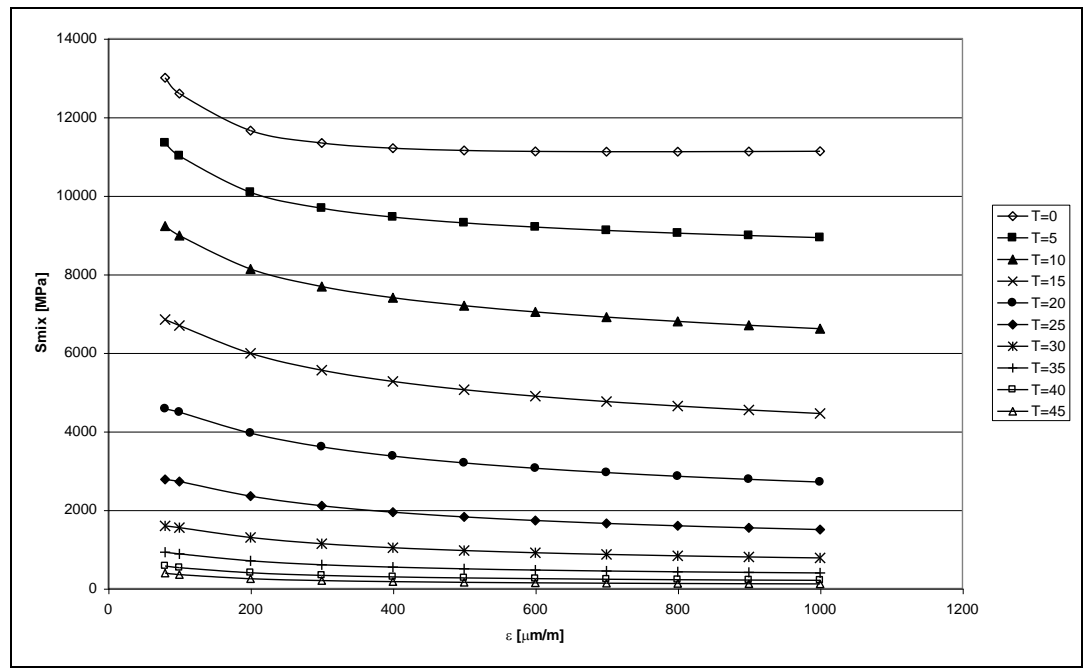


Figure 7.32: Strain dependency of the mix stiffness for t=0.02s

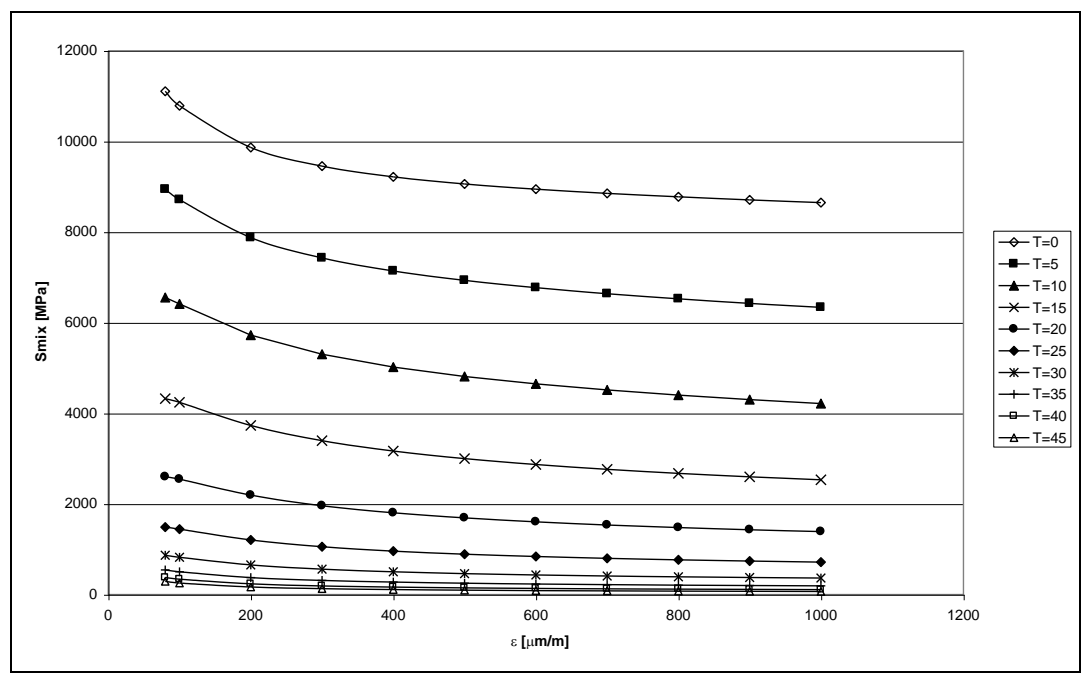


Figure 7.33: Strain dependency of the mix stiffness for t=0.1s

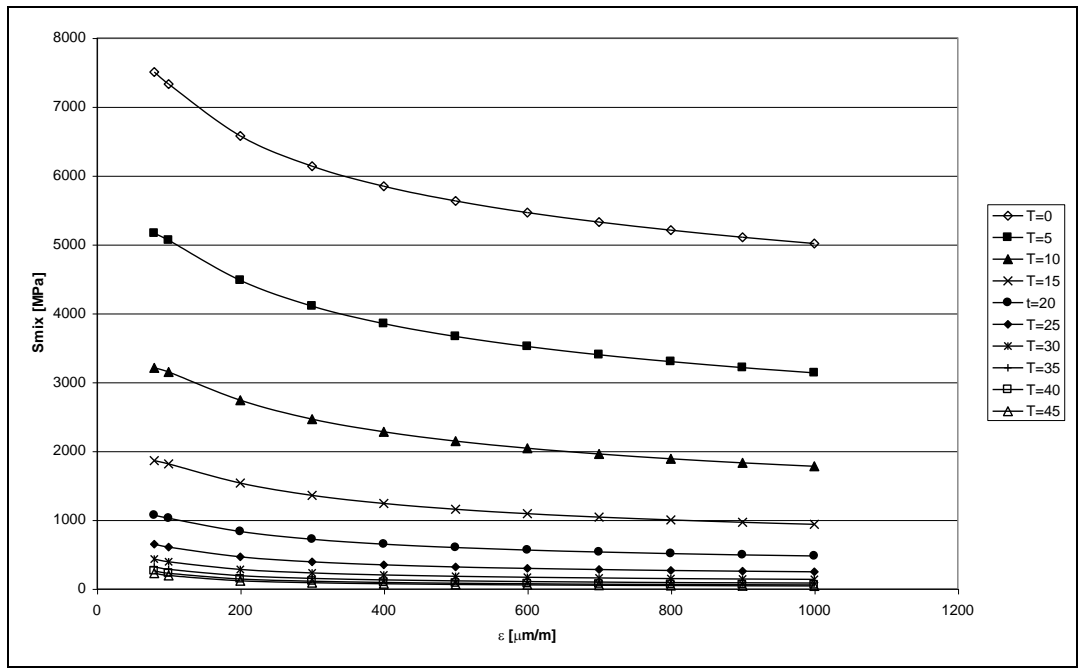


Figure 7.34: Strain dependency of the mix stiffness for t=1.0s

With this large influence of the stiffness on the strain level it is clear that this behaviour cannot be neglected. However, it should be noticed that the function for the mix stiffness is based on measurements on the Lintrack mix only. More testing is needed to verify if the function can be applied for all the mastic asphalt mixes. It should be emphasised here that the relationship is based merely on linear elastic theory and hence no viscous or visco-plastic behaviour was considered. The relationship is namely based on measurements with the four-point bending testing machine that calculates the stiffness by assuming linear elastic behaviour. However, at high temperatures and strain levels linear behaviour is not expected. Nevertheless, for practical purposes, this relationship may be considered very useful.

7.3.8 Determination of the shift-factor for mastic asphalt

In paragraph 7.3.4 the shift-factor between the mix stiffness at 80 μ m/m and 800 μ m/m was determined. It is clear that also the shift-factor for an arbitrarily strain level is of interest. The shift-factor is defined as:

$$SHIFT_{80 \to \varepsilon}(\varepsilon, t, T) = \frac{S_{mix}(\varepsilon, t, T)}{S_{mix}(80, t, T)}$$
 Equation 7.26

In which:

 $SHIFT_{80\rightarrow\varepsilon}$: Shift-factor

T : Temperature [°C] t : Loading time [s] ε : Strain level [μm/m]

The expression for the shift-factor as a function of loading time, temperature and strain level is rather complex (combination of equation 7.24 and 7.26). Therefore some tables and graphs are made from which the shift-factor can easily be read. Tables 7.21-7.23 and the figures 7.35-7.37 can be used to determine the shift factor for strain levels of 200, 600 and 1000 μ m/m.

Table 7.21: SHIFT₈₀₋₂₀₀ for different temperatures and loading times

SHIFT _{80→200}	<i>t</i> =0.01s	<i>t</i> =0.02s	t=0.1s	t=1.0s
0°C	0.90	0.90	0.89	0.88
5°C	0.89	0.89	0.88	0.87
10°C	0.89	0.88	0.87	0.85
15°C	0.88	0.87	0.86	0.83
20°C	0.87	0.86	0.84	0.78
25°C	0.86	0.85	0.81	0.72
30°C	0.83	0.81	0.75	0.65
35°C	0.79	0.76	0.69	0.59
40°C	0.73	0.70	0.63	0.55
45°C	0.66	0.63	0.57	0.51

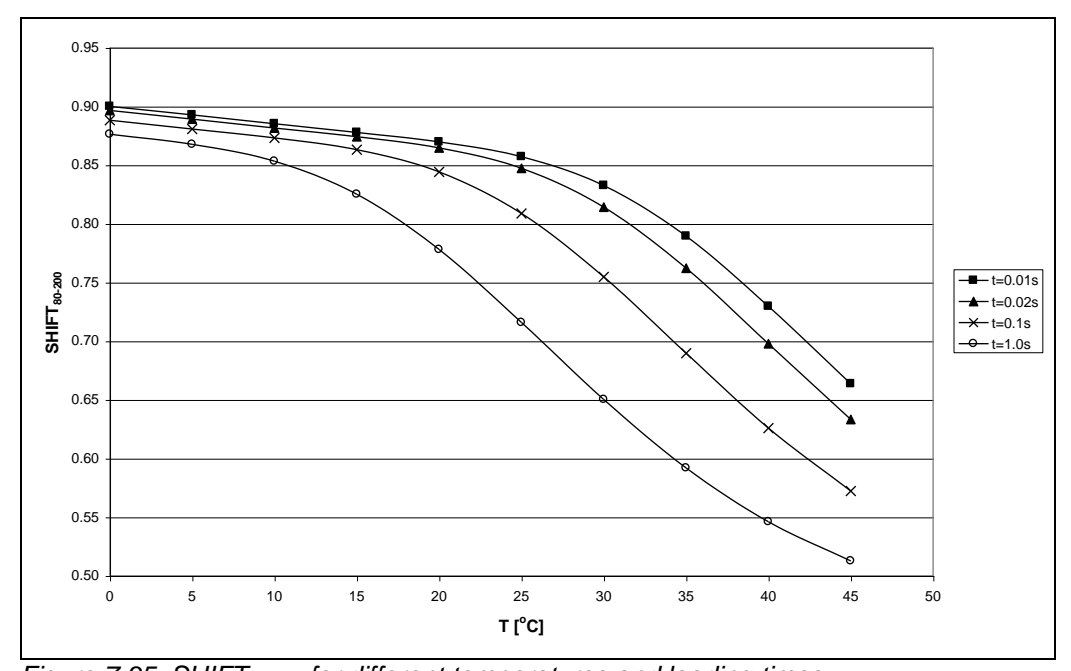


Figure 7.35: SHIFT₈₀₋₂₀₀ for different temperatures and loading times

Figure 7.35 shows that for low temperatures the factor SHIFT₈₀₋₂₀₀ is nearly constant (\approx 0.88) for different loading times. For temperatures higher than 10°C the shift-factor decreases and the difference in shift-factor between the different loading times increases.

Table 7.22: SHIFT₈₀₋₆₀₀ for different temperatures and loading times

	00 000			
SHIFT _{80→600}	t=0.01s	<i>t</i> =0.02s	t=0.1s	t=1.0s
0°C	0.88	0.86	0.81	0.73
5°C	0.83	0.81	0.76	0.68
10°C	0.79	0.76	0.71	0.64
15°C	0.74	0.72	0.66	0.59
20°C	0.69	0.67	0.62	0.53
25°C	0.65	0.62	0.56	0.46
30°C	0.60	0.57	0.50	0.39
35°C	0.54	0.51	0.43	0.32
40°C	0.47	0.44	0.36	0.28
45°C	0.40	0.37	0.30	0.24

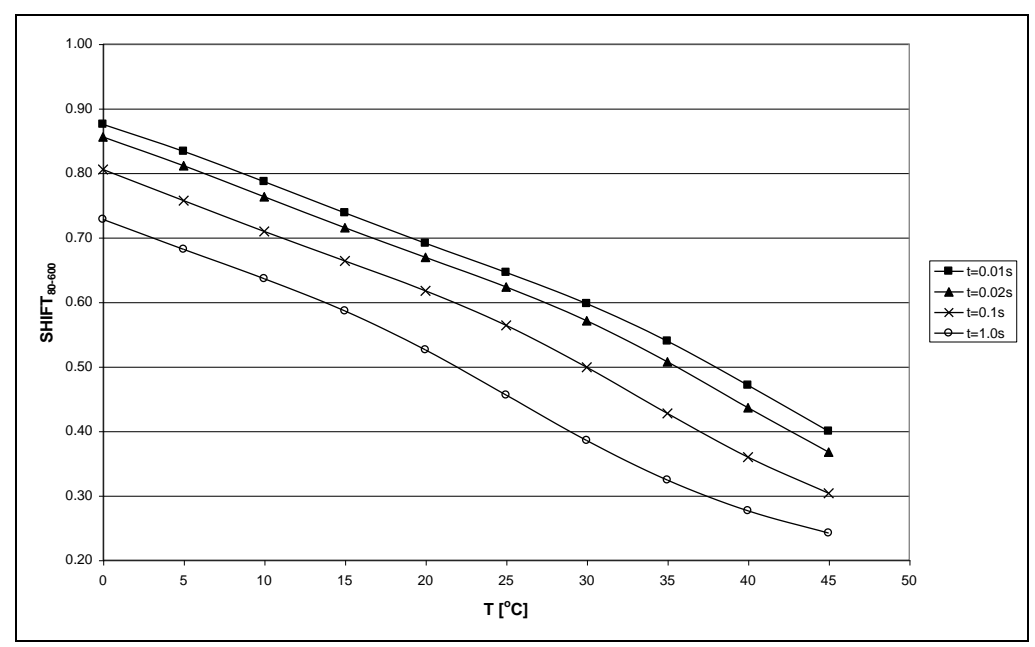


Figure 7.36: SHIFT₈₀₋₆₀₀ for different temperatures and loading times

The trend in figure 7.36 is different from the trend in figure 7.35. The difference in shift-factor for the different loading times is almost constant and the decrease of the shift-factor is almost constant for the whole range of temperatures.

Table 7.23: SHIFT₈₀₋₁₀₀₀ for different temperatures and loading times

SHIFT _{80→1000}	t=0.01s	t=0.02s	t=0.1s	t=1.0s
0°C	0.89	0.86	0.78	0.67
5°C	0.82	0.79	0.71	0.61
10°C	0.75	0.72	0.64	0.55
15°C	0.68	0.65	0.59	0.50
20°C	0.62	0.59	0.53	0.45
25°C	0.56	0.54	0.48	0.38
30°C	0.51	0.49	0.42	0.31
35°C	0.46	0.43	0.35	0.26
40°C	0.39	0.36	0.29	0.21
45°C	0.33	0.30	0.24	0.18

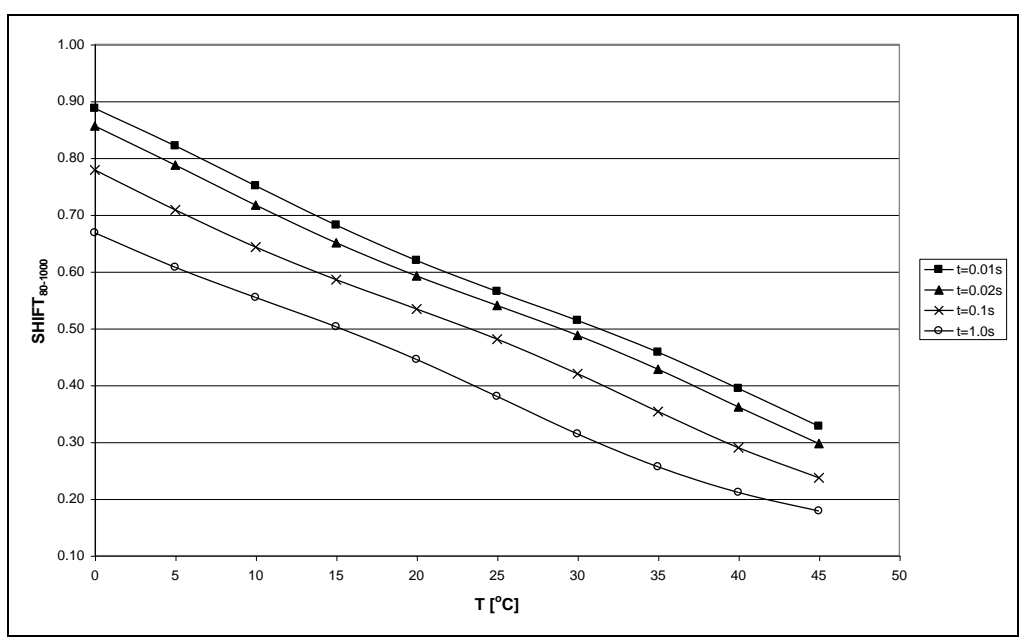


Figure 7.37 SHIFT₈₀₋₁₀₀₀ for different temperatures and loading times

Figures 7.36 and 7.37 show a similar trend.

These tables and graphs allow researchers to calculate the stiffness of mastic asphalt at an arbitrarily strain level from the stiffness at a strain level of 80 μ m/m, which is more or less used as a standard for modulus testing in the Netherlands. The advantage is twofold. First of all information of the stiffness at an arbitrarily strain level is obtained by carrying out tests at only one low strain level. Secondly, testing at this low strain level means limited or even no damage to the specimens. That means that the specimen can be used again later for other tests. However, one has to be aware of the fact that the shift-factor that is determined in this report is the result of testing on just one mastic asphalt mix, which means that it is not applicable for every mastic asphalt mix. More testing is therefore needed to investigate the existence of such a relationship for other types of mastic asphalt.

7.3.9 Effect of neglecting the strain dependency of the mix stiffness

In the previous sections it is shown that the determination of the mix stiffness is highly dependent on the strain. It was shown that the difference between the stiffness at a strain level of 80 μ m/m and the stiffness at a strain level of 1000 μ m/m could be a factor 5 for high loading times and temperatures.

In the past often master curves for mastic asphalt were determined for a strain level of 80 μ m/m (Kolstein, 1989). If the dependency of the stiffness on the strain in neglected, this would lead to overestimation of the value of the mix stiffness.

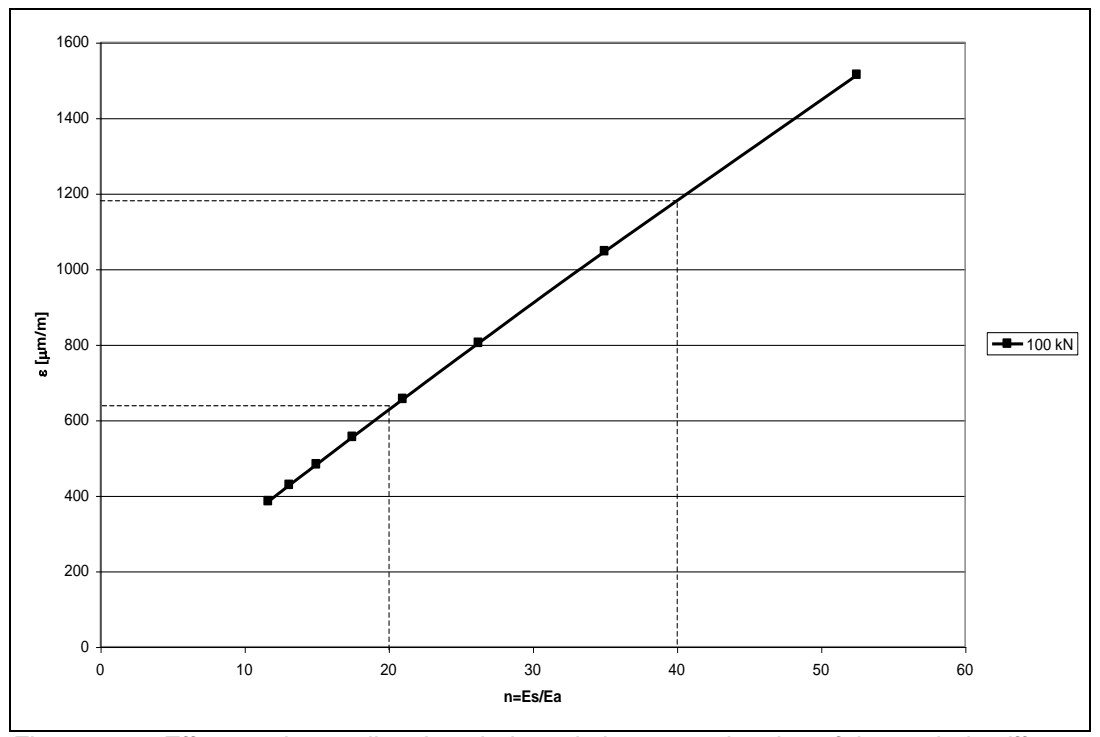


Figure 7.38: Effect on the predicted asphalt strain by overestimation of the asphalt stiffness

Figure 7.38 shows the relationship between the modular ratio E_s/E_a and the asphalt strain using Metcalfs composite action theory (section 3.3.2.1) for an axle load of 100 kN. E_s is the elastic modulus of the steel, which is assumed to be 2.1*10¹¹ Pa. For determining the asphalt strain use is made of the model shown in figure 3.24.

Ignoring the influence of the strain, the modular ratio is for example 20, which results in an asphalt strain of 625 μ m/m. However, when for example the real asphalt stiffness is a factor 2 lower, because of the strain dependency, the modular ratio becomes 40. This results in a asphalt strain of 1175 μ m/m. This means that the real asphalt strain is a factor 1.9 higher, and this implies that the asphalt fatigue pavement life in reality is 1.9 $^{\rm n}$ times smaller (where n=slope of the fatigue relationship). For T=10 $^{\rm o}$ C and f=5 Hz n is equal to 6.7 (see paragraph 7.2.2.1) resulting in an asphalt fatigue pavement life that is 74 times smaller.

7.4 Uniaxial monotonic compression test

7.4.1 Standardisation compression curves

The influence of the temperature and the strain rate on the stress-strain curves becomes clearer when the curves are standardised. The curves are standardised by plotting the ratio σ/σ_{max} against the strain, where σ_{max} is the maximum compression strength. Figure 7.39 shows the standardised curves

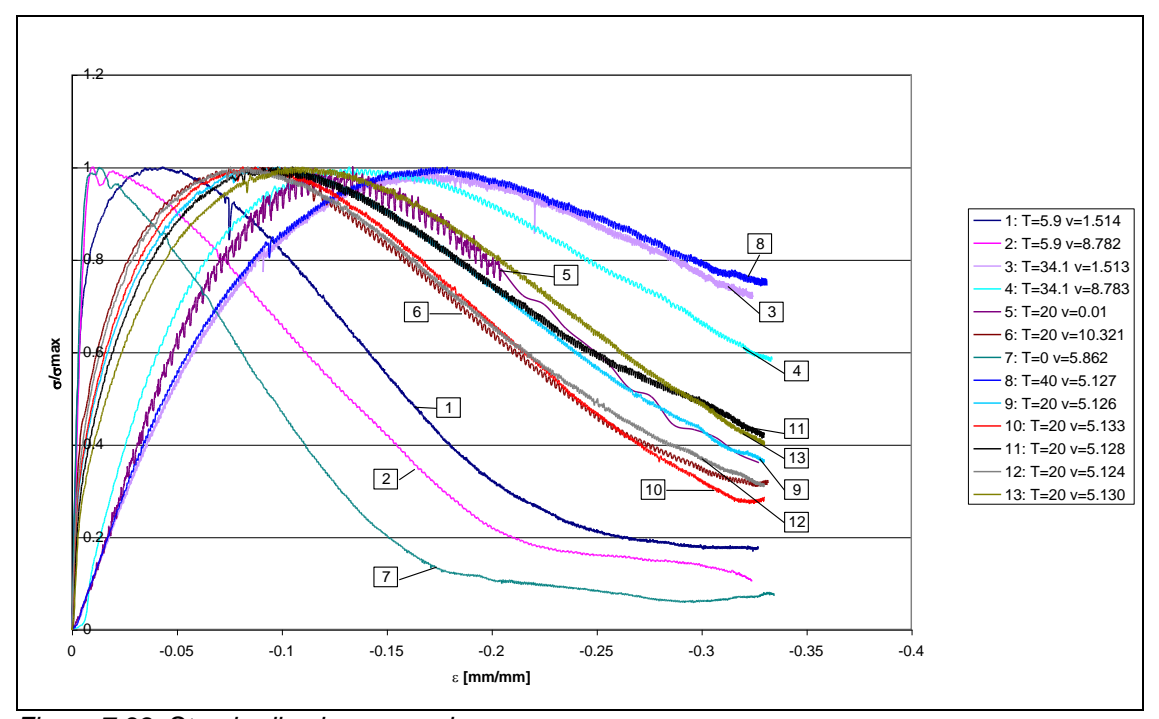


Figure 7.39: Standardised compression curves

This figure shows clearly that the slope of the elastic part (elastic modulus) increases with decreasing temperature and increasing loading rate. Also the strain at peak stress increases with increasing temperature and decreasing loading rate. Furthermore it can be observed that at increasing temperatures and decreasing loading rates the plastic part of the deformation starts at a lower strain level.

7.4.2 Determination of the compression strength as a function of temperature and strain rate

The relationship between the compressive strength, temperature and strain rate is described best with [Erkens, 1998]:

$$f_c = a \left(c - \frac{1}{1 + \left(\dot{\varepsilon} \exp\left(\left(\frac{b}{T_k} \right)^2 + d \right) \right)^e} \right)$$

Equation 7.27

in which:

f_c : compression strength [MPa]

 $\dot{\mathcal{E}}$: strain rate [x100/s] T_k : temperature [K]

a :-50.669 b :1812.644 c :1.022 d :-45.023 e :0.355 Appendix E shows the results from the regression analysis that has been carried out to obtain equation 7.27.

Table 7.24 shows a comparison between the measured and the predicted compression strength.

Table 7.24: Comparison between the measured and predicted compressive strength

				<u> </u>
Temperature [°C]	strain rate [1/s]	f _{c measured} [MPa]	f _{c predicted} [MPa]	difference [%]
5.9	1.68E-02	-16.96	-16.80	0.94
5.9	9.75E-02	-24.22	-24.19	0.12
34.1	1.70E-02	-2.58	-2.72	-5.49
34.1	9.78E-02	-4.71	-4.02	14.70
20.0	9.97E-05	-1.80	-2.01	-11.49
20.0	1.03E-01	-9.70	-9.87	-1.74
0	5.86E-02	-30.12	-30.16	-0.13
40.0	5.68E-02	-2.65	-2.67	-0.74
20.0	5.12E-02	-8.01	-8.22	-2.59
20.0	5.15E-02	-8.46	-8.23	2.68
20.0	5.12E-02	-7.97	-8.22	-3.14
20.0	5.11E-02	-8.38	-8.21	1.98
20.0	5.12E-02	-7.98	-8.22	-3.02

This table shows that the compressive strength can be predicted quite well with equation 7.27. Figure 7.40 shows the predicted compressive strength for different temperatures and strain rates.

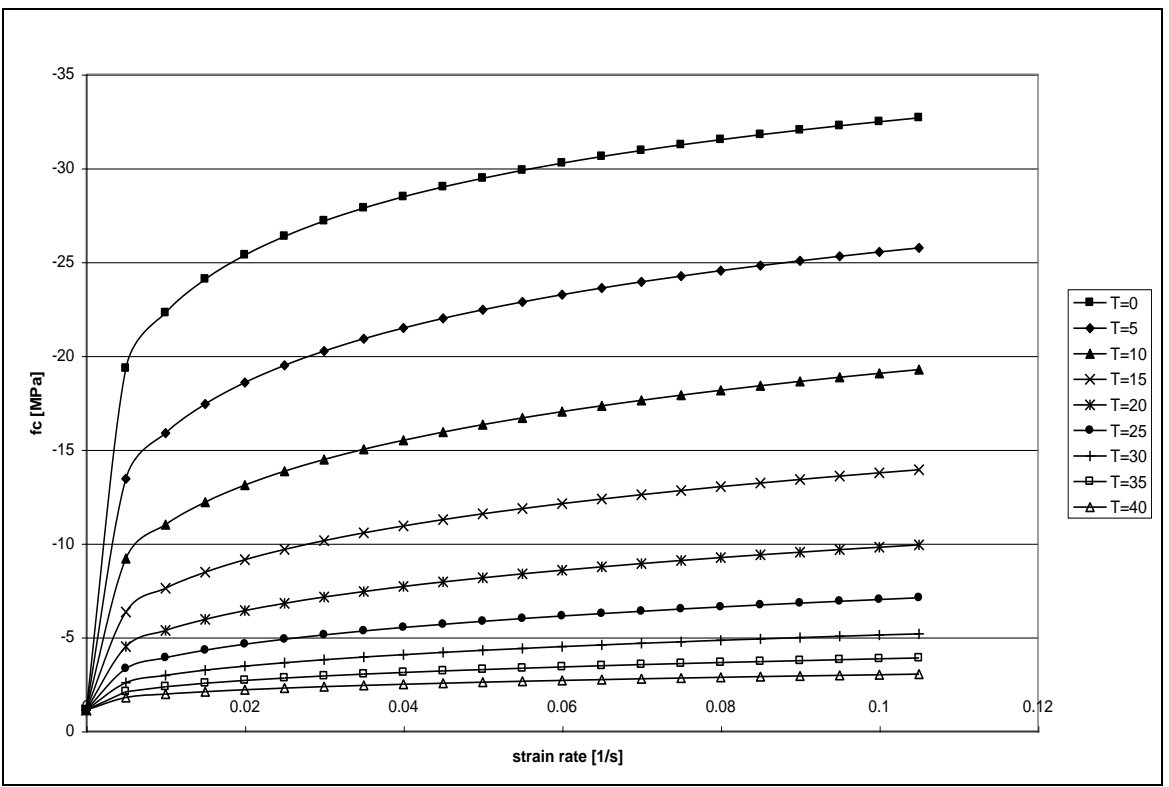


Figure 7.40: Compressive strength for different temperatures and strain rates

As expected, the predicted compressive strength decreases with increasing temperature and increases with increasing strain rate.

7.5 Uniaxial monotonic tension test

7.5.1 Standardisation of tension curves

The influence of the temperature and the strain rate on the stress-strain curves becomes clearer when the curves are standardised. The tension curves are standardised by plotting the ratio σ/σ_{max} against the strain, where σ_{max} is the maximum tension strength. Figure 7.41 shows the standardised curves.

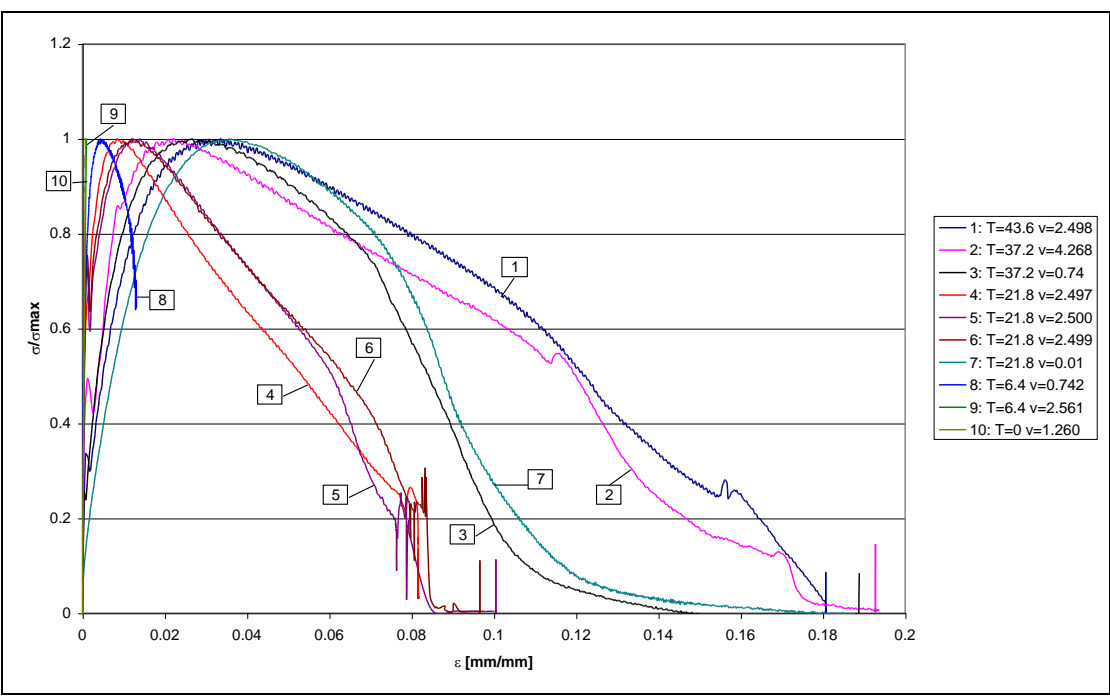


Figure 7.41: Standardised tension curves

This figure shows clearly that also for the tension tests the slope of the elastic part (elastic modulus) increases with decreasing temperature and increasing loading rate. Also the strain at peak stress increases with increasing temperature and decreasing loading rate. Furthermore it can be observed that at increasing temperatures and decreasing loading rates the plastic part of the deformation starts at a lower strain level.

7.5.2 Determination of the tension strength as a function of temperature and strain rate

Regression analysis resulted in the following relationship between tensile strength, temperature and loading rate [Erkens, 1998]:

$$f_{t} = a \left(c - \frac{1}{1 + \left(\dot{\varepsilon} \exp\left(\left(\frac{b}{T_{k}} \right)^{2} + d \right) \right)^{e}} \right)$$
 Equation 7.28

in which:

 f_t : tension strength [MPa] $\dot{\varepsilon}$: strain rate [x100/s] T_k : temperature [K]

a : 12.231 b : 1655.379 c : 1.039 d :-34.888 e : 0.758

Appendix E shows the results from the regression analysis that has been carried out to obtain equation 7.28. Table 7.25 shows a comparison between the measured and predicted tensile strength.

Table 7.25: Comparison between the measured and predicted tensile strength

Temperature [°C] strain rate [1/s]		f _{t measured} [MPa]	f _{t predicted} [MPa]	difference [%]
6.4	1.01E-02	5.90	7.12	-20.68
-			–	
6.4	3.50E-02	10.80	9.69	10.29
37.2	8.14E-03	0.50	0.56	-12.73
37.2	4.80E-02	0.80	0.79	1.63
21.8	1.11E-04	0.50	0.51	-2.89
21.8	5.56E-02	3.20	3.22	-0.59
0	1.72E-02	10.50	11.03	-5.05
43.6	2.77E-02	0.50	0.57	-13.79
21.8	2.78E-02	2.40	2.26	5.64
21.8	2.78E-02	2.40	2.27	5.58
21.8	2.78E-02	2.20	2.26	-2.90
21.8	2.77E-02	2.40	2.26	5.74
21.8	2.78E-02	2.20	2.26	-2.88

From table 7.25 it seems that the tensile strength can be predicted with equation 7.28 quite well. However, the differences between the measured and predicted values are larger than the differences for the compression tests. Equation 7.28 is used to predict the tensile strength for different temperatures and strain rates. This is shown in figure 7.42.

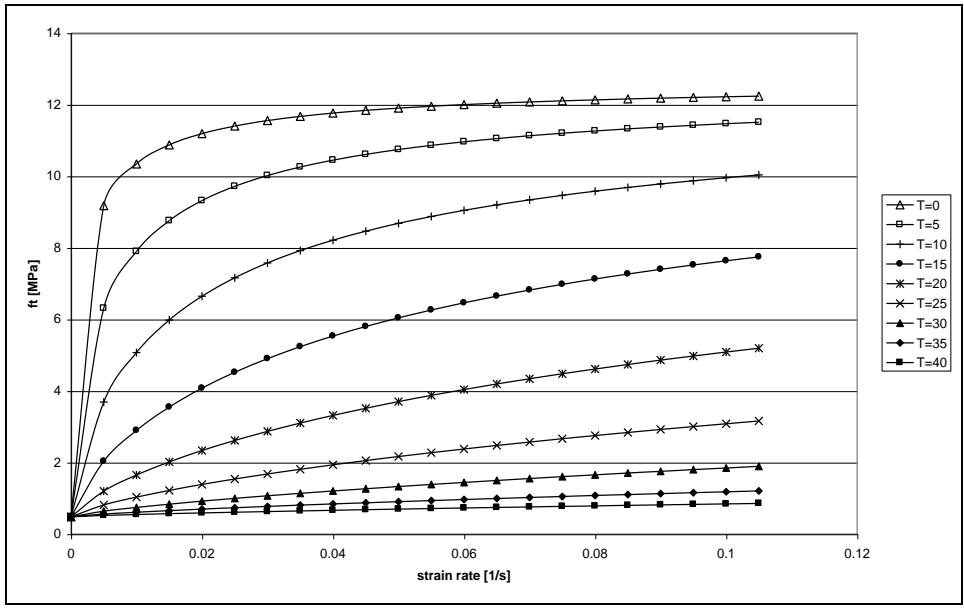


Figure 7.42: Tensile strength for different temperatures and strain rates

As expected, the tensile strength increases with decreasing temperature and increasing loading rate.

7.5.3 Ratio compressive strength/tensile strength

For different strain rates and temperatures the ratio f_o/f_t is calculated. The result is shown in figure 7.43.

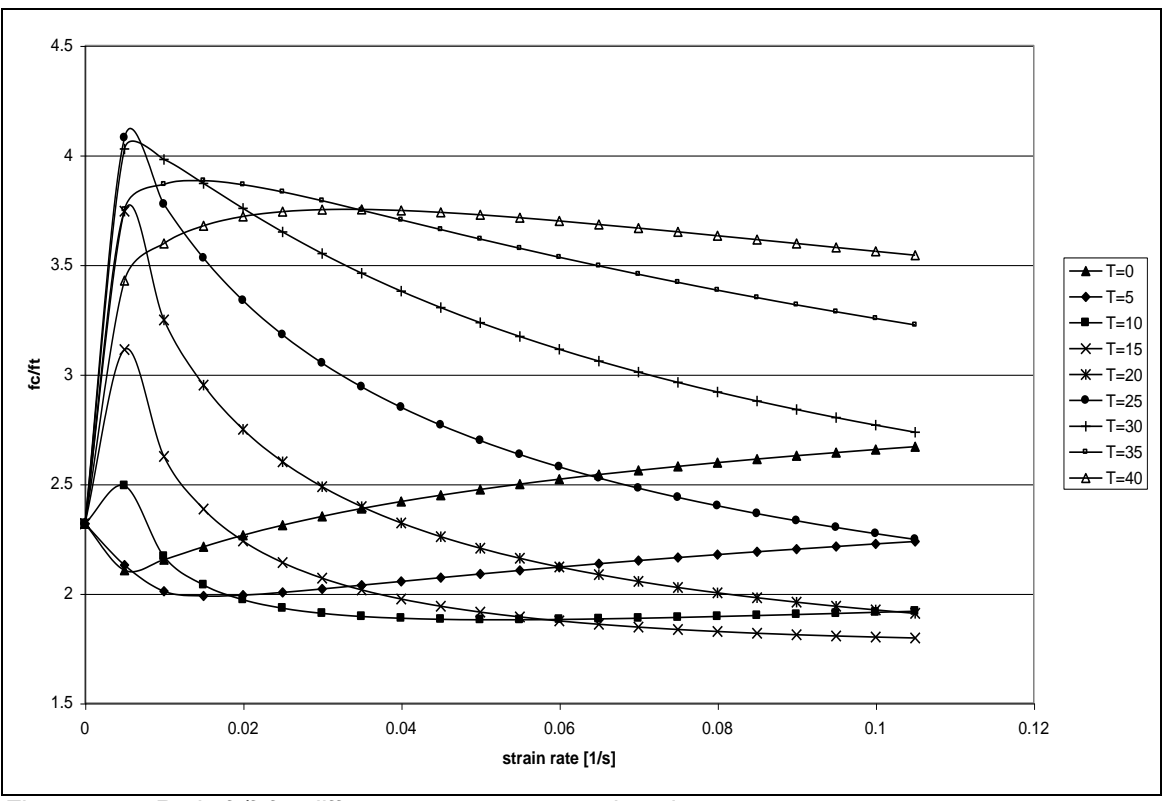


Figure 7.43: Ratio f_c/f_t for different temperatures and strain rates

The trends in figure 7.43 are rather remarkable, since the trend for $T=0^{\circ}C$ and $T=5^{\circ}C$ is different from the trend at the other temperatures. For the lower temperatures first the ratio f_c/f_t decreases at low strain rates and at a strain rate of approximately 0.01/s the ratio starts to increase. The opposite can be observed for the higher temperatures. Further, figure 7.44 shows that the ratio between the compressive and tensile strength varies between 1.8 and 4.2. Compared to concrete this is a rather small value, since the ratio for concrete is approximately 8-10. Also, for concrete the value is constant and varies not with temperature and loading rate, which is the case for asphalt.

7.6 Determination of the model parameters

7.6.1 Introduction

For the determination of all the model parameters in this section work carried by Erkens [1998, 2001, 2002] is gratefully used.

For uniaxial states of stress, the expression for the flow surface simplifies considerably. In that case:

$$\sigma_1 = \sigma$$
, $\sigma_2 = \sigma_3 = 0 \Rightarrow$

$$I_1 = \sigma_1 + \sigma_2 + \sigma_3 = \sigma$$

$$J_{2} = \frac{1}{2} \left[\left(\sigma_{1} - \frac{I_{1}}{3} \right)^{2} + \left(\sigma_{2} - \frac{I_{1}}{3} \right)^{2} + \left(\sigma_{3} - \frac{I_{1}}{3} \right)^{2} \right] = \frac{1}{2} \left[\left(\frac{2\sigma}{3} \right)^{2} + \left(-\frac{\sigma}{3} \right)^{2} + \left(-\frac{\sigma}{3} \right)^{2} \right] = \frac{1}{3} \sigma^{2}$$

$$J_3 = \left(\sigma_1 - \frac{\sigma}{3}\right)\left(\sigma_2 - \frac{\sigma}{3}\right)\left(\sigma_3 - \frac{\sigma}{3}\right) = \frac{2}{27}\sigma^3$$

$$\cos(3\theta) = \frac{3\sqrt{3}}{2} \frac{J_3}{(J_2)^{\frac{3}{2}}} = \frac{3\sqrt{3}}{2} \frac{\frac{2}{27}\sigma^3}{\left(\frac{1}{3}\sigma^2\right)^{\frac{3}{2}}} = \frac{\sqrt{27}}{2} \frac{\frac{2}{27}\sigma^3}{\sigma^3\sqrt{\frac{1}{27}}} = 1$$

Substitution in equation 4.1 yields:

$$\frac{\frac{1}{3}\sigma^2}{p_a^2} = \left[-\alpha \left(\frac{\sigma - R}{p_a} \right)^n + \gamma \left(\frac{\sigma - R}{p_a} \right)^2 \right] \cdot (1 - \beta)^{-\frac{1}{2}}$$
Equation 7.29

Until results from multiaxial tests are available, β is assumed to be zero, which means that the shape of the model on the π -plane is circular. In that case equation 7.29 reduces to:

$$\frac{\sigma^2}{3p_a^2} = \left[-\alpha \left(\frac{\sigma - R}{p_a} \right)^n + \gamma \left(\frac{\sigma - R}{p_a} \right)^2 \right]$$
 Equation 7.30

7.6.2 Determination of R

The three-dimensional tensile strength R can be determined from the uniaxial tension and compression results. R can be found as the intercept with the I_1 axis of a line through the tensile and compressive strength, plotted in the I_1 - $\sqrt{J_2}$ space (figure 7.44).

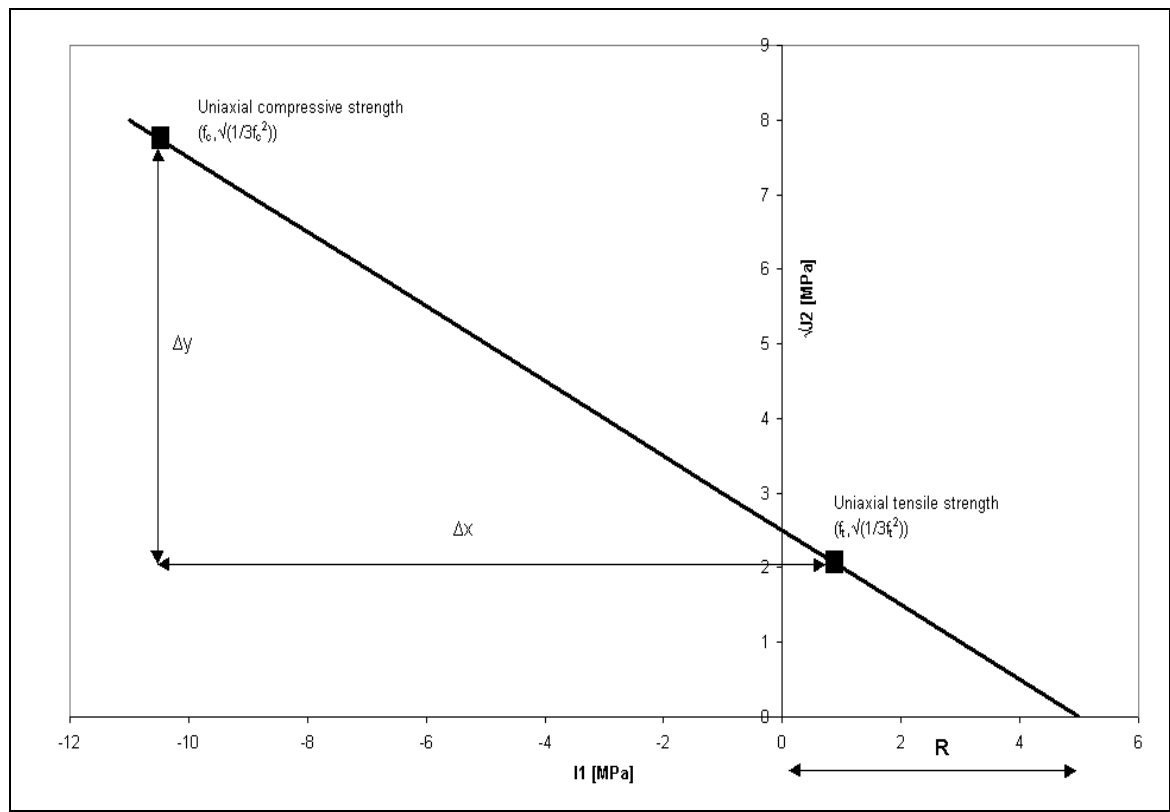


Figure 7.44: Determination of R by using the tension and the compression strength

In that case R is defined as:

$$R = f_t + \sqrt{\frac{1}{3} f_t^2} \frac{\Delta x}{\Delta y}$$
 Equation 7.31

in which:

$$\Delta x = f_t + \left| f_c \right|$$

$$\Delta y = \frac{1}{\sqrt{3}} \left\| f_c \right| - f_t \right|$$

and:

 f_t : tension strength [MPa] (equation 7.28) f_c : compression strength [MPa] (equation 7.27)

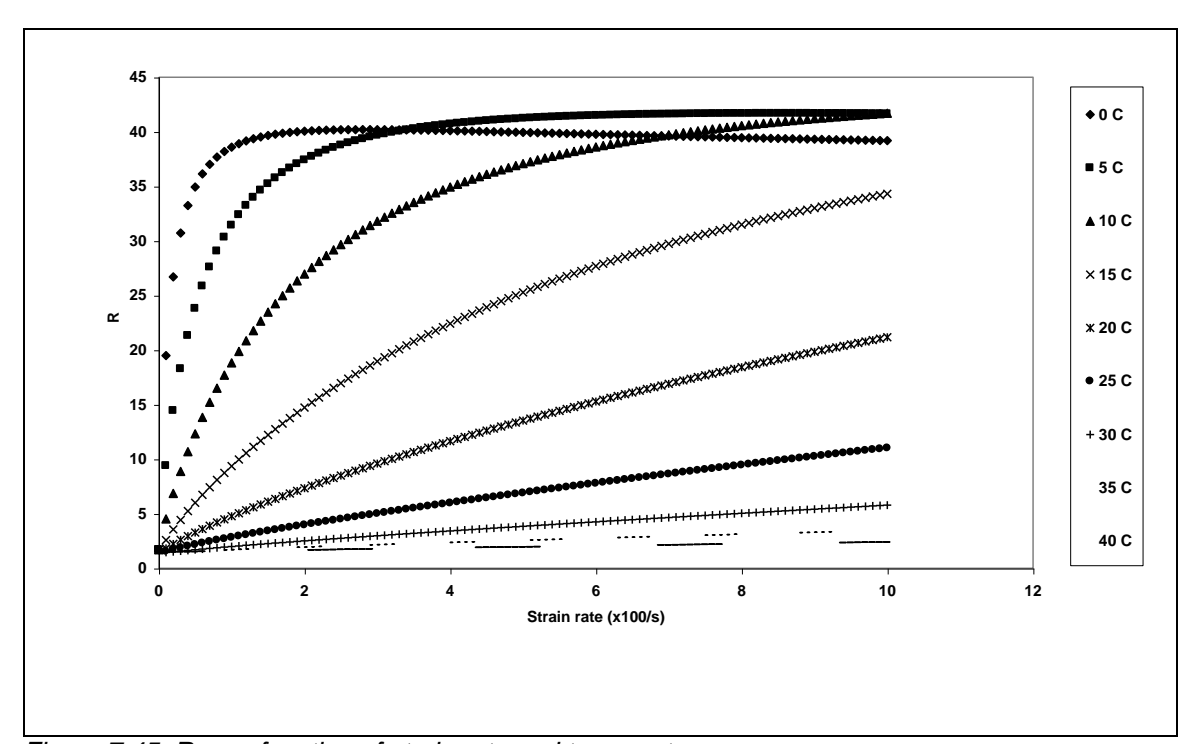


Figure 7.45 shows the results for parameter R as a function of strain rate and temperature.

Figure 7.45: R as a function of strain rate and temperature

From this figure it becomes clear that R decreases with temperature and increases with strain rate. This is to be expected since R is highly related to the tensile strength. This strength decreases with temperature due to a lower stiffness and increases with strain rate since in that case the material behaves stiffer. For low strain rates R converges to a value of 1.7. For high strain rates and a temperature of 10°C R reaches the maximum value of 41.7 at a strain rate of 0.1/s.

The figure also shows that for T=5°C R seems to reach to a maximum value and for lower temperatures (T=0°C) R starts to decrease. This can be explained by figure 7.43 that shows the ratio f_c/f_t . That figure shows that for T=0°C and T=5°C the trend in the ratio f_c/f_t is different from the trend at higher temperatures. Since R is related to f_c and f_t the different trend is to be expected for T=0°C and T=5°C, since the ratio f_c/f_t shows different trend at these temperatures also.

7.6.3 Determination of γ

The hardening parameter α is zero at peak stress (σ =apparent compressive strength= f_c). Then equation 7.30 becomes:

$$\frac{1}{3}f_c^2 = \gamma(f_c - R)^2$$
 Equation 7.32

Rewriting equation 7.32 results in the relation for γ :

$$\gamma = \frac{\frac{1}{3}f_c^2}{(f_c - R)^2}$$
 Equation 7.33

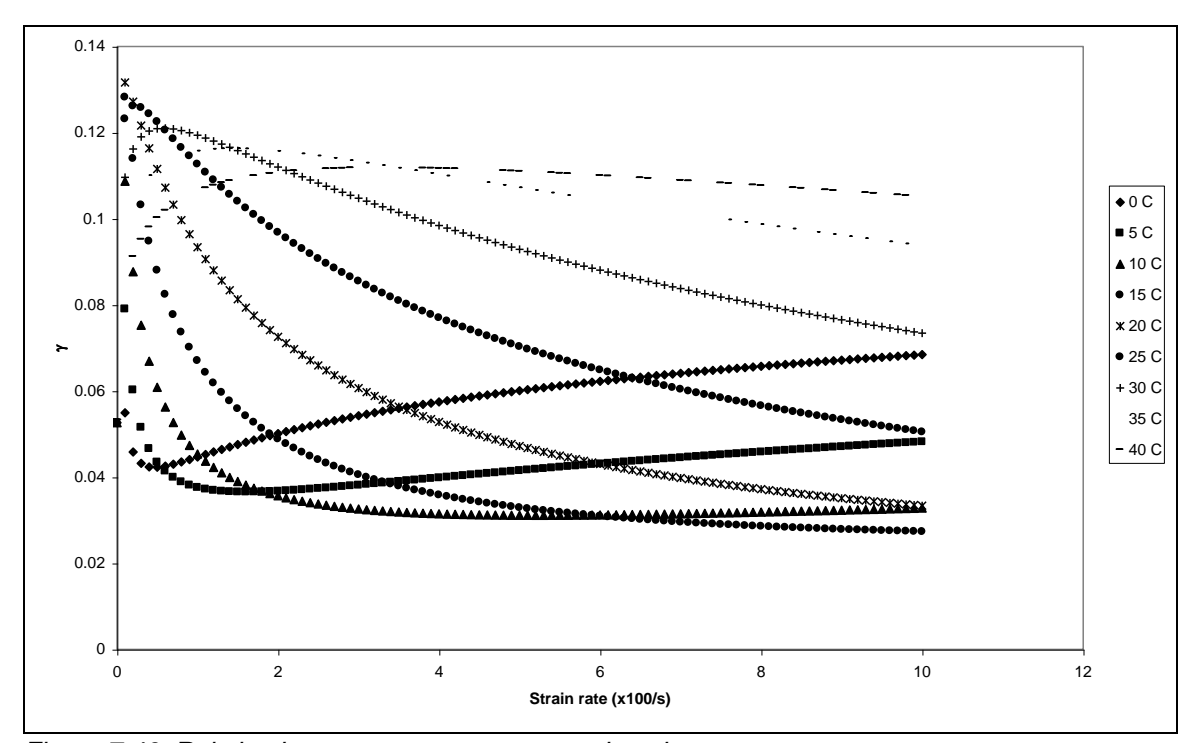


Figure 7.46 shows the relation between γ and both temperature and strain rate.

Figure 7.46: Relation between γ , temperature and strain rate

Also here different trend at T=0°C and T=5°C can be observed, since γ is also related to f_c and f_t. At high strain rates the minimum value of γ converges to 0.03. For low strain rates and a temperature of 20°C the maximum value of γ is 0.13.

7.6.4 Determination of n

The model parameter n is related to the onset of dilation in the specimen. Dilation is the increase in volume that results from the opening of internal cracks. At the beginning of a compression test, the axial strain is larger than the radial strain, which leads to decrease in volume. Once dilation starts, the volume increases. For dilation volumetric strains are of interest since they are related to the change in volume [Erkens, 2001, 2002]. The volumetric strains are calculated with:

$$\varepsilon_v = (1 + \varepsilon_r)^2 (1 - |\varepsilon_{ax}|) - 1$$
 Equation 7.34

in which:

 ε_{v} : volumetric strains [m/m] ε_{r} : radial strains [m/m] ε_{ax} : axial strains [m/m]

The radial and axial strains follow directly from the test output. For the determination of n the stresses at which dilation starts are of interest. This stress can be determined by means of the axial versus volumetric strain plot and the axial strain versus stress plot. The first plot is used to determine the axial strain at minimum volumetric strain (start of dilation), the second plot is used to determine the corresponding state of stress (figure 7.47).

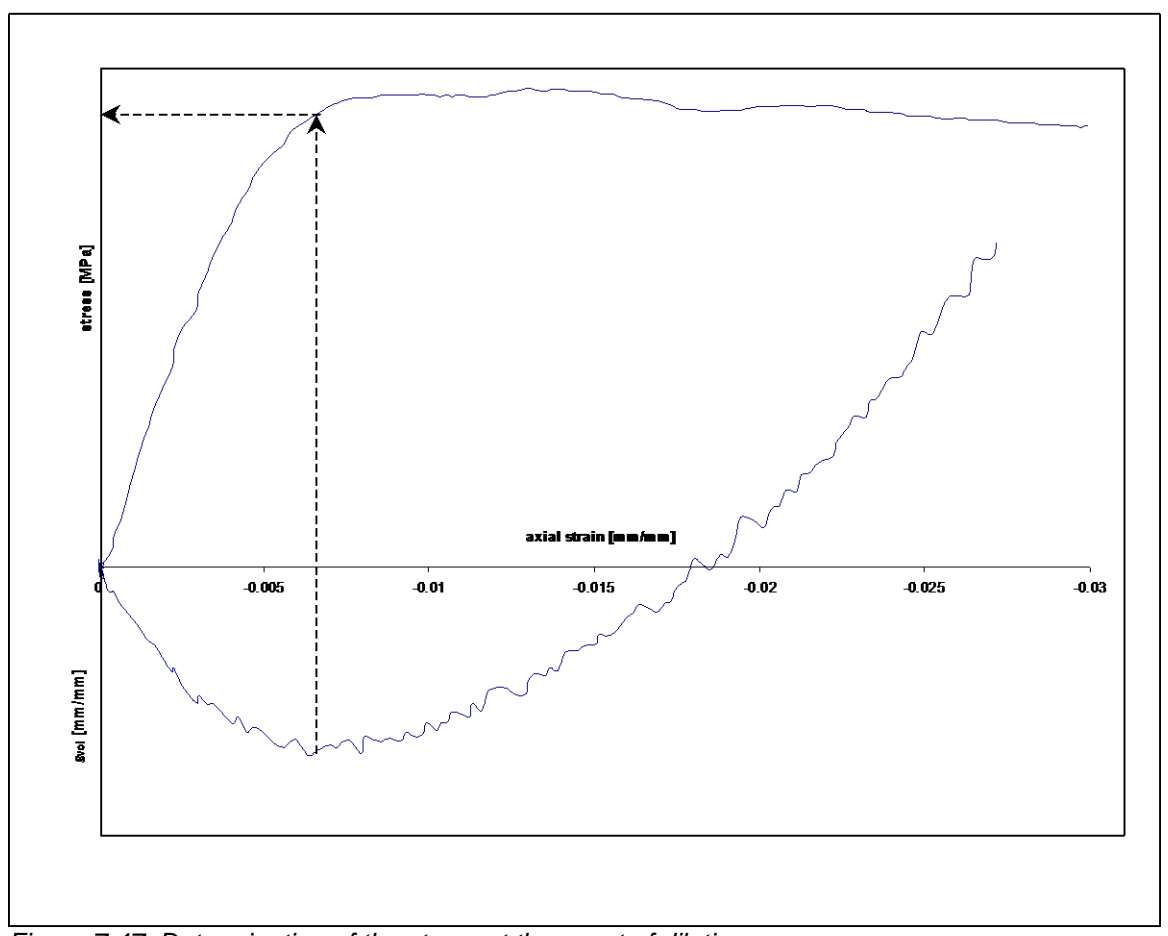


Figure 7.47: Determination of the stress at the onset of dilation

This figure shows that in first instance the volumetric strain decreases, indicating that the material is densified (plastic contraction). This is caused by the closure of cracks or the reorientation of grains. The volume reduction finally stops and an increase of volume follows (plastic dilation). During this dilation phase whole groups of grains are shifted with respect to each other [Sitters, 1998].

Regression analysis showed that the relation between the stress at the start of dilation and temperature and strain rate is best described with:

$$\sigma_{dilation} = a \left(1 - \frac{1}{1 + \left(\dot{\varepsilon} \exp\left(\left(\frac{b}{T_k} \right)^2 + c \right) \right)^d} \right)$$
 Equation 7.35

in which:

 $\sigma_{\! ext{dilation}}$: stress at the onset of dilation [MPa]

 $\dot{\varepsilon}$: strain rate [x100/s] T_k : temperature [K]

a : -42.612 b : 1841.544 c : -46.068 d : 0.581

Appendix G shows the results from the regression analysis that has been carried out to obtain equation 7.35.

Figure 7.48 shows the relation between σ_{dilation} and both temperature and strain rate.

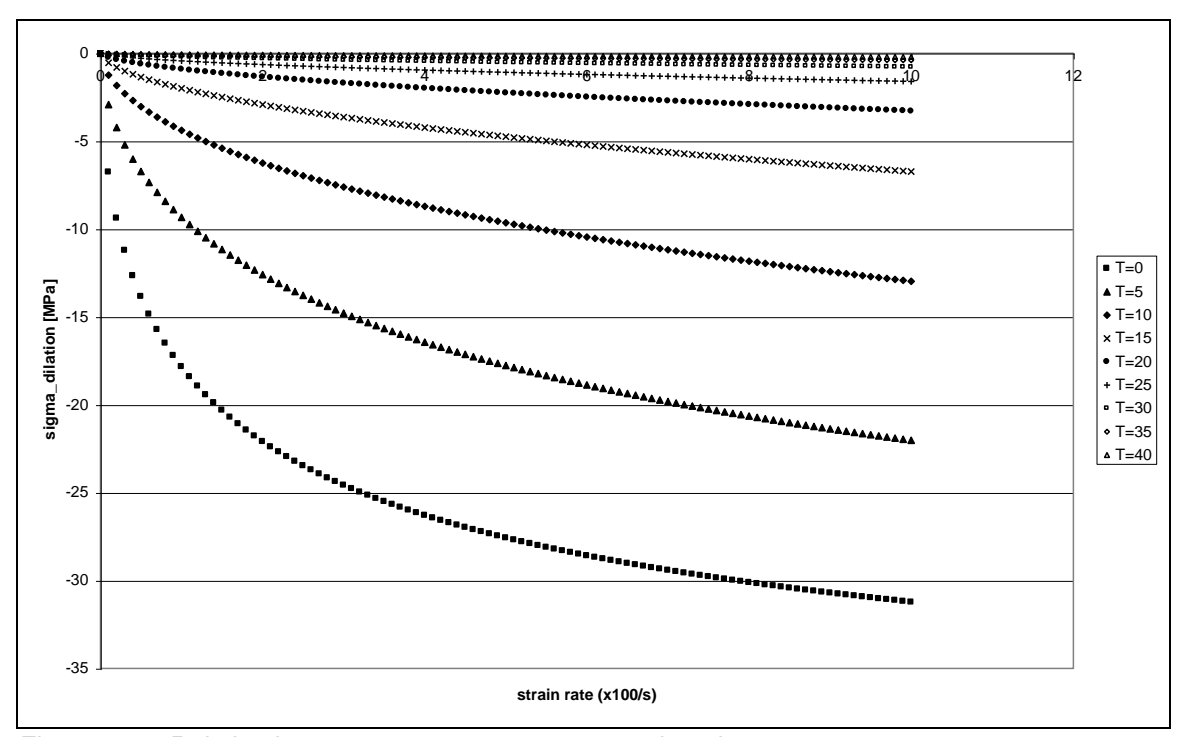


Figure 7.48: Relation between $\sigma_{dilation}$, temperature and strain rate

This figure shows clearly that σ_{dilation} increases with increasing strain rate and decreases with increasing temperature. Figure 7.49 shows the ratio $\sigma_{\text{dilation}}/f_c$ for different temperatures and strain rates.

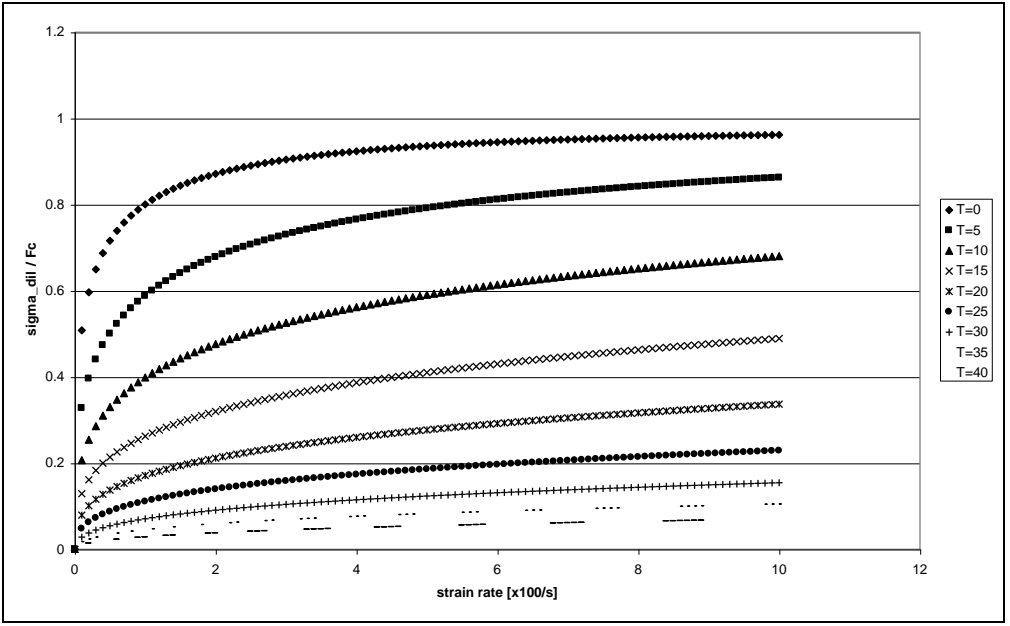


Figure 7.49: $\sigma_{\text{dilation}}/f_c$ for different temperatures and strain rates

This figure shows that for low temperatures the stress at which dilation starts is close to the maximum compressive stress. The difference between the stress at the beginning of dilation and the compressive strength depends on the difference in axial strain between these points and the slope of the stress-strain diagram. In case of plastic response, the difference in strain is considerable since dilation starts early in the test. This explains the decreasing value for $\sigma_{\text{dilation}}/f_{\text{c}}$ for increasing temperatures. For high strain rates the elastic response increases, which means that dilation starts at a stress level that is closer to the maximum compressive strength.

After the determination of σ_{dilation} , n is calculated with:

$$n = \frac{2}{\left(1 - \frac{\sigma_{dilation}^2}{3\gamma(\sigma_{dilation} - R)^2}\right)}$$
 Equation 7.36

Table 7.26 shows a comparison between the predicted σ_{dilation} and the real stress at the start of dilation that follows from the test results.

Table 7.26: Comparison between the predicted and real $\sigma_{dilation}$

specimen	strain rate [x100/s]	T [K]	σ_{dilation} [MPa]	σ _{dilation} predicted [MPa]	difference [%]
M5-3	1.680355	278.9	-10.45	-10.37	0.8
M4-3	9.746948	278.9	-20.00	-20.11	-0.5
M4-4	1.703829	307.1	-0.16	-0.16	-1.5
M3-10	9.780624	307.1	-0.54	-0.45	18.1
M10-10	0.00997	293	-0.16	-0.06	58.5
M10-2	10.29013	293	-4.00	-3.35	16.2
M11-4	5.856144	273	-28.50	-28.46	0.1
M2-5	5.684035	313	-0.15	-0.15	0.1
M11-3	5.115768	293	-2.12	-2.29	-8.1
M6-4	5.153614	293	-2.35	-2.30	2.2
M7-4	5.122877	293	-2.00	-2.29	-14.7
M9-2	5.108674	293	-2.12	-2.29	-8.1
M6-6	5.124875	293	-2.00	-2.29	-14.7

Immediately the large difference of 58% for specimen M10-10 catches the eye. However, this results of the rather small value for σ_{dilation} , which results in large relative differences when the real difference is very small. In this case the real difference is only 0.1MPa, which is negligible. A plot of n as a function of the stress at the onset of dilation is shown in figure 7.50. This plot shows that for states of stress close to the compressive strength the value of n increases considerable.

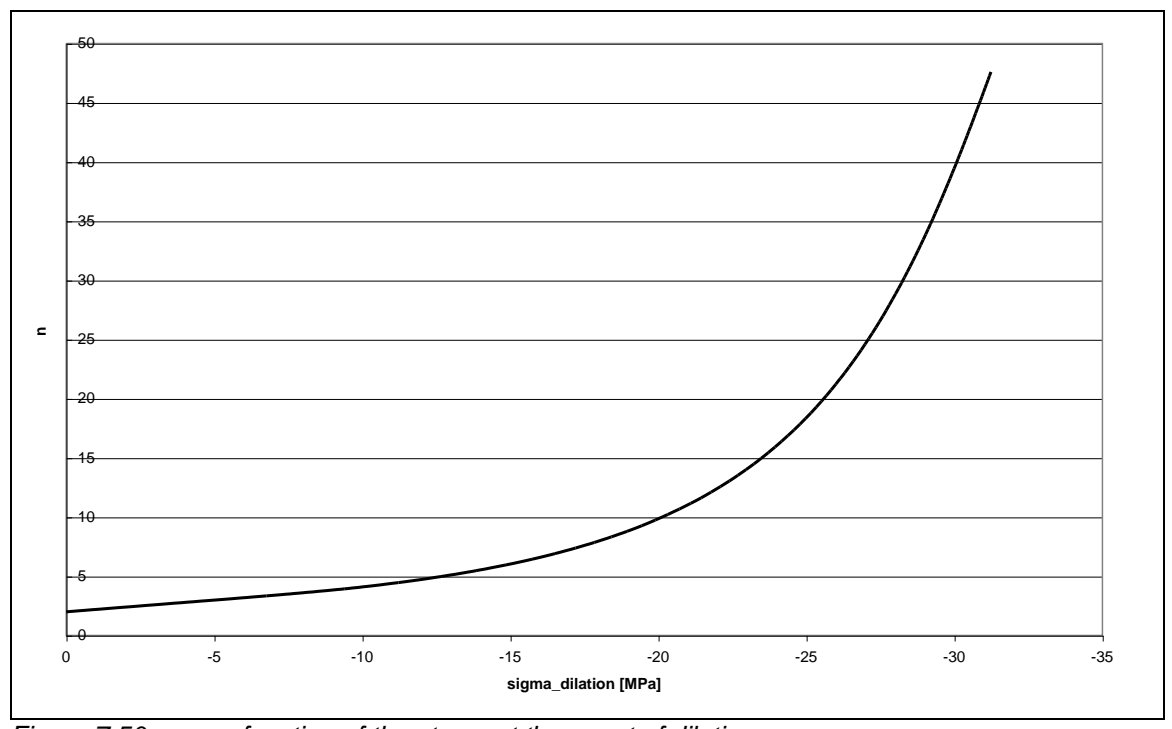


Figure 7.50: n as a function of the stress at the onset of dilation

For states of stress that differ considerably from the compressive strength the value of n reaches the value of 2.

7.6.5 Determination of α

7.6.5.1 Determination of α_0 at the onset of dilation

The last parameter to be determined is the hardening parameter α . "This parameter has a constant, non-zero, value during the linear elastic part of the response, its value diminishes during the non-linear phase until it is zero at peak stress. After peak stress, α remains zero. Now that the other parameters are known, α can be determined directly form the expression for the flow surface for each state of stress" as shown in equation 7.37 [Erkens et al., 1998].

$$f = \frac{J_2}{p_a^2} - \frac{\left[-\alpha \left(\frac{I_1 - R}{p_a} \right)^n + \gamma \left(\frac{I_1 - R}{p_a} \right)^2 \right]}{\sqrt{\left(1 - \beta \cos(3\theta)\right)}} = 0 \Rightarrow \alpha = \frac{-\frac{J_2}{p_a^2} \sqrt{\left(1 - \beta \cos(3\theta)\right)} + \gamma \left(\frac{I_1 - R}{p_a} \right)^2}{\left(\frac{I_1 - R}{p_a} \right)^n}$$
Equation 7.37

"Based on equation 7.32 values for α for all states of stress throughout the stress strain curves can be found. However, based on the definition for α , only the values between the onset of non-

linearity and peak strength have to be determined. The value found for the state of stress at the onset of non-linearity gives α_0 and from peak strength until complete annihilation of strength, α =0" [Erkens et al., 1998]. The peak strength is already determined as a function of temperature and strain rate (equation 7.27), the next step is determining the stress at the onset of non-linearity (σ_{plas}) as a function of temperature and strain rate. First the values for σ_{plas} for each compression test are determined. These values can not be exactly determined from the stress versus axial strain plot. Therefore use is made of the radial measurements to determine the stress at which non-linearity starts. During the first (linear) part of the test the ratio between the radial and the axial strains is approximately constant. This ratio is defined as Poisson's ratio. Once non-linearity starts, Poisson's ratio starts to increase. The strain at which non-linearity starts can be obtained by plotting the axial versus the radial strain (figure 7.51). For the linear elastic part the relation between the axial and the plastic strains is linear, as soon as non-linearity starts the relation is no longer linear.

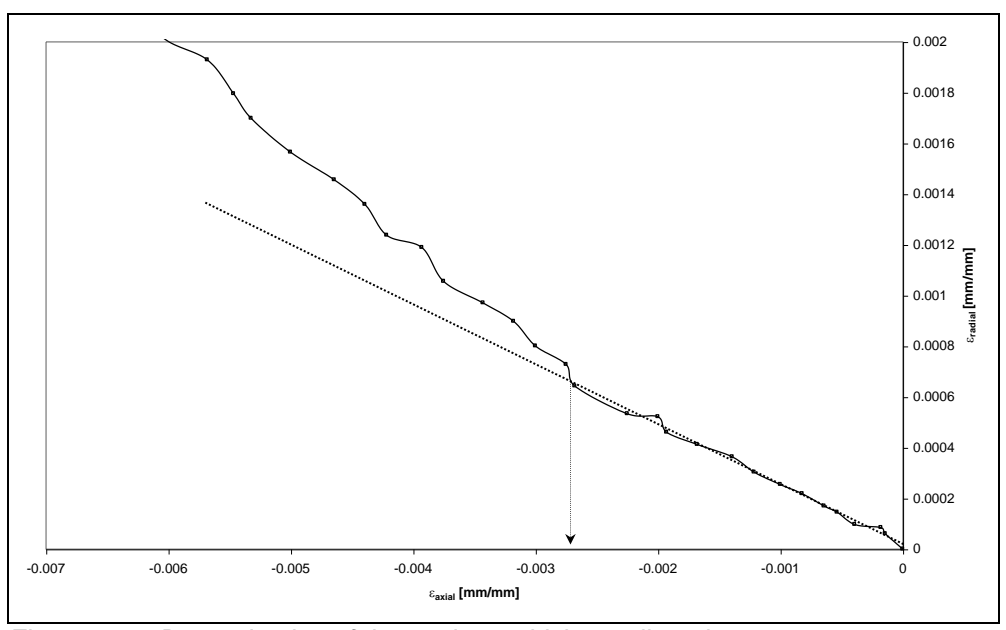


Figure 7.51: Determination of the strain at which non-linearity starts

By using the relation between the axial strain and the radial strain the strain at which non-linearity starts can be obtained for each compression test. Next, the stress at which non-linearity starts (σ_{plas}) can be obtained by using the plot between the axial strain and the stress. Table 7.27 shows the values for the compressive plastic stress σ_{plas} .

Table 7.27: Stress at the start of non-linearity for the compression tests

			•
Specimen	strain rate [x100/s]	T [K]	σ _{plas} [MPa]
M5-3	1.68	278.9	-6.51
M4-3	9.75	278.9	-7.22
M4-4	1.70	307.1	-0.11
M3-10	9.78	307.1	-0.41
M10-10	0.01	293	-0.04
M11-4	5.86	273	-16.28
M2-5	5.68	313	-0.08
M11-3	5.12	293	-2.16
M6-4	5.15	293	-2.29
M7-4	5.12	293	-1.86
M9-2	5.11	293	-2.62
M6-6	5.12	293	-1.45

It can be noted that in table 7.27 the data for specimen M10-2 is missing. The reason behind that is that during the test the radial measurement system failed during the first part of the test.

Erkens [2001, 2002] proposed the following type of equation for the relationship between σ_{plas} , temperature and strain rate:

$$\sigma_{plas} = a \left(1 - \frac{1}{1 + \left(\dot{\varepsilon} e^{\left(b + \frac{c}{T} \right)} \right)^d} \right)$$
 Equation 7.38

where:

 σ_{plas} : stress at the onset of non-linearity

 $\dot{\mathcal{E}}$: strain rate [1/s] T_k : temperature [K] a, b, c, d : regression constants

Regression analysis of the data from the compression tests showed that equation 7.38 is not quite suitable, since the standard error of the estimate became too. Additional is needed to determine the relationship between the stress at the onset of non-linearity, the strain rate and the temperature.

However, the stress at the onset of dilation can be obtained indirectly. Regression analysis showed that the relationship between α_0 , temperature and strain rate can be expressed as (equation 7.39):

$$\alpha_0 = a \left(1 - \frac{1}{1 + \left(\dot{\varepsilon} \exp\left(\left(\frac{b}{T_k} \right)^2 + c \right) \right)^d} \right)$$
 Equation 7.39

in which:

 α_0 : initial α value (material parameter)

 $\dot{\mathcal{E}}$: strain rate [x100/s] T_k : temperature [K]

a : 0.104 b : 1382.115 c : -22.723 d : -2.234

The constants a, b, c and d were determined using SPSS computer package, from which the output is shown in appendix H.

By combining equation 7.39 and equation 7.37 the stress at the onset of non-linearity can be determined by iteration.

Table 7.28 shows the comparison between the α_0 from the data and the predicted one. The values for α_0 -data in this table are determined by using σ_{plas} from table 7.27 in combination with equation 7.37.

Table 7.28: Comparison between the α_0 from the data and the predicted one

	-	0 -		· · /- · · · · · · · · · · · · · · · · ·	
specimen	strain rate [x100/s]	T [K]	α_0 -data	α_0 - predicted	Difference [%]
M5-3	1.68	278.9	2.38E-07	5.38E-04	-300835
M4-3	9.75	278.9	1.07E-21	1.07E-05	-1.3E+18
M4-4	1.70	307.1	0.097077	0.102855	0.57
M3-10	9.78	307.1	0.079719	0.0628668	0.07
M10-10	0.01	293	0.090973	0.104217	-0.16
M11-4	5.86	273	3.43E-24	3.02E-06	-3.7E+77
M2-5	5.68	313	0.09939	0.100588	-0.46
M11-3	5.12	293	0.006361	0.007248	-1.15
M6-4	5.15	293	0.007835	0.007137	-2.38
M7-4	5.12	293	0.006494	0.007226	3.08
M9-2	5.11	293	0.007316	0.007269	-8.63
M6-6	5.12	293	0.006851	0.007221	7.66

The prediction is quite good except for specimens M5-3, M4-3 and M11-4. For these three specimens a very small value has to be predicted and a small absolute difference between the real and the predicted value leads to a very large difference in percents. The small value of α_0 is the result from very large n-values. The three tests were all carried out at low temperatures (0°C and 5.9°C) which resulted in stresses at the onset of non-linearity that are close to the maximum compressive stress. Figure 7.50 showed that for states of stress close to the compressive strength the value of n increases considerable. Equation 7.37 shows that for very high n-values the denominator increases, which leads to a decrease in the α_0 -value.

Erkens [2001, 2002] also indicates the very small values for α_o for large n-values. According to Erkens the small α_0 -values are equal to zero and especially in any numerical application, values smaller than $10^{\cdot 16}$ are equivalent to zero. Therefore a cut-off value of 10 is used for high n-values. This cut-off means that for n-values higher than 10, or when the difference between f_c and $\sigma_{dilation}$ is smaller than 20%, n is set to 10. The latter requirement is used because the expressions for f_c and $\sigma_{dilation}$ as functions of temperature and strain rate can, for some conditions lead to $\sigma_{dilation} > f_c$. When n is set to 10, α_o is set to zero, which means that no hardening response occurs.

When these requirements are applied for the compression data, n is set to 10 and $\alpha_{\rm o}$ is set to 0 for the tests at specimen M4-3 ($\dot{\varepsilon}$ =9.75*10⁻², T=278.9K) and at specimen M11-4 ($\dot{\varepsilon}$ =5.86*10⁻², T=273K). Since in that case no hardening occurs these tests are neglected in the determination of α .

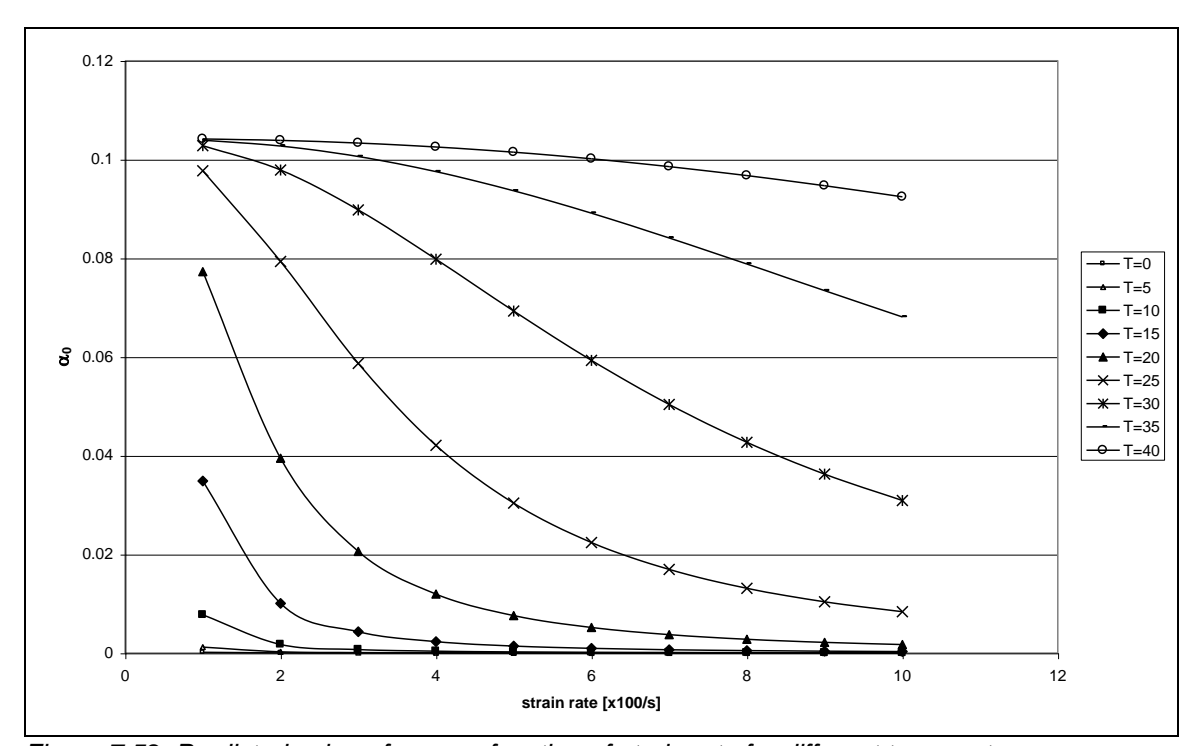


Figure 7.52 shows the predicted α_0 as a function of strain rate for different temperatures.

Figure 7.52: Predicted value of α_0 as a function of strain rate for different temperatures

Although the fact that the prediction for small values of α_0 (low temperatures, high strain rates) could be not exact, the trend in figure 7.52 has a physical meaning. The value of α_0 decreases namely with increasing strain rate and decreasing temperature, as to be expected.

Because α_o is known as a function of temperature and strain rate, α can then be determined. According to Erkens [2001, 2002] the degradation from α_o at the onset of plasticity to zero at peak stress can be expressed either as a function of the equivalent plastic strain ξ or as a function of plastic work W_p .

7.6.5.2 Determination of α as a function of the equivalent plastic strain

The equivalent plastic strain is defined as:

$$\xi = \sum \sqrt{\varepsilon_{p,ij}^T \cdot \varepsilon_{p,ij}} \qquad ; i, j = x, y, z$$
 Equation 7.40

For the compression tests equation 7.40 becomes:

$$\xi = \sum \sqrt{\varepsilon_r^2 + \varepsilon_{ax}^2}$$
 Equation 7.41

in which:

 $\begin{array}{ll} \xi & : \text{the equivalent plastic strain} \\ \epsilon_r & : \text{radial strain [mm/mm]} \\ \epsilon_{\text{ax}} & : \text{axial strain [mm/mm]} \end{array}$

0.8 0.7 - 1: T=278.9K strain rate=0.017 0.6 2: T=307.1K strain rate=0.017 3: T=307.1K strain rate=0.098 **2** 0.5 4: T=293K strain rate=9.97E-5 4 5: T=313K strain rate=0.057 6: T=293K strain rate =0.051 3 0.3 0.2 0.1 5 0 0.25 0.05 0.2

Figure 7.53 shows the relationship between $\alpha_{i}\alpha_{0}$ and ξ . For the 5 measurements at T=293K and $\dot{\varepsilon}$ =0.051 s⁻¹ the average is taken.

Figure 7.53: Relationship between $\alpha_0 \alpha_0$ and ξ

The relation used by Erkens to describe the degradation of α is [Erkens, 2001, 2002]:

$$\alpha = \alpha_0 e^{-\kappa \xi}$$
 Equation 7.42

where:

 α : hardening parameter

 α_0 : the initial α value (material parameter)

κ : controls the rate of degradation (material parameter)

 ξ : the equivalent plastic strain

Table 7.29 shows the value κ for each curve that was determined by regression analysis as well as the corresponding n-value.

Table 7.29: κ and n for different strain rates and temperatures

T [K]	strain rate [1/s]	κ	n
278.9	0.0168	-202.792	3.942395
307.1	0.0170	-15.6472	2.037674
307.1	0.0978	-25.8191	2.081955
293	0.0001	-21.2799	2.011656
313	0.0568	-15.9168	2.030734
293	0.0513	-35.2061	2.344905

According to Erkens κ is related to n, the model parameter that is related to dilation (see paragraph 7.6.4). Regression analysis resulted in the following relation between κ and n:

 $\kappa = a + bn^3$ Equation 7.43

in which:

κ : controls the rate of degradation (material parameter)

n : model parameter that is related to dilation

a : 9.782 b : -3.470

Figure 7.54 shows the relation between n and κ , in which the line the predicted relation between n and κ represents (equation 7.43).

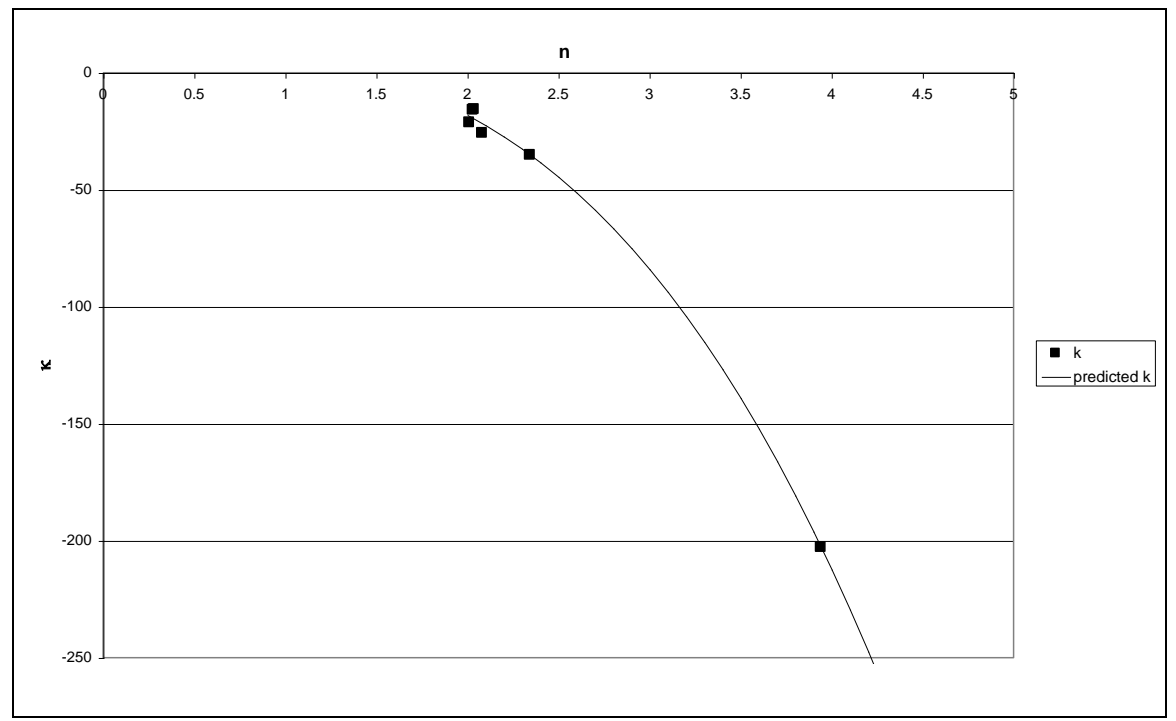
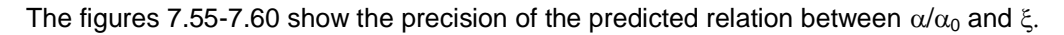


Figure 7.54: Relationship between κ and n

From figure 7.54 it becomes clear that the equivalent plastic strain ξ can be predicted quite good by using equation 7.43. However, the relationship is based on 6 data points, from which 4 data points are very close to each other. Further there are no data points in the range of n between 2.5 and 4. Therefore equation 7.43 is just the best fit for the available data points and has no physical meaning.



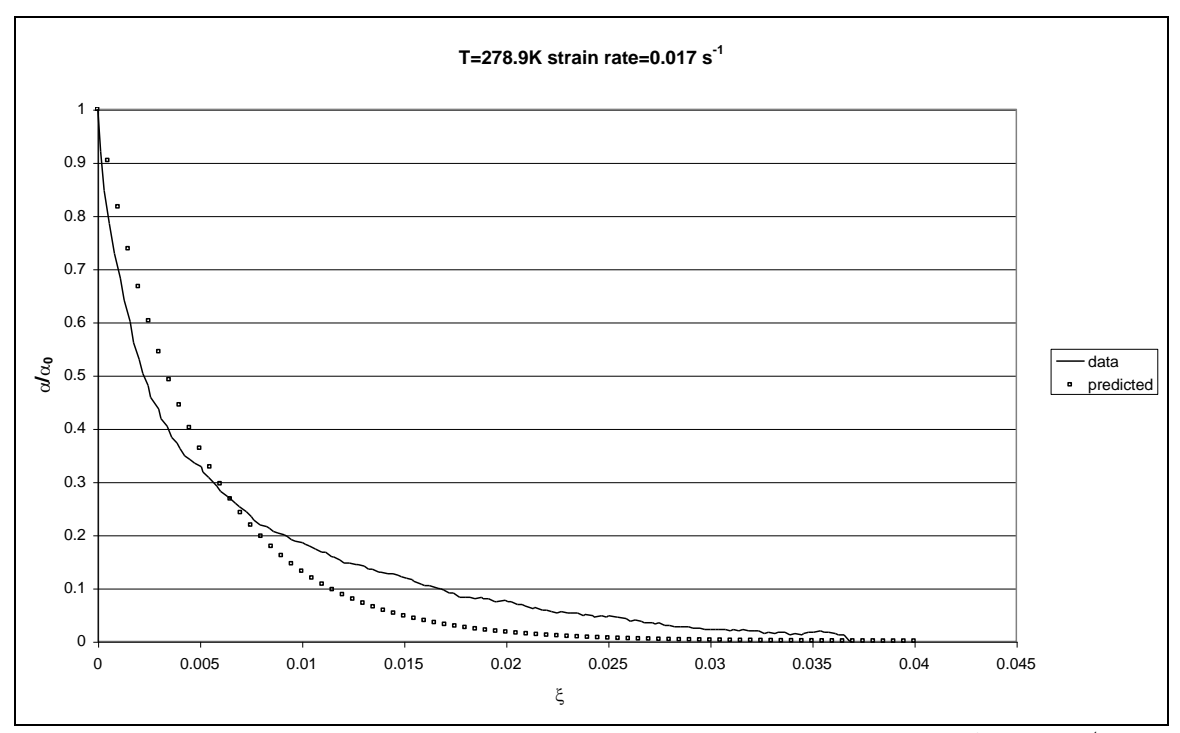


Figure 7.55: Precision of the predicted relationship between α/α_0 and ξ for T=278.9K and $\dot{\varepsilon}$ =0.017 s⁻¹

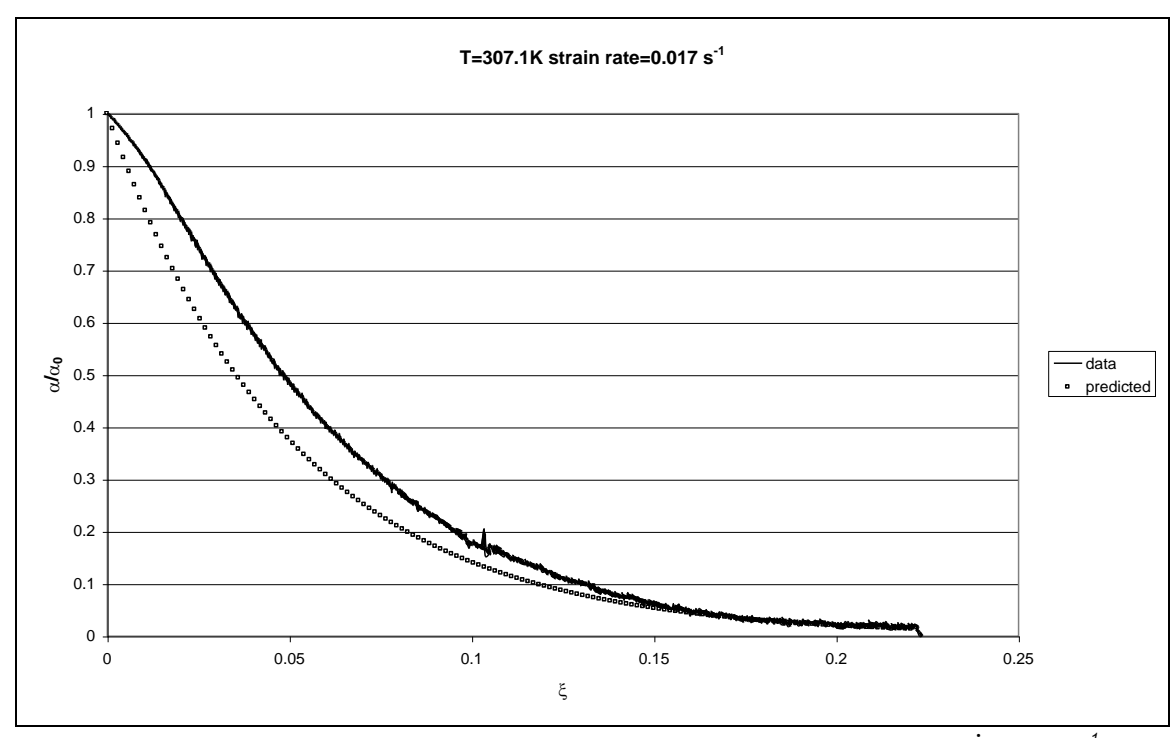


Figure 7.56: Precision of the predicted relationship between α/α_0 and ξ for T=307.1K and $\dot{\varepsilon}$ =0.017 s⁻¹

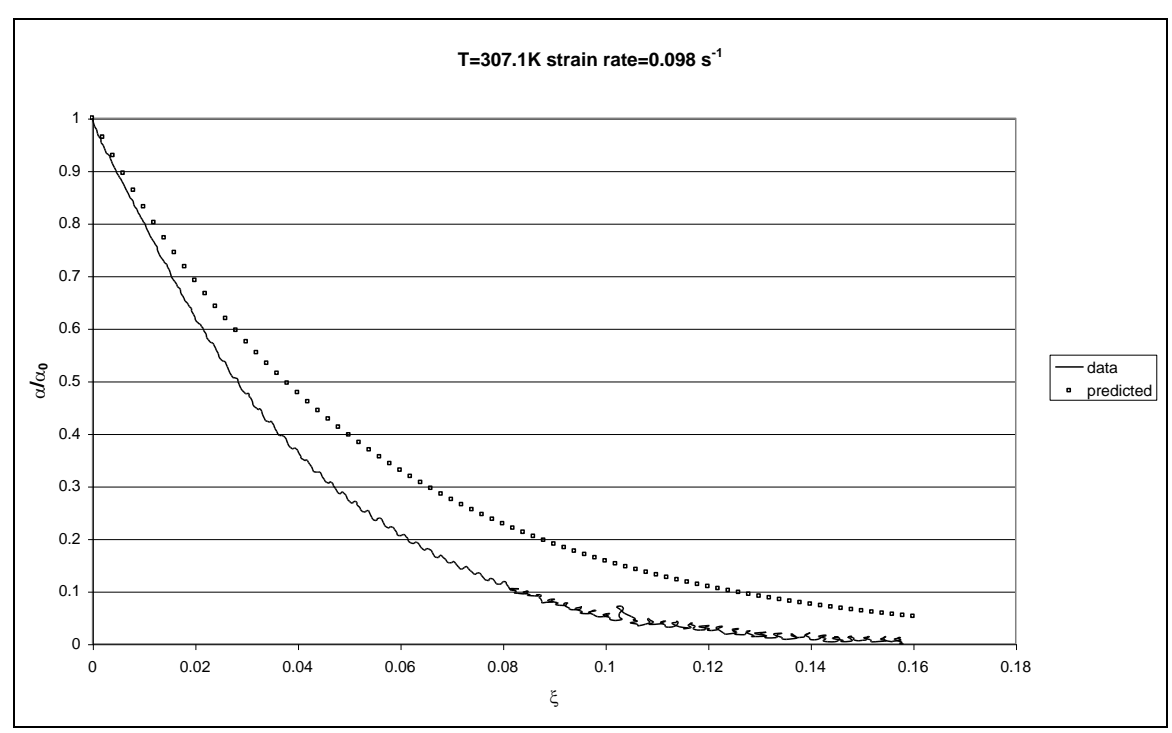


Figure 7.57: Precision of the predicted relationship between α/α_0 and ξ for T=307.1K and $\dot{\varepsilon}$ =0.098 s⁻¹

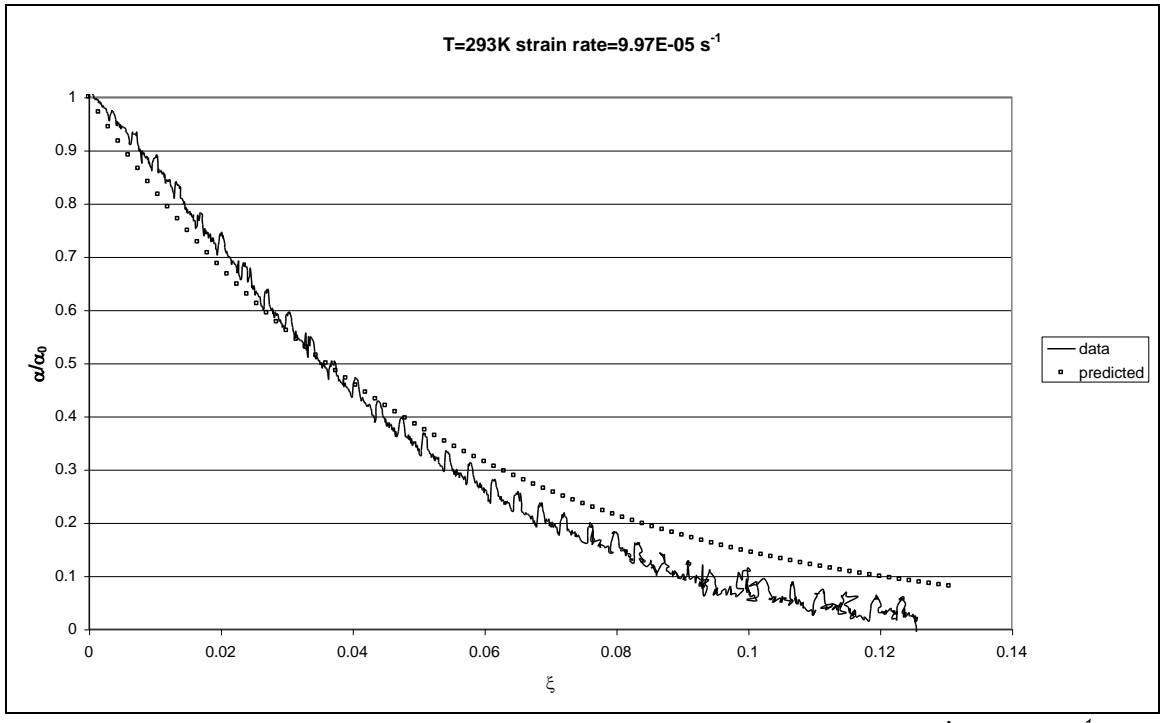


Figure 7.58: Precision of the predicted relationship between α/α_0 and ξ for T=293K and $\dot{\varepsilon}$ =9.97E-5 s⁻¹

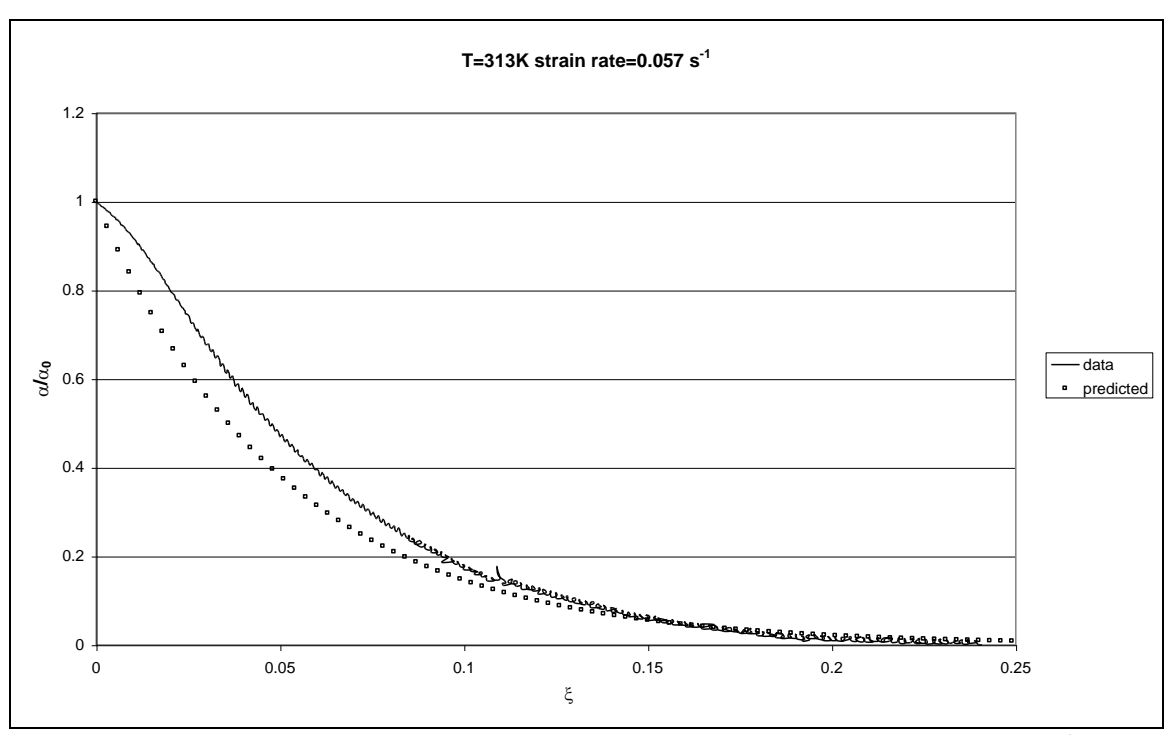


Figure 7.59: Precision of the predicted relationship between α/α_0 and ξ for T=313K and $\dot{\varepsilon}$ =0.057 s⁻¹

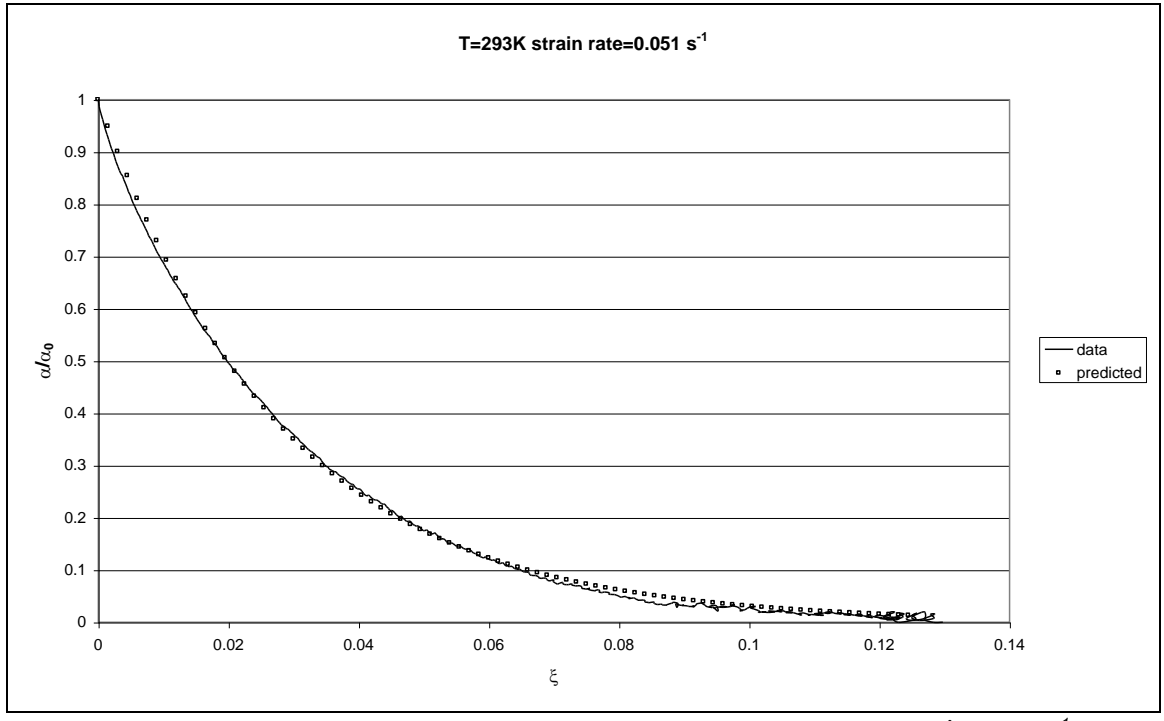


Figure 7.60: Precision of the predicted relationship between α/α_0 and ξ for T=293K and $\dot{\varepsilon}$ =0.051 s⁻¹

From the figures above it becomes clear that equation 7.42 is not good enough to predict the relationship between the ratio α/α_0 and ξ . Only for T=293K and $\dot{\varepsilon}$ =0.051 s⁻¹ the prediction is very close to the line based on the data. The fact that equation 7.42 is not good enough is not

attributed to the fact that κ is not predicted precisely but to the fact that the relation between α/α_0 and ξ can not be described by a simple exponential relation in this case.

Therefore another relationship between α and the equivalent plastic strain is analysed:

$$\alpha = \alpha_0 \frac{a + c\xi}{1 + b\xi}$$
 Equation 7.44

in which:

ξ : the equivalent plastic strain

 α : hardening parameter

 α_0 : the initial α value (material parameter)

a, b, c : constants

The constants are determined by regression analysis and are shown in table 7.30. Also the n-value is included in this table.

Table 7.30: Constants a, b and c for different strain rates and temperatures

strain rate [s ⁻¹]	T [K]	n	а	b	С
0.0168	278.9	3.942395	1.0	329.7	-20.5
0.0170	307.1	2.037674	1.1	14.7	-5.7
0.0978	307.1	2.081955	1.1	26.5	-7.9
0.0001	293	2.011656	1.1	15.0	-8.8
0.0568	313	2.030734	1.1	16.1	-5.6
0.0513	293	2.344905	1.0	38.0	-9.2

From table 7.30 it becomes clear that a has a constant value of approximately 1. This is to be expected since the parameter a determines the ratio α/α_0 for ξ =0. Therefore a is set to 1.0 for all the test conditions.

The parameters b and c are not constant and are assumed to be dependent on the n-value, just like the parameter κ in equation 7.43. Regression analysis resulted in the following relation between b and n:

$$b = -38.713 + 7.139e^n$$

Equation 7.45

in which:

b : constant

n : parameter related to the onset of dilation

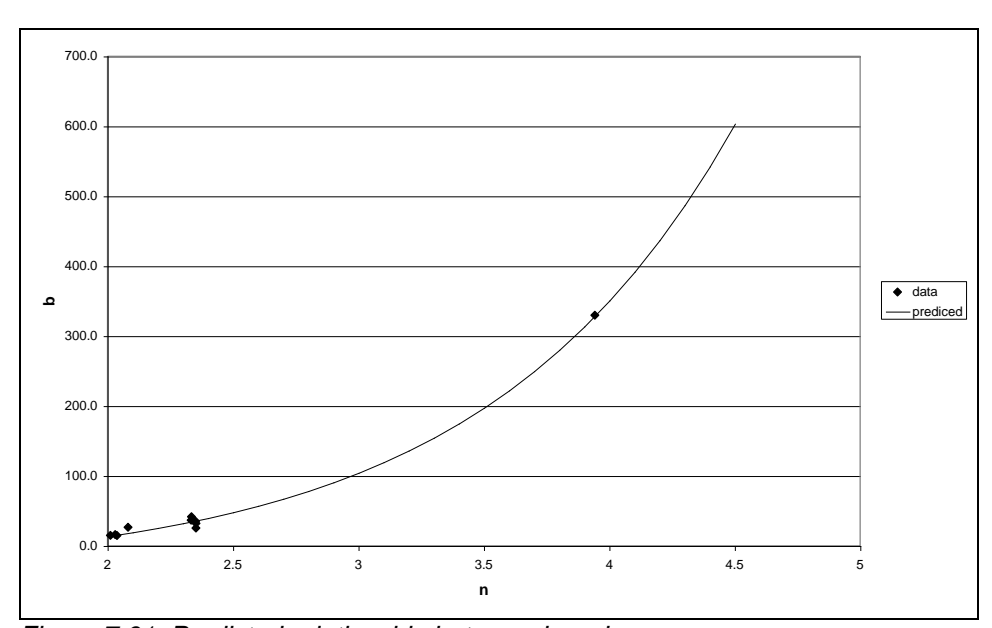


Figure 7.61 shows the predicted relation between b and n.

Figure 7.61: Predicted relationship between b and n

Figure 7.61 shows that the predicted relationship between b and n is quite good. However, the relationship has no physical meaning.

The relationship between *c* and *n* is best described with:

$$c = 7.375 - 20.386 \ln(n)$$

Equation 7.46

in which:

c : constant

n : parameter related to the onset of dilation



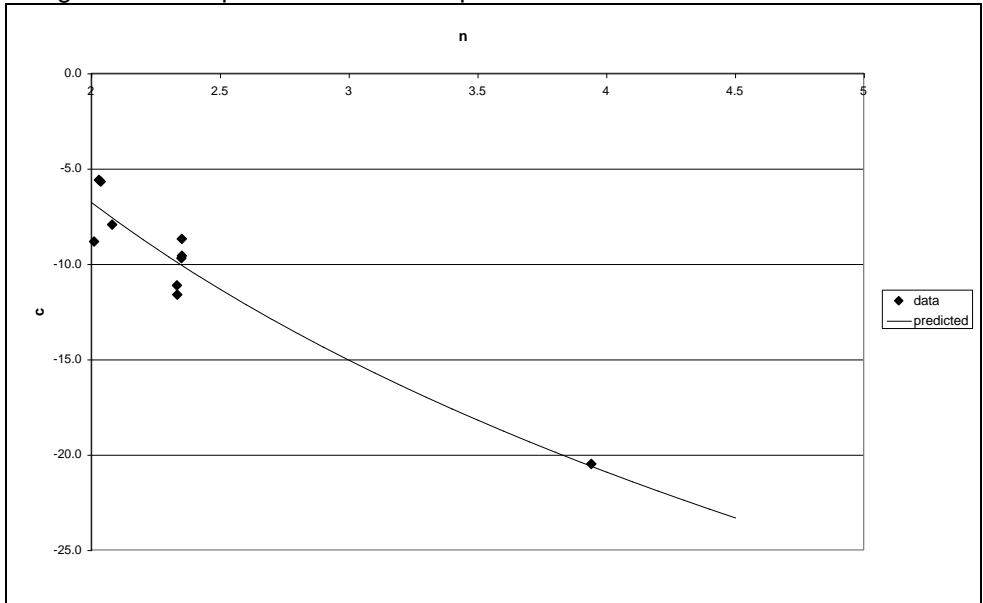


Figure 7.62: Relationship between c and n

It can be noted that the scatter for the equation between c and n is higher than for the equation between b and n. Additional analysis should be carried out to investigate for example a relation between c, strain rate and temperature instead of a straight relation between c and n.

Combination of the equations 7.44, 7.45 and 7.46 result in the following relationship between α and n:

$$\frac{\alpha}{\alpha_0} = \frac{1.0 + (7.375 - 20.368 \ln(n))\xi}{1 + (-38.713 + 7.139e^n)\xi}$$
 Equation 7.47

in which:

 α : hardening parameter

 $\begin{array}{ll} \alpha_0 & \text{ : the initial } \alpha \text{ value (material parameter)} \\ \text{n} & \text{ : parameter related to the onset of dilation} \end{array}$

ξ : the equivalent plastic strain

The precision of equation 7.47 is analysed in figures 7.63-7.68.

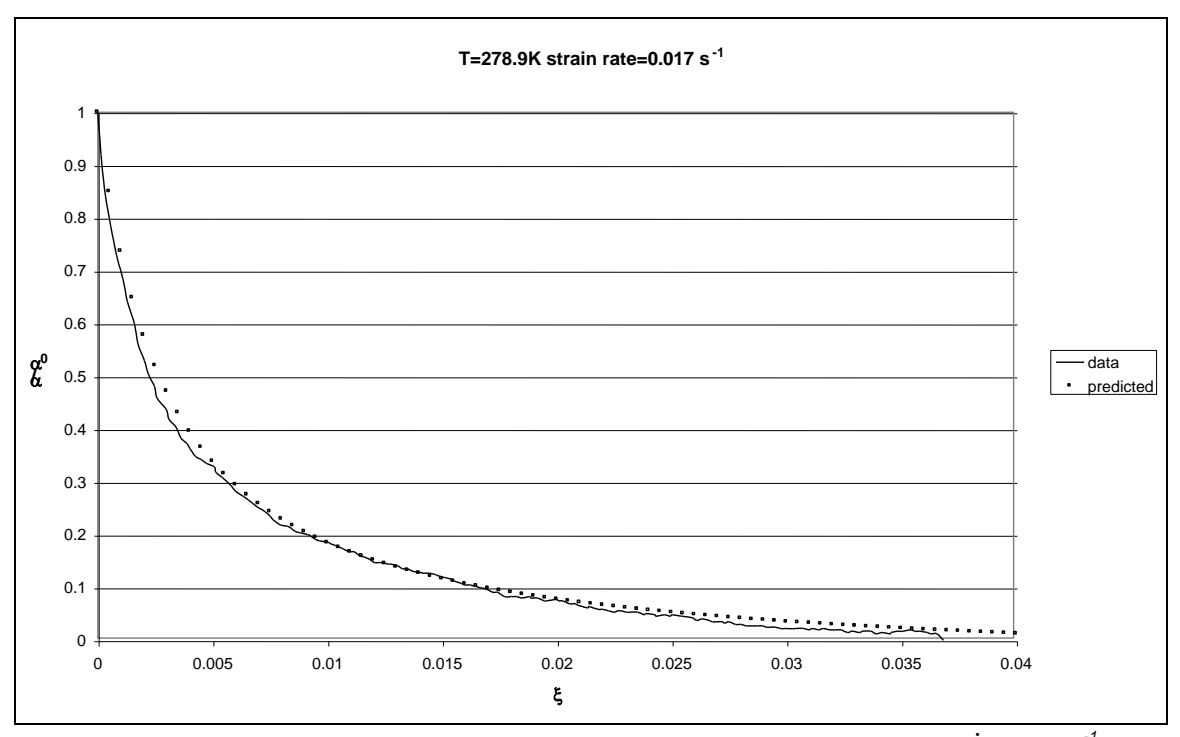


Figure 7.63: Precision of the predicted relationship between α/α_0 and ξ for T=278.9K and ε =0.017 s⁻¹

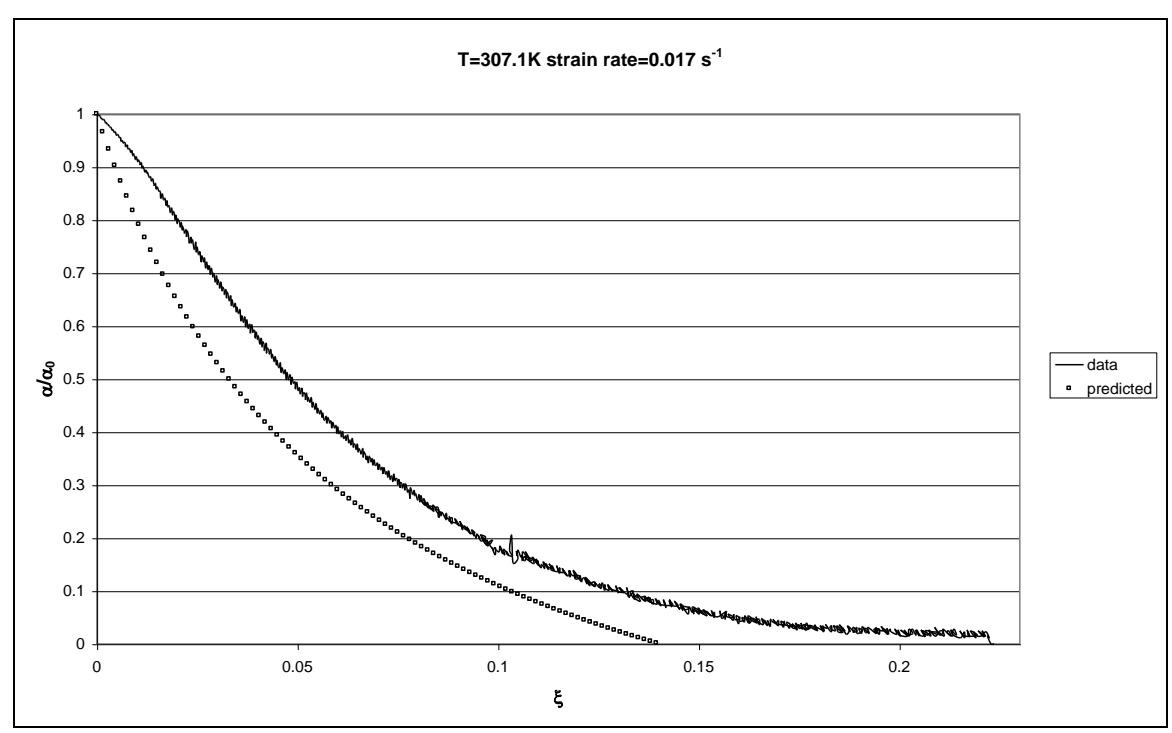


Figure 7.64: Precision of the predicted relationship between α/α_0 and ξ for T=307.1K and $\dot{\varepsilon}$ =0.017 s⁻¹

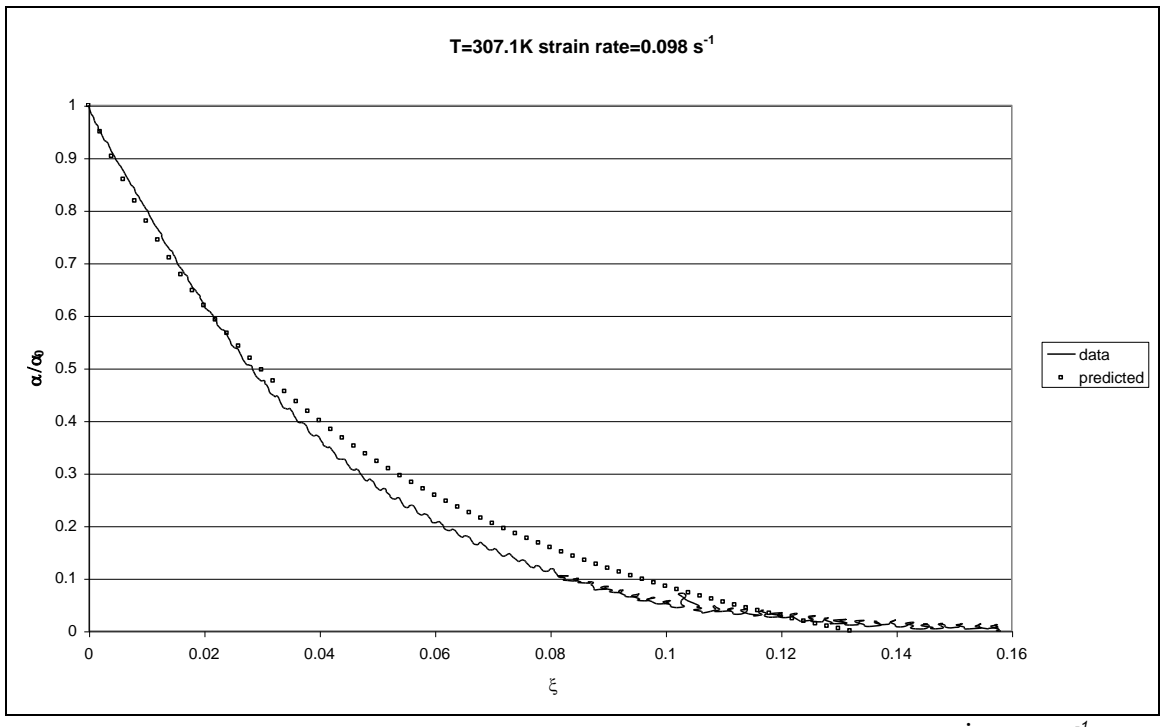


Figure 7.65: Precision of the predicted relationship between α/α_0 and ξ for T=307.1K and $\dot{\varepsilon}$ =0.098 s⁻¹

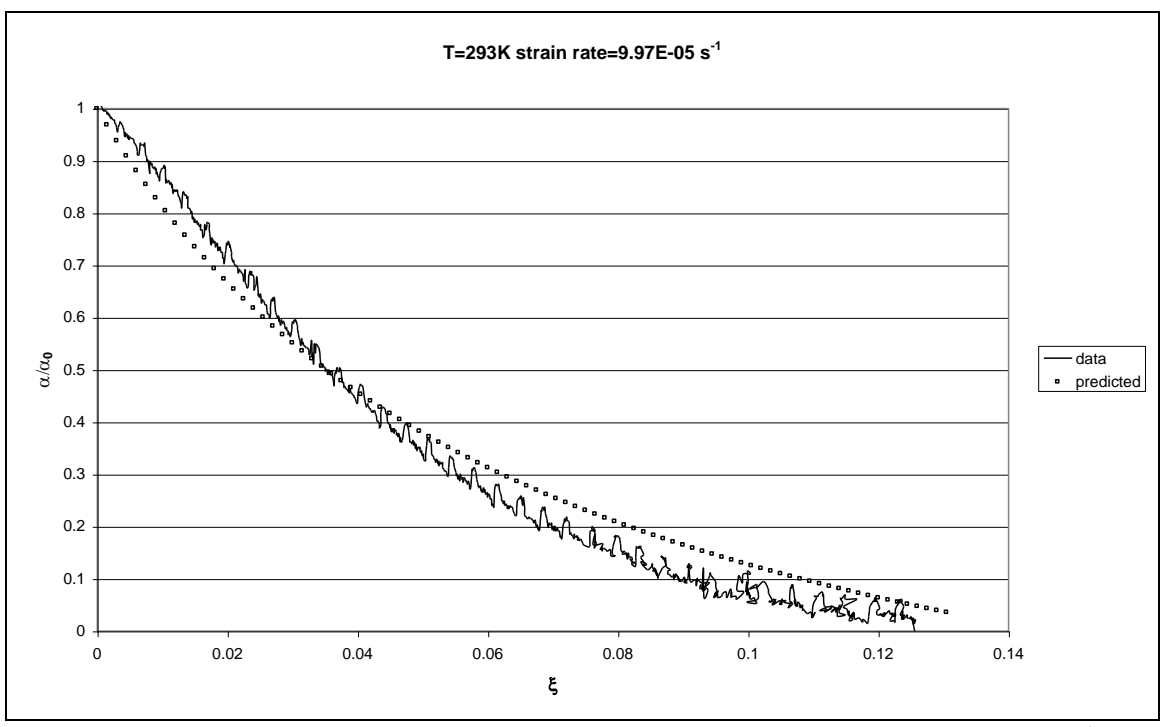


Figure 7.66: Precision of the predicted relationship between α/α_0 and ξ for T=293K and $\dot{\varepsilon}$ =9.97E-5 s⁻¹

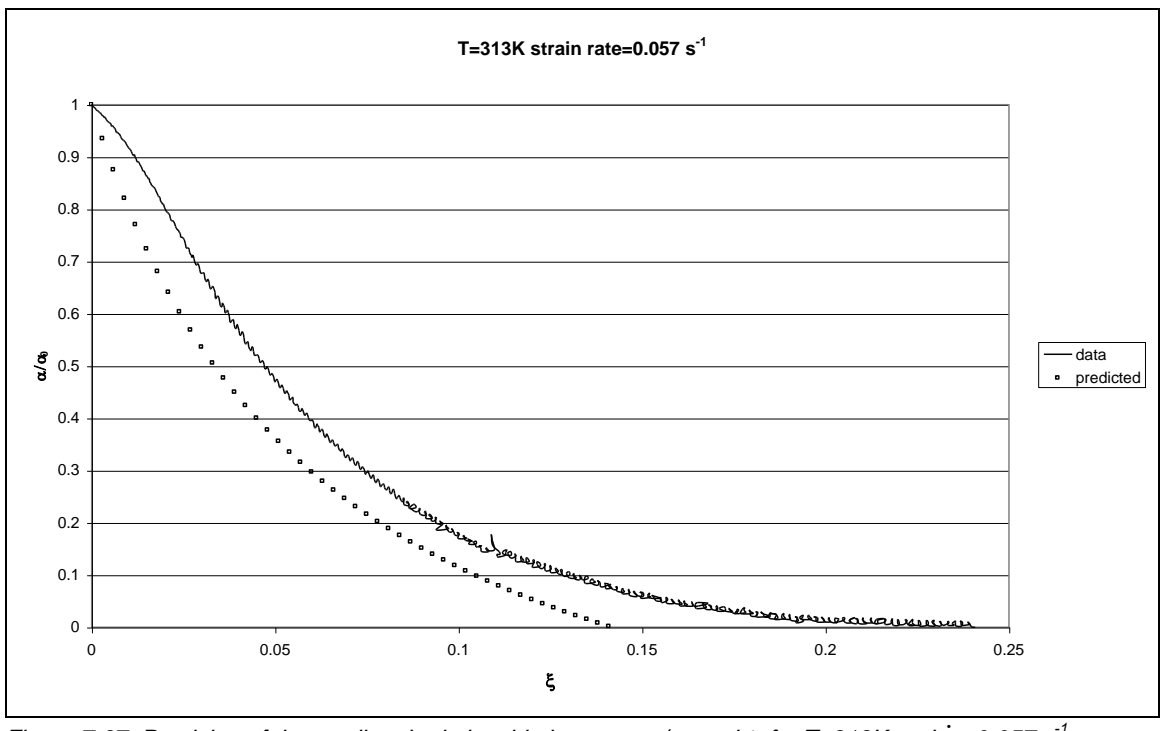


Figure 7.67: Precision of the predicted relationship between α/α_0 and ξ for T=313K and $\dot{\varepsilon}$ =0.057 s⁻¹

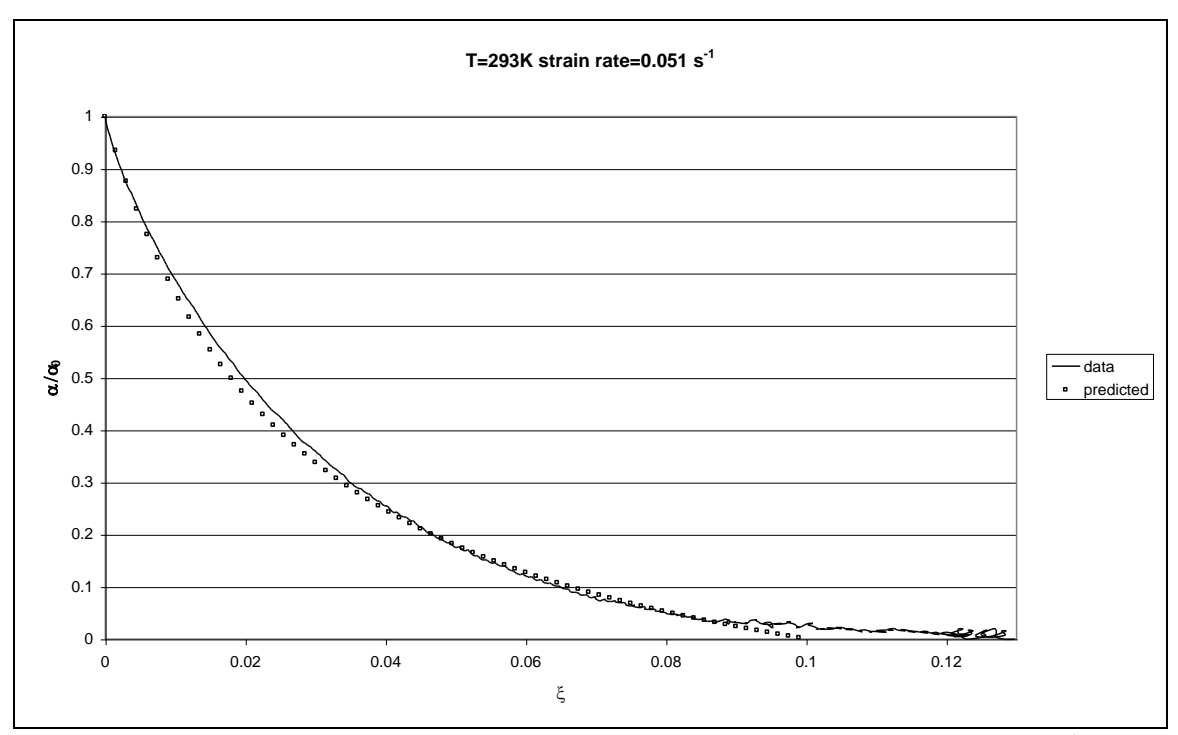


Figure 7.68: Precision of the predicted relationship between α/α_0 and ξ for T=293K and $\dot{\varepsilon}$ =0.051 s⁻¹

The prediction is reasonable for figures 7.63, 7.65, 7.66 and 7.68. The prediction in the figures 7.64 and 7.67 is not good. A closer look to these curves shows that both have a different trend in the relationship between the ratio α/α_0 and ξ . Both curves have a kind of S-shape, whereas the other curves have an exponential shape. These different shapes make the prediction of a relationship difficult. Therefore in paragraph 7.6.5.3 a different approach is used to determine a function for α .

7.6.5.3 Determination of α as a function of plastic work

A second way to describe α is expressing α as a function of plastic work W_p , which is defined as:

$$W_p = \int \sigma d\varepsilon_p$$
 Equation 7.48

in which:

W_p : plastic work σ : stress vector

 $d\varepsilon_p$: vector of the increment op plastic strain

Equation 7.48 shows that W_p is equal to the area under the stress-plastic strain curve. For the different measurements the relation between α/α_0 and W_p is plotted, as shown in figure 7.69. For the 5 measurements at T=293K and $\dot{\mathcal{E}}$ =0.051 s⁻¹ the average is taken.

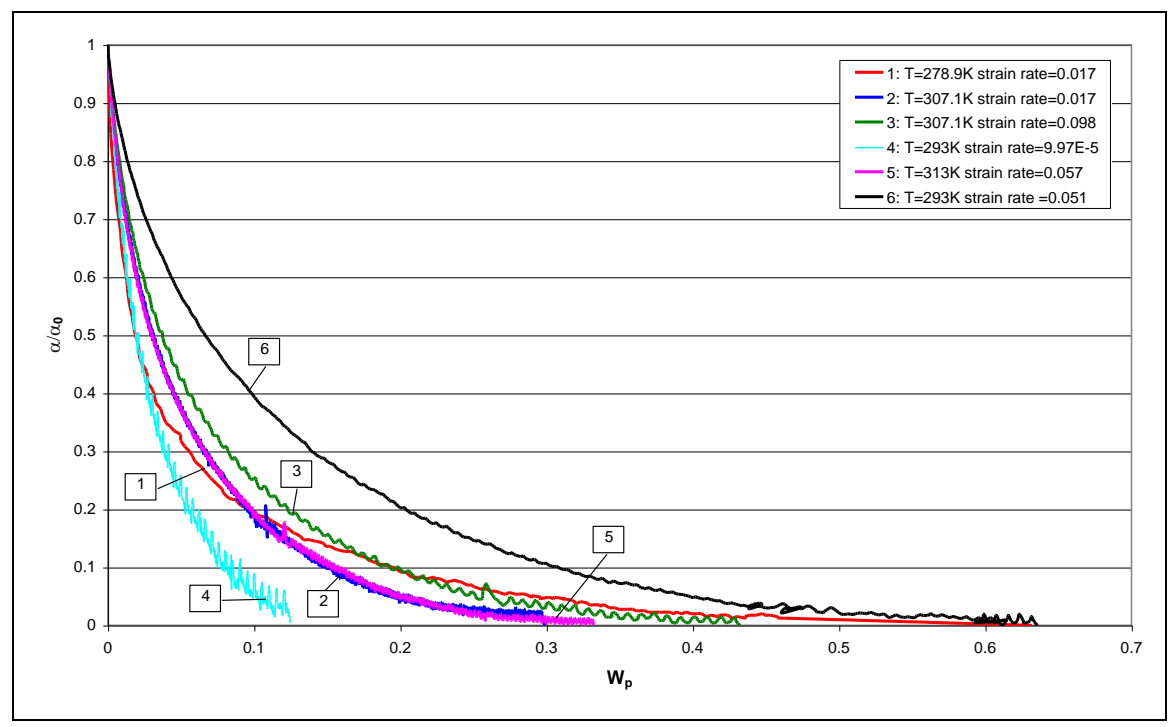


Figure 7.69: Relationship between α/α_0 and the plastic work W_p

In this case all the curves have the same shape, which makes the prediction of a relation easier. Analysis has shown that the curves could not be expressed in the form of a simple exponential equation. Therefore the following relationship is used to express α/α_0 as a function of W_p .

$$\alpha = \alpha_0 \frac{a + cW_p}{1 + bW_p}$$
 Equation 7.49

Table 7.31 shows the parameters that were determined by regression analysis for the different test conditions.

Table 7.31: Constants a, b and c for different strain rates and temperatures

strain rate [s ⁻¹]	T [K]	n	а	b	С
0.0168	278.9	3.942	0.9	34.9	-1.1
0.0170	307.1	2.038	1.0	24.6	-3.2
0.0978	307.1	2.082	1.0	19.9	-2.3
0.0001	293	2.012	1.0	36.1	-7.1
0.0568	313	2.031	1.0	25.0	-3.1
0.0513	293	2.345	1.0	10.2	-1.7

The constant a is chosen to be 1.0 since in that case $\alpha/\alpha 0$ becomes 0 at W_p=0. For b and c it is assumed that they are related to the parameter n, just like the parameter κ in equation 7.43. Next a relationship is determined between b and n. Figure 7.70 shows the relationship between b and n.

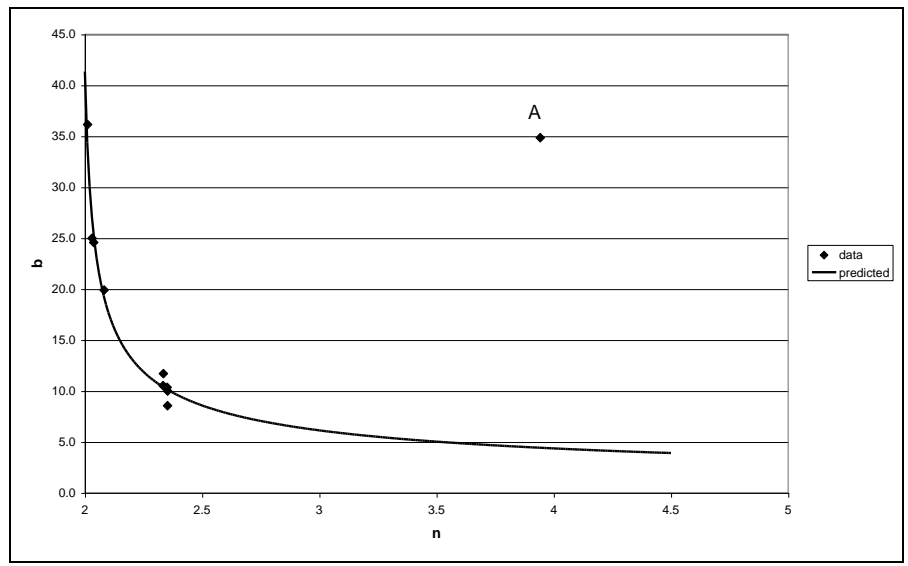


Figure 7.70: Predicted relationship between b and n

From this figure it becomes clear that point A seems to be an outlier. This point is related to the test at T=278.9K and a strain rate of $0.0168 \, \mathrm{s}^{-1}$. This point also gave problems in determining the relation for α_0 as a function of temperature and strain rate (hardly any hardening). A closer look to figure 7.69 shows that the line for these test conditions is different from the other test conditions, because it crosses the different lines. Because point A seems to be an outlier it is neglected in determining the relationship between b and a. For the model this means that for this condition there is no hardening response. The relationship between a0 and a1 becomes:

$$b = \sqrt{\frac{38.419}{n-1.978}}$$
 Equation 7.50

Figure 7.70 also shows the predicted relationship between b and n.

The same procedure is carried out to determine a relationship between c and n. This relationship is shown in figure 7.71.

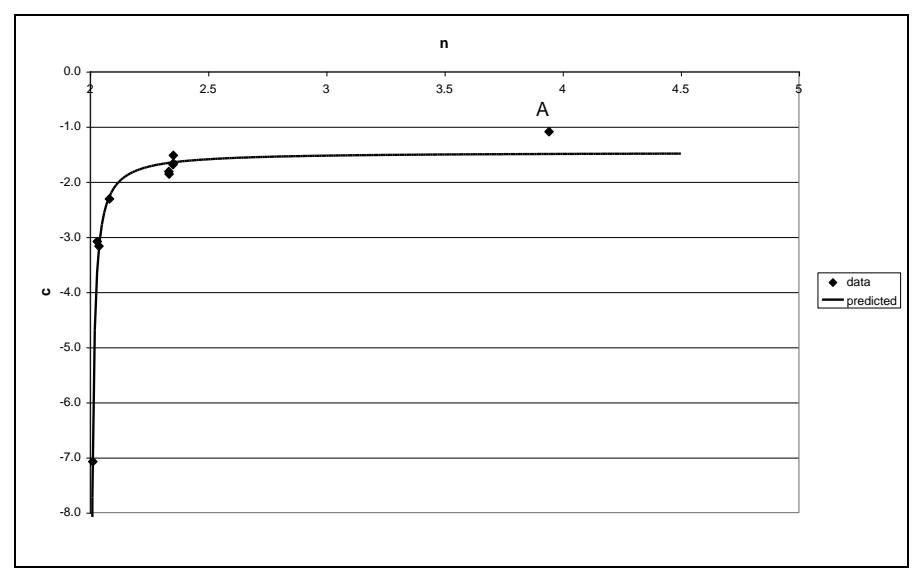


Figure 7.71: Predicted relationship between c and n

Again point A, which is related to the test conditions of T=278.9K and a strain rate of 0.0168 s⁻¹, is neglected, because it seems to be an outlier. The best relationship between c and n becomes:

$$c = \frac{\left(-1.405 + 0.368n^2\right)}{\left(1 - 0.250n^2\right)}$$
 Equation 7.51

Combination of equation 7.49, 7.50 and 7.51 results in the following relationship between α and $W_{\text{\tiny D}}$:

$$\alpha = \alpha_0 \frac{1 + \frac{\left(-1.405 + 0.368n^2\right)}{\left(1 - 0.250n^2\right)} W_p}{1 + \sqrt{\frac{38.419}{n - 1.978}} W_p}$$
 Equation 7.52

With equation 7.52 the lines in figure 7.69 are predicted, except for the line for T=278.9K and a strain rate of 0.0168 s⁻¹. This test was namely neglected in the determination of b and c as a function of n. The predicted lines as well as the original lines are shown in figures 7.72-7.76.

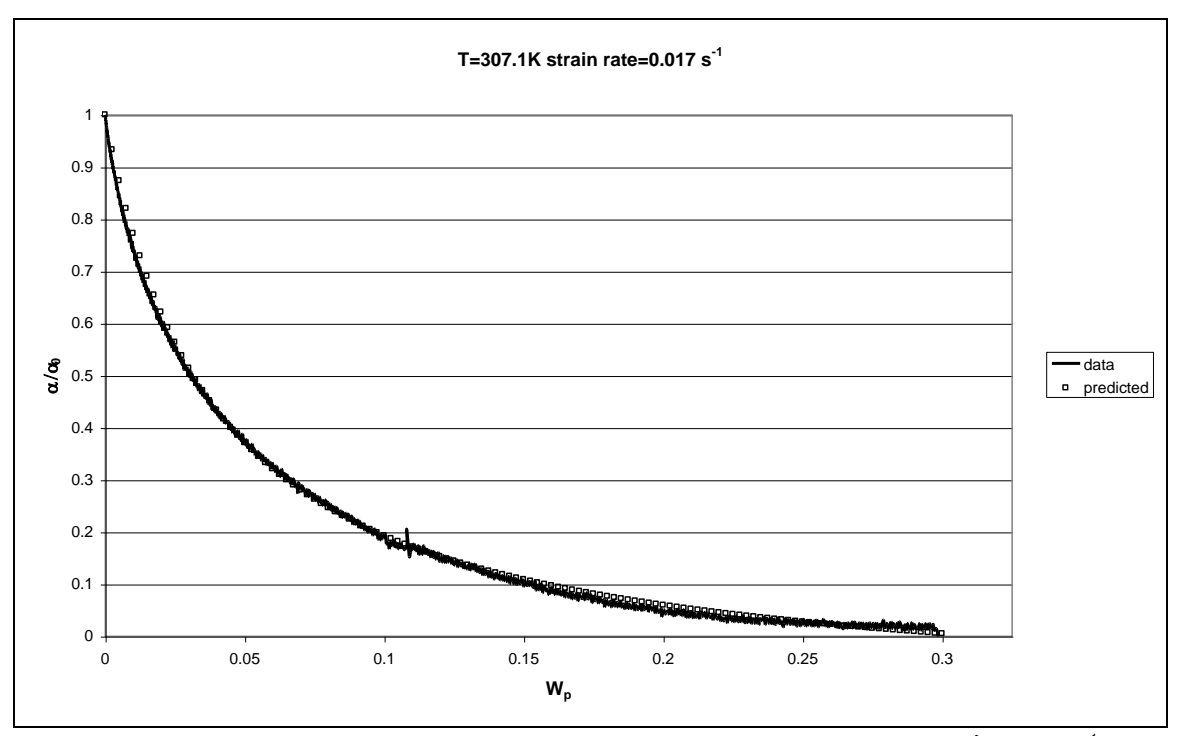


Figure 7.72: Precision of the predicted relationship between α/α_0 and ξ for T=307.1K and $\dot{\varepsilon}$ =0.017 s⁻¹

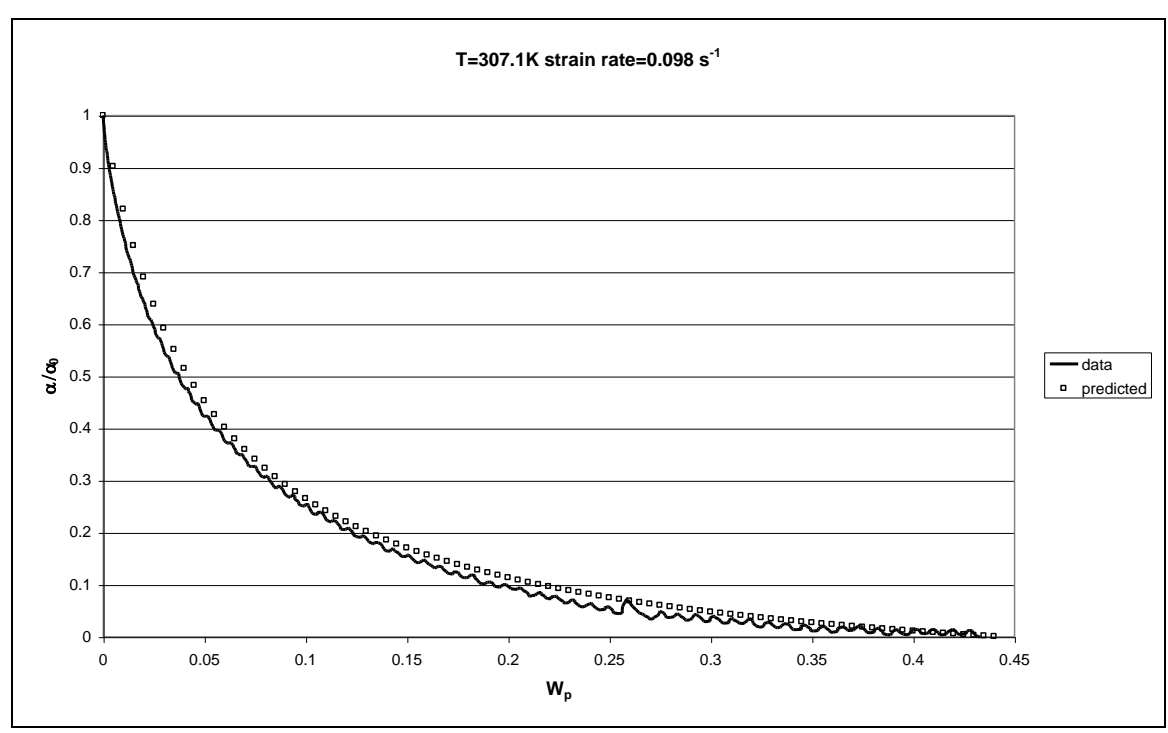


Figure 7.73: Precision of the predicted relationship between α/α_0 and ξ for T=307.1K and $\dot{\varepsilon}$ =0.098 s⁻¹

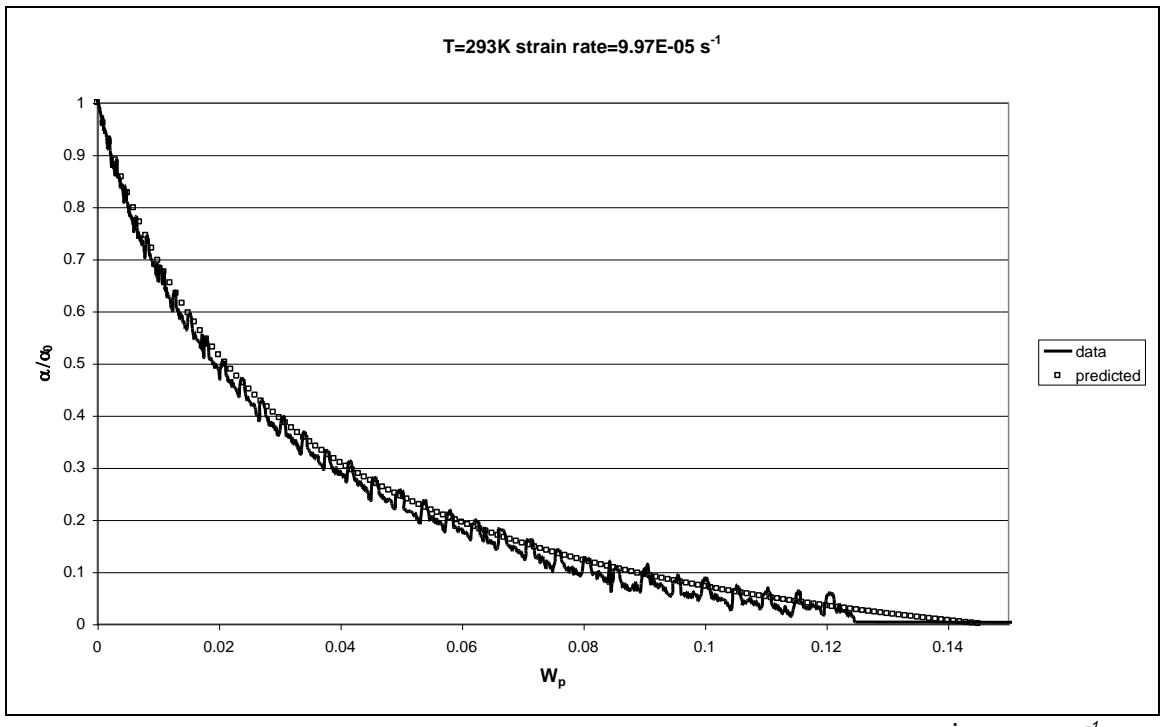


Figure 7.74: Precision of the predicted relationship between α/α_0 and ξ for T=293K and $\dot{\varepsilon}$ =9.97E-5 s⁻¹

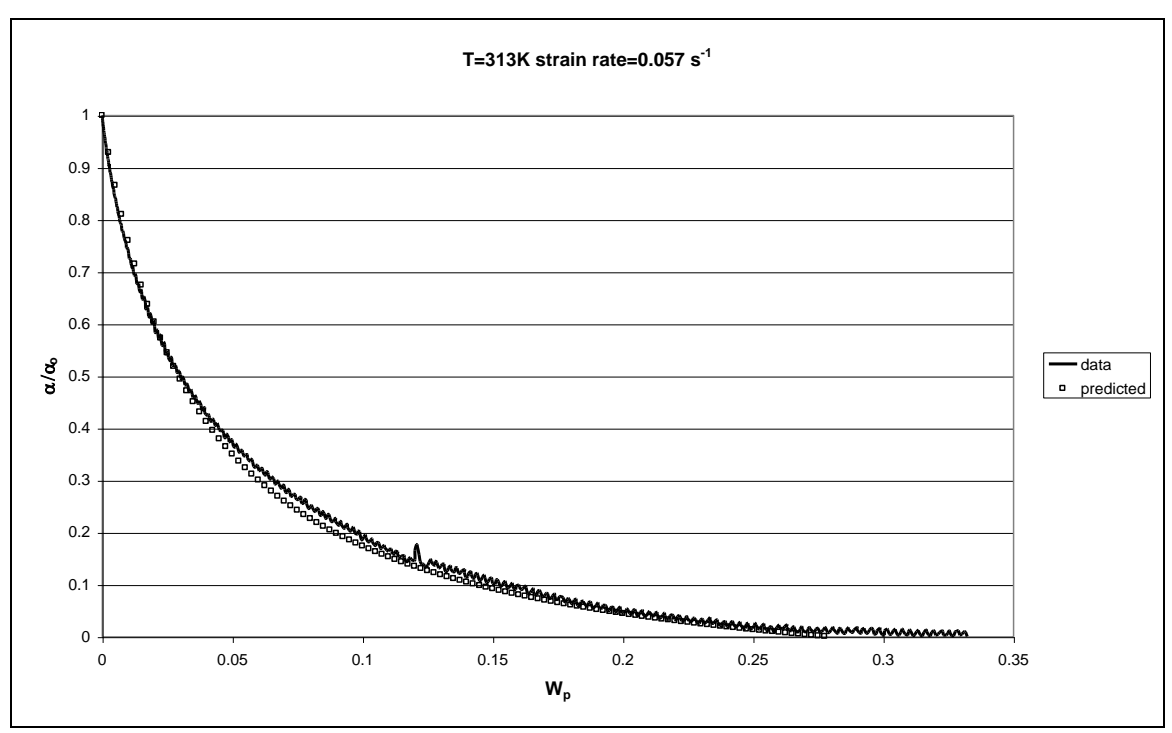


Figure 7.75: Precision of the predicted relationship between α/α_0 and ξ for T=313K and $\dot{\varepsilon}$ =0.057 s⁻¹

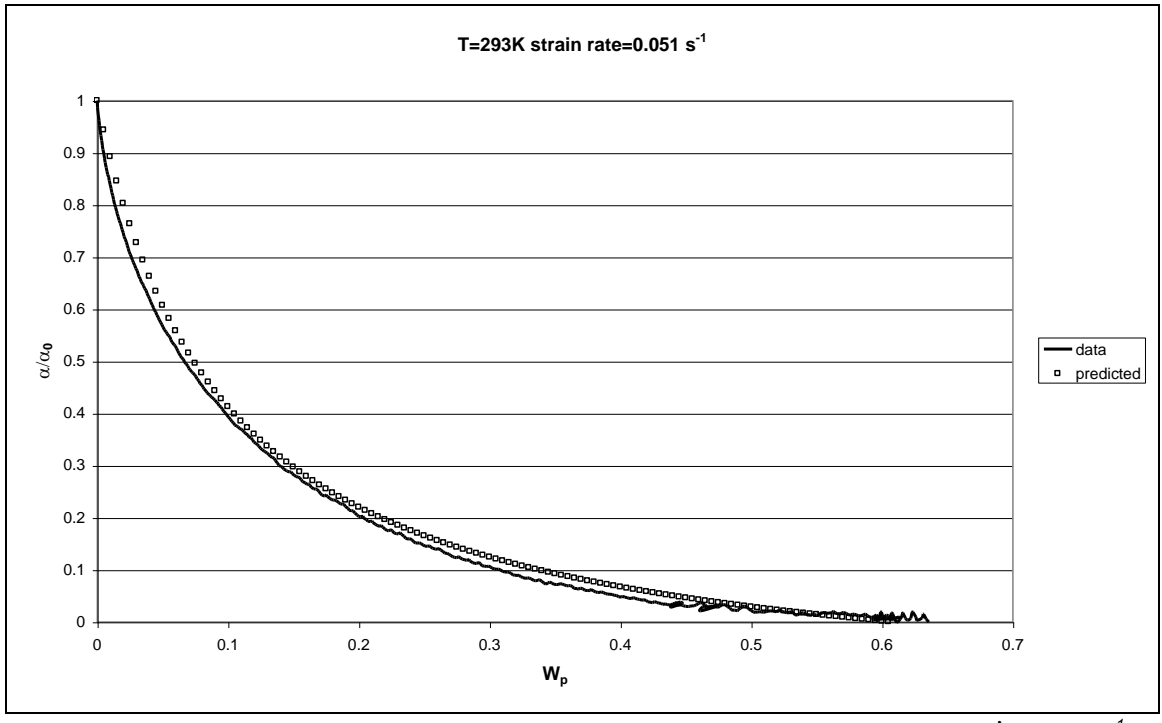


Figure 7.76: Precision of the predicted relationship between α/α_0 and ξ for T=293K and $\dot{\varepsilon}$ =0.051 s⁻¹

The prediction of the relationship between α/α_0 and W_p is good in all the figures. However, one has to keep in mind that one measurement has been neglected in the previous analysis.

7.6.6 The influence of the model parameters on the response surface

7.6.6.1 Effect of temperature on the response surface

Two cases have been considered, namely α = α_0 (figure 7.77) and α =0 (figure 7.78). The situation α = α_0 represents the change from linear-elastic to plastic behaviour. Furthermore, α =0 figure 7.78 represents the ultimate response surface.

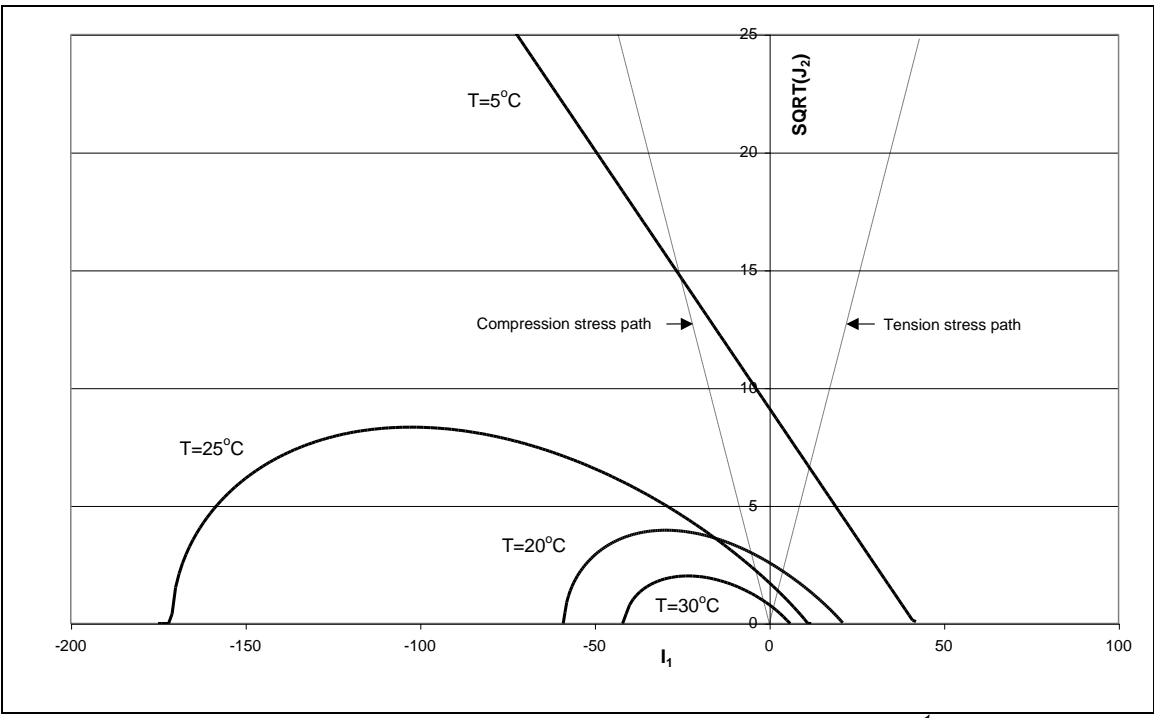


Figure 7.77: Effect of temperature on the flow-surface for a strain rate of 0.1 s⁻¹ and $\alpha = \alpha_0$

The influence of temperature on the linear elastic part becomes clear from figure 7.77. With decreasing temperature the linear-elastic part increases. The straight line for $T=5^{\circ}C$ shows that for low temperatures $\alpha_0 \cong 0$, meaning that no hardening occurs. Figure 7.78 shows the flow-surfaces for different temperatures for $\alpha=0$.

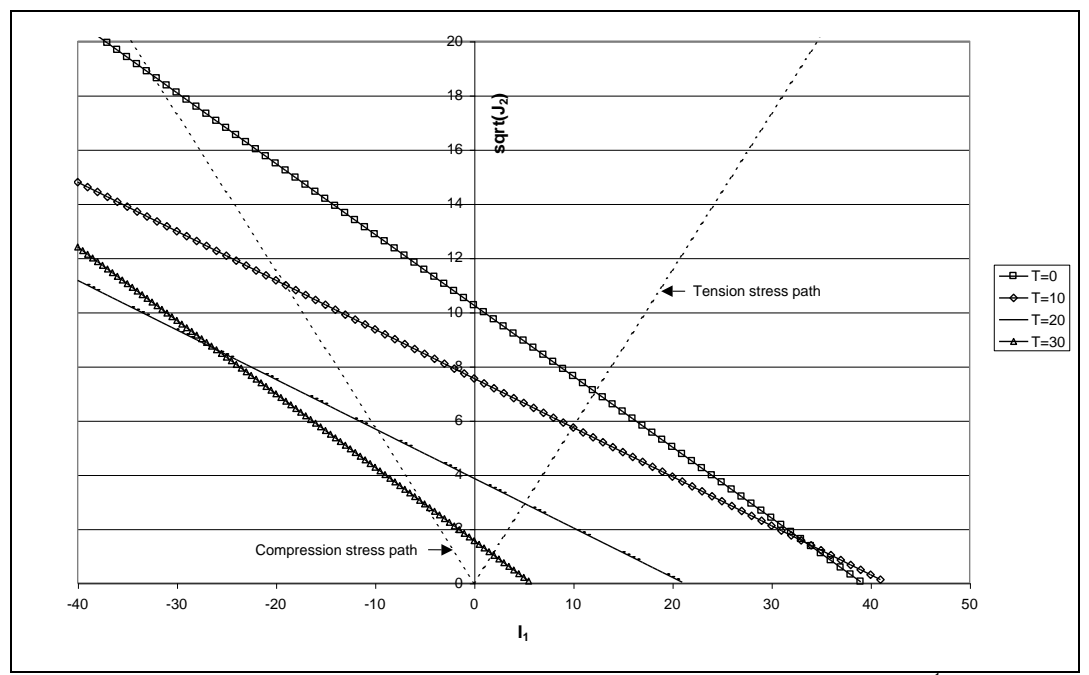


Figure 7.78: Effect of temperature on the flow-surface for a strain rate of 0.1 s⁻¹ and α =0

In figure 7.78 the intersections between both stress paths and the flow surfaces represent the tension and the compression strength for the specific temperature. As expected, both the tension and compression strength increase for decreasing temperature.

7.6.6.2 Effect of strain rate on the response surface

Figure 7.79 shows the influence of the strain rate on the flow-surface for $\alpha = \alpha_0$ and T=20°C. The situation $\alpha = \alpha_0$ represents the change from linear-elastic into plastic behaviour.

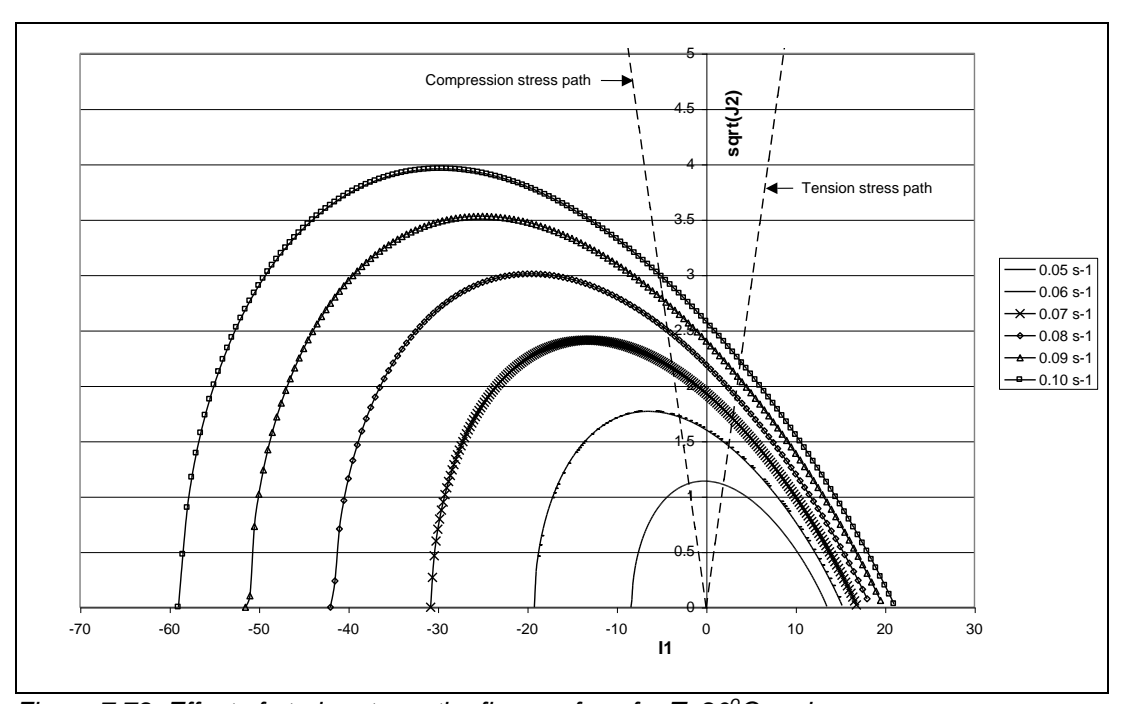


Figure 7.79: Effect of strain rate on the flow-surface for T=20°C and α = α_0

By following the stress paths for tension and compression the influence of strain rate becomes clear. An increasing strain rate means an increasing linear-elastic part, as to be expected. Figure 7.80 shows the influence of the strain rate on the flow surface at $T=20^{\circ}C$ and $\alpha=0$, i.e. the influence of the strain rate on the tension and compression strength of the material.

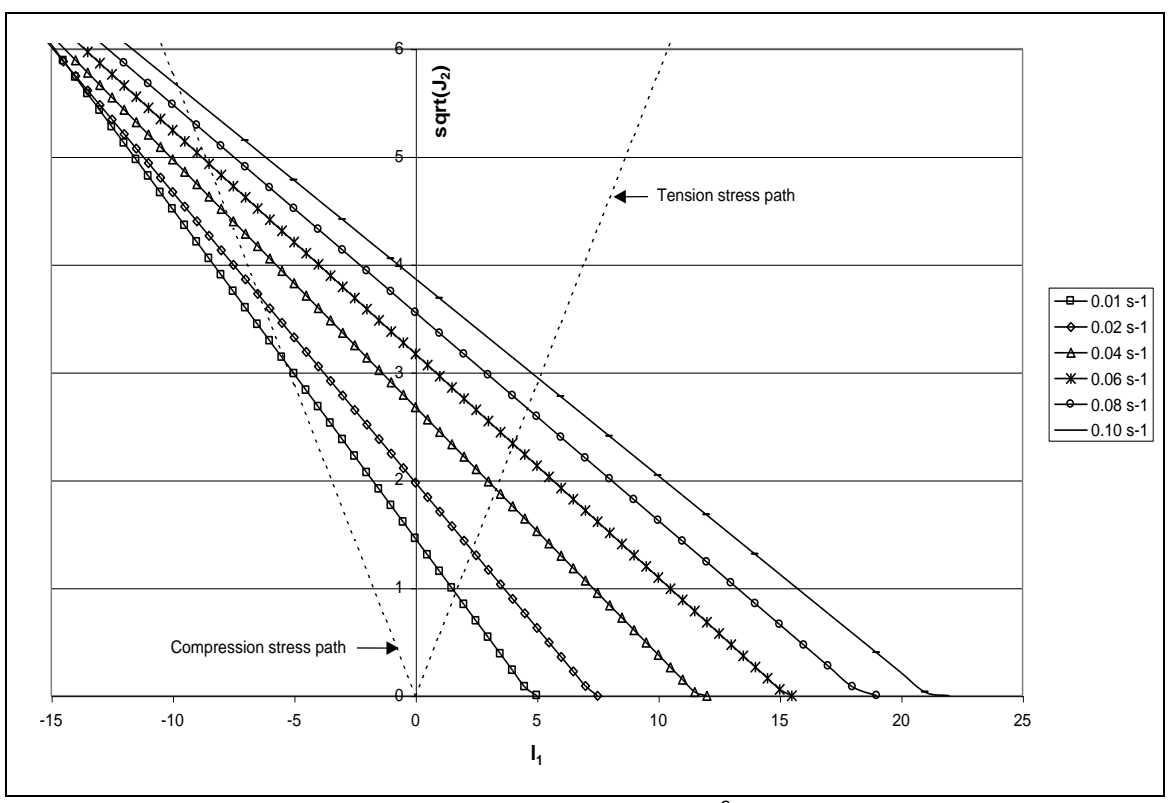


Figure 7.80: Effect of strain rate on the flow-surface for T=20 $^{\circ}$ C and α =0

Again the intersection point between both stress paths and the flow-surfaces represent the tension and the compression strength for the specific strain rate. From figure 7.80 it becomes clear that with increasing strain rate both the tension and compression strength increase.

7.6.6.3 Effect of α on the response surface

Finally the effect of α on the flow surface is investigated for T=20°C and strain rate of 0.05 s⁻¹. For α =0.0076, 0.005, 0025 and 0 the flow surfaces are plotted in figure 7.81. The value α =0.0076 represents the start of the hardening phase and for α =0 the tension and compression strength has been reached.

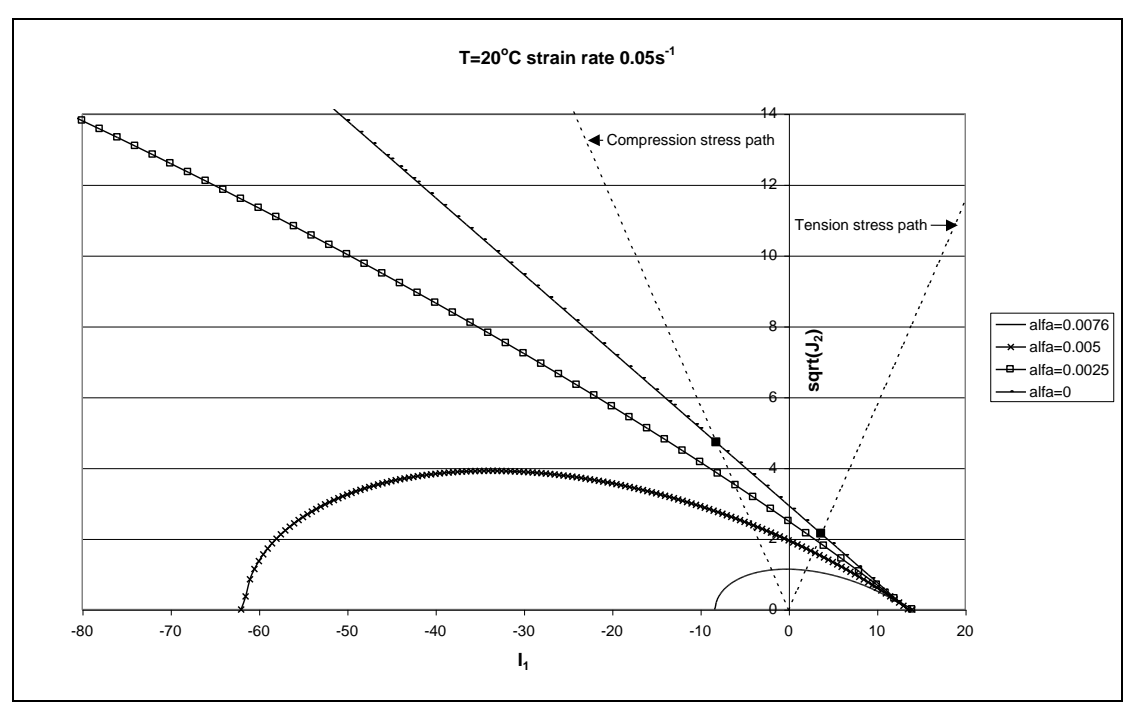


Figure 7.81: Flow surface for a decreasing value of α

As expected the flow surface increases for decreasing value of α . At the moment α becomes equal to zero the flow surface reduces to a straight line (ultimate response). The tension and compression strength of the material has been reached.

It should be noted here that only strain rates higher than 0.05 s⁻¹ are shown in figures 7.77-7.81. This is because the determination of the flow surfaces for α = α ₀ is impossible for the lower strain rates. In that case J₂ becomes negative for all the values of I₁ and the square root of J₂ can not be calculated. Mathematically this means the following: J₂ is calculated with equation 7.53:

$$J_2 = p_a^2 \left[-\alpha_0 \left(\frac{I_1 - R}{p_a} \right)^n + \gamma \left(\frac{I_1 - R}{p_a} \right)^2 \right]$$
 Equation 7.53

To avoid that J_2 becomes negative the following condition has to be valid:

$$\alpha_0 \le \gamma \left(\frac{I_1 - R}{p_a}\right)^{2-n}$$
 Equation 7.54

The problems are caused by the fact that the prediction of α_0 at low strain levels is too high. This is a pure mathematical point of view, physically equation 7.39 seems good to predict α_0 . The expected trend of a decreasing α_0 for increasing strain rate and decreasing temperature is clearly shown in figure 7.52.

Physically the problems at lower strain rates may be attributed to the fact that there is hardly any elastic response, meaning that the material starts to flow immediately. For the model this means that α has to decrease until the condition in equation 7.54 is valid.

8 Case study Moerdijk bridge

8.1 Introduction

The lifetime of mastic asphalt on orthotropic steel bridges is short compared to the lifetime of asphalt mixtures on road pavements. For example the asphalt on the Hagestein bridge had to be replaced after only 5 years, for the Ewijk bridges the lifetime has been even shorter, namely 3 respectively 4 years. On the Moerdijk bridge a new asphalt surface had been applied in June 2000, which contains a new type of SBS modified bitumen. In this case study an attempt is made to predict the lifetime of the Moerdijk mix by using the experimental results described in this report. It has to be noted that several factors influence the lifetime of asphaltic mixes. Some of them are neglected over here because their influence is simply not clear. Also some assumptions were made.

8.2 Traffic loading

For the traffic distribution use is made from measurements carried out on the Moerdijk bridge in 1999. From this traffic distribution the number of 100 kN equivalent axles per year is determined. The following data was used:

Estimated total number of truck axles per day: 35000 Working days per year: 275 n (slope of the fatigue line): 6.74

The n-value that is used to calculate the number of 100 kN equivalent axle loads is the real n-value obtained from the fatigue line of the Moerdijk mix for a temperature of 10°C and a frequency of 5 Hz.

Table 8.1 shows the traffic loading for the Moerdijk bridge, as well as the number of 100 kN equivalent axle loads.

Table 8.1: Traffic loading and number of 100kN equivalent axle loads

axle load [kN]	percentage [%]	axles per day	100 kN equivalent axles per day
10	4.5	1575	0
30	21.01	7354	2
50	29.58	10353	97
70	27.07	9475	857
90	10.92	3822	1880
110	5.24	1834	3485
130	1.44	504	2951
150	0.22	77	1182
170	0.02	7	250
Number of 100 kN equivalent axles per day:			10704
Number of 100 kN equivalent axles per year:			2943706

Combining this information with the experimental fatigue relation results in a prediction for the fatigue lifetime. However, this lifetime is the experimental lifetime and the lifetime in practice is longer due to healing of the asphalt and lateral wandering of the traffic. The lifetime in practice is calculated with:

$$N_{field} = N_{\text{experimental}} \times H \times LW$$
 Equation 8.1

in which:

 N_{field} : Predicted number of load repetitions in practice.

 $N_{\text{experimental}}$: Predicted number of load repetitions from the fatigue relation.

H : Healing factor.

LW : Factor for lateral wandering of the traffic.

8.3 Healing

Healing can be defined as the self-restoring capacity of the mix. This means that a mix can sustain more load repetitions if rest periods are introduced during cyclic loading. Healing is highly dependent on the bitumen content of a mix, the degree of filling and the hardness of the bitumen. An increasing bitumen content tends to increase the healing capacity of the mix. The Dutch Ministry of Transport, Public Works and Water Management uses a healing factor of 4 for standard asphalt concrete mixes in fatigue lifetime predictions. Molenaar [1993] developed a relationship between the bitumen content, void content and the healing factor, shown in figure 8.1.

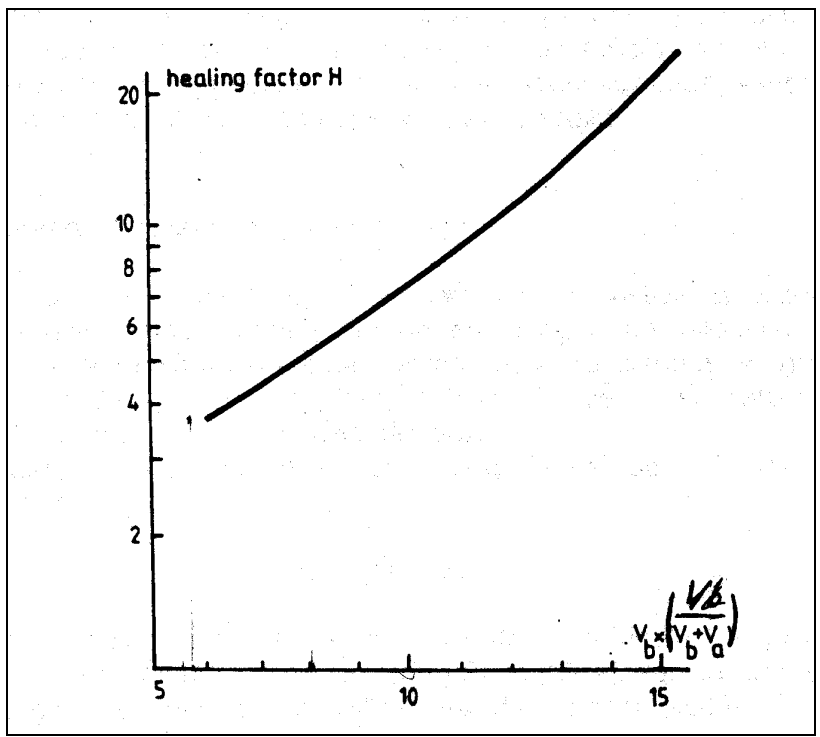


Figure 8.1: Relation between bitumen content an the healing factor

With a bitumen content of 18.5% by volume and a void content of 2% the healing factor is approximately 20, which is 5 times the healing factor that the Dutch Ministry of Transport, Public Works and Water Management uses. This high healing factor is to be expected for mastic asphalt since the bitumen content is very high compared to other types of asphalt mixes. Also during the experimental program that was carried out, the effect of healing has been observed. After a rest period of 2.5 months the stiffness of the tested specimens has increased again to values approaching the original stiffness values. The increase of the stiffness can be attributed to the healing capacity of the mix.

8.4 Lateral wander

In practice not all the wheels will pass exactly at the same lateral position. Instead the wheel positions of vehicles will be transversely distributed over the pavement, which is called 'lateral wander'. The factor for traffic wander is highly dependent on the width of the traffic lane. For traffic lanes of 3.6 m, a lateral wander factor of 2.5 is proposed by the Dutch Ministry of Transport, Public Works and Water Management. On an orthotropic bridge this factor might be different, since the pavement structure on a subgrade is essentially different from that on an orthotropic bridge, which leads to different strain conditions in the pavement. To investigate the lateral wander factor on an orthotropic bridge a 10-span beam model was used (figure 8.2).

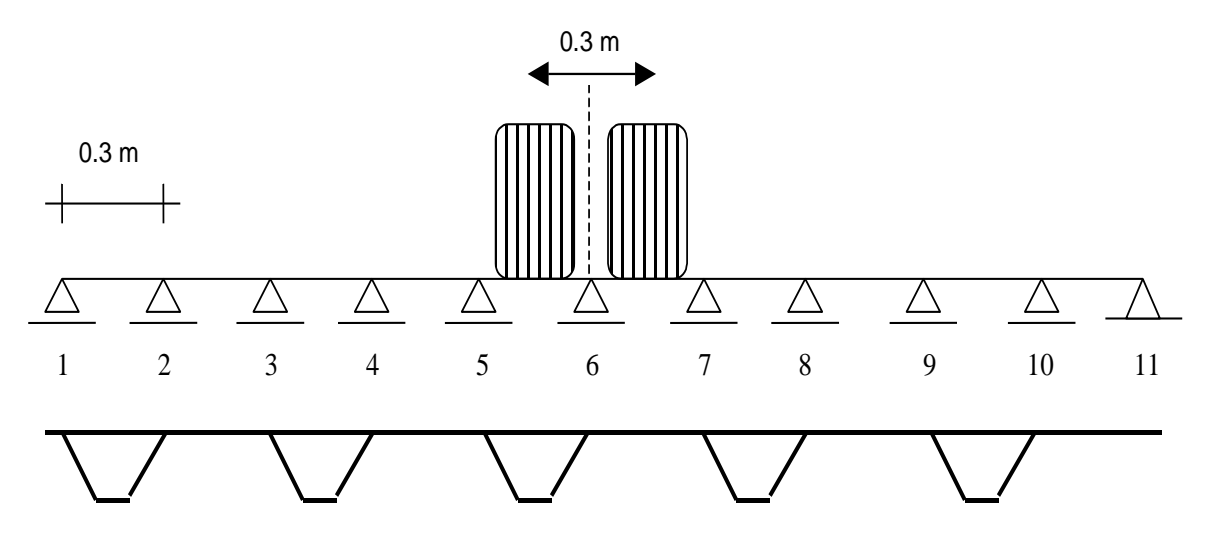


Figure 8.2: Beam model to investigate the effect of traffic wander

Each span of the beam is 0.3 m, which corresponds to the width of the stiffener and also the distance between the troughs. The width of the beam is taken as 0.1 mm. The structure consists of a 10 mm steel plate and a 50 mm thick asphalt layer on top. The dual tyre wheel is schematised as two line loads of 0.7 N/mm/mm, with a length of 190 mm. This corresponds to an axle load of 100 kN.

For the traffic wander a Gaussian distribution is used with σ =0.29 m. The distribution is truncated at 0.80 m on either side of the centre line, which results in a trafficked width of 1.60 m. This traffic loading was also used for the Lintrack control program [Groenendijk, 1998]. Figure 8.3 shows the traffic distribution when the Gaussian distribution is divided in steps of 0.1 m.

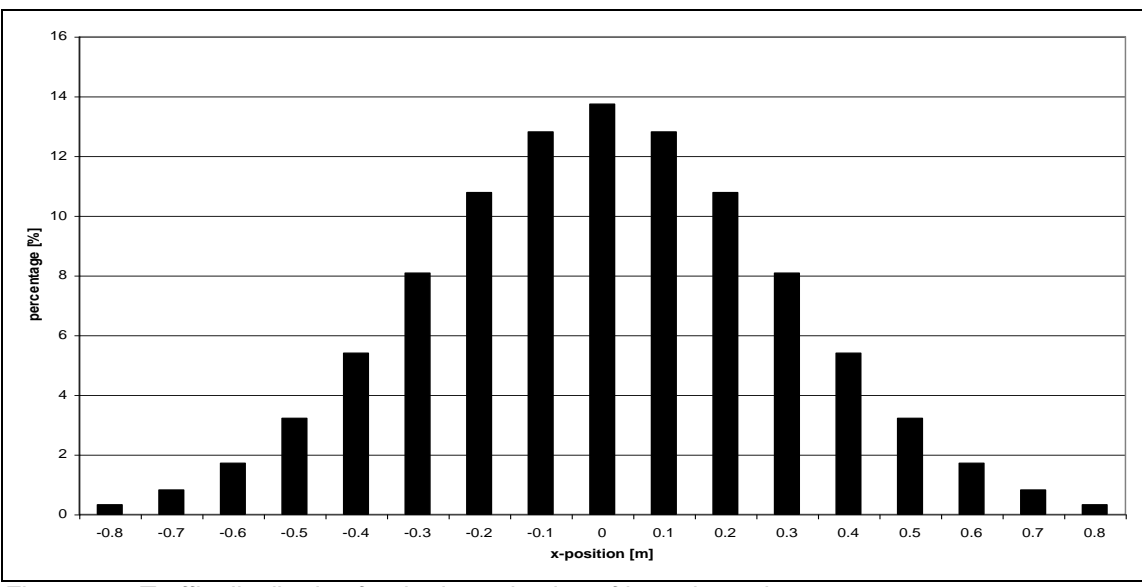


Figure 8.3: Traffic distribution for the investigation of lateral wander

The average position of the centre of the dual tyre wheel is chosen to be above support number 6. Next the effect of shifting the centre of the dual tyre load on the bending moment above support 6 is determined by using Metcalf's linear-elastic theory (see paragraph 3.3.2.1). Therefore the load is shifted in steps of 0.1 m to both the left and the right side of support 6, with a maximum of 0.8 m. Figure 8.4 shows the relation between the position of the centre of the dual tyre wheel and the bending moment at support 6 for an axle load of 100 kN.

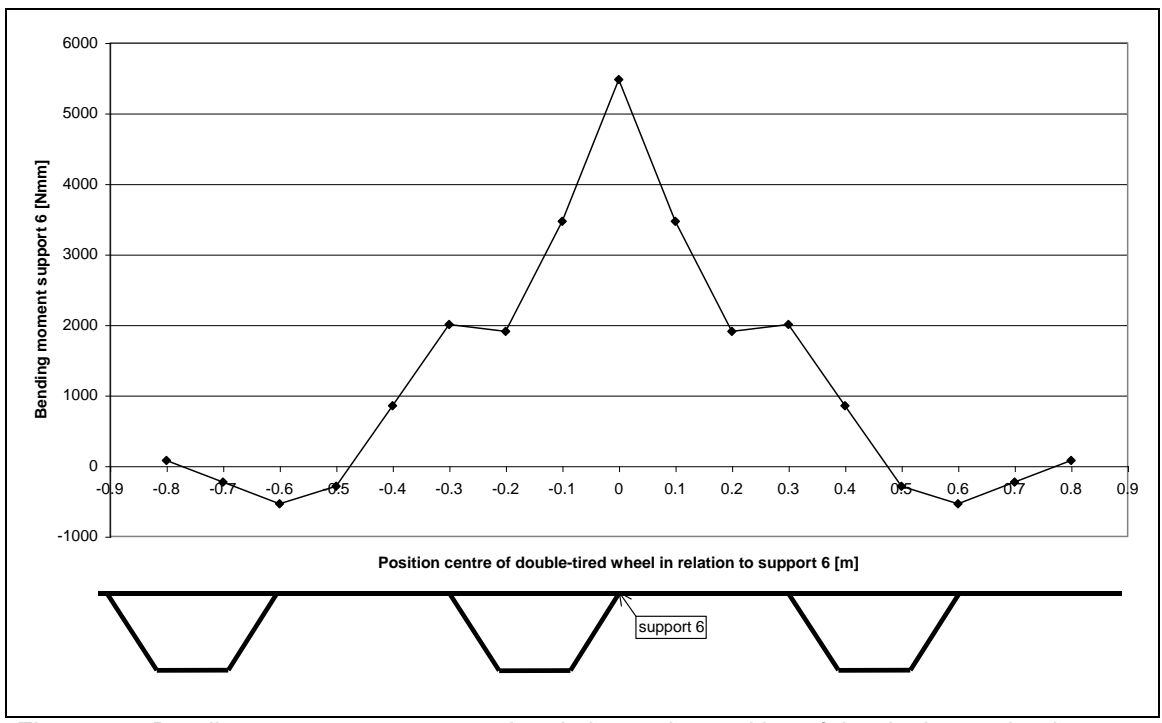


Figure 8.4: Bending moment at support 6 in relation to the position of the dual tyre wheel

This figure clearly shows that by shifting the load the bending moment above support 6 increases. When the dual tyre wheel is shifted over a distance of ≈0.5-0.8 m the bending moment becomes negative, meaning a compression strain at the top of the asphalt above support 6.

The positive effect of traffic wander on the fatigue life is shown in table 8.2, in which the factor for lateral wander is calculated. This lateral wander factor is dependent on the slope of the fatigue relation, thus in this case the factor is valid for a temperature of 10°C and a frequency of 5 Hz. The factor will decrease for increasing temperatures. When use is made of the n-value of 4 proposed by Rijkswaterstaat the factor LW decreases to 5.4.

Table 8.2: Calculation of the factor for lateral wander for T=10°C and f=5 Hz

		Bending moment		100kN
distance to supp. 6	traffic [%]	support 6 [Nmm]	axle load supp. 6 [kN]	axles [-]
-0.8	0.3	77	1.41	1.10E-15
-0.7	0.8	-229	-	-
-0.6	1.7	-537	-	-
-0.5	3.2	-288	-	-
-0.4	5.4	854	15.59	1.97E-07
-0.3	8.1	2005	36.61	9.28E-05
-0.2	10.8	1908	34.83	8.84E-05
-0.1	12.8	3468	63.30	5.89E-03
0	13.7	5478	100.00	1.37E-01
0.1	12.8	3468	63.30	5.89E-03
0.2	10.8	1908	34.83	8.84E-05
0.3	8.1	2005	36.61	9.28E-05
0.4	5.4	854	15.59	1.97E-07
0.5	3.2	-288	-	-
0.6	1.7	-537	-	-
0.7	0.8	-229	-	-
0.8	0.3	77	1.41	1.10E-15
	·		wander effect:	0.14953
			LW:	6.7

It has to be noted that is assumed that 100% of the axles consist of dual tyre wheels and that the average position of the centre of the dual tyre wheel is exactly above a support.

8.5 Shifting the traffic lanes

In the previous sections it has been shown that both healing and lateral wander play an important role in increasing the lifespan of mastic asphalt. Both effects may be increasing when the traffic lanes are shifted on the bridge for a certain period during a year. When the traffic lanes are shifted in the right way this will lead to release of strains. It will also result in extra rest periods for the heaviest loaded part, which results in better healing of the asphalt. Specially on bridges with heavy traffic this may play an important role, since in that case very little rest periods are available to heal the material.

To estimate a reasonable shift distance for the traffic lanes the total width of a bridge is considered. The most critical part is the right lane, which is used by most of the heavy trucks. Switching the left and the right lanes might be an option, however, this might lead to chaotic situations for the traffic that has to change lanes before and after the bridge.

A better shift distance is obtained when use is made of figure 8.4, which shows the effect of shifting a dual tyre wheel. Shifting this dual tyre wheel over more than 1.0 m is not useful, since in that case the second dual tyre wheel on the axle starts to load the asphalt above support 6. Reckoning with this fact, figure 8.4 shows that the best distance to shift the lane lies between 0.5 and 1.0 m, since in that case a large part of the load causes a negative or very small bending

5000
4000
2000
1000
2000
1000
Distance between centre load and support 6 [m]

moment above support 6. From figure 8.5 it becomes clear that the best distance to shift the traffic lane is 1.0 m.

Figure 8.5: The effect of shifting the traffic lane over 1.0 m.

In that case the largest percentage (96%) of the traffic distribution (figure 8.3) causes a compressive or negligible tensile strain above support 6. This means that due to the shift of the lane over 1.0 m the asphalt above the critical point is hardly loaded for a certain time, which has two supplementary effects. Firstly, the total number of load repetitions will increase because the critical point (above support 6) is less loaded. Secondly, the material will have some time to heal, which has also a positive effect on increasing the total number of load repetitions to failure. The application of shifting traffic depends of coarse on the geometry of the bridge.

- bending moment above support 6

8.6 Prediction of the fatigue lifetime by neglecting the strain dependency of the mix stiffness

8.6.1 Prediction of the fatigue lifetime for the Moerdijk mix using common method for T=10°C and f=5 Hz

In this section the lifetime is predicted in a way that is commonly used for road engineering. For this procedure the experimental fatigue line as well as Metcalf's theory were used.

Three following phenomena were neglected:

- Strain dependent behaviour of the mix stiffness.
- Temperature distribution during the year.

In this case Metcalf's composite action theory was used and the following assumptions were made:

- 100% bonding between the steel and the asphalt.
- Linear-elastic relation between load and strain.

For the calculation of the bending moment the same 10-span beam that has been used for calculation of the lateral wander (figure 8.2) was used. By using that model the bending moment above the middle support due to an axle load of 100 kN is 5478 Nmm. This bending moment is overestimated because the beam-theory is assumed, while in reality plate-theory is more applicable. It is assumed that the bending moment by using plate theory is approximately 70% of the bending moment that is determined with beam theory. Taking this into account results in a bending moment of 3835 Nmm. Normally the strain dependent behaviour of the mix stiffness is neglected. In that case the stiffness is determined by using the master curve at a low strain level, say 80 $\mu m/m$. For T=10°C and f=5 Hz the stiffness of the Moerdijk mix is 5500 MPa. Metcalf's theory was used to determine the corresponding strain, by assuming an asphalt thickness of 50 mm and a steel plate of 10 mm. In this case the strain is 673 $\mu m/m$ and the corresponding number of load repetitions is 71240 (see figure 8.6).

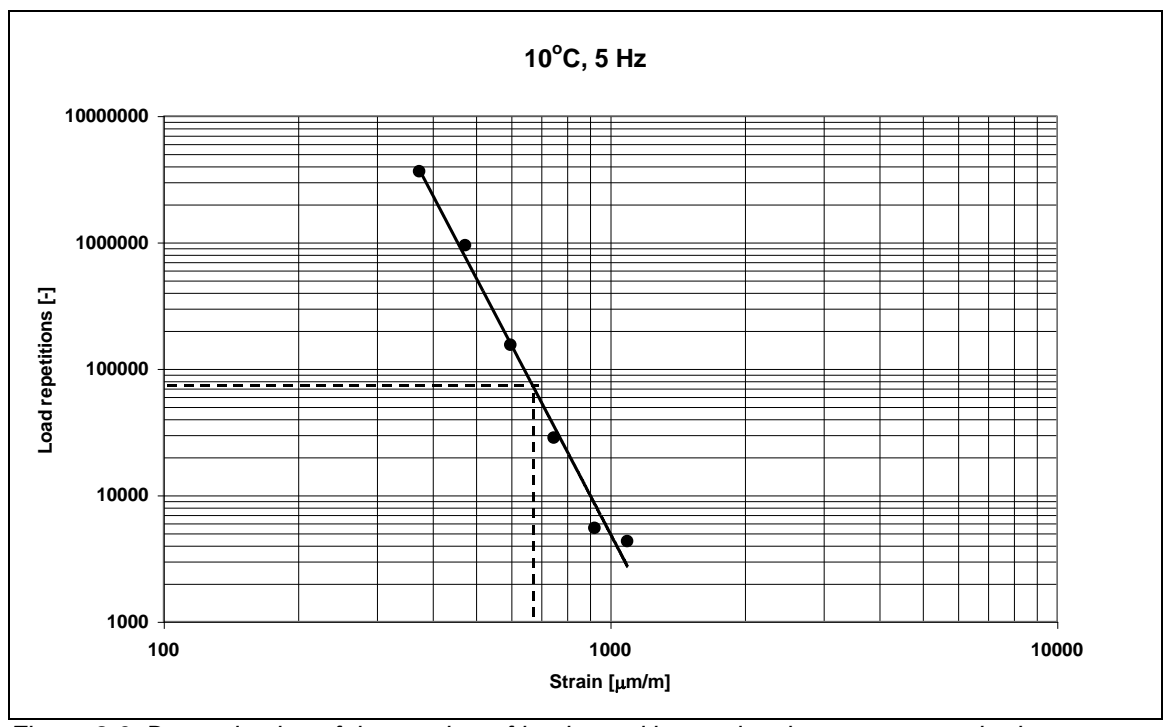


Figure 8.6: Determination of the number of load repetitions using the common method

To obtain the anticipated number of load repetitions in practice and the predicted fatigue lifetime, the experimental number is multiplied by different factors for healing and lateral wander (table 8.3).

Table 8.3: Determination of the fatigue lifetime for different healing and wander factors

	N _{experimental}	Н	LW	$N_{\it field}$	Lifetime [years]
ľ	71240	4	2.5	712400	0.2
	71240	20	2.5	3562000	1.2
	71240	4	6.7	1909232	0.6
	71240	20	6.7	9546160	3.2

Table 8.3 shows that the predicted fatigue lifetime varies between 0.2 and 3.2 years. In reality the fatigue life time of mastic asphalt on orthotropic steel bridges varies between 3 and 5 years. This means that only the prediction of 3.2 years seems to be reasonable. However, the following has to be noted for the previous fatigue lifetime prediction. The calculation is based on a temperature of 10°C and a loading frequency of 5 Hz. These are not representative values since the average asphalt temperature in the Netherlands is approximately 20°C and a reasonable loading

frequency is 50 Hz (0.02 s). An increasing temperature decreases the asphalt stiffness, increases the strains and results in a shorter fatigue lifetime. A higher temperature also causes a lower value for the lateral wander factor, which also results in a shorter fatigue lifetime. Another phenomenon that was neglected in the fatigue lifetime prediction is the variation in stiffness for the different fatigue measurements. By using the fatigue line in figure 8.6 it is assumed that the stiffness is constant for a temperature of 10°C and a frequency of 5 Hz irrespective of the strain level. This is certainly not the case, since the 4-point bending tests on the Lintrack mix showed a decreasing stiffness for increasing strain levels (paragraph 7.3.7). In paragraph 8.6.2 a fatigue lifetime prediction is done by using a more reasonable temperature and loading time. Also the variation of the stiffness is included.

8.6.2 Prediction of the fatigue lifetime for the Moerdijk mix using common method for T=20°C and f=50 Hz

In this paragraph the fatigue lifetime is predicted using figure 7.8 and equation 7.8. This means that also the stiffness is included in the fatigue lifetime prediction. The calculation of the strains is the same as in the previous section. Only the temperature of 20° C and loading time of 0.02 s (50 Hz) were chosen. It is assumed that figure 7.8 and equation 7.8 (in which the stiffness is included) are valid under these conditions, in spite of the fact that they are based on measurements at 10° C and 5 Hz.

In practice, normally the variation of the mix stiffness with strain level is neglected and the mix stiffness is determined at a low strain level, say 80 μ m/m. In this case the stiffness is 4404 MPa, which is determined by using equation 7.1 and table 7.2. For the calculation of the strains Metcalf's method is used by using the same conditions as in the previous section. For an asphalt stiffness of 4404 MPa the strain in the asphalt is 824 μ m/m.

With the fatigue relationship (equation 7.8) of the Moerdijk mix the number of load repetitions becomes 12168.

This value is the experimental number of load repetitions. Table 8.4 shows the calculation of the expected number of load repetitions for the different healing and traffic wander factors. The lifetime in years is predicted by using the traffic on the Moerdijk bridge, i.e. 2943706 100 kN axles per year. It should be noted that the calculation of this number is based on a temperature of 10°C and a frequency of 5 Hz.

Table 8.4: Determination of the fatigue lifetime for different healing and wander factors

N _{experimental}	Н	LW	$N_{\it field}$	Lifetime [years]
12168	4	2.5	121680	0.0
12168	20	2.5	608400	0.2
12168	4	6.7	326102	0.1
12168	20	6.7	1630512	0.6

Table 8.4 shows that the predicted lifetime varies between 0.0 and 0.6 years. This example indicates that the normal procedure to predict the fatigue lifetime seems not to be valid for mastic asphalt on orthotropic steel bridges, since in practice the fatigue lifetime of mastic asphalt varies between 3 and 5 years. However, in the previous prediction the stiffness is calculated by using the master curve at a strain level of 80 μ m/m and next the asphalt strain is determined by using this mix stiffness. This is only possible when the stiffness doesn't vary with strain level. However, in paragraph 7.3.7 it is shown that the stiffness varies with strain level.

The procedure followed in paragraph 8.6.1 is carried out for the mixes tested by Kolstein, to investigate the lifetime prediction for these mixes.

8.6.3 Prediction of the fatigue lifetime for mixes tested by Kolstein using common method

The fatigue lines determined by Kolstein are valid for a temperature of 20°C and 30 Hz. Table 8.5 shows the mix stiffness of four mixes for these conditions as determined by using the master curves (chapter 7, figure 7.4).

Table 8.5: Mix stiffness at T=20°C and 30 Hz

Mix	Stiffness [MPa]
SEAL1	5000
EVAL2	5000
STYLO	9000
REFBLO	12000

Again Metcalf's theory is assumed and the strain dependent behaviour of the mix stiffness and the temperature variation are neglected. The same beam and the same conditions are used as in paragraph 8.6.1. For an axle load of 100 kN Metcalf's composite action theory results in the strains as shown in table 8.6 for the different mixes.

Table 8.6: Strains for an axle load of 100 kN

Mix	Strain [μm/m]
SEAL1	734
EVAL2	734
STYLO	429
REFBLO	330

With the fatigue lines in figure 8.7 the lifetime can be predicted. However, the fatigue lines are determined at very low strain levels in a very small range, so extrapolation has been carried out to make lifetime predictions at higher strain levels possible.

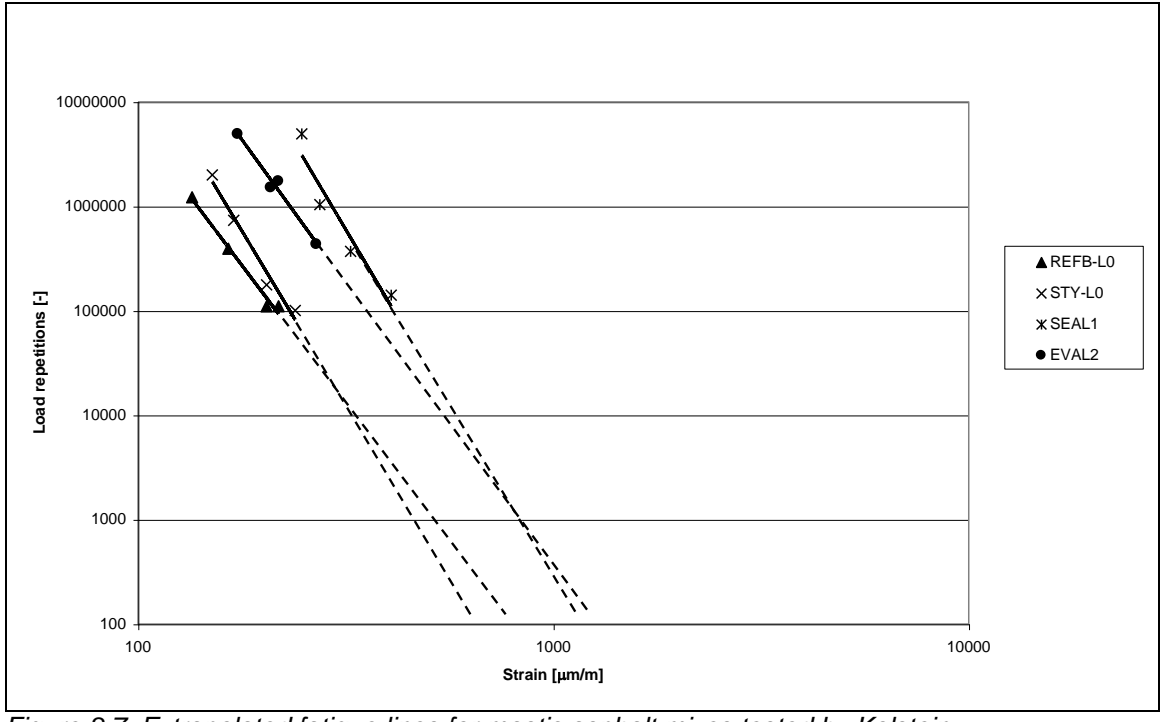


Figure 8.7: Extrapolated fatigue lines for mastic asphalt mixes tested by Kolstein

After extrapolation the lifetime is predicted for different healing and wander factors as shown in table 8.7.

Table 8.7: Lifetime prediction for mixes tested by Kolstein

Mix	N _{experimental}	Н	LW	N_{field}	Lifetime [years]
SEAL1	2139	4	2.5	21390	0.0
	2139	20	2.5	106950	0.0
	2139	4	6.7	57325.2	0.0
	2139	20	6.7	286626	0.1
EVAL2	1696	4	2.5	16960	0.0
	1696	20	2.5	84800	0.0
	1696	4	6.7	45452.8	0.0
	1696	20	6.7	227264	0.1
STYLO	1747	4	2.5	17470	0.0
	1747	20	2.5	87350	0.0
	1747	4	6.7	46819.6	0.0
	1747	20	6.7	234098	0.1
REFBLO	10128	4	2.5	101280	0.0
	10128	20	2.5	506400	0.2
	10128	4	6.7	271430.4	0.1
	10128	20	6.7	1357152	0.5

It can be seen that the estimated lifetime lies between 0 and 0.5 years. This may be attributed to the fact that the common procedure seems not to be valid to predict the lifetime of mastic asphalt on orthotropic steel bridges. However, also in this example assumptions have been made, which could have effected the results. Also the fact that the fatigue lines have been extrapolated could heave effect on the results.

8.7 A proposed procedure for estimating the fatigue lifetime

8.7.1 Definition of the procedure

The procedure normally adopted in road engineering for estimating the lifespan of asphaltic pavements neglect the dependency of stiffness on strain. Due to the high strain levels encountered at the surfacing of orthotropic steel bridges it is thought that a procedure which takes into account this dependency is needed. This procedure will be combined with equation 7.8 in chapter 7 that describes the fatigue life as a function of strain as well as the stiffness.

The determination of the stiffness and the strain requires actually a complex procedure since they are dependent on each other; the stiffness is required to calculate the asphalt strain, while the stiffness is in turn dependent on the strain. This non-linearity necessitates the use of a complex model to calculate the asphalt strains as a result of a certain applied load on orthotropic steel bridges. For such a complex model the use of a finite element program is inevitable.

However, in this case linear behaviour is assumed, in order to use a simple linear-elastic theory to determine the asphalt strains. The use of such a theory requires an iteration procedure, which is described by a flow chart in figure 8.8:

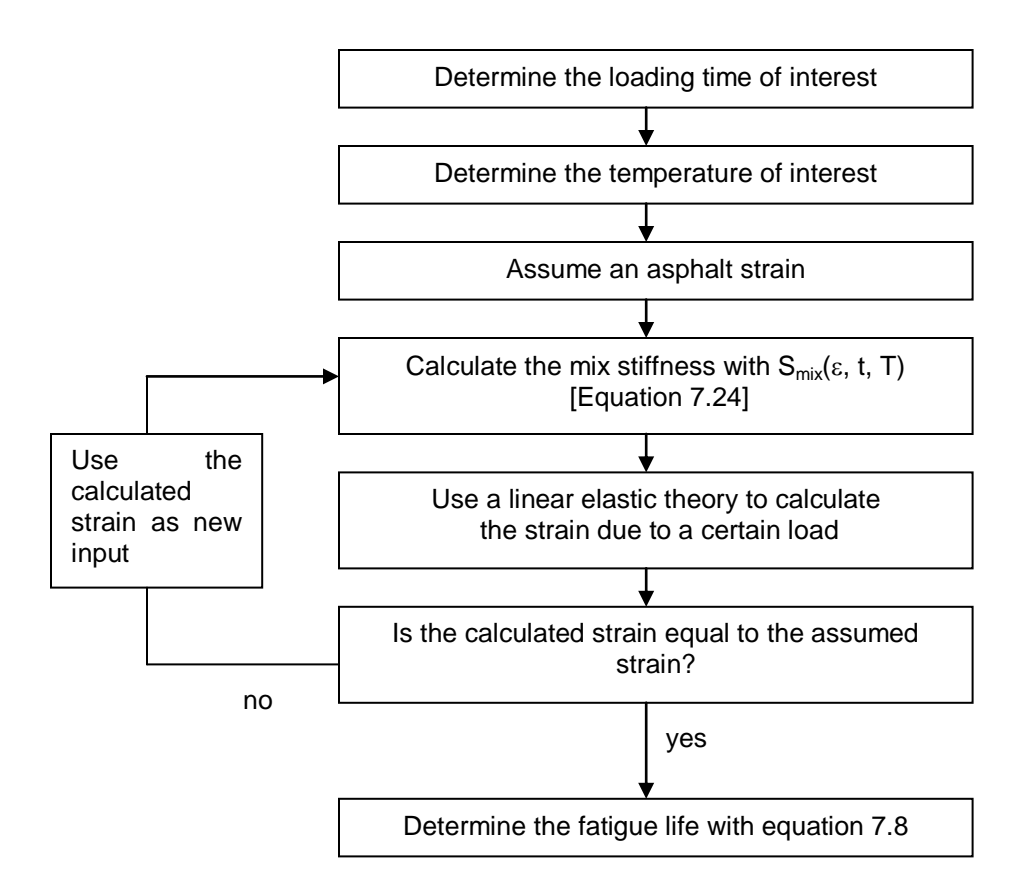


Figure 8.8: Flow chart for determining the fatigue life

When the strain is known, the fatigue life can be determined by using the design nomographs in appendix D.

8.7.2 Estimating the fatigue life using a simple beam model and a constant temperature of 20°C

In the following steps the procedure is carried out for the Moerdijk mix:

- 1. A loading time of 0.02 s is chosen, which corresponds to a speed of 54 km/h.
- 2. A temperature of 20°C is chosen, since this is close to the average asphalt temperature in the Netherlands.
- 3. For the calculation of the asphalt strains Metcalf's theory was used. An axle load of 100 kN is assumed. The bending moment is determined with the 10-span beam shown in figure 8.2. The bending moment is 3835 Nmm. After iteration the estimated stiffness is 2516 MPa and the strain level 1358 μ m/m.
- 4. With equation 7.8 the number of load repetitions is 951.

The lifetime after multiplication with the factors for healing and traffic wander is shown in table 8.8.

Table 8.8: Predicted fatigue lifetime for the Moerdijk mix

	N _{experimental}	Н	LW	N_{field}	Lifetime [years]
ſ	951	4	2.5	9510	0.0
	951	20	2.5	47550	0.0
	951	4	6.7	25486.8	0.0
	951	20	6.7	127434	0.0

The table shows that the predicted lifetime is 0. This may be attributed to the following:

- The strains become too high to use equation 7.24, which is valid for strains of maximal 1000 μm/m.
- The strains are calculated by using a linear-elastic theory with a simple beam model.
- In practice the temperature is not constant, but varies during the year.

The fact that the proposed procedure is too simple becomes even clearer when under the same conditions for different temperatures the strains and corresponding mix stiffness is calculated. Table 8.9 shows the results:

Table 8.9: Asphalt strains and mix stillness for dilierent temperature						
T [°C]	ε [μ m /m]	S _{mix} [MPa]				
0	349	11261				
5	410	9437				
10	529	7148				
15	782	4663				
20	1358	2516				
25	2577	1165				
30	4489	532				
35	6586	262				
40	8364	139				

Table 8.9: Asphalt strains and mix stiffness for different temperatures

From this table it becomes clear that the procedure doesn't work for high temperatures. At high temperatures the iteration procedure leads to asphalt strains that might be higher than the maximum strain the material can take. Also measurements showed that the maximum asphalt strain is approximately $1300 \, \mu \text{m/m}$.

Two facts my have influenced the iteration procedure. First of all the determination is based on linear-elastic behaviour, while at high strain levels and temperatures non-linear behaviour may be expected. Secondly the determination of the bending moment is based on some assumptions, which may result in an overestimated bending moment and subsequently in an overestimated strain.

8.7.3 Estimating the fatigue life using a finite element model and a constant temperature of 20°C

De Jong [2000] used a two-dimensional linear-elastic finite element model to calculate the strains in the asphalt. The model is shown in figure 8.9.

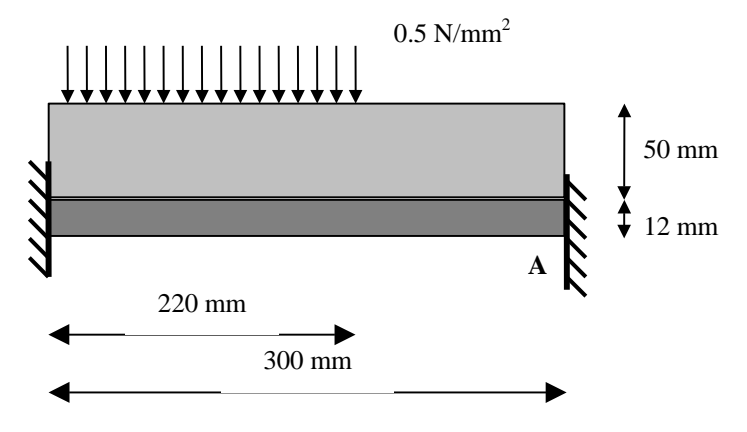


Figure 8.9: Model to calculate the asphalt strains

The model consists of a beam that is clamped at both the left and the right side. A wheel load of 35 kN was assumed, acting on an area of 220x320 mm at the left side of the beam. This results in a uniform pressure of 0.5 N/mm². This load combination leads to a maximum asphalt strain at clamp A. The thickness of the asphalt is 50 mm and the thickness of the steel plate is 12 mm. For calculations 100% bond (no slip) between the asphalt and the steel is assumed.

Using this model the relationship between the strain and mix stiffness is obtained as shown in figure 8.10.

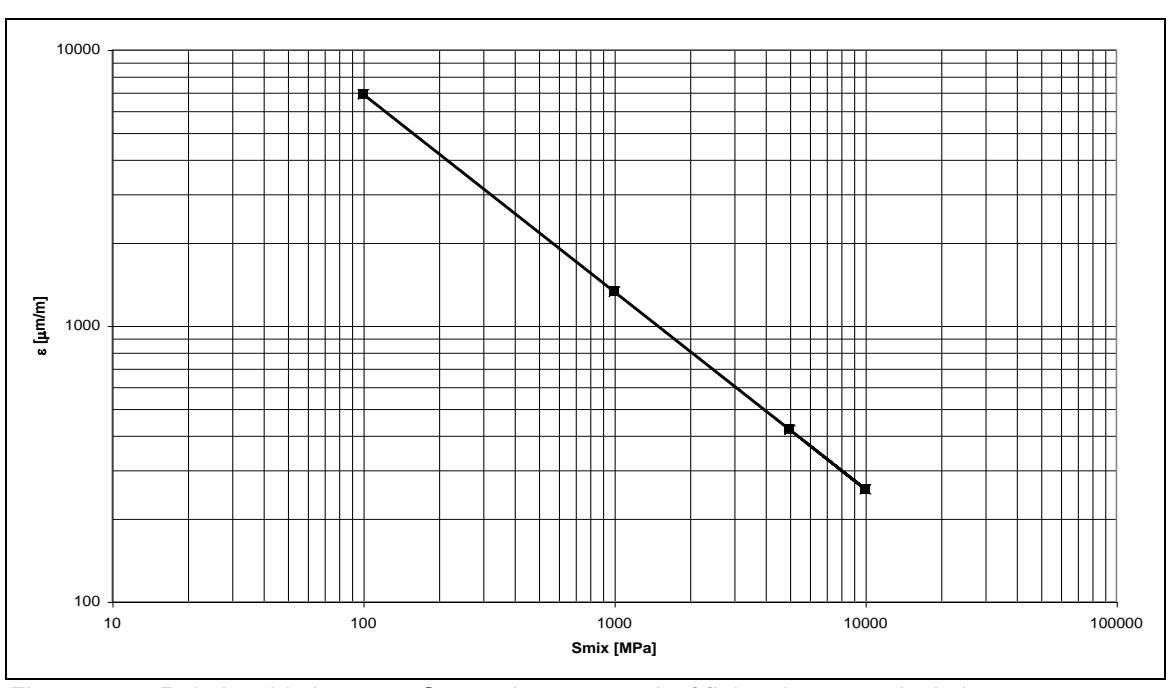


Figure 8.10: Relationship between S_{mix} and ε as a result of finite element calculations

This relationship is described best with the following equation:

$$\varepsilon = 186192 \times S_{mix}^{-0.7156}$$
 Equation 8.2

For T=20 $^{\circ}$ C and a loading time of 0.02 s the combination of the strain dependent mix stiffness with equation 8.2 results after iteration in an asphalt strain of 596 μ m/m and an asphalt stiffness of 3065 MPa. By using equation 7.8 the number of load repetitions becomes 288475. Table 8.10 shows the number of load repetitions for different factors of traffic wander and healing.

Table 8.10: Predicted fatigue lifetime for the Moerdijk mix

N _{experimental}	Н	LW	$N_{\it field}$	Lifetime [years]
288475	4	2.5	2884750	1.0
288475	20	2.5	14423750	4.9
288475	4	6.7	7731130	2.6
288475	20	6.7	38655650	13.1

From this table it becomes clear that the predicted fatigue lifetime varies between 1.0 and 13.1 years. These values are more reasonable than the previous predictions, although the fatigue lifetime of 13.1 years seems far too high, compared to the findings in practice. However, to compare these lifetimes with the ones determined in previous sections, one should be aware of the fact that for these calculations different models were used.

8.7.4 Estimating the fatigue life using a finite element model and variable temperature

The same two-dimensional finite element model is used to calculate the strains in the asphalt. Table 8.11 shows the results for different temperatures in the range of 0 to 40°C after iteration.

Table 8 11:	Asphalt strains	and mix stiffnes	s for differen	t temperatures
1 4010 0.11.	Aspirali sirali is	and mix sumics	o ioi ailicicii	licinporalares

T [°C]	$arepsilon$ [μ m/m]	S _{mix} [MPa]
0	231	11525
5	259	9815
10	310	7652
15	405	5259
20	596	3065
25	992	1503
30	1786	661
35	3193	293
40	5342	143

From this table it is clear that using a finite element model gives less conservative estimate of the fatigue life than the beam model. However, for higher temperatures (>35°C) the calculated strains become too large. This may be attributed to the fact that at these temperatures and strains the material behaves no longer linear-elastic. This requires the use of a non-linear material model. Also a beam model was used instead of a plate model.

8.8 Conclusion

From the previous case study it becomes clear that the normal procedure used in road engineering to estimate the fatigue lifetime seems not to be applicable for mastic asphalt on orthotropic steel bridges. That is because the predicted lifetime is underestimated compared to the findings in practice. An attempt has been made to make a more reasonable lifetime prediction by using an iterative procedure that uses the strain dependent behaviour of the mix stiffness and a reasonable temperature distribution. For this procedure use is made of the linear-elastic theory of Metcalf. This procedure still gives a too short estimate of the lifetime. However, the procedure itself is better than the normal procedure because it describes the real asphalt behaviour in a better way and uses a reasonable temperature distribution. The reason that the predicted lifetime is still underestimated may be attributed to the fact that:

- for the calculation of the bending moment a simplified model has been used, which may lead to an overestimated bending moment.
- linear-elastic behaviour has been assumed in calculation of the strains, while at high temperatures and high strain levels non-linear behaviour should be expected.

Some preliminary calculations showed indeed that a more reasonable lifetime is predicted when use is made of a finite element model to calculate the bending moment and the asphalt strains. However, further calculations are needed with a non-linear model to deal with higher strain levels and temperatures.

9 CONCLUSIONS AND RECOMMENDATIONS

9.1 Conclusions

This report describes the material characterisation of a typical mastic asphalt mix that is used for surfacing orthotropic steel bridges. These types of bridges consist of a steel deck plate supported into two perpendicular directions, which results in different elastic properties of the deck in the two orthogonal directions. Normally, the steel decks are surfaced with asphalt, which has four main objectives:

- To provide a running surface with suitable skid resistance.
- To provide a flat running surface to compensate for the rough surface of the steel plate.
- To protect the deck plate with a waterproofing layer.
- To reduce the stresses in the steel deck plate.

To fulfil these objectives the asphalt surfacing can be divided in four functional layers:

- Bonding layer to ensure sufficient adhesion between the steel plate and the isolation layer.
- Isolation layer to protect the underlying steel deck against corrosion.
- Adhesion layer to ensure the adhesion between the isolation layer and the wearing coarse.
- Wearing coarse to take and transfer the loading from traffic to the underlying structure.

The deformation of the steel deck and the asphalt on orthotropic steel bridges are larger than the deformations of normal pavements on a basecoarse and a subgrade. Due to this large deformations a flexible type of asphalt is needed for deck surfacing. Mastic asphalt fulfils this requirement. The main properties of mastic asphalt are:

- The voids are overfilled with mastic.
- The asphalt is not compacted.
- The stability is obtained from a stiff, often modified, type of bitumen.
- The production and processing take place at relative high temperatures (220-240°C).
- The thickness of the asphalt layers varies between 20 mm and 50 mm.

The requirements for mastic asphalt are different in different countries. The requirements in the Netherlands are:

- The maximum aggregate size is 8 mm.
- The maximum void ratio is 2.5%.
- Penetration 10-40 (*0.1 mm) with the stempel test (300 sec, 5.25 N/mm², 100 mm², 25°C).
- Deformation of 6-10% after 100.000 load repetitions in the wheel track test.

In practice composite action theories are used to calculate stresses and strains that occur in the mastic asphalt due to bending moment produced by loading. They are based on one of both of the following assumptions:

- Linear strain distribution in the asphalt and the steel.
- The slopes of the strain distribution through the depth of the asphalt and the steel are equal. From the comparison between the composite action theories from Metcalf, Kolstein, Cullimore, Nakanishi and Sedlacek/Bild the following can be concluded:
- The maximum asphalt strains for a low bonding stiffness between steel and asphalt are ≈1300 μm/m which is 10 times higher than the strains in normal pavements on a subgrade.
- For these high strain levels linear elastic behaviour of the asphalt, which is currently assumed, is doubtful.
- The strains/stresses in the steel/asphalt are calculated using a beam model. However, plate theory may be more applicable.
- According to Nakanishi's theory the asphalt strains at ±15% bonding are higher than the strains at 0% bonding.

- For certain conditions the presented theories might be true, but these conditions might not be representative for the real structure.
- For extreme values of the bond (0% and 100% bonding) the theories give the same results, but for values of the bond stiffness between both extremes the theories give different results.

From a dynamic analysis the following can be concluded:

- Vibration of the deck could lead to increasing strains in the pavement due to an increasing impact of the dynamic axle loads compared to pavements on a subgrade, because of the interaction between the bridge deck and the vehicle.
- Vibration of the deck could lead to a faster alternation between tensile and compressive strains in the pavement compared to pavements on a subgrade. This alternation might have influence on the fatigue behaviour.

On orthotropic steel bridges problems, like rutting and fatigue cracking, arise in a relative early stage of lifetime, which results in an asphalt lifetime of only 3-5 years. Therefore, a better understanding of the mastic asphalt behaviour is needed. For that purpose the following experimental program has been carried out on the mastic asphalt that was placed on the Moerdijk bridge in June 2000:

- 1. Determination of the relationship between the mix stiffness, loading time and temperature (master curves) for temperatures between 5°C and 30°C and loading times between 0.1 and 2 s. Comparison of the mix stiffness of the Moerdijk mix with some other types of modified mastic asphalt mixes showed that the master curves are more or less comparable. After 2.5 months the master curves for the Moerdijk mix were determined again by using the specimen that were tested before in the fatigue test. The stiffness of this repeated testing is comparable to that of the first measurements, which can be attributed to the fact that the material has a very good healing capacity.
- 2. Comparison of the fatigue characteristics for the Moerdijk mix with some other types of modified mastic asphalt mixes showed that the Moerdijk mix has rather good fatigue characteristics. The determination of the fatigue characteristics has been repeated after 2.5 months, which showed a similar fatigue line, which gives indication of the healing capacity of the mix.
- 3. It has been noticed that the stiffness of mastic asphalt is not only a function of loading time and temperature, but also of the strain level. This indicates non-linear elastic behaviour of mastic asphalt. Therefore a relationship is determined for the mix stiffness as a function of loading time, temperature and strain level. This relationship is valid for temperatures between 0 and 45°C, loading times between 0.01 and 1 s. and strain levels between 80 and 1000 $\mu m/m$. The mix stiffness decreases with increasing strain level. When the strain dependency is neglected and for determination of the stiffness a strain level of 80 $\mu m/m$ is used (which is representative for normal pavements) the maximum overestimation of the stiffness is 5 times for 45°C, t=1.0 s. and a strain level of 1000 $\mu m/m$. For road engineering often the strain dependency is neglected. This results in an overestimated asphalt stiffness and an underestimated asphalt strain. When this asphalt strain is used for determination of the fatigue life this lifetime will be overestimated. Therefore the strain dependency can not be neglected.
- Determination of the parameters of the ACRe material model by carrying out uniaxial monotonic tension and compression tests. The following can be concluded:
 - Both tension and compression strength increase with decreasing temperature and increasing strain rate.
 - No relationship was found for the stress at the start of plasticity as a function of strain rate and temperature. Instead a function of α_0 as a function of strain rate and temperature is determined, from which the stress at the start of plasticity can be obtained indirectly.
 - For high strain rates and low temperatures a cut-off value for parameter n is used of 10 and α is set to zero. This means that under these conditions no hardening occurs.

- It was not possible to determine the hardening parameter α as a function of equivalent plastic strain.
- The hardening parameter α is expressed as a function of equivalent plastic work.
- For strain rates lower than $0.05~\text{s}^{-1}$ the flow surface can not be determined. Mathematically this is a result of the fact that the determination of α_0 is too high for low strain levels. Physically this might be attributed to the fact that in that case there is hardly any elastic response, meaning that the material starts to flow immediately.

From a case study for the Moerdijk bridge the following can be concluded:

- Shifting the traffic lanes over a distance of 1.0 m during a certain period of the year on a bridge has two positive effects:
 - 1. The repetition of strains at a certain point of the structure decreases, because the shift of the traffic lane leads to less deformation at the specific point.
 - 2. Because mastic asphalt has excellent healing properties the material can heal during the period that the lanes are shifted.

Both effects lead to an increased lifetime of the asphalt mix.

• The procedure normally adopted in road engineering practice to estimate the fatigue lifetime seems not to be applicable for mastic asphalt surfacings on orthotropic steel bridges.

9.2 Recommendations

The comparison of the composite action theories gives approximately the same strains for full and no adhesion between the steel and the asphalt. For values of the bond stiffness between these extreme values, which is the case in practice, the theories give different results. Because the bond stiffness is highly related to the degradation of the asphalt more research has to be carried out on the behaviour of the bonding layer between the asphalt and the steel. For this research shear tests on the bonding layer are recommended.

Further the composite action theories might be true for certain conditions, but these conditions might not be representative for the real structure. To calculate the representative asphalt strains in a better way, a representative part of the structure has to be analysed and plastic behaviour of the asphalt has to be included.

For the determination of the dynamic axle loads on orthotropic steel bridges use has been made of simple models. These simple models showed that the axle loads might increase on orthotropic steel bridges due to interaction between vehicle and bridge deck. More research is recommended, by using more complex dynamic models to investigate the effect of dynamic axle loads on orthotropic steel bridges.

The relationship describing the strain dependent behaviour of the mix stiffness is valid for the Lintrack mix only. More four-point bending tests on mastic asphalt at different strain levels have to be carried out to determine the strain dependent behaviour of the other mastic asphalt mixes in general. The relationship that was determined is valid for maximum strain levels of 1000 μ m/m, while in practice maximal strain levels of 1300 μ m/m were measured. Further research at these high strain levels is recommended to increase the validity of the relationship for the mix stiffness as a function of the strain level.

By using a simple beam model it has been shown that shifting the traffic lanes over a distance of 1.0 m, during a certain period of the year has positive effects on the fatigue lifetime. Therefore it is recommended to investigate this possibility by using a more representative part of the structure and a good material model, for example the ACRe material model.

The prediction of the fatigue lifetime using the methods normally used in road engineering seems not to be valid for asphalt on orthotropic steel bridges. This might be attributed to the fact that the asphalt strains are overestimated and to the fact that the common theories are based on linear-

elastic behaviour. However, for higher strain levels linear-elastic behaviour is doubtful. To calculate the fatigue lifetime of mastic asphalt in a better way the following is proposed:

- Include the strain dependent behaviour of the asphalt stiffness in the calculation of the asphalt strains.
- Use a finite element program to calculate a reasonable bending moment, but take a representative part of the structure.
- Use a non-linear material model to calculate the asphalt strains, for example the ACRe material model.

In the determination of the model parameters the parameter β is assumed to be zero. It is recommended to carry out multiaxial tests to determine this parameter. Also further research is recommended to investigate the behaviour of the ACRe material model for low values of hardening parameter α . For these low values of α (for high temperatures and small loading times) the model gives some problems. Extra testing under these conditions might lead to a better relationship between α , temperature and loading time.

REFERENCES

- 1. Backer, C. de, *Bitumineuze Bedekkingen op Orthotrope Brugplaten* (in Dutch). De Wegentechniek/ La Technique Routiĕre, No. 1,1978.
- 2. Bouma, A.L., *Mechanica van constructies, elastostatica van slanke structuren* (in Dutch). Delft: Delftsche Uitgevers Maatschappij, 1993.
- 3. Brants, J.P., *Slijt-en Isolatielagen op Kunsterken* (in Dutch), Werkgroep H2, Stichting Studie Centrum Wegenbouw, Arnhem, the Netherlands, 1972.
- 4. Company, S.I., Shell Pavement Design manual. London: Shell International Petroleum Company Ltd., 1978.
- 5. CROW, Standaard RAW bepalingen 2000 (in Dutch). Ede: CROW, 2000.
- 6. Cullimore, M.S.G. et al., 'Flexure of Steel Bridge Deck Plate with Asphalt Surfacing', *IABSE Periodical*, 1 (1983), p.58-83.
- 7. Desai, C.S., S. Somasundaram and G. Frantziskonis, 'A Hierarchical Approach for Constitutive Modelling of Geologic Materials', *International Journal of Numerical and Analytical Methods in Geomechanics*, 10, 3, (1986), p. 225-257.
- 8. Dieterman, H.A., *Algemene Mechanica II, deel II Inleiding Dynamica van Constructies.* Delft: Delft University of Technology, Faculty of Civil Engineering, 1997.
- 9. Dijk W. van, 'Practical Fatigue Characterization of Bituminous Mixes', *Proceedings of the Association of asphalt Paving Technologists (AAPT)*, volume 44 (1975), pp 38-74.
- 10. Dijk W. van, and W. Visser, The Energy Approach to Fatigue for Pavement Design', Proceedings of the Association of asphalt Paving Technologists (AAPT), volume 46 (1977), pp 1-40.
- 11. Divine, *Dynamic interaction vehicle-infrastructure experiment*. Rotterdam, European concluding conference, September 17-19, 1997.
- 12. Erkens, S.M.J.G. and M.R. Poot, *The Uniaxial Compression Test*. Delft: Delft University of Technology, 1998.
- 13. Erkens, S.M.J.G. and M.R. Poot, *The Uniaxial Tension Test Asphalt Concrete Response (ACRe)*. Delft: Delft University of Technology, 2001, report nr. 7-01-117-7.
- 14. Erkens, S.M.J.G, *Asphalt Concrete Response Measuring, Modelling and Predicting, PhD.* Thesis Delft University of Technology, 2002 (under preparation).
- 15. Eurocode 3, *Design of Steel Structures-Part2: Steel Bridges.* Brussels, European Committee for Standards, 1997.
- 16. Ewalds, H.L. and R.J.H. Wanhil, *Fracture Mechanics*. London: Co-publication of Delftse Uitgevers Maatschapij and Edwards Arnold Publishers, 1986.
- 17. Francken, L. and C. Clauwaert, *Characterisation and structural assessment of bound materials for flexible road structures*, Proceedings 6th international conference on the structural design of asphalt pavements, Ann Arbor, MI, USA, (1988), p. 130-144.
- 18. Groenendijk, J., *Accelerated Testing and Surface Cracking of Asphaltic Concrete Pavements*, PhD. Thesis. Delft: University of Technology, Netherlands, 1998.
- 19. Gurney, T., *Fatigue of Steel Bridge Decks*, Transport Research Laboratory, Department of Transport. London: HMSO Publication centre, 1992.
- 20. Hardenberg, G. et al., *Gietasfalt: Toepassing op orthotrope stalen bruggen* (in Dutch). Werkgroep H2 "Slijt- en isolatielagen op kunstwerken", 1985.
- 21. Hopman, P.C. and R. Coorengel, *Development of a porous wearing coarse for orthotropic steel bridge decks.* Madrid: 4th Eurobitume symposium, 1989.
- 22. Huurman, M., *Permanent deformation in concrete block pavements*, PhD. Thesis. Delft: University of Technology, Netherlands, 1997.
- 23. Jacobs, M.M.J., *Crack growth is asphaltic mixes,* Ph.D. Dissertation. Delft: Delft University of Technology, Faculty of Civil Engineering, 1995.
- Jenq, Y.S. and J.D. Perng, Analysis of Crack Propagation in Asphalt Concrete Using a Cohesive Crack Model, Proceedings 70th Annual Meeting TRB, Washington D.C: Paper No. 910522, 1991.

- 25. Jong, P. de, *Internal report: Road and Hydraulic Engineering Division of the Ministry of Transport.* Public Works and Water Management of Rijkswaterstaat (RHED), 2000.
- 26. Kolstein, M.H., *Optimalisatie van Economische Bruikbaarheid van Dikke Stijl en Isolatielagen op Stalen Brugdekken (Criteria en Factoren)*, Report 26.6.90.12/A2/22.03, Road and Railway Research Laboratory (in Dutch). Delft: Faculty of Civil Engineering and Geosciences, 1990.
- 27. Kolstein, M.H. and J.H. Dijkink, *Behaviour of modified bituminous surfacings on orthotropic steel bridge decks*. Madrid: 4th Eurobitume symposium, 1989.
- 28. Kohler, Deters, Bituminöse Beläge auf Stahlbrücken mit orthotropen Fahrbahplatten, (in German), Bitumen, Teere, Asphalt, Peche 25, blz. 11-14, 1974.
- 29. Lytton, R.L., J. Uzan, E.M. Fernando, R. Roque, D. Hiltunen and S.M. Stoffels, *Development* and validation of performance prediction models and specifications for asphalt binders and paving mixes, SHRP report A-357. Washington, DC, USA: SHRP/NRC, 1993.
- 30. Medani, T.O., A simplified procedure for estimation of the fatigue and crack growth characteristics of asphaltic mixes, M. Sc Thesis. Delft: International Institute for Infrastructural, Hydraulic and Environmental Engineering, 1999.
- 31. Medani, T.O., A preliminary Review on Asphalt Surfacing Applied to orthotropical Steel Bridges. Delft: Delft University of Technology, 2000a.
- 32. Medani, T.O., Towards a new design philosophy for asphalt surfacings on orthotropic steel decks. Delft: Delft University of Technology, 2000b.
- 33. Metcalf, C.T., Flexural tests of paving Materials for Orthotropic Steel Plate Bridges, Highway research record No.155. Washington, D.C., 1967.
- 34. Molenaar, A.A.A., Structural Design of Pavements, part II: Stresses and strains in flexible pavements. Lecture notes e54. Delft: Delft University of Technology, Faculty of Civil Engineering, 1994.
- 35. Molenaar, A.A.A., *Road materials, part III: Asphaltic materials.* Delft: Delft University of Technology, Faculty of Civil Engineering, 1994.
- 36. Nakanishi, H. et al., *The structural evaluation for an asphalt pavement on a steel plate deck,* Proceedings of the First International Conference, World of Asphalt Pavement (AAPA), p.112-123. Sydney, Australia, 2000.
- 37. NPC, *Onderzoek gietasfaltmengsels brug Ewijk* (in Dutch). Hoevelaken: Netherlands Pavement Consultants, 1996.
- 38. Pronk, A.C., Fatigue lives of asphalt beams in 2 and 4 point dynamic bending tests based on a 'new' fatigue life definition using the "Dissipated Energy Concept", Phase II: DAB 0/8, rapport W-DWW-98-001. Delft: Rijkswaterstaat, Dienst Weg- en Waterbouwkunde, 1998.
- 39. Ramsamooj, D.V., 'Prediction of Fatigue Life of Asphalt Concrete Beams from Flexure Tests', Journal of Testing and Evaluation, Volume 19, No. 3 (1991), pp 231-239.
- 40. Robinson, G.K., Practical Strategies for Experimenting. John Willey & Sons, England, 2000.
- 41. Roik, K. and G. Sedlacek, 'Erweiterung der technischen Biege- und Verdrehtheorie unter Berücksichtigung von Schubverformungen' (in German), *Die Bautechnik 47*, (1970), p. 20-32.
- 42. Sassen, J.A., Onderzoek naar de initiële dynamsche stijfheidsmodulus van de Lintrackmeetvakken, rapport MAE-S-91150 (in Dutch). Delft: Rijkswaterstaat, Dienst Weg- en Waterbouwkunde DWW, 1991.
- 43. Saygeh, G., 'Viscoelastic properties of bituminous mixtures'. *Proceedings* 2nd *international on the structural design of asphalt pavements, Ann Arbor, MI, USA*, (1967).
- 44. Scarpas, A., C.A.P.M. van Gurp, R.I.N. Al-Khoury and S.M.J.G. Erkens, *Finite Elements Simulation of Damage Development in Asphalt Concrete Pavements*, 8th International Conference on Asphalt Pavements (ICAP), University of Washington, Seattle, U.S.A., August 10-14. Seattle, 1997.
- 45. Sedlacek G., *Stahlbau Handbuch Band 1, Zweiachsige Biegung und Torsion* (in German). 2^e Auflage. Köln, Stahlbau-Verlags-GmbH, 1982
- 46. Sedlacek G. and S. Bild, *Beitrag zur Verbesserung der Haltbarkeit von Fahrbahnbelägen auf Orthotropen Platten* (in German). Aachen, Bundesministers für Verkehr, 1985.
- 47. SHRP, Fatigue Response of Asphalt-Aggregate Mixes. Washington: National Research Council, DC, 1994.
- 48. Sitters, C.M.W., *Material Models for Soil and Rock*. Delft: Delft University of Technology, Faculty of Civil Engineering, 1998.

- 49. Spijkers, J., *Dynamica van Constructies*. Delft: Delft University of Technology, Faculty of Civil Engineering, 1996.
- 50. Ullidtz, P., T.L. Kieler and A. Kargo, *Finite Element Simulation of Asphalt Fatigue Testing,* Proceedings of the 5th International Rilem Symposium MTBM Lyon, France, May 1997.
- 51. VBW asfalt, Asfalt in wegen- en waterbouw (in Dutch). 9^e herziene druk. Breukelen: VBW asfalt, 1996.
- 52. Volker, N., 'Brückenbeläge auf Stahl Bauvorbereitung und Bauüberwachung des Auftraggebers' (in German), *Bitumen 1/93*,1993.
- 53. Wattimena, J.S., *Vermoeiingsonderzoek G.A.B. mei 1991 (Lintrack)*, rapport 91482 (in Dutch). Hoevelaken: Netherlands Pavement Cosultants NPC, 1991.
- 54. Whiteoak C.D., The Shell bitumen handbook. Chertsey. Surrey: Shell bitumen U.K., 1990.
- 55. Williams, M.L., R.F. Landel and J.D. Ferry, 'The temperature dependence of relaxation mechanism in amorphous polymers and other glass forming liquids', Journal of ACS, vol. 77, (1955), p.3701.

Appendix A: Specimens' dimensions

In this appendix the results of the dimension measurements are presented. Table 1 shows the dimensions of the 8 specimens from the Moerdijk mix. Table 2 and 3 show the dimensions of the specimens for the uniaxial compression and tension tests respectively. Finally, table 4 shows the dimensions of the 46 specimens from the Lintrack mix.

All dimensions were measured four times and the average was taken. The width and height were measured with a calippers, for the length a sliding rule was used.

Table 12: Dimensions of the 8 specimens from the Moerdijk mix

	specimen	1	2	3	4	5	6	7	8
height [mm]	measurement 1	50.91	51.71	51.18	51.84	51.61	51.76	51.57	50.21
	measurement 2	50.69	50.95	51.63	51.52	51.27	50.94	50.97	50.82
	measurement 3	50.67	50.52	51.58	51.23	50.74	50.41	50.71	51.01
	measurement 4	50.28	50.67	51.9	51.15	50.43	49.91	50.3	51.56
	average	50.64	50.96	51.57	51.44	51.01	50.76	50.89	50.90
width [mm]	measurement 1	52.24	52.19	51.73	51.58	52.05	52.39	52.49	52.16
	measurement 2	53.04	53.28	52.68	53.25	53.49	53.65	53.38	53.3
	measurement 3	53.51	53.75	52.69	53.73	53.91	53.86	53.35	53.4
	measurement 4	52.53	52.52	51.74	51.83	52.35	52.32	52.13	52.66
	average	52.83	52.94	52.21	52.60	52.95	53.06	52.84	52.88
length [mm]	measurement 1	449	449	449	450	450	450	450	450
	measurement 2	450	449	449	450	450	450	450	451
	measurement 3	449	449	449	449	450	450	450	450
	measurement 4	450	449	449	450	449	450	451	450
	average	450	449	449	450	450	450	450	450

Table 2: Dimensions of the specimens for the uniaxial monotonic compression test

			height [mm]				Diameter [mr	n]		
Specimen					average					average
M4-3	90.0	90.1	90.2	90.1	90.1	49.8	49.8	49.9	49.9	49.8
M11-4	100.1	100.1	100.0	100.1	100.1	49.7	49.7	49.9	49.9	49.8
M5-3	90.1	89.9	90.1	90.1	90.1	49.7	49.7	49.9	49.9	49.8
M4-4	89.8	89.8	90.0	90.0	89.9	51.0	50.0	50.0	50.0	50.0
M3-10	89.6	90.0	89.8	89.7	89.8	49.6	49.9	49.7	49.8	49.8
M2-5	90.2	90.2	90.2	90.1	90.2	49.9	49.9	49.9	49.8	49.9
M11-3	100.3	100.1	100.2	100.1	100.2	50.3	50.1	49.8	49.9	50.0
M6-4	99.6	99.6	99.6	99.5	99.6	49.7	49.6	49.7	49.7	49.7
M7-4	100.1	100.0	100.2	100.0	100.1	50.0	50.0	50.1	50.1	50.1
M9-2	100.3	100.3	100.2	100.4	100.3	49.8	49.8	49.8	49.9	49.8
M10-2	100.3	100.3	100.3	100.3	100.3	49.8	49.8	49.8	49.9	49.8
M10-10	100.1	100.4	100.3	100.2	100.3	49.7	49.8	49.7	49.9	49.8
M6-6	100.1	100.1	100.1	100.2	100.1	49.8	49.9	49.8	49.7	49.8

Table 3: Dimensions of the specimens for the uniaxial monotonic tension test

			height [mm]				Diameter [mr	n]		
Specimen					average					average
M11-5*	89.3	89.4	89.5	89.4	89.4	49.9	49.9	50.0	49.9	49.9
M2-1*	89.1	89.1	89.0	89.1	89.1	49.7	49.7	49.9	49.9	49.8
M11-8	90.9	90.7	90.9	90.9	90.9	49.5	49.5	49.7	49.7	49.6
M2-3	88.9	88.9	89.1	89.1	89.0	49.9	49.8	49.8	49.8	49.8
M3-9	90.1	90.5	90.3	90.2	90.3	49.8	49.9	50.0	50.0	50.0
M3-1	90.0	90.0	90.0	89.9	90.0	50.0	50.0	50.0	49.9	50.0
M1-10*	89.4	89.2	89.3	89.2	89.3	50.0	49.8	49.5	49.6	49.7
M3-7	90.2	90.2	90.2	90.1	90.2	49.6	49.5	49.6	49.6	49.6
M5-2	90.1	90.0	90.2	90.0	90.1	49.8	49.8	49.9	49.9	49.9
M3-4	90.0	90.0	89.9	90.1	90.0	49.9	49.9	49.9	50.0	49.9
M2-4	90.0	90.0	90.0	90.0	90.0	49.7	49.7	49.7	49.8	49.7
M4-7	89.8	90.1	90.0	89.9	90.0	49.8	49.9	49.8	50.0	49.9
M1-3	90.0	90.0	90.0	90.1	90.0	49.5	49.6	49.5	49.4	49.5

Table 4: Dimensions of the specimens from the Lintrack mix

, abic i	. Diiii	71131011			SIIIIGII	3 110111		ntrack	IIIIX						
		l	height [mn	n] I			'	width [mm]	I	1		, 	ength [mm]		1
specimen					average					average					average
ML/4pb/1/1	50.4	50.6	50.5	50.4	50.5	50.6	50.1	50.2	50.7	50.4	420	421	420	420	420
ML/4pb/1/2	50.2	50.0	50.3	51.1	50.4	50.3	49.9	50.0	50.1	50.1	420	420	420	420	420
ML/4pb/1/3	50.6	50.2	50.7	50.1	50.4	51.4	50.8	50.4	50.1	50.7	420	420	420	421	420
ML/4pb/1/4	50.5	50.4	50.5	50.4	50.5	50.9	50.3	50.4	50.7	50.6	421	421	421	421	421
ML/4pb/1/5	50.4	50.4	50.3	50.4	50.4	50.7	51.1	51.2	51.4	51.1	422	422	421	421	422
ML/4pb/1/6	50.5	50.7	50.5	50.6	50.6	53.3	52.1	51.5	52.9	52.5	421	421	421	421	421
ML/4pb/1/7	52.2	52.3	52.7	53.2	52.6	50.6	50.6	50.4	50.4	50.5	422	421	422	422	422
ML/4pb/1/8	50.7	50.6	50.7	50.6	50.7	50.4	50.6	50.7	50.6	50.6	421	421	421	420	421
ML/4pb/1/9	50.6	50.7	50.4	50.6	50.6	50.7	50.9	51.1	51.1	51.0	423	422	421	422	422
ML/4pb/1/10	50.2	50.3	50.5	50.6	50.4	50.9	51.0	51.4	51.0	51.1	421	421	421	421	421
ML/4pb/2/1	49.8	49.7	49.6	49.3	49.6	51.6	51.3	52.3	53.3	52.1	420	420	420	420	420
ML/4pb/2/2	49.8	49.3	49.4	49.1	49.4	50.1	50.4	50.4	51.1	50.5	419	419	420	421	420
ML/4pb/2/3	49.4	49.2	49.2	48.9	49.2	49.3	49.4	48.1	49.3	49.0	420	420	420	420	420
ML/4pb/2/4	49.2	49.2	49.2	49.1	49.2	52.4	53.0	54.1	55.5	53.8	420	420	420	420	420
ML/4pb/2/5	49.4	49.2	49.1	49.0	49.2	53.2	54.5	56.1	56.2	55.0	421	419	420	420	420
ML/4pb/2/6	49.3	49.4	49.6	49.5	49.5	53.7	56.8	57.6	58.0	56.5	420	420	420	420	420
ML/4pb/2/7	49.7	49.1	49.3	49.2	49.3	51.1	51.6	52.4	52.6	51.9	420	420	420	420	420
ML/4pb/2/8	49.3	49.1	49.3	49.0	49.2	51.2	53.5	52.8	53.4	52.7	420	420	420	420	420
ML/4pb/2/9	49.3	49.1	49.1	48.9	49.1	52.4	52.2	52.8	52.7	52.5	420	421	421	420	421
ML/4pb/2/10	49.6	49.2	49.2	48.8	49.2	50.9	50.7	51.1	51.3	51.0	421	421	421	420	421
ML/4pb/3/1	50.1	50.3	50.7	50.7	50.5	50.2	50.5	50.6	50.6	50.5	421	421	421	420	421
ML/4pb/3/2	50.0	50.4	50.6	50.8	50.5	50.2	50.4	50.4	50.5	50.4	422	422	421	421	422
ML/4pb/3/3	50.4	50.5	50.7	50.9	50.6	50.8	50.7	50.6	50.6	50.7	422	422	422	422	422
ML/4pb/3/4	50.0	49.9	50.2	50.6	50.2	50.5	50.7	50.8	50.4	50.6	422	422	421	421	422
ML/4pb/3/5	49.8	49.8	49.8	50.2	49.9	49.6	49.7	50.0	49.9	49.8	422	422	422	422	422
ML/4pb/3/6	50.0	49.4	49.4	49.8	49.7	50.1	49.8	49.4	48.9	49.6	422	422	421	423	422
ML/4pb/3/7	50.0	50.0	50.2	50.5	50.2	49.2	49.0	49.4	49.2	49.2	422	422	422	422	422
ML/4pb/3/8	50.8	50.4	50.3	50.2	50.4	49.3	49.7	50.0	49.3	49.6	422	422	422	422	422
ML/4pb/3/9	50.3	50.5	50.7	50.9	50.6	50.1	50.0	49.9	49.4	49.9	422	422	422	422	422
ML/4pb/3/10	50.3	50.5	51.0	51.0	50.7	51.0	50.4	50.4	50.0	50.5	421	422	422	421	422
ML/4pb/4/1	50.8	50.4	50.0	49.9	50.3	50.2	50.5	50.7	50.7	50.5	420	420	420	420	420
ML/4pb/4/2	51.1	50.6	50.6	50.3	50.7	50.2	50.6	51.0	51.4	50.8	421	421	421	420	421
ML/4pb/4/3	50.6	50.8	50.7	50.6	50.7	50.1	50.3	50.4	50.6	50.4	422	420	421	421	421
ML/4pb/4/4	51.2	50.8	50.4	50.3	50.7	50.3	51.1	51.4	51.2	51.0	421	421	421	420	421
ML/4pb/4/5	50.2	50.5	50.8	51.4	50.7	50.6	50.4	50.5	50.0	50.4	421	420	421	420	421
ML/4pb/4/6	51.1	50.7	50.6	50.9	50.8	49.8	50.0	50.2	50.7	50.2	422	422	422	422	422
ML/4pb/4/7	51.0	50.7	50.4	50.2	50.6	49.4	49.9	50.0	50.4	49.9	422	421	421	422	422
ML/4pb/4/8	51.1	51.0	50.4	50.4	50.7	49.4	50.2	50.3	50.4	50.1	422	420	421	421	421
ML/4pb/4/9	51.0	50.4	50.4	50.4	50.4	49.4	49.9	50.0	50.0	49.8	422	422	422	422	422
ML/4pb/4/10	51.0	50.6	50.3	50.3	50.4	50.2	50.8	51.1	51.4	50.9	421	421	421	420	421

Appendix B: Results four-point bending tests

B.1. Introduction

The four point bending test has been carried out at 5 frequencies, namely 10, 5, 2, 1 and 0.5 Hz. Finally, a reference measurement is carried out at 10 Hz.

B.2. First determination of master curves

At temperatures of 5°C, 10°C, 15°C, 20°C, 25°C and 30°C the stiffness is determined (table 1-table 6). For each temperature and frequency the measurement is carried out four times, from which the average is taken. The tests are all displacement controlled, by using a real sinusoidal displacement signal with a strain amplitude of 80 μ m/m.

Table 13: Mix stiffness at T=5°C

Temperature:	5	°C				f	requency	1		
Specimen	date	height [mm]	width [mm]	length [mm]	10	5	2	1	0.5	10
4	19-2-2001	51.44	52.6	450	10220	8869	7149	5889	4836	10495
6	19-2-2001	50.76	53.06	450	10626	9100	7607	6291	1	10532
2	20-2-2001	50.96	52.94	449	10250	8632	7153	5822	4796	10321
3	20-2-2001	51.57	52.21	449	10408	8883	7121	5866	4817	10297
1	,	•	Average stiff	ness [MPa]	10394	8871	7258	5967	4816	
			Standard dev	iation [MPa]	166	234	263	254	28	
			Variance	[%]	1.6	2.6	3.6	4.3	0.6	

Table 2: Mix stiffness at T=10°C

TUDIO Z. IVIII	Commode	1 dt 1 – 10 O								
Temperature:	10	°C				f	requency	,		
Specimen	date	height [mm]	width [mm]	length [mm]	10 Hz	5 Hz	2 Hz	1 Hz	0.5 Hz	10 Hz
4	21-2-2001	51.44	52.6	450	6958	5712	4276	3224	2439	6974
6	21-2-2001	50.76	53.06	450	6733	5510	4065	3252	2453	6786
2	21-2-2001	50.96	52.94	449	6714	5334	3962	3120	2357	6662
3	21-2-2001	51.57	52.21	449	6677	5417	4119	3193	2346	6776
,	•	,	Average stiff	fness [MPa]	6785	5493	4106	3197	2399	
			Standard dev	iation [MPa]	120	163	131	57	55	
			Variance	[%]	1.8	3.0	3.2	1.8	2.3	

Table 3: Mix stiffness at T=15°C

Temperature:	15	°C				f	requency	<u>'</u>		
Specimen	date	height [mm]	width [mm]	length [mm]	10 Hz	5 Hz	2 Hz	1 Hz	0.5 Hz	10 Hz
4	22-2-2001	51.44	52.6	450	4068	3031	2103	1568	1185	4008
6	22-2-2001	50.76	53.06	450	3907	3110	2015	1511	1166	4135
2	22-2-2001	50.96	52.94	449	4063	3068	2022	1578	1122	4127
3	22-2-2001	51.57	52.21	449	3973	3072	2094	1580	1076	3862
	•		Average stiff	ness [MPa]	4018	3070	2059	1559	1137	
			Standard dev	iation [MPa]	99	32	46	33	49	
			Variance	[%]	2.5	1.1	2.3	2.1	4.3	

Table 4: Mix stiffness at T=20°C

Temperature:	20	°C	•			f	requency	,		
Specimen	date	height [mm]	width [mm]	length [mm]	10 Hz	5 Hz	2 Hz	1 Hz	0.5 Hz	10 Hz
4	23-2-2001	51.44	52.6	450	2190	1783	1137	876	589	2195
6	23-2-2001	50.76	53.06	450	2208	1671	1025	782	601	2300
2	23-2-2001	50.96	52.94	449	2190	1728	1081	917	558	2248
3	23-2-2001	51.57	52.21	449	2447	1755	1088	828	587	2110
,			Average stiff	ness [MPa]	2236	1734	1083	851	584	
			Standard dev	iation [MPa]	101	48	46	59	18	
			Variance	[%]	4.5	2.8	4.2	6.9	3.1	

Table 5: Mix stiffness at T=25°C

Temperature:	25	°C				f	requency	<u>'</u>		
Specimen	date	height [mm]	width [mm]	length [mm]	10 Hz	5 Hz	2 Hz	1 Hz	0.5 Hz	10 Hz
4	26-2-2001	51.44	52.6	450	1364	906	662	485	421	1367
6	26-2-2001	50.76	53.06	450	1312	990	695	486	424	1394
2	26-2-2001	50.96	52.94	449	1429	941	593	561	386	1305
3	26-2-2001	51.57	52.21	449	1423	902	625	454	451	1369
4	26-2-2001	51.44	52.6	450	1274	•	-	1	-	-
6	26-2-2001	50.76	53.06	450	1332	•	1	1	-	-
2	26-2-2001	50.96	52.94	449	1314	ı	ı	ı	-	-
3	26-2-2001	51.57	52.21	449	1328	•	ı	1	-	-
	•		Average stiff	ness [MPa]	1351	935	644	497	421	
			Standard dev	iation [MPa]	46	41	44	45	27	
			Variance	[%]	3.4	4.4	6.9	9.2	6.3	

Table 6: Mix stiffness at T=30°C

Table 0. IVII	Commos	at 1-30 C								
Temperature:	30	°C				f	requency	!		
Specimen	date	height [mm]	width [mm]	length [mm]	10 Hz	5 Hz	2 Hz	1 Hz	0.5 Hz	10 Hz
4	28-2-2001	51.44	52.6	450	800	529	418	315	317	797
6	28-2-2001	50.76	53.06	450	776	492	457	351	283	804
2	28-2-2001	50.96	52.94	449	729	520	418	349	312	811
3	28-2-2001	51.57	52.21	449	804	518	380	314	343	803
		,	Average stiff	ness [MPa]	791	515	418	332	314	
			Standard dev	iation [MPa]	27	16	31	21	25	
			Variance	[%]	3.4	3.1	7.5	6.2	7.8	

For the determination of the master curves the data shown in table 7 was used.

Table 7: Summary of the mix stiffness at different temperatures and loading times

freq [Hz]	t [s]	PLUS5	PLUS10	PLUS15	PLUS20	PLUS25	PLUS30
0.5	2	4816	2399	1137	584	421	314
1	1	5967	3197	1559	851	497	332
2	0.5	7258	4106	2059	1083	644	418
5	0.2	8871	5493	3070	1734	935	515
10	0.1	10394	6785	4018	2236	1351	791

B.3. Repeated determination of master curves

After 2.5 moths the determination of master curves has been repeated for 3 temperatures, namely 10°C, 20°C and 30°C. The tests are carried out at a strain level of $80\mu\text{m/m}$ as well as 800 $\mu\text{m/m}$. Due to the lack of specimens the tests were carried out two times for each combination of frequency and temperature. Tables 8-13 show the results for the repeated determination of master curves.

Table 8: Mix stiffness at $T=10^{\circ}$ C and $\varepsilon=80 \ \mu\text{m/m}$

Temperature:	10	°C					1	requency			
Specimen	strain [µm/m]	date	height [mm]	width [mm]	length [mm]	10 Hz	5 Hz	2 Hz	1 Hz	0.5 Hz	10 Hz
1	80	14-5-2001	52.83	50.64	450	6168	5121	3663	2809	2217	6223
4	80	14-5-2001	51.44	52.6	450	6324	5136	3763	2962	2230	6340
		•		Average stift	ness [MPa]	6264	5129	3713	2886	2224	
				Standard dev	iation [MPa]	82	11	71	108	9	
				Variance	[%]	1	0	2	4	0	

Table 9: Mix stiffness at $T=10^{\circ}$ C and $\varepsilon=800 \ \mu\text{m/m}$

Temperature:	10		1	requency							
Specimen	strain [µm/m]	date	height [mm]	width [mm]	length [mm]	10 Hz	5 Hz	2 Hz	1 Hz	0.5 Hz	10 Hz
1	800	14-5-2001	52.83	50.64	450	5629	3504	2137	1529	1104	4813
4	800	14-5-2001	51.44	52.6	450	5489	3476	2126	1510	1091	4718
				Average stiff	ness [MPa]	5162	3490	2132	1520	1098	
				Standard dev	iation [MPa]	463	20	8	13	9	
				Variance	[%]	9	1	0	1	1	

Table 10: Mix stiffness at $T=20^{\circ}$ C and $\varepsilon=80 \mu m/m$

emperature: 20 °C							frequency				
Specimen	strain [µm/m]	date	height [mm]	width [mm]	length [mm]	10 Hz	5 Hz	2 Hz	1 Hz	0.5 Hz	10 Hz
7	80	15-5-2001	50.89	52.84	450	2323	1696	1102	782	640	1978
8	80	15-5-2001	50.9	52.88	450	2048	1534	1034	732	564	2047
	•			Average stiff	ness [MPa]	2099	1615	1068	757	602	
				Standard dev	iation [MPa]	153	115	48	35	54	Ì
				Variance	[%]	7	7	5	5	9	Ì

Table 11: Mix stiffness at $T=20^{\circ}$ C and $\varepsilon=800 \ \mu\text{m/m}$

emperature: 20 °C							f	requency			10 Hz 1428 1400		
Specimen	strain [µm/m]	date	height [mm]	width [mm]	length [mm]	10 Hz	5 Hz	2 Hz	1 Hz	0.5 Hz	10 Hz		
7	800	15-5-2001	50.89	52.84	450	1452	1121	546	386	264	1428		
8	800	15-5-2001	50.9	52.88	450	1437	1068	534	362	261	1400		
		•		Average stiff	iness [MPa]	1429	1095	540	374	263			
				Standard dev	riation [MPa]	22	37	8	17	2			
				Variance	[%]	2	3	2	5	1			

Table 12: Mix stiffness at $T=30^{\circ}$ C and $\varepsilon=80 \ \mu\text{m/m}$

emperature: 30 °C							1	requency						
Specimen	strain [µm/m]	date	height [mm]	width [mm]	length [mm]	10 Hz	5 Hz	2 Hz	1 Hz	0.5 Hz	10 Hz			
3	80	15-5-2001	51.57	52.21	449	730	486	384	382	278	700			
5	80	15-5-2001	51.01	52.95	450	703	494	383	317	245	693			
	•			Average stiff	iness [MPa]	707	490	384	350	262				
				Standard deviation [MPa]		16	6	1	46	23				
				Variance	[%]	2	1	0	13	9				

Table 13: Mix stiffness at $T=30^{\circ}$ C and $\varepsilon=800 \,\mu\text{m/m}$

emperature: 30 °C							ſ	requency						
Specimen	strain [μm/m]	date	height [mm]	width [mm]	length [mm]	10 Hz	5 Hz	2 Hz	1 Hz	0.5 Hz	10 Hz			
3	800	15-5-2001	51.57	52.21	449	470	339	158	112	84	435			
5	800	15-5-2001	51.01	52.95	450	556	352	160	107	82	422			
		•		Average stiff	ness [MPa]	471	346	159	110	83				
				Standard deviation [MPa]		60	9	1	4	1				
				Variance [%]		13	3	1	3	2				

For the determination of the master curves the data shown in table 14 and 15 was used.

Table 14: Summary of the mix stiffness for ε =80 μ m/m

freq [Hz]	t [s]	PLUS10	PLUS20	PLUS30
0.5	2	2224	602	262
1	1	2886	757	350
2	0.5	3713	1068	384
5	0.2	5129	1615	490
10	0.1	6264	2099	707

Table 15: Summary of the mix stiffness for ε =800 μ m/m

and the community of the state of the parties of th											
freq [Hz]	t [s]	PLUS10	PLUS20	PLUS30							
0.5	2	1098	263	83							
1	1	1520	374	110							
2	0.5	2132	540	159							
5	0.2	3490	1095	346							
10	0.1	5162	1429	471							

B.4. Determining the strain dependent behaviour of the mix stiffness

For these tests 46 specimens of the Lintrack mix were used. The tests were carried out at temperatures of 5°C, 12.5°C, 20°C, 27.5°C, 35°C and 42.5°C. All tests are displacement controlled with a real sinusoidal displacement. The strain amplitudes that were applied are 80 $\mu\text{m/m}$, 200 $\mu\text{m/m}$, 600 $\mu\text{m/m}$ and 1000 $\mu\text{m/m}$. Each test combination is repeated once, the average of both measurements is used for the determination of the master curves. Table 16 shows the results of the measurements.

Table 16: Stiffness at different temperatures, loading times and strain levels

14510 10.00	iiiiiess at ui	nerent temper	frequency						
Specimen	T [°C]	strain [µm/m]	10Hz	5Hz	2Hz	1Hz	0.5Hz	10Hz	
ML/4pb/1/1	5	80	8870	7726	6109	5117	4062	8946	
ML/4pb/1/2	5	80	8963	7623	6176	5091	4196	9113	
ML/4pb/1/1 ML/4pb/1/1	5	200	8704	7210	5591	4473	3575	8617	
ML/4pb/1/1 ML/4pb/1/2	5	200	8823	7355	5635	4562	3639	8777	
ML/4pb/1/2 ML/4pb/1/3	5	600	9143	6532	4564	3513	2698	7854	
ML/4pb/1/3 ML/4pb/1/4	5	600	9356	6829	4848	3745	2873	8050	
ML/4pb/1/4 ML/4pb/1/5	5	1000	9414	6589	3975	2865	2118	7648	
ML/4pb/1/6	12.5	1000	8748	6089	3914	2837	2107	7225	
ML/4pb/1/7	12.5	80	5859	4583	3377	2486	1919	5721	
ML/4pb/1/8	12.5	80	5223	3939	3025	2374	1744	5239	
ML/4pb/1/7	12.5	200	5511	4214	2853	2050	1531	5427	
ML/4pb/1/8	12.5	200	4931	3797	2549	1874	1461	4878	
ML/4pb/1/9	12.5	600	4034	2786	1781	1281	922	3714	
ML/4pb/1/10	12.5	600	4094	2806	1791	1293	937	3770	
ML/4pb/2/1	12.5	1000	3840	2323	1438	1017	725	3140	
ML/4pb/2/2	12.5	1000	3638	2268	1398	994	715	3121	
ML/4pb/2/3	20	80	2190	1875	1271	1013	774	2296	
ML/4pb/2/4	20	80	2388	1904	1329	928	743	2319	
ML/4pb/2/3	20	200	2269	1658	1002	707	542	2217	
ML/4pb/2/4	20	200	2250	1687	998	748	536	2175	
ML/4pb/2/5	20	600	1819	1319	727	498	367	1776	
ML/4pb/2/6	20	600	1818	304	728	502	367	1654	
ML/4pb/2/7	20	1000	1497	932	597	403	279	1418	
ML/4pb/2/8	20	1000	1462	910	579	395	279	1406	
ML/4pb/2/9	27.5	80	1155	842	565	536	379	1188	
ML/4pb/2/10	27.5	80	1023	857	581	431	354	1084	
ML/4pb/2/9	27.5	200	1016	732	399	322	261	999	
ML/4pb/2/10	27.5	200	959	679	425	316	268	963	
ML/4pb/3/1	27.5	600	803	489	267	202	151	809	
ML/4pb/3/2	27.5	600	802	491	274	192	147	759	
ML/4pb/3/3	27.5	1000	706	461	236	150	114	728	
ML/4pb/3/4	27.5	1000	709	477	245	152	116	669	
ML/4pb/3/5	35	80	590	393	391	272	272	544	
ML/4pb/3/6	35	80	589	435	295	393	277	566	
ML/4pb/3/5	35	200	460	267	219	188	173	451	
ML/4pb/3/6	35	200	431	302	206	175	159	476	
ML/4pb/3/7	35	600	506	295	131	105	84	427	
ML/4pb/3/8	35	600	469	294	119	98	83	422	
ML/4pb/3/9	35	1000	432	306	125	73	58	459	
ML/4pb/3/10	35	1000	495	305	132	66	54	451	
ML/4pb/4/1	42.5	80	379	305	301	339	205	459	
ML/4pb/4/2	42.5	80	327	297	220	259	222	374	
ML/4pb/4/1	42.5	200	319	167	152	152	107	257	
ML/4pb/4/2	42.5	200	298	149	13	119	134	334	
ML/4pb/4/3	42.5	600	320	215	75	65	60	286	
ML/4pb/4/4	42.5	600	-	198	79	59	60	278	
ML/4pb/4/5	42.5	1000	-	-	82	48	42	-	
ML/4pb/4/6	42.5	1000	-	-	97	54	42	-	

For the determination of master curves use is made of the average stiffness that is shown in table 17.

Table 17: Summary of the mix stiffness at different temperatures, frequencies and strain levels

temp	strainlevel	10Hz	5Hz	2Hz	1Hz	0.5Hz
-			_			
T=5°C	80	8973	7675	6143	5104	4129
	200	8730	7283	5613	4518	3607
	600	8601	6681	4706	3629	2786
	1000	8259	6339	3945	2851	2113
T=12.5°C	80	5511	4261	3201	2430	1832
	200	5187	4006	2701	1962	1496
	600	3903	2796	1786	1287	930
	1000	3435	2296	1418	1006	720
T=20°C	80	2298	1890	1300	971	759
	200	2228	1673	1000	728	539
	600	1792	1312	728	500	367
	1000	1446	921	588	399	279
T=27.5°C	80	1113	850	573	484	367
	200	984	708	412	319	265
	600	793	490	271	197	149
	1000	703	469	241	151	115
T=35°C	80	572	414	393	333	275
	200	455	285	213	182	166
	600	456	295	125	102	84
	1000	437	306	129	70	56
T=42.5°C	80	385	301	261	259	214
	200	302	158	143	136	121
	600	295	207	77	62	60
	1000	Х	Х	90	51	42

Appendix C: Determination of S_{mix} as a function of temperature, loading time and strain level

C.1. Determination of the function parameters

For each combination of strain level and temperature there is a master curve as a function of the loading time t. To determine the relationship for S_{mix} as a function of t, T and ϵ , first each master curve is expressed as a function of t for a constant T and ϵ Each master curve can be expressed as follows:

$$\log S_{mix} = a + \frac{b}{\left(1 + e^{\frac{-(\log t - c)}{d}}\right)}$$
 Equation 1

The constants *a*, *b*, *c* and *d* are determined for each master curve. Tables 1-24 show the output for this parameter determination. Therefore use is made of the computer program TableCurve2D.

Table 1: Master curve ε =80 μ m/m T=5°C

	able 1. Madel daive e-de primit 1-0 C										
[Sigmoid] y=	= a+ b/(1+ ex	p(-(x-c)/d))									
		Parameters	Values	Std Error	TValue	95% Conf Lim	95% Conf Lim				
Eqn	[Sigmoid] y=	а	2.253402	0.023197	97.14304	2.205806011	2.300997571				
Eqn #	8011	b	1.942615	0.037956	51.18019	1.864734593	2.020494705				
r2	0.998197	С	1.420732	0.044066	32.24092	1.330315557	1.511147897				
DF Adj r2	0.99792	d	-1.252728	0.040864	-30.65572	-1.336574853	-1.168881143				
Fit Std Err	0.024431										
F-stat	4983.172										
Date	Jun 22, 200	1			·						
Time	11:37:02 A	М									

Table 2: Master curve ε =80 μ m/m T=12.5 °C

Table 2. IVI	Table 2. Master curve ε =00 μ m/m 1=12.0 \odot										
[Sigmoid] y=	a+ b/(1+ ex	p(-(x-c)/d))									
		Parameters	Values	Std Error	T Value	95% Conf Lim	95% Conf Lim				
Eqn	[Sigmoid] y=	а	2.253317	0.023222	97.03374	2.20566927	2.300964463				
Eqn #	8011	b	1.942923	0.038042	51.07313	1.864867515	2.020978919				
r2	0.998197	С	0.388627	0.044075	8.817324	0.298191466	0.479061757				
DF A dj r2	0.99792	d	-1.252992	0.040945	-30.60179	-1.337004289	-1.16897964				
Fit Std Err	0.024433										
F-stat	4982.458										
Date	Jun 22, 200	1									
Time	11:37:45 A	M									

Table 14: Master curve ε =80 μ m/m T=20 $^{\circ}$ C

[Sigmoid] y=	a+ b/(1+ ex	p(-(x-c)/d))					
		Parameters	Values	Std Error	T V alue	95% Conf Lim	95% Conf Lim
Eqn	[Sigmoid] y=	а	2.253135	0.023272	96.81869	2.205385527	2.300884682
Eqn #	8011	b	1.943581	0.038209	50.86765	1.865183275	2.021978332
r2	0.998196	С	-0.590893	0.044097	-13.39976	-0.68137357	-0.500413148
DF A dj r2	0.997919	d	-1.253555	0.041102	-30.49893	-1.337888898	-1.169221772
Fit Std Err	0.024437						
F-stat	4980.92						
Date	Jun 22, 200	1					
Time	11:38:25 A	М					

Table 4: Master curve ε =80 μ m/m T=27.5 °C

[Sigmoid] y=	a+ b/(1+ ex	p(-(x-c)/d))					
		Parameters	Values	Std Error	T Value	95% Conf Lim	95% Conf Lim
Eqn	[Sigmoid] y=	а	2.25276	0.023366	96.41061	2.204816667	2.300704091
Eqn #	8011	b	1.944933	0.038522	50.48894	1.865892223	2.02397328
r2	0.998195	С	-1.522022	0.044147	-34.476	-1.612604694	-1.431439185
DF Adj r2	0.997918	d	-1.254714	0.041395	-30.31068	-1.339650255	-1.169778704
Fit Std Err	0.024445						
F-stat	4977.672						
Date	Jun 22, 200	1					
Time	11:39:00 A	М					

Table 5: Master curve ε =80 μ m/m T=35 $^{\circ}$ C

	able of macter curve of the primitive of										
[Sigmoid] y=	= a+ b/(1+ ex	p(-(x-c)/d))									
		Parameters	Values	Std Error	T Value	95% Conf Lim	95% Conf Lim				
Eqn	[Sigmoid] y=	а	2.252013	0.023542	95.65926	2.203708478	2.300316971				
Eqn #	8011	b	1.947629	0.039097	49.81563	1.867408803	2.027848569				
r2	0.998193	С	-2.40878	0.044258	-54.42621	-2.49958929	-2.317970623				
DF A dj r2	0.997915	d	-1.257025	0.041931	-29.97856	-1.3430601	-1.170990275				
Fit Std Err	0.024462										
F-stat	4970.821										
Date	Jun 22, 200	1									
Time	11:39:53 A	М									

Table 6: Master curve ε =80 μ m/m T=42.5 $^{\circ}$ C

[Sigmoid] y=	= a+ b/(1+ ex	p(-(x-c)/d))					
		Parameters	Values	Std Error	T Value	95% Conf Lim	95% Conf Lim
Eqn	[Sigmoid] y=	а	2.250561	0.023864	94.30666	2.201595717	2.299526659
Eqn #	8011	b	1.952877	0.040138	48.65466	1.870521883	2.035232651
r2	0.998187	С	-3.255248	0.044499	-73.15376	-3.346551339	-3.16394374
DF A dj r2	0.997908	d	-1.261514	0.042894	-29.41013	-1.349525341	-1.17350341
Fit Std Err	0.024498						
F-stat	4956.035						
Date	Jun 22, 200	1					
Time	11:40:33 A	M					

Table 7: Master curve ε=200 μm/m T=5 $^{\circ}$ C

[Sigmoid] y=	: a+ b/(1+ ex	p(-(x-c)/d))					
		Parameters	Values	Std Error	T V alue	95% Conf Lim	95% Conf Lim
Eqn	[Sigmoid] y=	а	1.892585	0.0396	47.79304	1.811187044	1.973983314
Eqn #	8011	b	2.304665	0.059311	38.85704	2.1827483	2.426580857
r2	0.997447	С	1.667883	0.059178	28.18418	1.54624136	1.7895256
DF Adj r2	0.997039	d	-1.327189	0.054293	-24.44484	-1.43879023	-1.21558763
Fit Std Err	0.033613						
F-stat	3386.221						
Date	Jun 22, 200	1					
Time	11:41:12 A	М					

Table 8: Master curve ε =200 μ m/m T=12.5 $^{\circ}$ C

[Sigmoid] y	[Sigmoid] y= a+ b/(1+ exp(-(x-c)/d))									
		Parameters	Values	Std Error	T Value	95% Conf Lim	95% Conf Lim			
Eqn	[Sigmoid] y=	а	1.892416	0.039659	47.71668	1.810894869	1.973937102			
Eqn #	8011	b	2.305173	0.059481	38.75503	2.182908574	2.427436835			
r2	0.997447	С	0.635757	0.059187	10.74157	0.514097316	0.757416906			
DF A dj r2	0.997038	d	-1.327587	0.054436	-24.38802	-1.4394824	-1.215692571			
Fit Std Err	0.033614									
F-stat	3385.922									
Date	Jun 22, 200	1								
Time	11:41:46 A	М								

Table 9: Master curve ε =200 μ m/m T=20 $^{\circ}$ C

[Sigmoid] v=	Sigmoid] $y = a + b/(1 + exp(-(x-c)/d))$									
[aginola] y-	. ` ` ` ` ` ` ` ` ` ` ` ` ` ` ` ` ` ` `	, , , ,,								
		Parameters	Values	Std Error	T Value	95% Conf Lim	95% Conf Lim			
Eqn	[Sigmoid] y=	а	1.892071	0.039772	47.57285	1.810318272	1.973823619			
Eqn #	8011	b	2.306207	0.059796	38.56784	2.183294705	2.429120109			
r2	0.997446	С	-0.343787	0.059209	-5.806354	-0.465491866	-0.222081437			
DF Adj r2	0.997038	d	-1.328399	0.054702	-24.28441	-1.440840351	-1.215958297			
Fit Std Err	0.033617									
F-stat	3385.294									
Date	Jun 22, 200	1								
Time	11:42:18 A	M								

Table 10: Master curve ε=200 μm/m T=27.5 °C

[Sigmoid] y=	a+ b/(1+ ex	p(-(x-c)/d))					
		Parameters	Values	Std Error	T Value	95% Conf Lim	95% Conf Lim
Eqn	[Sigmoid] y=	а	1.891391	0.039978	47.31094	1.809215246	1.973566649
Eqn #	8011	b	2.308246	0.060367	38.23709	2.184160605	2.432331593
r2	0.997445	С	-1.274926	0.059261	-21.51371	-1.39673855	-1.153112768
DF Adj r2	0.997037	d	-1.329999	0.055181	-24.10267	-1.44342376	-1.216573298
Fit Std Err	0.033624						
F-stat	3383.983						
Date	Jun 22, 200	1					
Time	11:43:22 A	М					

Table 11: Master curve ε =200 μ m/m T=35 $^{\circ}$ C

[Sigmoid] y=	a+ b/(1+ ex	p(-(x-c)/d))					
		Parameters	Values	Std Error	T Value	95% Conf Lim	95% Conf Lim
Eqn	[Sigmoid] y=	а	1.89009	0.040346	46.8473	1.807157802	1.973021575
Eqn #	8011	b	2.312154	0.061376	37.67194	2.18599347	2.438313891
r2	0.997443	С	-2.161638	0.059379	-36.40419	-2.283693091	-2.039583208
DF Adj r2	0.997034	d	-1.33306	0.056024	-23.79464	-1.448218418	-1.217902246
Fit Std Err	0.033638						
F-stat	3381.188						
Date	Jun 22, 200	1					
Time	11:43:51 A	М					

Table 12: Master curve ε =200 μ m/m T=42.5 $^{\circ}$ C

[Sigmoid] y	= a+ b/(1+ ex	p(-(x-c)/d))					
		Parameters	Values	Std Error	T Value	95% Conf Lim	95% Conf Lim
Eqn	[Sigmoid] y=	а	1.887658	0.040997	46.04413	1.803388459	1.971928407
Eqn #	8011	b	2.319487	0.063144	36.73329	2.189692348	2.449281053
r2	0.997439	С	-3.007906	0.059636	-50.43793	-3.130489471	-2.88532319
DF Adj r2	0.997029	d	-1.338792	0.05749	-23.28728	-1.456964503	-1.22061871
Fit Std Err	0.033669						
F-stat	3374.942						
Date	Jun 22, 200	1					
Time	11:44:23 A	М					

Table 13: Master curve ε =600 μ m/m T=5 $^{\circ}$ C

[Sigmoid] y=	Sigmoid] y= a+ b/(1+ exp(-(x-c)/d))								
		Parameters	Values	Std Error	T Value	95% Conf Lim	95% Conf Lim		
Eqn	[Sigmoid] y=	а	1.490625	0.073642	20.24146	1.338284743	1.642965709		
Eqn #	8011	b	2.730722	0.103274	26.44165	2.517084754	2.944359846		
r2	0.995414	С	1.736468	0.095372	18.2074	1.539177009	1.933759108		
DF Adj r2	0.99458	d	-1.449282	0.084448	-17.16184	-1.623975696	-1.274588078		
Fit Std Err	0.051416								
F-stat	1663.933								
Date	Jun 22, 200	1							
Time	11:45:12 A	М							

Table 14: Master curve ε =600 μ m/m T=12.5 °C

[Sigmoid] y=	: a+ b/(1+ ex	p(-(x-c)/d))					
		Parameters	Values	Std Error	T Value	95% Conf Lim	95% Conf Lim
Eqn	[Sigmoid] y=	а	1.490057	0.073838	20.17996	1.337310134	1.642802998
Eqn #	8011	b	2.732128	0.103766	26.32969	2.517471564	2.946784503
r2	0.995416	С	0.704253	0.095385	7.38326	0.506934033	0.901572395
DF Adj r2	0.994583	d	-1.450321	0.084823	-17.09817	-1.625791032	-1.274850926
Fit Std Err	0.051401						
F-stat	1664.907						
Date	Jun 22, 200	1					
Time	11:45:43 A	М					

Table 15: Master curve ε =600 μ m/m T=20 $^{\circ}$ C

[Sigmoid] $y= a+ b/(1+ exp(-(x-c)/d))$							
		Parameters	Values	Std Error	T Value	95% Conf Lim	95% Conf Lim
Eqn	[Sigmoid] y=	а	1.488996	0.074183	20.07188	1.335536386	1.642455575
Eqn #	8011	b	2.73478	0.104628	26.1381	2.51834067	2.951220142
r2	0.995421	С	-0.275456	0.095419	-2.886813	-0.47284449	-0.07806729
DF A dj r2	0.994589	d	-1.452274	0.085478	-16.99009	-1.62909832	-1.27545003
Fit Std Err	0.051372						
F-stat	1666.762						
Date	Jun 22, 200	1					
Time	11:47:03 A	М					

Table 16: Master curve ε =600 μ m/m T=27.5 $^{\circ}$ C

[Sigmoid] y=	[Sigmoid] $y= a+ b/(1+ exp(-(x-c)/d))$						
		Parameters	Values	Std Error	T Value	95% Conf Lim	95% Conf Lim
Eqn	[Sigmoid] y=	а	1.487067	0.074774	19.88736	1.332384256	1.641749895
Eqn #	8011	b	2.739662	0.106101	25.82117	2.520174864	2.959149751
r2	0.995431	С	-1.206898	0.095495	-12.63837	-1.404443994	-1.00935204
DF Adj r2	0.9946	d	-1.455855	0.086591	-16.81293	-1.634982392	-1.276726631
Fit Std Err	0.05132						
F-stat	1670.182						
Date	Jun 22, 200	1					
Time	11:47:51 A	М					

Table 17: Master curve ε =600 μ m/m T=35 $^{\circ}$ C

[Sigmoid] y=	a+ b/(1+ ex	p(-(x-c)/d))					
		Parameters	Values	Std Error	T Value	95% Conf Lim	95% Conf Lim
Eqn	[Sigmoid] y=	а	1.483624	0.075774	19.57952	1.326873037	1.64037505
Eqn #	8011	b	2.748487	0.108585	25.31189	2.523862516	2.973112122
r2	0.995447	С	-2.094164	0.095658	-21.89209	-2.29204901	-1.896279752
DF A dj r2	0.994619	d	-1.462296	0.088457	-16.53123	-1.64528286	-1.279309977
Fit Std Err	0.051227						
F-stat	1676.296						
Date	Jun 22, 200	1					
Time	11:48:30 A	М					

Table 18: Master curve ε =600 μ m/m T=42.5 °C

[Sigmoid] y=	: a+ b/(1+ ex	p(-(x-c)/d))					
		Parameters	Values	Std Error	T Value	95% Conf Lim	95% Conf Lim
Eqn	[Sigmoid] y=	а	1.477544	0.077463	19.07429	1.317300581	1.637787763
Eqn #	8011	b	2.76429	0.112771	24.51251	2.531006449	2.997573974
r2	0.995476	С	-2.941463	0.096002	-30.63961	-3.140058005	-2.7428676
DF Adj r2	0.994653	d	-1.473765	0.091572	-16.09403	-1.663196894	-1.2843339
Fit Std Err	0.051066						
F-stat	1686.868						
Date	Jun 22, 200	1					
Time	11:49:11 A	М					

Table 19: Master curve ε =1000 μ m/m T=5 $^{\circ}$ C

ταδίο το: Madio earve ε-τουσ μπηπ τ-ο σ							
[Sigmoid] y=	[Sigmoid] $y= a+ b/(1+ exp(-(x-c)/d))$						
		Parameters	Values	Std Error	T Value	95% Conf Lim	95% Conf Lim
Eqn	[Sigmoid] y=	а	1.280908	0.135065	9.483624	1.000799801	1.561016131
Eqn #	8011	b	2.96179	0.178354	16.60623	2.591906446	3.331674451
r2	0.989465	С	1.745278	0.167896	10.39497	1.397081758	2.093473498
DF A dj r2	0.987458	d	-1.573894	0.138391	-11.37284	-1.86089881	-1.286889539
Fit Std Err	0.079155						
F-stat	688.7429						
Date	Jun 22, 200	1					
Time	11:49:52 A	M					

Table 20: Master curve ε =1000 μ m/m T=12.5 $^{\circ}$ C

[Sigmoid] y=	a+ b/(1+ ex	p(-(x-c)/d))					
		Parameters	Values	Std Error	T Value	95% Conf Lim	95% Conf Lim
Eqn	[Sigmoid] y=	а	1.279578	0.135675	9.431228	0.99820595	1.560949614
Eqn #	8011	b	2.964782	0.179725	16.49626	2.592056424	3.337508273
r2	0.989475	С	0.713004	0.168009	4.243834	0.364573673	1.061433755
DF Adj r2	0.98747	d	-1.57605	0.139399	-11.30603	-1.865145507	-1.286953533
Fit Std Err	0.079118						
F-stat	689.3982						
Date	Jun 22, 200	1					
Time	11:50:21 A	М					

Table 21: Master curve ε =1000 μ m/m T=20 $^{\circ}$ C

		σ σ τουο μιπ					
[Sigmoid] y=	[Sigmoid] y= a+ b/(1+ exp(-(x-c)/d))						
		Parameters	Values	Std Error	T Value	95% Conf Lim	95% Conf Lim
Eqn	[Sigmoid] y=	а	1.277248	0.136697	9.343623	0.993755091	1.560740731
Eqn #	8011	b	2.970118	0.182019	16.31765	2.592634062	3.347601337
r2	0.989493	С	-0.266853	0.168222	-1.586318	-0.615722835	0.082017247
DF Adj r2	0.987491	d	-1.579874	0.141083	-11.19821	-1.872461652	-1.287286312
Fit Std Err	0.07905						
F-stat	690.5908						
Date	Jun 22, 200	1					
Time	11:50:56 A	M					

Table 22: Master curve ε =1000 μ m/m T=27.5 $^{\circ}$ C

[Sigmoid] y=	a+ b/(1+ ex	p(-(x-c)/d))					
		Parameters	V alues	Std Error	T Value	95% Conf Lim	95% Conf Lim
Eqn	[Sigmoid] y=	а	1.273241	0.138386	9.20066	0.986246282	1.560235574
Eqn #	8011	b	2.979464	0.185799	16.03593	2.594139776	3.364787869
r2	0.989524	С	-1.198626	0.168611	-7.108802	-1.548304418	-0.848946794
DF Adj r2	0.987529	d	-1.586538	0.143846	-11.02942	-1.884856159	-1.288219326
Fit Std Err	0.078931						
F-stat	692.709						
Date	Jun 22, 200	1					
Time	11:51:27 A	М					

Table 23: Master curve ε =1000 μ m/m T=35 $^{\circ}$ C

		0 0 1000 pt					
[Sigmoid] y=	[Sigmoid] $y= a+ b/(1+ exp(-(x-c)/d))$						
		Parameters	Values	Std Error	T Value	95% Conf Lim	95% Conf Lim
Eqn	[Sigmoid] y=	а	1.266422	0.141158	8.97167	0.973678254	1.559165208
Eqn #	8011	b	2.995676	0.192003	15.60226	2.597486374	3.39386464
r2	0.989579	С	-2.086596	0.169319	-12.32345	-2.437742366	-1.735449674
DF A dj r2	0.987594	d	-1.598028	0.148353	-10.7718	-1.905692744	-1.290362558
Fit Std Err	0.078724						
F-stat	696.3976						
Date	Jun 22, 200	1					
Time	11:52:07 A	М					

Table 24: Master curve ε =1000 μ m/m T=42.5 $^{\circ}$ C

[Sigmoid] y=	[Sigmoid] $y= a+ b/(1+ exp(-(x-c)/d))$						
		Parameters	V alues	Std Error	T V alue	95% Conf Lim	95% Conf Lim
Eqn	[Sigmoid] y=	а	1.254824	0.14575	8.609434	0.952556933	1.557090236
Eqn #	8011	b	3.023813	0.2023	14.9472	2.604269363	3.443356742
r2	0.989672	С	-2.935371	0.170603	-17.20586	-3.289179384	-2.58156163
DF A dj r2	0.987705	d	-1.617828	0.155767	-10.38619	-1.940869833	-1.294786578
Fit Std Err	0.078372						
F-stat	702.7211						
Date	Jun 22, 200	1					
Time	11:52:39 A	M					

Tables 25-28 show a summary of the output parameters:

Table 25: Parameters for ε =80 μ m/m

and the second s								
T [°C]	а	b	С	d				
5.0	2.25	1.94	1.42	-1.25				
12.5	2.25	1.94	0.39	-1.25				
20.0	2.25	1.94	-0.59	-1.25				
27.5	2.25	1.94	-1.52	-1.25				
35.0	2.25	1.95	-2.41	-1.26				
42.5	2.25	1.95	-3.26	-1.26				

Table 26: Parameters for ε =200 μ m/m

T [°C]	а	b	С	d
5.0	1.89	2.30	1.67	-1.33
12.5	1.89	2.31	0.64	-1.33
20.0	1.89	2.31	-0.34	-1.33
27.5	1.89	2.31	-1.27	-1.33
35.0	1.89	2.31	-2.16	-1.33
42.5	1.89	2.32	-3.01	-1.34

Table 27: Parameters for ε =600 μ m/m

asio 21.1 diamotoro for a coo piritim								
T [°C]	а	b	С	d				
5.0	1.49	2.73	1.74	-1.45				
12.5	1.49	2.73	0.70	-1.45				
20.0	1.49	2.73	-0.28	-1.45				
27.5	1.49	2.74	-1.21	-1.46				
35.0	1.48	2.75	-2.09	-1.46				
42.5	1.48	2.76	-2.94	-1.47				

Table 28: Parameters for ε =1000 μ m/m

	0101010 1000 pillin	•		
T [°C]	а	b	С	d
5.0	1.28	2.96	1.75	-1.57
12.5	1.28	2.96	0.71	-1.58
20.0	1.28	2.97	-0.27	-1.58
27.5	1.27	2.98	-1.20	-1.59
35.0	1.27	3.00	-2.09	-1.60
42.5	1.25	3.02	-2.94	-1.62

From these tables it becomes clear that *a*, *b* and *d* vary with strain level and that *c* varies with strain level and temperature, so:

$$a = f(\varepsilon)$$

$$b = f(\varepsilon)$$

$$c = f(\varepsilon, T)$$

$$d = f(\varepsilon)$$

With the computer program TableCurve2D the relationship between a and ϵ is determined. This relationship is best described with:

$$a = a_1 + b_1 \ln \varepsilon$$
 Equation 2

Table 29 shows the output for the determination of the constants of equation 2.

Table 29: Determination of a as a function of ε

y= a1 + b1 ln	X						
		Parameters	V alues	Std Error	T Value	95% Conf Lim	95% Conf Lim
Eqn	y= a+ blnx	a1	3.936725	0.031141	126.4162	3.802736381	4.070714177
Eqn #	13	b1	-0.384815	0.005342	-72.03081	-0.407801125	-0.361828455
r2	0.999615						
DF Adj r2	0.998844						
Fit Std Err	0.010461						
F-stat	5188.438						
Date	Jun 22, 200	1					
Time	12:09:06 PM	M					

The relationship between b and ε is best described with:

$$b = c_1 + d_1(\log \varepsilon)^2$$
 Equation 3

Table 30 shows the output from TableCurve2D for the determination of c₁ and d₁.

Table 30: Determination of b as a function of ε

y = c1 + d1(l)	nx)^2						
		Parameters	Values	Std Error	T Value	95% Conf Lim	95% Conf Lim
Eqn	y= a+ b(lnx)^2	c1	1.273163	0.037569	33.88878	1.111517584	1.434809228
Eqn #	10	d1	0.035955	0.001051	34.20064	0.031431594	0.040478306
r2	0.998293054						
DF Adj r2	0.994879163						
Fit Std Err	0.023275391						
F-stat	1169.683554						
Date	Jun 22, 2001						
Time	12:11:01 PM						

The determination of c as a function of T and ϵ is carried out in two steps: First c is expressed as a function of T for each strain level, which is described best with:

$$c = e_1 + f_1 T$$
 Equation 4

In this equation e_1 and f_1 are dependent on the strain level. First the parameters e_1 and f_1 are determined for each strain level. The output for each strain level is shown in the tables 31-34.

Table 31: Parameter c for ε =80 μ m/m

[Line Robust None, Gaussian Errors] c= e1+ f1x								
		Parameters	Values	Std Error	T Value		95% Conf Lim	
Eqn	[Line Robust	e1	1.964268	0.061005	32.19848	1.794890594	2.133644566	
Eqn #	8160	f1	-0.124584	0.002261	-55.10604	-0.130860779	-0.118306799	
r2	0.998685							
DF A dj r2	0.997808							
Fit Std Err	0.070932							
F-stat	3036.676							
Date	Jul 9, 2001							
Time	10:35:20 PM	Л						

Table 32: Parameter c for ε =200 μ m/m

[Line Robust None, Gaussian Errors] c= e1+ f1x							
•	,	Parameters	Values	Std Error	T Value	95% Conf Lim	95% Conf Lim
Eqn	[Line Robust	e1	2.211341	0.061069	36.21078	2.041787532	2.380894716
Eqn #	8160	f1	-0.12458	0.002263	-55.04701	-0.130863626	-0.118296556
r2	0.998682						
DF A dj r2	0.997803						
Fit Std Err	0.071006						
F-stat	3030.173						
Date	Jul 9, 2001						
Time	10:36:05 PN	M					

Table 33: Parameter c for ε =600 μ m/m

[Line Robust None, Gaussian Errors] c= e1+ f1x							
		Parameters	Values	Std Error	T Value	95% Conf Lim	95% Conf Lim
Eqn	[Line Robust	e1	2.280507	0.060778	37.52201	2.111760937	2.449253745
Eqn #	8160	f1	-0.124634	0.002252	-55.33413	-0.13088733	-0.11838009
r2	0.998695						
DF Adj r2	0.997826						
Fit Std Err	0.070668						
F-stat	3061.866						
Date	Jul 9, 2001						
Time	10:36:34 PM	M					

Table 34: Parameter c for ε =1000 μ m/m

[Line Robust None, Gaussian Errors] y= e1+ f1x							
		Parameters	Values	Std Error	T Value	95% Conf Lim	95% Conf Lim
Eqn	[Line Robust	e1	2.290103	0.060347	37.9492	2.122554538	2.457652278
Eqn #	8160	f1	-0.1247	0.002236	-55.75937	-0.13090948	-0.118491
r2	0.998715						
DF Adj r2	0.997859						
Fit Std Err	0.070166						
F-stat	3109.107						
Date	Jul 9, 2001						
Time	10:37:12 PN	M					

Table 35 shows an overview of the parameters e_1 and f_1 for different strain levels.

Table 35: Overview of the parameters e_1 and f_1 for different strain levels

ε μm/m	e ₁	f ₁
80	1.964268	-0.12484
200	2.211341	-0.12458
600	2.280507	-0.12463
1000	2.290103	-0.12470

From this table it becomes clear that e_1 is a function of ε and that f_1 is constant, namely -0.124624 (average of the four values in table 35)

The second step is the determination of e_1 as a function of ϵ . This relationship is best described with:

$$e_1 = g_1 + h_1 \varepsilon^{-1.5}$$
 Equation 5

Table 36 shows the determination of the parameters g₁ and h₁.

Table 36: Determination of g_1 and h_1

e1 = g1 + h1/	x^(1.5)						
		Parameters	Values	Std Error	T Value	95% Conf Lim	95% Conf Lim
Eqn	$y = a + b/x^{(1.5)}$	g1	2.296692	0.000724	3171.604	2.293576674	2.299808138
Eqn #	18	h1	-238.0479	1.003299	-237.2651	-242.3647937	-233.731096
r2	0.999964474						
DF Adj r2	0.999893422						
Fit Std Err	0.001111548						
F-stat	56294.73836						
Date	Jun 25, 2001						
Time	1:17:43 PM						

The relationship for c as a function of ε and T is obtained by combining equation 4 and 5:

$$c = f_1 T + g_1 + \frac{h_1}{\varepsilon \sqrt{\varepsilon}}$$
 Equation 6

The relationship between d and ε is best described with:

$$d = i_1 + j_1 \sqrt{\varepsilon}$$
 Equation 7

Table 37 shows the output for the determination of i_1 and j_1 .

Table 37: Determination of i_1 and j_1

$y = i1 + j1x^{0.5}$	5)						
		Parameters	Values	Std Error	T Value	95% Conf Lim	95% Conf Lim
Eqn	$y= a+ bx^{(0.5)}$	i1	-1.124671	0.018917	-59.45162	-1.206065681	-1.0432756
Eqn #	12	j1	-0.014312	0.000873	-16.40178	-0.018066583	-0.01055764
r2	0.992620425						
DF Adj r2	0.977861274						
Fit Std Err	0.015405155						
F-stat	269.0183046						
Date	Jun 22, 2001						
Time	12:12:15 PM						

The relationship for the mix stiffness is obtained by combining the equations 2, 3, 6 and 7:

$$\log S_{mix}(\varepsilon,t,T) = a_1 \ln \varepsilon + b_1 + \frac{c_1 + d_1 (\ln \varepsilon)^2}{1 + e^{\left(\frac{-(\log t + f_1 T + g_1 + h_1 \varepsilon^{-1.5})}{i_1 + j_1 \varepsilon^{0.5}}\right)}}$$
Equation 8

The parameters in this equation are:

```
: -0.38481
b_1
        : 3.936725
C_1
        : 1.273163
d_1
        : 0.035955
        : 0.124624
f_1
        : -2.296692
g_1
h_1
        : 238.0479
        : -1.124671
i_1
        :-0.014312
```

The final step is rewriting $a_1 ln \varepsilon$ as $alog \varepsilon$ and $d_1 (ln \varepsilon)^2$ as $d(log \varepsilon)^2$. Therefore equation 9 is used:

```
\ln \varepsilon = 2.3025851 \log \varepsilon
```

Equation 9

The final equation that describes the mix stiffness as a function of loading time, temperature and strain level becomes:

$$\log S_{mix}(\varepsilon,t,T) = a\log \varepsilon + b + \frac{c + d(\log \varepsilon)^2}{1 + e^{\frac{-(\log t + fT + g + h\varepsilon^{-1.5})}{i + j\varepsilon^{0.5}}}}$$
 Equation 10

in which:

 S_{mix} : mix stiffness [MPa] ε : strain [μ m/m] t : loading time [s] T : temperature [°C]

The constants a-j are:

```
: -0.88607
а
       : 3.936725
b
С
       : 1.273163
d
       : 0.190629
f
       : 0.124624
       : -2.296692
g
h
       : 238.0479
i
       : -1.124671
       :-0.014312
```

C.2. Accuracy of the function for S_{mix}

The accuracy of equation 10 is analysed by comparing the predicted stiffness ($S_{mixpred}$) with the measured stiffness (S_{mix}). Tables 38 and 39 show the comparison for the stiffness at ϵ =80 μ m/m.

Table 38: Comparison between the predicted and measured stiffness for 5, 12.5 and 20 $^{\circ}$ C and ε =80 μ m/m

eps=80 T=5		·	
t = 5	Smix	Smixpred	diff
2	4129	4148	0
1	5104	5160	1
0.5	6143	6267	2
0.2	7675	7797	2 2
0.1	8973	8944	0
21.5238	1832	1719	-6
10.7619	2430	2253	-7
5.380951	3201	2929	-9
2.15238	4261	4048	-5
1.07619	5511	5048	-8
205.1072	759	741	-2
102.5536	971	946	-3
51.27681	1300	1226	-6
20.51072	1890	1752	-7
10.25536	2298	2295	0
1746.511	367	401	9
873.2554	484	477	-1
436.6277	573	581	1
174.6511	850	783	-8
87.32554	1113	1003	-10
13398.62	275	277	1
6699.31	333	308	-8
3349.655	393	349	-11
1339.862	414	427	3
669.931	572	513	-10
93299.24	214	226	5
46649.62	259	239	-8
23324.81	261	258	-1
9329.924	301	292	-3
4664.962	385	328	-15

eps=80			
T=12.5			
t	Smix	Smixpred	diff
2.00	1832	1877	2
1.00	2430	2455	1
0.50	3201	3179	-1
0.20	4261	4358	2
0.10	5511	5394	-2
0.19	4129	4462	8
0.09	5104	5509	8
0.05	6143	6637	8
0.02	7675	8171	6
0.01	8973	9304	4
19.06	759	800	5
9.53	971	1027	6
4.76	1300	1337	3
1.91	1890	1913	1
0.95	2298	2501	9
162.29	367	423	15
81.14	484	507	5
40.57	573	623	9
16.23	850	846	0
8.11	1113	1091	-2
1245.00	275	286	4
622.50	333	320	-4
311.25	393	365	-7
124.50	414	452	9
62.25	572	547	-4
8669.40	214	230	7
4334.70	259	245	-5
2167.35	261	265	2
866.94	301	302	0
433.47	385	342	-11

T=20			
t	Smix	Smixpred	diff
2	759	829	9
1	971	1067	10
0.5	1300	1391	7
0.2	1890	1990	5
0.1	2298	2599	13
0.019502	4129	4610	12
0.009751	5104	5672	11
0.004875	6143	6807	11
0.00195	7675	8341	9
0.000975	8973	9466	5
0.209879	1832	1953	7 5
0.104939	2430	2552	
0.05247	3201	3298	3
0.020988	4261	4504	6
0.010494	5511	5555	1
17.03022	367	434	18
8.515111	484	522	8
4.257555	573	643	12
1.703022	850	878	3
0.851511	1113	1134	3 2 5
130.6499	275	290	5
65.32495	333	325	-2
32.66248	393	373	-5
13.06499	414	464	12
6.532495	572	564	-1
909.7607	214	232	8
454.8803	259	247	-4
227.4402	261	268	3
90.97607	301	307	3 2 -9
45.48803	385	349	-9

Table 39: Comparison between the predicted and measured stiffness for 27.5, 35 and 42.5°C and ε =80 μ m/m

eps=80		7	-
T=27.5			
t	Smix	Smixpred	diff
2	367	433	18
1	484	520	7
0.5	573	641	12
0.2	850	874	3
0.1	1113	1129	1
0.00229	4129	4595	11
0.001145	5104	5655	11
0.000573	6143	6790	11
0.000229	7675	8323	8
0.000115	8973	9450	5
0.024648	1832	1945	6
0.012324	2430	2542	5
0.006162	3201	3286	3
0.002465	4261	4489	5
0.001232	5511	5538	0
0.234877	759	826	9
0.117438	971	1063	9
0.058719	1300	1386	7
0.023488	1890	1982	5
0.011744	2298	2589	13
15.3433	275	290	5
7.671651	333	325	-2
3.835825	393	372	-5
1.53433	414	463	12
0.767165	572	562	-2
106.8407	214	231	8
53.42037	259	247	-5
26.71018	261	268	3
10.68407	301	307	2
5.342037	385	348	-10

	eps=80					
ı	T=35			1:77		
	t	Smix	Smixpred	diff		
	2	275	285	4		
	1	333	318	-4		
	0.5	393	364	-8		
	0.2	414	449	9		
	0.1	572	543	-5 7		
	0.000299	4129	4430			
	0.000149	5104	5473	7 7		
	7.46E-05	6143	6599	7		
	2.99E-05	7675	8133	6		
	1.49E-05	8973	9268	3		
	0.003213	1832	1860	2		
	0.001606	2430	2434	0		
	0.000803	3201	3153	-2 2 -3		
	0.000321	4261	4326	2		
	0.000161	5511	5358	-3		
	0.030616	759	794	5		
	0.015308	971	1018	5		
	0.007654	1300	1325	2		
	0.003062	1890	1896	0		
	0.001531	2298	2479	8		
	0.2607	367	421	15		
	0.13035	484	504	4		
	0.065175	573	618	8		
	0.02607	850	840	-1		
	0.013035	1113	1081	-3		
	13.92669	214	229	7		
	6.963347	259	244	-6		
	3.481674	261	264	1		
	1.392669	301	301	0		
	0.696335	385	340	-12		

eps=80					
T=42.5					
t	Smix	Smixpred	diff		
2	214	225	5		
1	259	239	-8		
0.5	261	258	-1		
0.2	301	291	-3		
0.1	385	327	-15		
4.28728E-05	4129	4134	0		
2.14364E-05	5104	5144	1		
1.07182E-05	6143	6249	2		
4.28728E-06	7675	7779	1		
2.14364E-06	8973	8927	-1		
0.000461393	1832	1712	-7		
0.000230696	2430	2244	-8		
0.000115348	3201	2917	-9		
4.61393E-05	4261	4034	-5		
2.30696E-05	5511	5032	-9		
0.004396761	759	738	-3 -3		
0.00219838	971	942	-3		
0.00109919	1300	1222	-6		
0.000439676	1890	1745	-8		
0.000219838	2298	2286	-1		
0.037438905	367	400	9		
0.018719452	484	476	-2		
0.009359726	573	579	1		
0.00374389	850	780	-8		
0.001871945	1113	999	-10		
0.287218201	275	276	0		
0.143609101	333	307	-8		
0.07180455	393	348	-11		
0.02872182	414	426	3		
0.01436091	572	511	-11		

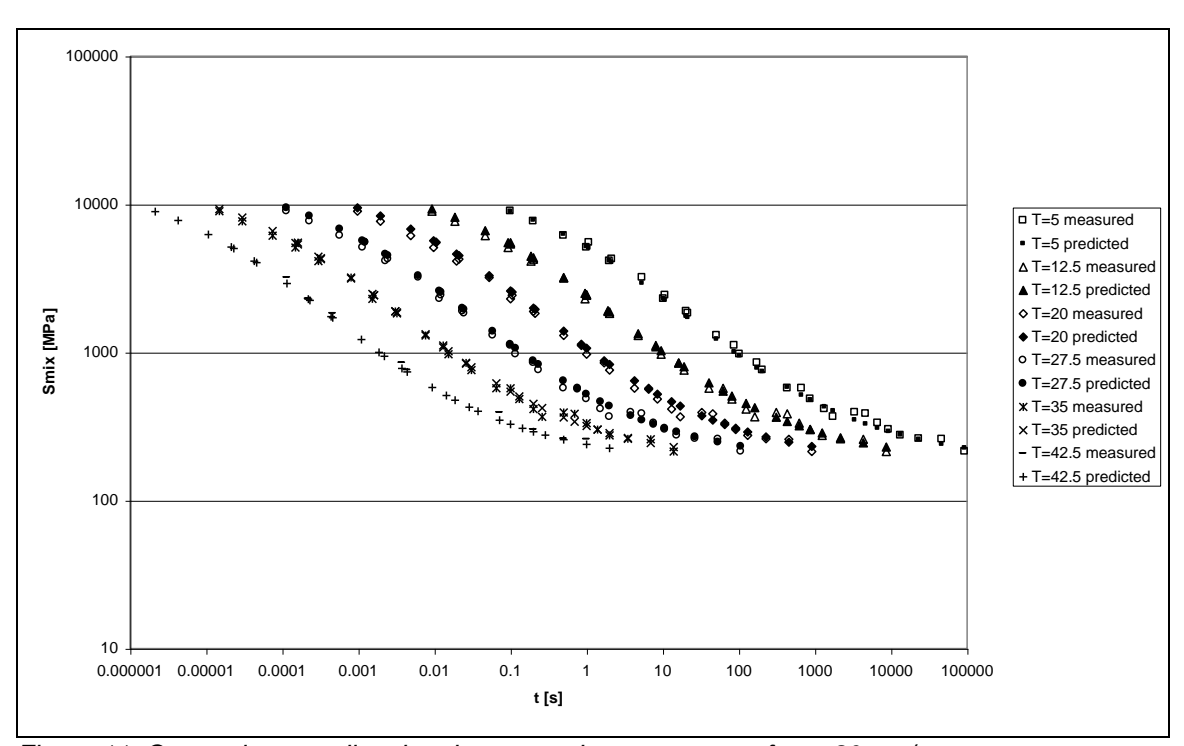


Figure 1 shows the comparison for the predicted and measured master curves.

Figure 11: Comparison predicted and measured master curves for ε =80 μ m/m

eps=200

For ϵ =200 μ m/m the comparison between the predicted and measured stiffness is shown in Tables 40 and 41.

Table 40: Comparison between the predicted and measured stiffness for 5, 12.5 and 20 $^{\circ}$ C and ε =200 μ m/m

	eps=200					
	T=5					
I	t	Smix	Smixpred	diff		
I	2	3607	3575	-1		
	1	4518	4478	-1		
	0.5	5613	5466	-3		
ı	0.2	7283	6839	-6		
	0.1	8730	7877	-10		
	21.5238	1496	1409	-6		
	10.7619	1962	1885	-4		
	5.380951	2701	2488	-8		
	2.15238	4006	3486	-13		
	1.07619	5187	4378	-16		
	205.1072	539	544	1		
	102.5536	728	723	-1		
	51.27681	1000	971	-3		
	20.51072	1673	1439	-14		
	10.25536	2228	1923	-14		
	1746.511	265	256	-3		
	873.2554	319	319	0		
	436.6277	412	407	-1		
	174.6511	708	581	-18		
ı	87.32554	984	774	-21		
	13398.62	166	155	-6		
	6699.31	182	180	-1		
	3349.655	213	213	0		
I	1339.862	285	277	-3		
I	669.931	455	349	-23		
١	93299.24	121	116	-4		
١	46649.62	136	126	-7		
١	23324.81	143	141	-2		
l	9329.924	158	167	6		

T=12.5			
t	Smix	Smixpred	diff
2	1496	1550	4
1	1962	2066	5
0.5	2701	2711	0
0.2	4006	3762	-6
0.1	5187	4686	-10
0.185841	3607	3855	7
0.09292	4518	4789	6
0.04646	5613	5797	3
0.018584	7283	7177	-1
0.009292	8730	8205	-6
19.05864	539	596	11
9.529321	728	795	9
4.76466	1000	1069	7
1.905864	1673	1582	-5
0.952932	2228	2106	-5
162.2864	265	274	3
81.14322	319	344	8
40.57161	412	442	7
16.22864	708	636	-10
8.114322	984	851	-14
1245.005	166	163	-2
622.5024	182	189	4
311.2512	213	226	6
124.5005	285	298	5
62.25024	455	378	-17
8669.401	121	119	-2
4334.701	136	131	-4
2167.35	143	146	2
866.9401	158	176	11

T=20			
t	Smix	Smixpred	diff
2 1	539	621	15
1	728	830	14
0.5	1000	1117	12
0.2	1673	1651	-1 -2
0.1	2228	2194	-2
0.019502	3607	3987	11
0.009751	4518	4934	9
0.004875	5613	5950	6
0.00195	7283	7330	1
0.000975	8730	8353	-4
0.209879	1496	1618	8
0.104939	1962	2153	10
0.05247	2701	2818	4
0.020988	4006	3892	-3 -7
0.010494	5187	4830	-7
17.03022	265	283	7
8.515111	319	356	12
4.257555	412	460	12
1.703022	708	664	-6
0.851511	984	889	-10
130.6499	166	166	0
65.32495	182	194	7
32.66248	213	233	9
13.06499	285	308	8
6.532495	455	392	-14
909.7607	121	120	0
454.8803	136	133	-2
227.4402	143	149	4
90.97607	158	180	14

eps=200

Table 41: Comparison between the predicted and measured stiffness for 27.5, 35 and 42.5°C and ε =200 μ m/m

eps=200			μ,	eps=200				eps=200			
T=27.5				T=35				T=42.5			
t	Smix	Smixpred	diff	t	Smix	Smixpred	diff	t	Smix	Smixpred	diff
2	265	282	6	. 2	166		-3	2		116	
1	319	355	-	1	182	188	4	1	136	-	
0.5		458		0.5	213		6	0.5	143	-	
0.2		661	-7	0.2	285		4	0.2	158		6
0.1	984	885	-10	0.1	455	375	-18	4.28728E-05	3607	3562	-1
0.00229	3607	3974	10	0.000299	3607	3826	6	2.14364E-05	4518	4463	-1
0.001145	4518	4919	9	0.000149	4518	4757	5	1.07182E-05	5613	5450	-3
0.000573	5613	5934	6	7.46E-05	5613	5763	3	4.28728E-06	7283	6823	-6
0.000229	7283	7315	0	2.99E-05	7283	7142	-2	2.14364E-06	8730	7861	-10
0.000115	8730	8338	-4	1.49E-05	8730	8172	-6	0.000461393	1496	1403	-6
0.024648	1496	1611	8	0.003213	1496	1535	3	0.000230696	1962	1877	-4
0.012324	1962	2144	9	0.001606	1962	2047	4	0.000115348	2701	2478	-8
0.006162	2701	2807	4	0.000803	2701	2688	0	4.61393E-05	4006	3473	-13
0.002465	4006	3879	-3	0.000321	4006	3734	-7	2.30696E-05	5187	4363	-16
0.001232	5187	4815	-7	0.000161	5187	4654	-10	0.004396761	539	542	1
0.234877	539	619	15	0.030616	539	590	10	0.00219838	728	720	-1
0.117438	728	827	14	0.015308	728	787	8	0.00109919	1000	967	-3
0.058719	1000	1112	11	0.007654	1000	1059	6	0.000439676	1673	1432	-14
0.023488	1673	1644	-2 -2	0.003062	1673	1567	-6	0.000219838	2228	1915	-14
0.011744	2228	2185	-2	0.001531	2228	2087	-6	0.037438905	265	255	-4
15.3433		166		0.2607	265		3	0.018719452	319		
7.671651	-	194	-	0.13035	319	-	7	0.009359726	412		
3.835825	_	232	9	0.065175	412		6	0.00374389	708	578	-
1.53433		307	8	0.02607	708		-11	0.001871945	984	771	-22
0.767165		391	-14	0.013035	984		-14	0.287218201	166		
106.8407	1	120		13.92669	121	119	-2	0.143609101	182	179	
53.42037		132	-3	6.963347	136		-4	0.07180455	213		
26.71018	_	149		3.481674	143	-	2	0.02872182	285		-3
10.68407	158	179	13	1.392669	158	175	11	0.01436091	455	348	-24

The predicted and measured master curves for ε =200 μ m/m are compared in figure 2.

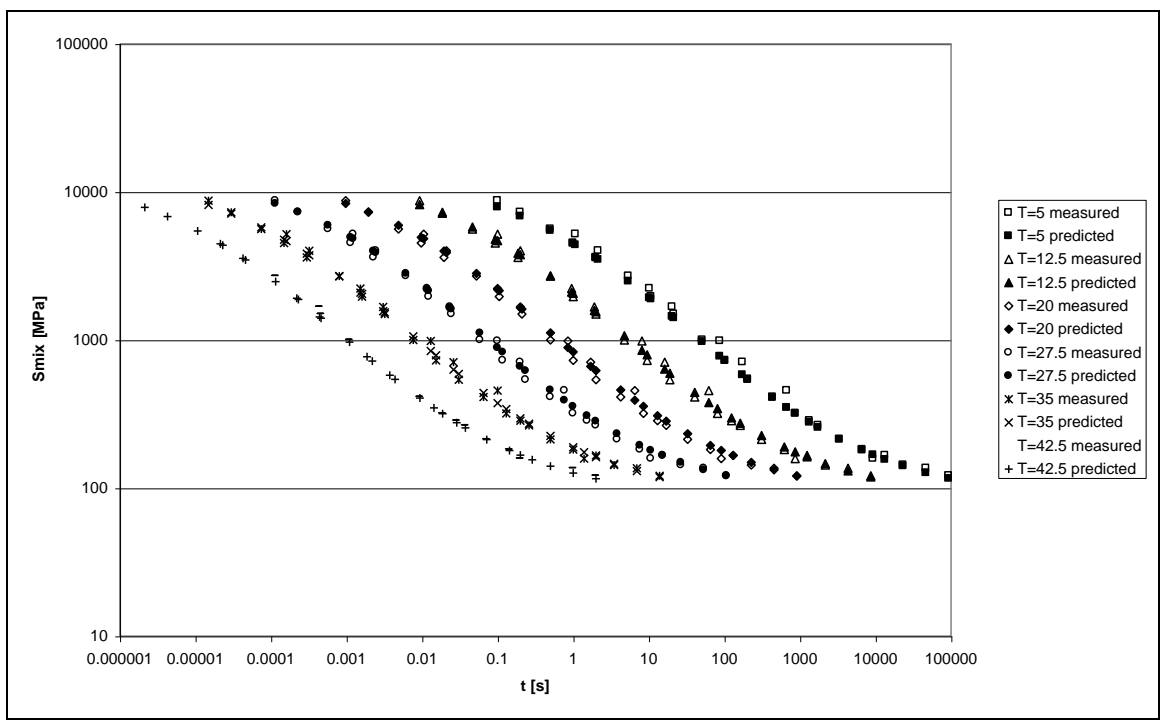


Figure 2: Comparison predicted and measured master curves for ε =200 μ m/m

For ϵ =600 μ m/m the comparison between the predicted and measured stiffness is shown in Tables 42 and 43.

Table 42: Comparison between the predicted and measured stiffness for 5, 12.5 and 20°C and ε =600 μ m/m

eps=600

T=12.5			
t	Smix	Smixpred	diff
2	930	1102	18
1	1287	1503	17
0.5	1786	2019	13
0.2	2796	2895	4
0.1	3903	3702	-5
0.185841	2786	2975	7
0.09292	3629	3794	5
0.04646	4706	4718	0
0.018584	6681	6057	-9
0.009292	8601	7115	-17
19.05864	367	390	6
9.529321	500	535	7
4.76466	728	738	1
162.2864	149	162	9
81.14322	197	211	7
40.57161	271	280	3
1245.005	84	86	2
622.5024	102	104	2
311.2512	125	129	3 2 2 3 -5
8669.401	60	57	-5
4334.701	62	64	4
2167.35	77	75	-3

T=20				
t	Smix	Smixpred	diff	
2	367	408	11	
1	500	561	12	
0.5	728	774	6	
0.2	1312	1180	-10	
0.1	1792	1605	-10	
0.019502	2786	3088	11	
0.009751	3629	3924	8	
0.004875	4706	4862	3	
0.00195	6681	6212	-7	
0.000975	8601	7272	-15	
0.05247	1786	2106	18	
0.020988	2796	3007	8	
0.010494	3903	3830	-2	
17.03022	149	168	13	
8.515111	197	219	11	
4.257555	271	293	8	
130.6499	84	88	5	
65.32495	102	107	5	
32.66248	125	133	7	
909.7607	60	58	-4	
454.8803	62	66	6	
227.4402	77	77	0	

Table 43: Comparison between the predicted and measured stiffness for 27.5, 35 and 42.5 $^{\circ}$ C and ε =600 μm/m

eps=600

46649.62 23324.81

T=27.5			
t	Smix	Smixpred	diff
2	149	167	12
1	197	218	11
0.5	271	291	8
0.2	490	437	-11
0.00229	2786	3077	10
0.001145	3629	3911	8
0.000573	4706	4847	3
0.000229	6681	6196	-7
0.000115	8601	7256	-16
0.002465	2796	2995	7
0.001232	3903	3817	-2
0.234877	367	407	11
0.117438	500	558	12
0.058719	728	770	6
0.023488	1312	1174	-11
0.011744	1792	1597	-11
15.3433	84	88	4
7.671651	102	107	5
3.835825	125	133	6
106.8407	60	58	-4
53.42037	62	66	6
26 71010	77	76	4

eps=600
T=35

t	Smix	Smixpred	diff
2	84	85	1
1	102	103	1
0.5	125	128	2
0.000299	2786	2950	6
0.000149	3629	3765	4
7.46E-05	4706	4686	0
2.99E-05	6681	6023	-10
0.003213	930	1090	17
0.001606	1287	1488	16
0.000803	1786	2000	12
0.000321	2796	2871	3
0.000161	3903	3673	-6
0.030616	367	386	5
0.015308	500	529	6
0.007654	728	730	0
0.2607	149	160	8
0.13035	197	209	6
0.065175	271	277	2
0.02607	490	415	-15
13.92669	60	57	-6
6.963347	62	64	4
3.481674	77	74	-3

eps=600

eps=600

T=42.5						
t	Smix	Smixpred	diff			
2	60	55	-9			
1	62	62	-1			
0.5	77	71	-8			
4.28728E-05	2786	2725	-2			
2.14364E-05	3629	3504	-3			
1.07182E-05	4706	4395	-7			
4.28728E-06	6681	5705	-15			
2.14364E-06	8601	6755	-21			
0.000461393	930	990	6			
0.000230696	1287	1355	5			
0.000115348	1786	1831	3			
4.61393E-05	2796	2650	-5			
2.30696E-05	3903	3416	-12			
0.004396761	367	351	-4			
0.00219838	500	480	-4			
0.00109919	728	662	-9			
0.037438905	149	149	0			
0.018719452	197	192	-2			
0.009359726	271	254	-6			
0.287218201	84	81	-4			
0.143609101	102	97	-5			
0.07180455	125	119	-4			

The predicted and measured master curves for $\epsilon \!\!=\!\! 600~\mu\text{m/m}$ are compared in figure 3.

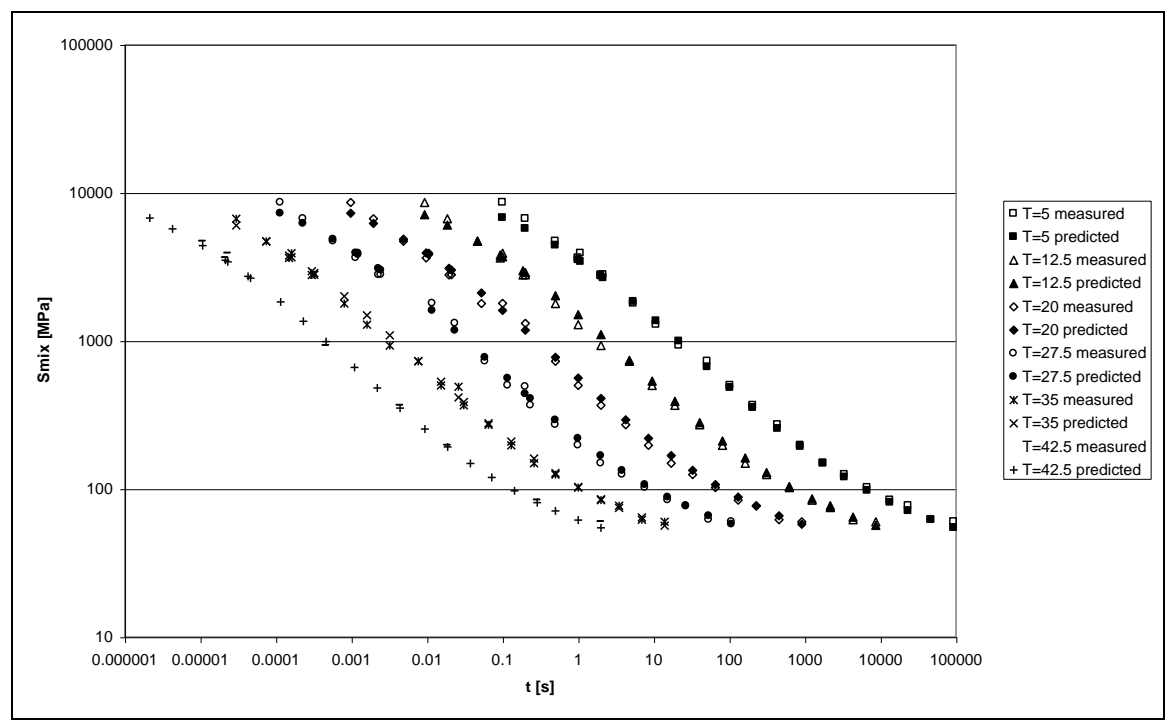


Figure 3: Comparison predicted and measured master curves for ε =600 μ m/m

Finally, the predicted and measured stiffness at a strain level of 1000 μ m/m is compared in Tables 44 and 45.

Table 44: Comparison between the predicted and measured stiffness for 5, 12.5 and 20 $^{\circ}$ C and ε =1000 μ m/m

eps=1000			
T=5			
t	Smix	Smixpred	diff
2	2113	2410	14
1	2851	3135	10
0.5	3945	3983	1
0.2	6339	5271	-17
10.7619	1006	1173	17
5.380951	1418	1597	13
2.15238	2296	2341	2
1.07619	3435	3052	-11
205.1072	279	296	6
102.5536	399	408	2
51.27681	588	565	-4
20.51072	921	871	-5
10.25536	1446	1199	-17
1746.511	115	121	5
873.2554	151	158	5
436.6277	241	212	-12
13398.62	56	63	12
6699.31	70	77	9
93299.24	42	40	-4
46649.62	51	46	-9

eps=1000			
T=12.5			
t	Smix	Smixpred	diff
0.5	1418	1759	24
0.2	2296	2556	11
0.1	3435	3308	-4
0.185841	2113	2630	24
0.09292	2851	3396	19
0.04646	3945	4282	9
0.018584	6339	5608	-12
0.009292	8259	6692	-19
19.05864	279	328	17
9.529321	399	453	13
4.76466	588	628	7
1.905864	921	967	5
0.952932	1446	1327	-8
162.2864	115	132	14
81.14322	151	174	15
40.57161	241	233	-3
1245.005	56	67	19
622.5024	70	82	17
8669.401	42	42	0
4334,701	51	49	-5

eps=1000			
T=20			
t	Smix	Smixpred	diff
2	279	344	23
1	399	475	19
0.5	588	659	12
0.2	921	1014	10
0.1	1446	1388	-4
0.019502	2113	2735	29
0.009751	2851	3519	23
0.004875	3945	4422	12
0.00195	6339	5764	-9
0.000975	8259	6856	-17
0.05247	1418	1837	30
0.020988	2296	2659	16
0.010494	3435	3430	0
17.03022	115	137	19
8.515111	151	181	20
4.257555	241	244	1
130.6499	56	69	23
65.32495	70	85	21
909.7607	42	43	2
454.8803	51	50	-2

ans-1000

Table 45: Comparison between the predicted and measured stiffness for 27.5, 35 and 42.5°C and ε =1000 μ m/m

ps=1000 =27.5				eps=1000 T=35				eps=1000 T=42.5	
	Smix	Smixpred	diff	t	Smix	Smixpred	diff	t	1
2	115	136	19	2	56	66	18		2
1	151	180	19	1	70	82	17		1
0.5	241	243	1	0.000299	2113	2607	23	4.28728E-0	5
0.00229	2113	2724	29	0.000149	2851	3368	18	2.14364E-0	5
0.001145	2851	3506	23	7.46E-05	3945	4251	8	1.07182E-0	5
0.000573	3945	4408	12	2.99E-05	6339	5573	-12	4.28728E-0	6
0.000229	6339	5749	-9	1.49E-05	8259	6656	-19	0.00023069	6
0.000115	8259	6839	-17	0.000803	1418	1742	23	0.00011534	8
0.006162	1418	1829	29	0.000321	2296	2534	10	4.61393E-0	5
0.002465	2296	2649	15	0.000161	3435	3282	-4	2.30696E-0	5
0.001232	3435	3418	-1	0.030616	279	324	16	0.00439676	1
0.234877	279	342	23	0.015308	399	448	12	0.0021983	8
0.117438	399	473	18	0.007654	588	622	6	0.0010991	9
0.058719	588	656	12	0.003062	921	956	4	0.00043967	6
0.023488	921	1009	10	0.001531	1446	1313	-9	0.00021983	8
0.011744	1446	1382	-4	0.2607	115	131	14	0.03743890	5
15.3433	56	69	22	0.13035	151	172	14	0.01871945	2
7.671651	70	85	21	0.065175	241	231	-4	0.00935972	6
106.8407	42	43	2	13.92669	42	42	0	0.28721820	1
53.42037	51	50		6.963347	51	48	-5	0.14360910	1

The master curves for ϵ =1000 μ m/m are compared in figure 4.

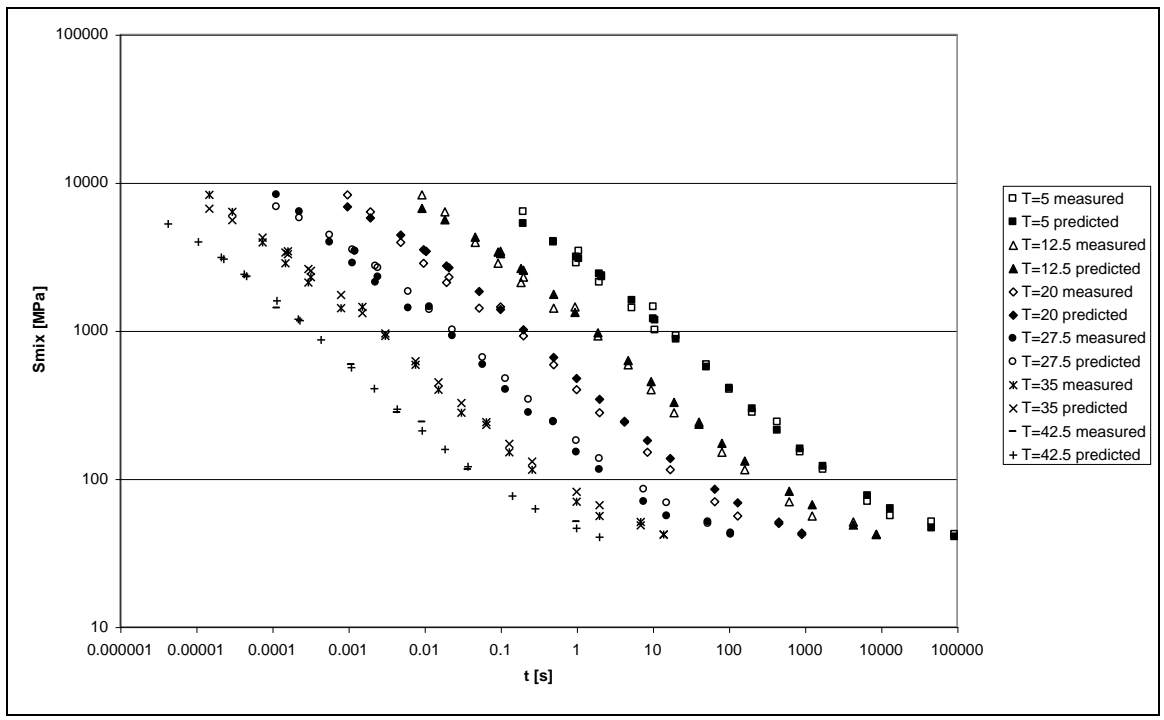


Figure 4: Comparison predicted and measured master curves for ε=1000μm/m

Smixpred diff

Appendix D: Nomographs

This appendix presents fatigue design nomographs for loading speeds of 1, 11, 54 and 108 km/h. They are shown in figures 1, 2, 3 and 4.

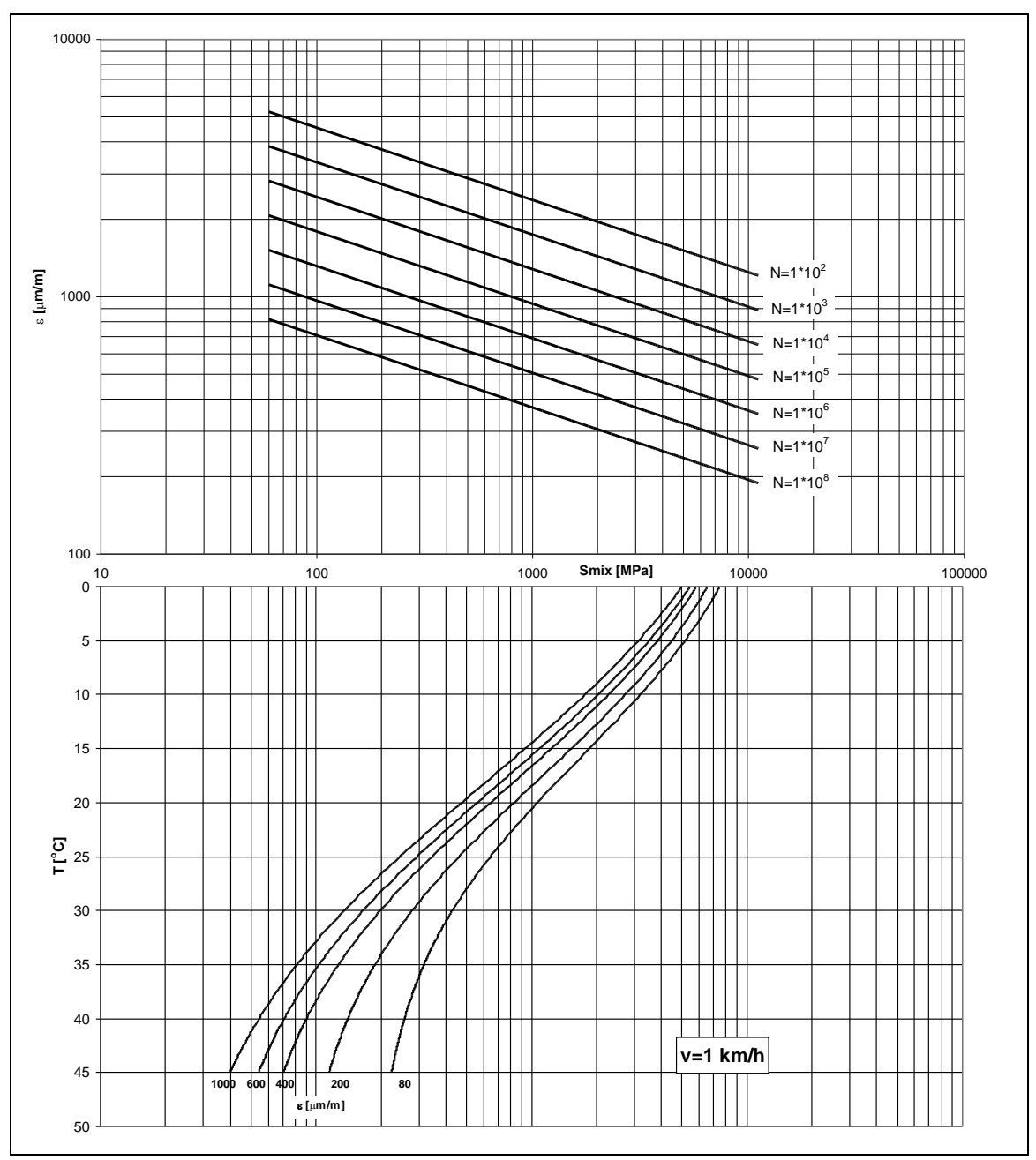


Figure 1: Fatigue design nomograph for 1 km/h

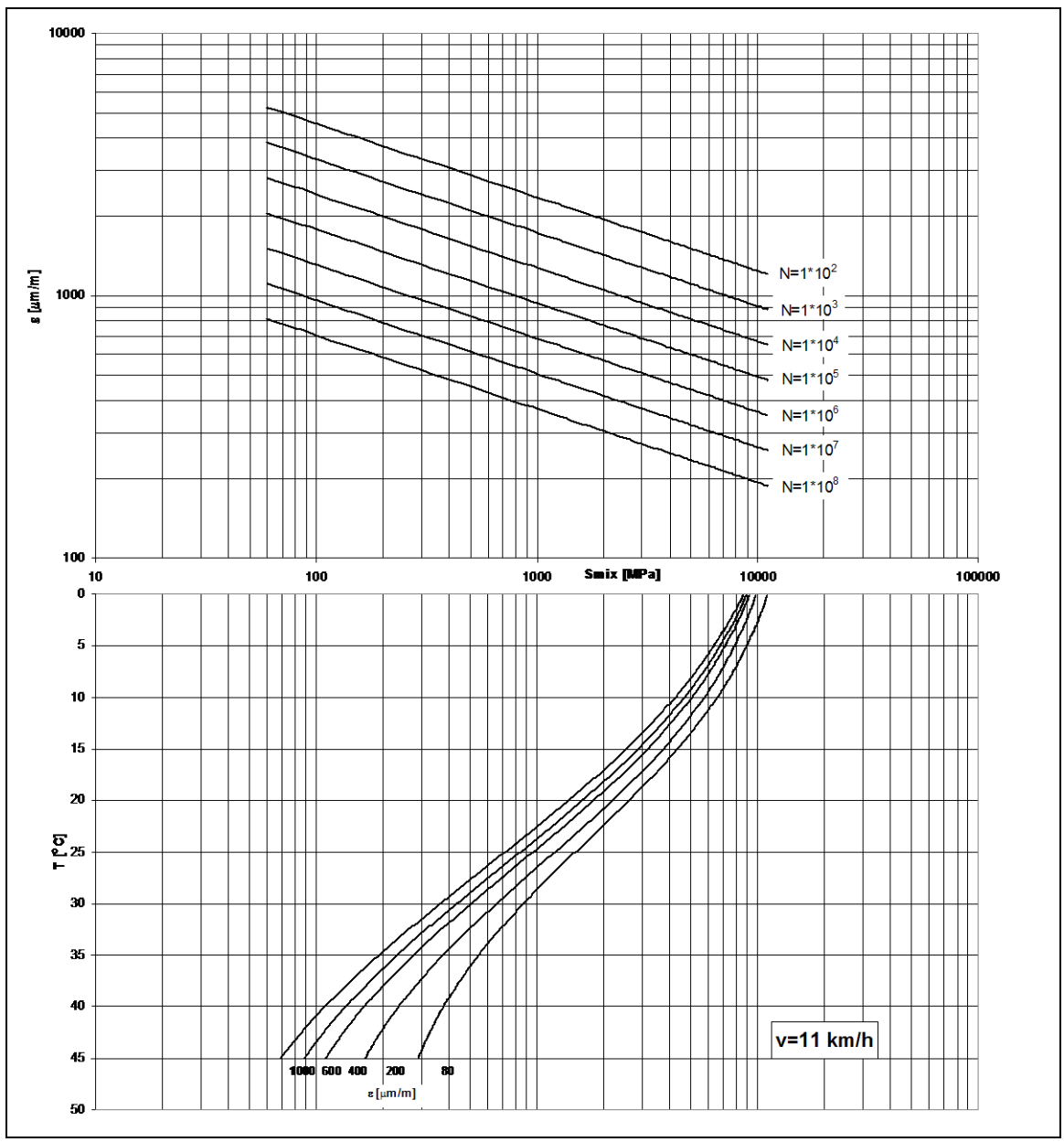


Figure 2: Fatigue design nomograph for 11 km/h

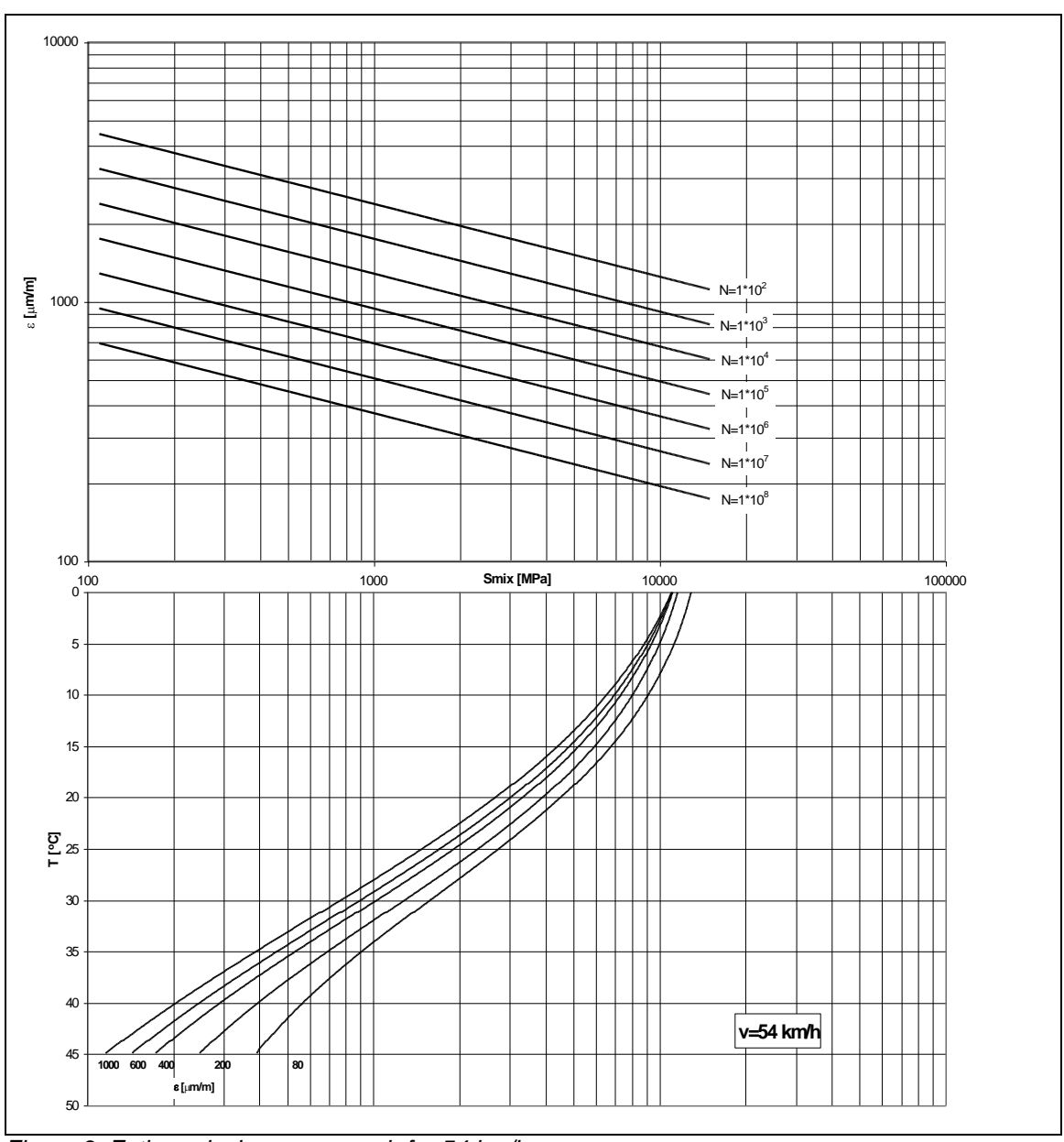


Figure 3: Fatigue design nomograph for 54 km/h

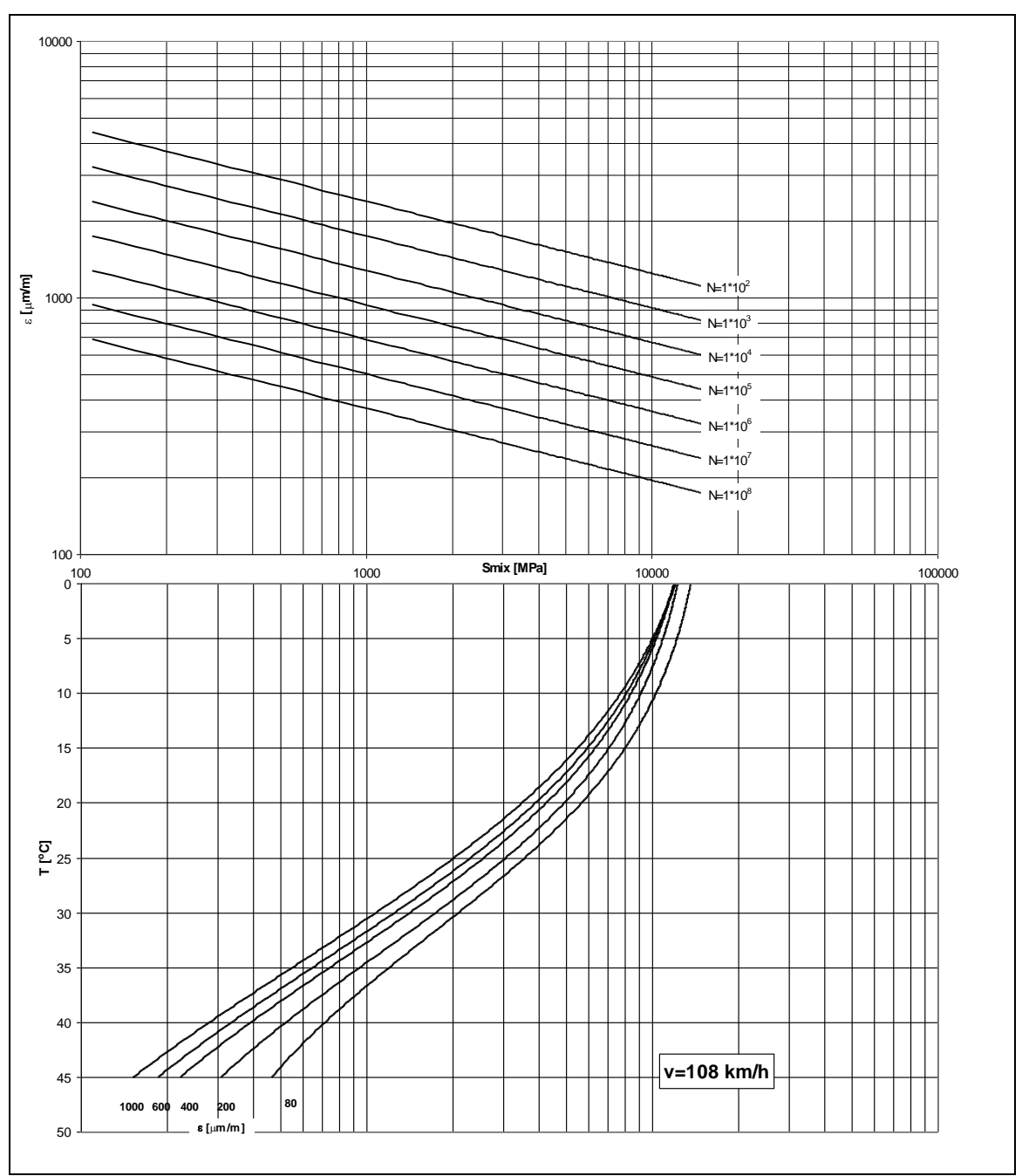


Figure 4: Fatigue design nomograph for 108 km/h

Appendix E: Determination of the tension and compression strength as a function of temperature and loading rate

E.1. Introduction

With the data from the tension and compression tests both the tension and compression strength can be expressed as a function of temperature and loading rate. Analysis showed that both can be expressed as follows (equation 1):

$$f = a \left(c - \frac{1}{1 + \left(v \exp\left(\left(\frac{b}{T_k}\right)^2 + d\right) \right)^e} \right)$$

Equation 1

in which:

 $\begin{array}{ll} f & : tension/compression \ strength \ [MPa] \\ v & : strain \ rate \ [100/s] \\ T_k & : temperature \ [K] \\ a, b, c, d, e & : parameters \\ \end{array}$

For both the tension and compression test the parameters a-e are determined by using a nonlinear regression analysis in SPSS. Paragraph E1 and E2 show the output from SPSS.

E.2. Compression strength

Notes

Output Created		17 Jul 01 14:23:42
Comments		
Input	Data	H:\SPSS\compression.sav
	Filter	<none></none>
	Weight	<none></none>
	Split File	<none></none>
	N of Rows in Working Data File	54
Sy ntax		MODEL PROGRAM A=-95 B=1800 E=0.35 D=-45 C=1 . COMPUTE PRED_ =
		a*(c-1/(1+(rate*exp((b/tempk)**2+d)) **e)).
		NLR ft /OUTFILE='C:\TEMP\SPSSFNLR.TM P'
		/PRED PRED_ /SAVE PRED RESID /CRITERIA SSCONVERGENCE 1E-8 PCON 1E-8.
Resources	Elapsed Time	0:00:00.54

All the derivatives will be calculated numerically.

Run stopped after 10 model evaluations and 5 derivative evaluations. Iterations have been stopped because the relative reduction between successive

residual sums of squares is at most SSCON = 1.000E-08

	Nonlinear	Regression	Summary	7 Statistics	Dependent	Variable	FT
--	-----------	------------	---------	--------------	-----------	----------	----

Source	DF	Sum of Squares	Mean Square
Regression Residual Uncorrected Total	5 8 13	2246.97351 .84129 2247.81480	449.39470 .10516
(Corrected Total)	12	876.05083	

R squared = 1 - Residual SS / Corrected SS = .99904

			Asymptot	tic 95 %
		Asymptotic	Confidence	e Interval
Parameter	Estimate	Std. Error	Lower	Upper
A	-50.66874508	6.716490664	-66.15700032	-35.18048983
В	1812.6438466	54.270704121	1687.4953785	1937.7923147
E	.354577057	.041769480	.258256464	.450897649
D	-45.02278207	2.899620308	-51.70931849	-38.33624565
С	1.022098411	.010195473	.998587608	1.045609213

Asymptotic Correlation Matrix of the Parameter Estimates

	A	В	E	D	С
A	1.0000	3404	.8677	.5441	.8675
В	3404	1.0000	7322	9738	3259
E	.8677	7322	1.0000	.8608	.8328
D	.5441	9738	.8608	1.0000	.4906
С	.8675	3259	.8328	.4906	1.0000

E.3. Tension strength

Notes

Output Created		17 Jul 01 13:51:11
Comments		
Input	Data	H:\SPSS\tensiongoed.sav
	Filter	<none></none>
	Weight	<none></none>
	Split File	<none></none>
	N of Rows in	54
	Working Data File	
Sy ntax		MODEL PROGRAM A=-95 B=1800 C=1 D=-45 E=0.35 .
		COMPUTE PRED_=
		a*(c-1/(1+(rate*exp((b/tempk)**2+d))
		**e)). NLR ft
		/OUTFILE='C:\TEMP\SPSSFNLR.TM
		P'
		/PRED PRED_ /SAVE PRED RESID
		/CRITERIA SSCONVERGENCE
		1E-8 PCON 1E-8 .
Resources	Elapsed Time	0:00:00.75

All the derivatives will be calculated numerically.

Run stopped after 69 model evaluations and 32 derivative evaluations. Iterations have been stopped because the relative reduction between successive $\frac{1}{2}$

residual sums of squares is at most SSCON = 1.000E-08

Nonlinear Regression Summary Statistics Dependent Variable FT

Source	DF	Sum of Squares	Mean Square
Regression Residual Uncorrected Total	5 9 14	344.55951 3.34049 347.90000	68.91190 .37117
(Corrected Total)	13	160.65429	

R squared = 1 - Residual SS / Corrected SS = .97921

			Asymptotic 95 %		
		Asymptotic	Confidence	e Interval	
Parameter	Estimate	Std. Error	Lower	Upper	
A	12.231241044	2.018784240	7.664433816	16.798048273	
В	1655.3789535	99.831090685	1429.5453366	1881.2125704	
С	1.039477399	.033230247	.964305357	1.114649441	
D	-34.88799962	4.495482800	-45.05748824	-24.71851100	
E	.757772269	.237640660	.220191747	1.295352791	

Asymptotic Correlation Matrix of the Parameter Estimates

	А	В	С	D	E
A	1.0000	.5100	6333	5816	8757
В	.5100	1.0000	1758	9951	7824
C	6333	1758	1.0000	.1994	.5594
D	5816	9951	.1994	1.0000	.8250
E	8757	7824	.5594	.8250	1.0000

Appendix F: Determination of N as function of ϵ and S_{mix}

The data from the first fatigue test on the Moerdijk mix is used to determine the fatigue relationship as a function of the stiffness and the strain. The relationship is described best with equation 1:

$$\log N = a_1 - n_1 \log \varepsilon - n_2 \log S_{mix}$$

Equation 1

The parameters a1, n1 and n2 are determined with a non-linear regression analysis by using SPSS. The output from SPSS is shown below.

Notes

Output Created		11 Jun 01 11:35:57
Comments		
Input	Filter	<none></none>
	Weight	<none></none>
	Split File	<none></none>
	N of Rows in Working Data File	6
Sy ntax		MODEL PROGRAM A1=1 N1=1 N2=1 . COMPUTE PRED_ = +a1+n1*logeps+n2*logsmix. NLR logn /OUTFILE='C:\TEMP\SPSSFNLR.TM P' /PRED PRED_ /CRITERIA SSCONVERGENCE 1E-8 PCON 1E-8 .
Resources	Elapsed Time	0:00:00.37

All the derivatives will be calculated numerically.

Iteration	Residual SS	A1	N1	N2
1	45.78211820	1 0000000	1 0000000	1 0000000
1.1		33.3774389		
2	.0789928294	33.3774389	-7.4391278	-2.0857776
2.1	.0789928294	33.3774209	-7.4391262	-2.0857738

Run stopped after 4 model evaluations and 2 derivative evaluations. Iterations have been stopped because the relative reduction between successive

residual sums of squares is at most SSCON = 1.000E-08

Nonlinear Re	egression	Summary	Statisti	.CS	Dependent	Variable	LOGN
Source		DF	Sum of S	quares	Mean Squa	are	
Regression Residual Uncorrecte		3 3 6		35149 07899 43048	50.78 .02	3383 2633	
(Corrected	d Total)	5	7.	14033			
R squared	= 1 - Res	idual SS	S / Corre	cted SS	.98	3894	
Parameter	Estimat			Con	Asymptotic Afidence In Wer	nterval	
A1 N1 N2	-7.439126	227 1.0	044463165	-10.76	5369306 74 5307417 -4 5110322 6	.115178287	7
Asymptotic	c Correlat	ion Matı	rix of th	ıe Param	neter Estir	mates	
	A1	1	11	N2			
A1 N1 N2	9505	1.000)59)0 .9)0 1.0	190			

Appendix G: Determination of $\sigma_{dilation}$ as a function of strain rate and temperature

Analyses showed that the relationship between σ_{dilation} , temperature and strain rate is best

$$\sigma_{dilation} = a \left(1 - \frac{1}{1 + \left(\dot{\varepsilon} \exp\left(\left(\frac{b}{T_k} \right)^2 + c \right) \right)^d} \right)$$

Equation 1

in which:

 $\begin{array}{ll} \sigma_{\textit{dilation}} & : \text{ stress at the onset of dilation [MPa]} \\ \hat{\mathcal{E}} & : \text{ strain rate [x100/s]} \\ T_k & : \text{ temperature [K]} \\ a, b, c , d & : \text{ constants} \\ \end{array}$

The constants a-d are determined with a non-linear regression analysis in SPSS. The output is shown below.

All the derivatives will be calculated numerically.

Run stopped after 14 model evaluations and 7 derivative evaluations. Iterations have been stopped because the relative reduction between successive

residual sums of squares is at most SSCON = 1.000E-08

Nonlinear Regression Summary Statistics Dependent Variable SIGMA

Source	DF	Sum of Squares	Mean Square
Regression Residual Uncorrected Total	4 9 13	1360.02910 .69455 1360.72365	340.00727 .07717
(Corrected Total)	12	933.08517	

R squared = 1 - Residual SS / Corrected SS = .99926

			Asymptotic 95 %		
		Asymptotic	Confidence	e Interval	
Parameter	Estimate	Std. Error	Lower	Upper	
A	-42.61158964	2.103272706	-47.36952306	-37.85365623	
В	1841.5436469	41.350556128	1748.0021902	1935.0851036	
C	-46.06791961	2.007463039	-50.60911650	-41.52672272	
D	.581261792	.030522390	.512215348	.650308235	

Asymptotic Correlation Matrix of the Parameter Estimates

	A	В	С	D	
A	1.0000	0508	.1451	.5937	
В	0508	1.0000	9954	7808	
С	.1451	9954	1.0000	.8312	
D	.5937	7808	.8312	1,0000	

Appendix H: Determination of α_0 as a function of strain rate and temperature

Analyses showed that the relationship between α_0 , temperature and strain rate is best described

$$\alpha_0 = a \left(1 - \frac{1}{1 + \left(\dot{\varepsilon} \exp\left(\left(\frac{b}{T_k} \right)^2 + c \right) \right)^d} \right)$$

Equation 1

in which:

: the initial α value (material parameter) α_0

 $\begin{array}{ll} \dot{\mathcal{E}} & \text{: strain rate [x100/s]} \\ T_k & \text{: temperature [K]} \\ a, b, c , d & \text{: constants} \\ \end{array}$

The constants a-d are determined with a non-linear regression analysis in SPSS. The output is shown below.

All the derivatives will be calculated numerically.

The following new variables are being created:

Name Label

Predicted Values Residuals PRED

Run stopped after 347 model evaluations and 164 derivative evaluations. Iterations have been stopped because the relative reduction between successive

residual sums of squares is at most SSCON = 1.000E-08

Nonlinear Regression Summary Statistics Dependent Variable ALFA

Source DF Sum of Squares Mean Square Regression Residual 4 .03577 8.942851E-03 8 1.662827E-06 2.078534E-07 Uncorrected Total 12 .03577 (Corrected Total) 11 .02199

R squared = 1 - Residual SS / Corrected SS = .99992 Asymptotic 95 % Asymptotic Confidence Interval Parameter Estimate Std. Error Lower Upper .000449987 .103180278 .105255620 .104217949 1382.1151026 42.713812618 1283.6168741 1480.6133311 В -22.72272379 1.266721780 -25.64378945 -19.80165813 D .203571604 -2.703885549 -1.765011627 Ε -2.234448588 Asymptotic Correlation Matrix of the Parameter Estimates Α В 1.0000 Α .7544 -.7523 .7783 1.0000 -1.0000 В .7544 .9916 1.0000 D **-.**7523 -1.0000 -.9913 Ε .7783 .9916 -.9913 1.0000